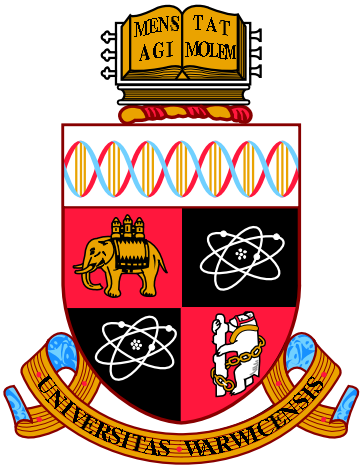

Modelling and Analysis of Hand Motion in Everyday Activities with Application to Prosthetic Hand Technology

by

Callum John Thornton

Thesis

Submitted to the University of Warwick

for the degree of

Doctor of Philosophy

School of Engineering

January 2023

Mason Dray is a close friend of the family and one of the kindest people anyone would ever come to know, no one has a single bad word to say about him. He overcame many struggles through his life, always having joy to give and making the world around him a better place to be. Having secured a dream job, he was settling down and enjoying his life.

On 2nd May 2022 Mason's life was taken, at the age of 19, two days after being hit by a drunk driver. This page remembers Mason and all those who's lives have meet unjust ends paying the consequences of others' wrongdoings. These words do not make up for his loss but hope they mean that a great, kind and always giving person will not be forgotten.

Thank you

Contents

List of Figures

List of Tables

Acknowledgements

I would like to open by thanking my mother, Tanya Claire Thornton, for the single greatest gift there is and continuing to push me to make the most of that life. I thank the surgeons and intensive care staff at Darent Valley Hospital and know I will forever owe my life to them.

My family have given me endless support and motivation to be the best me throughout my life, for which I gratefully thank: my mother, my brother (Leon Thornton), my grandparents (Christine Elizabeth Thornton and John Thornton) and my uncles (Lee Darren Thornton and Troy Matthew Thornton). To my wonderful wife, Makiko Tanada-Thornton, thank you for all of your support in my life and work, you have helped me more than words can describe.

I would like to thank my supervisors, Michael John Chappell, Neil Darren Evans and Joseph Hardwicke, for the opportunity to conduct this research and the help they have provided throughout the study. I would also like to thank Naomi Smerdon, Rebecca Grenfell, Ciara Dinneny and the Hand Therapy and Rheumatology team at UHCW for their time aiding the data collection performed during this study.

To all of my friends I am lucky to have close to me, thank you for keeping me motivated throughout the project. Particularly, I would like to thank those who have helped me learn and improve the skills applied throughout this study.

I thank all of the teaching staff I have had the opportunity to work with and Sotaro Kita's research group within the Department of Psychology for their support, particularly Suzanne Aussems for her help in moving this project forward.

To Yusuke Miyazaki, I thank you for the help you provided me when I was first living in Tokyo, and to Mitsunori Tada, thank you for your continued support of my job at AIST and move to Tokyo.

There have been so many people who have aided my life. To those not named here, please know I am forever grateful for the help you have given me.

I would like to close by thanking you, the reader, for, at the very least, considering my work to be of interest to you.

Declaration

This thesis is submitted to the University of Warwick in support of my application for the degree of Doctor of Philosophy. Except where specifically stated, all of the work described in this thesis was carried out by the author, under the supervision of Prof. Michael J. Chappell, Dr. Neil D. Evans and Dr. Joseph Hardwicke, during the period of October 2017 to April 2022. The research reported here has not been presented, nor submitted, in any previous application for any degree at another university.

C. J. Thornton
April 2022

Dissemination

The results of this research have been disseminated in the following publications and conferences.

Journal Publications

1. C. J. Thornton, M. J. Chappell, N. D. Evans, and J. Hardwicke, "Portable Markerless Hand Motion Capture System for Determining the Grasps Performed in Activities of Daily Living," *Computer Methods in Biomechanics and Biomedical Engineering: Imaging & Visualization*. Submitted May 2022, pending review.
2. N. Henry, C. J. Thornton, N. D. Evans, M. J. Chappell, S. Homer-Vanniasinkam, J. Hardwicke, "Identification of Commonly Used Grasps using the Leap Motion Capture System," *Journal of Hand Surgery Global Online*. Submitted January 2023, pending review.

Conference Presentations

1. C. J. Thornton, M. J. Chappell, N. D. Evans, and J. Hardwicke, "Modelling and Analysis of Hand Motion in Everyday Activities with Application to Prosthetic Hand Technology," *Workshop: Gesture & technology*, Warwick, June 2018. Oral presentation.
2. C. J. Thornton, M. J. Chappell, N. D. Evans, and J. Hardwicke, "Modelling and Analysis of Hand Motion in Everyday Activities," *UHCW Surgical Research Forum*, Coventry, February 2018. Oral presentation.

3. C. J. Thornton, M. J. Chappell, N. D. Evans, and J. Hardwicke, "Modelling and Analysis of Hand Motion in Everyday Activities," *School of Engineering 7th Postgraduate Symposium*, Warwick, April 2019. Poster presentation.

4. C. J. Thornton, M. J. Chappell, N. D. Evans, and J. Hardwicke, "Modelling and Analysis of Hand Motion in Everyday Activities with Application to Prosthetic Hand Technology," *BioMedEng21*, Sheffield, September 2021. Oral presentation.

5. C. J. Thornton, M. J. Chappell, N. D. Evans, and J. Hardwicke, "Predicting Muscle Excitations of the Hand from Kinematic Data," *IEEE Industrial Cyber-Physical Systems (ICPS22)*, May 2022. Oral presentation.

6. C. J. Thornton, M. J. Chappell, N. D. Evans, and J. Hardwicke, "Validation and Clinical Applications of the Leap Motion Controller," *IUPESM World Congress on Medical Physics and Biomedical Engineering (IUPESM WC2022)*, June 2022. Oral presentation.

Abstract

Upper-limb prostheses are either too expensive for many consumers or exhibit a greatly simplified choice of actions, this research aims to enable an improvement in the quality of life for recipients of these devices. Previous attempts at determining the hand shapes performed during activities of daily living (ADL) provide a limited range of tasks studied and data recorded. To avoid these limitations, motion capture systems and machine learning techniques have been utilised throughout this study.

A portable motion capture system created, utilising a Leap Motion controller (LMC), has captured natural hand motions during modern ADL. Furthering the use of these data, a method applying optimisation techniques alongside a musculoskeletal model of the hand is proposed for predicting muscle excitations from kinematic data. The LMC was also employed in a device (AirGo) created to measure joint angles, aiming to provide an improvement to joint angle measurements in hand clinics.

Hand movements for 22 participants were recorded during ADL over 111 hours and 20 minutes - providing a taxonomy of 40 and 24 hand shapes for the left and right hands, respectively. The predicted muscle excitations produced joint angles with an average correlation of 0.58 to those of the desired hand shapes. AirGo has been successfully employed within a hand therapy clinic to measure digit angles of 11 patients.

A taxonomy of the hand shapes used in modern ADL is presented, highlighting the hand shapes currently more appropriate to consider during upper-limb prostheses development. A method for predicting the muscle excitations of the hand from kinematic data is introduced, implemented with data collected during ADL. AirGo offered improved repeatability over traditional devices used for such measurements with greater ease of use.

Abbreviations

2D	Two-Dimensional
3D	Three-Dimensional
ADL	Activities of Daily Living
ADM	Abductor Digiti Minimi
AI	Artificial Intelligence
ANN	Artificial Neural Network
APB	Abductor Pollicis Brevis
API	Application Programming Interface
APL	Abductor Pollicis Longus
AUC	Area Under the Curve
BSREC	Biomedical & Scientific Research Ethics Committee
CH	Calinski-Harabasz
CMC	Carpometacarpal
CNN	Convolutional Neural Network
CSV	Comma-Separated Values
DB	Davies-Bouldin
DI	Dorsal Interossei
DIP	Distal Interphalangeal
DoF	Degrees of Freedom
ED	Extensor Digitorum

EDM	Extensor Digiti Minimi
EEG	Electroencephalography
EI	Extensor Indicis
EMG	Electromyography
EPB	Extensor Pollicis Brevis
EPL	Extensor Pollicis Longus
FDMB	Flexor Digiti Minimi Brevis
FDP	Flexor Digitorum Profundus
FDS	Flexor Digitorum Superficialis
FPB	Flexor Pollicis Brevis
FPL	Flexor Pollicis Longus
GA	Genetic Algorithm
GD	Gradient Descent
HMI	Human-Machine Interface
HTML	Hypertext Markup Language
ICC	Intraclass Correlation Coefficient
IMU	Inertial Measurement Unit
IoT	Internet of Things
IP	Interphalangeal
IR	Infra-Red
JS	JavaScript
KNN	k-Nearest Neighbours
LED	Light-Emitting Diode
LMC	Leap Motion Controller
MCP	Metacarpophalangeal

MDS	Multi-Dimensional Scaling
MU	Motor Unit
NUC	Next Unit of Computing
ODM	Opponens Digiti Minimi
OP	Opponens Pollicis
PCA	Principal Component Analysis
PCoA	Principal Co-Ordinate Analysis
PI	Palmar Interossei
PIP	Proximal Interphalangeal
PSO	Particle Swarm Optimisation
RAM	Random Access Memory
R-CNN	Region-Based Convolutional Neural Network
RNN	Recurrent Neural Network
ROC	Receiver Operating Characteristic
sEMG	Surface Electromyography
SVD	Singular Value Decomposition
TAM	Total Active Motion
t-SNE	t-Distributed Stochastic Neighbour Embedding
TENS	Transcutaneous Electrical Nerve Stimulation
TMR	Targeted Muscle Reinnervation
UHCW	University Hospitals Coventry & Warwickshire
USB	Universal Serial Bus
VR	Virtual Reality

Chapter 1

Introduction

Modern day upper-limb prostheses are either too expensive for many consumers or provide a greatly simplified choice of actions available. The intended impact of this research is to provide the knowledge of what is demanded from the human hand during average typical everyday tasks. This aims to lead to improvements in the quality of life for recipients of upper-limb prosthetic devices whilst also offering a reduction in the cost. Consequential improvements to the quality of life for the recipients would aid the adoption rate of these prosthetic devices and a reduction to the cost would enable the offering of these devices to a greater number of amputees. The objective of this study is to implement a, novel, portable motion capture device to capture the natural hand motions of modern activities of daily living (ADL). Alongside this the data collected has been inputted into a method combining an existing musculoskeletal model and optimisation techniques to predict the hand muscle excitations from kinematic data, aimed at aiding the development of myoelectric-controlled prostheses, and a device for measuring the hand digit joint angles has been proposed, aimed at improving the currently employed clinical methods used. This chapter outlines the motivation for this work, the aims and objectives and summarises the discussions of the succeeding chapters.

1.1 Motivation

Modern day upper-limb prostheses do not support the requirements of many consumers [1–4]. Grasp taxonomies presented in the literature [5–8] offer an insight into the grasping actions performed during certain tasks, attempting to aid functional imitations of the human hand. The latest taxonomy of grasps was introduced by Feix et al. [8]; however, this only considered two professions (housekeepers and machinists). Due to the limited range of activities studied in previous work, there is a need for these taxonomies to be updated to include modern activities of daily living (ADL) - such as the use of mobile phones and keyboards. The use of video recorded data to shape previous taxonomies limits the possible length of the recordings, due to the requirement to watch over the collected data; this has led to a limited amount data being collected and used to create these taxonomies.

This study aims to update the currently accepted standard set of grasp taxonomies. By providing this as an updated taxonomy of functional hand shapes, upper-limb prostheses can be designed with new knowledge surrounding the importance of each different hand shape. The results will highlight the functionality demanded from the hand during an average typical day - a basic desire from the hand. Through the utilisation of this information, upper-limb prostheses could potentially be developed to ensure that this base level of functionality is met. With this improved functionality of upper-limb prostheses, it is hoped that the quality of life for recipients will increase; with improvements to rehabilitation time, ease of use and the adoption rate of these devices among amputees. The proposed solution, using a motion capture system to record the data, will offer the ability to collect more data, due to the enabled application of machine learning techniques to process and analysis the data. Furthermore, making this system portable removes the requirement for performing such data collection within a fixed motion capture environment - allowing for the recording of more natural ADL. The introduced portable motion capture system has been validated against a state-of-the-art motion capture studio, to ensure confidence in the collected hand motion data. This has also provided a validation of the Leap Motion controller (LMC) for application in the acquisition of clinically relevant measurements.

Knowledge of hand shapes performed in everyday life has not been used to determine the muscle excitations required. Extracting the muscle excitations performed during collections of hand motions in ADL would provide aid to electromyography (EMG) controlled upper-limb prostheses. A method which could predict the muscle excitations occurring within kinematic data would enable the utilisations of existing data, collected during ADL, to provide muscle excitation measurements. This

would indicate the shapes associated with expected EMG patterns within ADL. In addition, a method predicting these muscle excitations from kinematic data would enable the collection of muscle excitation data without a need for encumbering or invasive devices to be place on the participant. The observed inaccuracy of current measurement systems employed also supports the introduction of alternative means for indicating muscle excitations.

In light of this, this study aims to provide the muscle excitations performed during everyday activities of modern life. Within this work, in an attempt to further utilise the kinematic data collected during ADL, a method combining an existing musculoskeletal model [9] and optimisation techniques is introduced. The obtained knowledge has been highlighted for the aid of myoelectric protheses. The introduced method offers a means of capturing the muscle excitations occurring from, exclusively, a single frame of kinematic data - information previously only obtainable through contact or invasive devices. Ascertained knowledge of the muscle excitations of the hand during common hand shapes aids upper-limb prostheses design for myoelectric prostheses. From this knowledge, devices could be designed to cater for certain cases of muscle excitation inputs. This would aid the quality of the responses from myoelectric upper-limb prostheses, with known information supporting the development of each movement produced by the prostheses. Furthermore, there is the potential for cheaper development with use case limited prostheses, providing the most used hand shapes for a reasonable cost performance balance.

During physiotherapy, acquiring the range of motion available to a patient is a useful measure of progress. In the deployment of prosthetic hands, the measurement of enabled hand movement is also key to evaluating these devices. Additionally, evaluating the rehabilitation progress for users of full and partial prostheses provides support during the recovery process. Currently a goniometer is used for most clinical assessments; however, there is limited knowledge of the accuracy of this device and it often fails to show agreement across different users. Furthermore, this method requires contact between the patient and the observer, takes a significant amount of time to complete a full collection of hand digit joint angles and requires expertise to operate. Improvements to the repeatability of this method would provide confident knowledge of patient progress. Knowledge of the accuracy of the method used would provide a useful indication to the confidence allowed in the collected data. A contactless system would reap several benefits - in particular, the removal of potential contamination of the measurements. Faster collection times would result in an ability to collect more information and see more patients within a set time. Additionally, if the device was able to run with no expertise it would enable the completion of measurements by the patients, independently from their clinical visit time. A means to store and easily refer to collected observations would aid rehabilitation by enabling

a fast indication of patient progress.

This study aims to provide improvements to measurements taken of the hand digit joint angles, through further utilisation of the LMC. The LMC offers several benefits to the, currently employed, goniometer: validation of the device highlights a known accuracy, the results are repeatable, quick and no contact is required to achieve a measurement of the joint angles. Additionally, this is able to aid in the assessment of partial and full hand prostheses. Provided the structure of a complete hand is presented, the LMC is able to capture motion data. This enables quick and accurate evaluation of the quality of a prosthesis and rehabilitation progress. A device (named AirGo) is introduced within this work, aiming to alleviate the issues present in the application of manual goniometers for the collection of hand digit joint angle measurements. This device provides a faster and more reliable means for collecting measurements of patient hand digit joint angles, whilst remaining contactless from the patient, within hand therapy clinics. Additionally, the operator of the device does not require previous experience of the device - enabling the ability for patients to perform their own measurements independent of their clinical visit. Patient progress assessment is aided by the quick and easy referral of the electronically stored measurements.

1.2 Aims and Objectives

The aims of this project and objectives by which these aims were achieved are as shown below. These were created based on the project outline and findings from the literature.

Aims:

- Create a means by which the quality of life of recipients of upper-limb prostheses can be increased and the cost of the devices reduced.
- To ascertain the most commonly used hand motions in everyday tasks, including the use of modern day technology.
- Provide a greater understanding of hand motion through mechanistic musculoskeletal modelling of the hand.
- Improve the clinical methods employed to obtain angular displacement measurements for the hand digits.

Objectives:

- Collect and analyse motion capture data of the hand to provide an understanding of the typical everyday hand motions.

- Determine the common hand shapes performed in everyday activities and compare these with previously developed taxonomies in the literature.
- Develop and implement a musculoskeletal model based technique to determine muscle excitations from hand shapes observed in everyday life.
- Utilise motion capture technology to provide faster and more reliable measurements of the hand digit angle than the current clinical standard.

1.3 Thesis Outline

This thesis discusses the biomechanical properties of the hand and analysis of the hand shapes seen throughout regular ADL. The motivation, aims and objectives have been achieved through the work presented in the following chapters.

Chapter 2, **Background**, reviews the current state-of-the-art in upper-limb prosthetic devices and the capture and analysis of human hand motions. To begin, the structure of the hand is presented, discussing the roles of each bone, joint and muscle. A discussion of the development of upper-limb prostheses is provided. The existing taxonomies of grasps are introduced and discussed. The current state-of-the-art methods for the capture of hand motions are displayed. Following this the analysis methods utilised in the literature are reviewed - with focus placed on developments surrounding artificial intelligence (AI) and data manipulation techniques. Existing models aimed to capture the intricacy of hand motions are identified and discussed. The currently utilised measurement methods for muscle excitations are introduced and their limitations promulgated. Subsequently, literature surrounding the deployment of optimisation techniques are highlighted to aid their envisaged utilisation within a prediction model. A review of the currently employed and suggested techniques for joint angle measurements closes this chapter.

Chapter 3, **Methodology**, introduces the methods used the collection and analysis of hand motions. The chapter opens with a description of the proposed alternatives to the current methods used for capturing the movement of the hands, predicting muscle excitations from kinematic data and obtaining measurements of hand joint angles. A detailed breakdown of the methods employed to collect data is given. The methods used to analyse this collected data are also introduced, highlighting the strengths and weakness for the use of each with the collected data. A description of how the final results were displayed has been given - collecting utilisable outputs to provide the outcome of the project.

Chapter 4, **Analysis**, examines the data collected and applies the, previously described, analysis techniques. The results of validations undertaken for each of the techniques employed are reviewed. Results of the analysis methods mentioned in the

previous chapter are presented and the final results displayed. The validation and evaluation results of several muscle excitation prediction methods are provided. The results of a clinical trial undertaken for a new hand joint angle measurement device are shown and discussed.

Chapter 5, **Taxonomy of Functional Hand Shapes**, discusses how the obtained results could be used to influence a taxonomy of hand shapes. Current grasp taxonomies are revisited, highlighting their similarities and any possible extensions which could be made. The taxonomy of functional hand shapes developed from the results of this project has been provided here. Comparisons are then drawn between the the presented taxonomy and current state-of-the-art, observing any differences and deducing the reasoning for such.

Chapter 6, **Predicting Hand Muscle Excitations**, reviews current musculoskeletal hand models and presents the selected model for implementation with optimisation techniques, to predict muscle excitations from kinematic data. A review over the selected musculoskeletal model is given and the steps taken to implement it reported. The selection of optimisation techniques chosen for this application is highlighted, with each implementation described. The results obtained following utilisation of the proposed prediction technique are transcribed and discussed.

Chapter 7, **AirGo**, highlights a novel device created for the measurement of hand joint angles. A brief review of the current state-of-the-art has been given and a proposed solution to the issues identified, named AirGo, presented. A revisit to the validation results for the LMC and performed clinical trial, with AirGo, provide argument for the deployment of this proposed device. The chapter closes with a discussion of the presented device and currently employed methods.

Chapter 8, **Conclusions and Future Work**, summarises the results found and discusses the potential future of the work performed.

Chapter 2

Background

This chapter provides a study of the required background knowledge. The included literature review examines existing ideas surrounding the motion of digits, provides a look into the progress seen in upper-limb prostheses design, reviews the development of grasp taxonomies throughout the literature, overviews potential techniques for the capture and analysis of the human hand movements, displays the current state-of-the-art models of the human hand and discusses the currently employed and suggested methods for measuring hand joint angles in a clinical environment. Methods introduced see their strengths and weaknesses highlighted, drawing conclusions of the optimal devices and techniques for this project. The required technical knowledge is presented, providing a detailed examination of the techniques employed to analyse the data collected. Included in this discussion are the machine learning approaches applied to highlight similarities within hand motion data and optimisation techniques explored to provide fast, reliable and accuracy estimations of the muscle excitations from singular frames of kinematic data. The utilisations of these described techniques are then reported in Chapter 3 and the results of implementation shown in the succeeding Chapter 4.

2.1 The Human Hand

The human hand is a complex mechanism, consisting of several elements interacting to enable the available range of motion. In a basic mechanical form the hand can be considered as rigid bodies, the bones, rotated around a pivot, the joints, by pulleys, the muscles and tendons. This interaction achieves 27 degrees of freedom (DoF) with 27 bones and 27 muscles, of which 16 are extrinsic and nine are intrinsic. This system of bones and muscles results in a vast capability for the hand - enabling a plenitude functions.

Many studies have tried to describe the reasons for the dexterity achieved by the human hand and recreate this ability in mathematical models [10–14]. Pons et al. [10] define manipulation to require the independent control of the fingers. It is argued that, though the independent flexion and extension of fingers may not be greatly important in grasping, it is for manipulation. A study performed by Montagnani et al. [11] tests the functionality of the human hand when different degrees of freedom are imposed on it; finding that independent abduction and adduction is more important than independent flexion and extension when grasping an object. In this study digits were physically constrained to move as one to create hands with varying degrees of freedom. It was also seen in this study that having an opposable thumb present gave a measurable advantage when performing activities of daily living (ADL). Research by Okada [12, 13] found that the introduction of abduction and adduction in a robotic hand allowed for greater functionality (e.g. fastening a nut to a bolt). This research supports the argument by Montagnani et al. that abduction and adduction is an important function in the use of the hand. Additionally, when testing different actuator configurations Tavakoli et al. [14] found that abduction and adduction of the thumb increased the overall performance of the hand. It is clear that there is a consensus in literature that, to adequately replicate the functionality of the human hand, enabling manipulative interaction with the world around it, independent control of the digit flexion and extension and abduction and abduction are required.

2.1.1 Bones and Joints

Bones give a rigid structure to the body, they provide support and enable mobility. The joints of the body act as fulcrums for these rigid structures to translate across and rotate about.

The human hand consists of 27 bones, each labelled in Figure 2.1. The phalanges (appropriately named distal, intermediate and proximal) and metacarpals form the

digits. The wrist is comprised of carpal bones - eight bones forming the carpus. The individual names of which have been deemed unimportant here. The hand attaches to the lower arm at the distal ends of the radius and ulna. Though there is a lot of complexity to the carpus the digits are simple rigid bodies with generalisable simple hinges, this allows for basic robotic mimicking.

The three joint which connect the bones in each finger (digits two to five): metacarpophalangeal (MCP), proximal interphalangeal (PIP) and distal interphalangeal (DIP); for the thumb (digit one) this is: MCP and interphalangeal (IP). The joints are secured through ligaments, a connective tissue which binds bone to bone. Three joints connect the hand to the arm, the radiocarpal, ulnocarpal and distal radioulnar joints. Additionally, there are several joints connecting the carpal bones, each with labels derived from the connected bones - the individual naming of each has been considered irrelevant for this project. Connecting the carpals to the metacarpals of each digit are the carpometacarpal (CMC) joints. From here the collection of joints within and around the wrist will be refereed to as the wrist joint, singularly. The MCP of each finger has two DoF and the PIP and DIP one DoF each. The MCP of the thumb exhibits four DoF and the IP one DoF. These with the six DoF of the wrist joint provides the human hand with an overall 27 DoF. Each joint of the hand can be seen described in Figure 2.1.

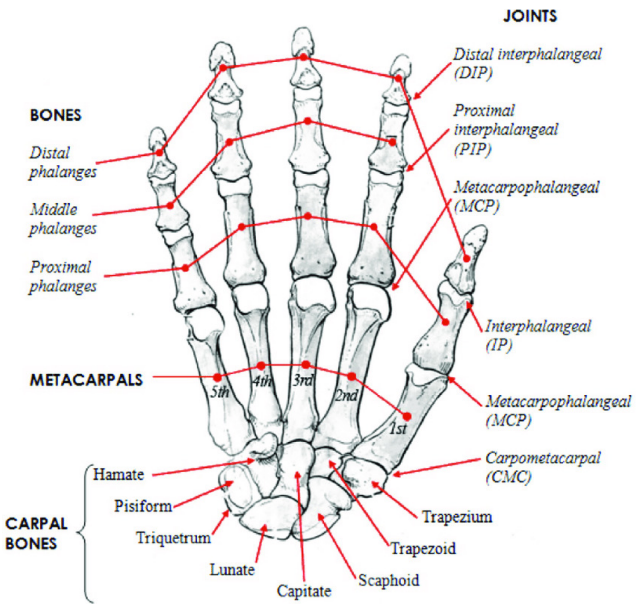

Figure 2.1: The bones and joints of the human hand [15].

2.1.2 Muscles and Tendons

Muscles provide the mechanical work required to move the body. The force each muscle is able to produce depends upon varying characteristics (length and velocity). Tendons act as an anchor between muscle and bone, they provide a conduit for the force from the muscles to be transferred to the bones.

The complex motions achieved by the human hand are actuated through the combined activation of intrinsic and extrinsic muscles. Intrinsic muscles are found within the hand structure and are, in general, responsible for the fine motor control seen by the hand. Extrinsic muscles are found externally to the hand and tend to produce larger motions, providing the gripping force possible by the hand. A descriptive breakdown of the intrinsic and extrinsic muscle of the hand can be seen in Tables 2.1 and 2.2, respectively. For simplicity, within these tables each digit has been referenced as a relative number (one to five in lateral to medial order) and similarly for the bones (one to four in proximal to distal order). The action column provides the resultant motion due to the activation of the respective muscles, with the digits and bones of these digits given this motion listed in the subsequent columns. Figures 2.2 and 2.3 visually depict each of these muscles, providing the location of each within the arm and hand.

Knowledge of extrinsic muscles is employed in prosthetic control and, with knowledge of intrinsic muscles, for development, training and validation of models of the hand. A price paid for examination of extrinsic muscles alone is their inability to describe the finer motor functions of the hand, responsible only for the overall, crude, motion. Due to their complex entanglement, intrinsic muscles are exceedingly difficult to record using surface electromyographys (EMGs) - the crosstalk seen in this area results in a near impossible to decode signal obtained with current surface EMGs technology.

Table 2.1: The extrinsic muscles of the human hand.

Name	Action	Digits	Bones
Extensor Digitorum (ED)	Extension	2 - 5	2 - 4
Extensor Indicis (EI)	Extension	1	2 - 4
Extensor Digiti Minimi (EDM)	Extension	5	2 - 4
Flexor Digitorum Superficialis (FDS)	Flexion	2 - 5	2, 3
Flexor Digitorum Profundus (FDP)	Flexion	2 - 5	2, 4
Flexor Pollicis Longus (FPL)	Flexion	1	2, 3
Extensor Pollicis Longus (EPL)	Extension	1	2 - 4
Extensor Pollicis Brevis (EPB)	Extension	1	1, 2
Abductor Pollicis Longus (APL)	Abduction	1	1

Table 2.2: The intrinsic muscles of the human hand.

Name	Action	Digits	Bones
Opponens Pollicis (OP)	Rotation, Flexion	1	1
Abductor Pollicis Brevis (APB)	Abduction	1	1
Flexor Pollicis Brevis (FPB)	Flexion	1	2
Opponens Digiti Minimi (ODM)	Rotation, Flexion	5	1
Abductor Digiti Minimi (ADM)	Abduction	5	1
Flexor Digiti Minimi Brevis (FDMB)	Flexion	5	2
Lumbricals	Flexion; Extension	2 - 5	2; 3, 4
Dorsal Interossei (DI)	Abduction	2 - 5	1
Palmar Interossei (PI)	Adduction	2 - 5	1

Similarly to ligaments, tendons are connective tissue. They are exceptionally durable and act like cords transmitting force, enabling the muscles to move the bones about and across the joints. There are two types of tendons: positional tendons, providing support for the bones and muscles, and energy storing tendons, acting as springs in aid of energy consumption during motion. The stretch experienced by the tendons aids muscle force generation. Within the hands the tendons enable the extrinsic muscle forces to affect the bones. From the forearm there are two groups of tendons: flexor and extensor tendons. Flexor tendons are located on the palmar side of the hand to enable digit flexion. Extensor tendons are located on the dorsal side of the hand to enable digit extension. Within the hand, the tendons connecting the

intrinsic muscles and bones provide structural support.

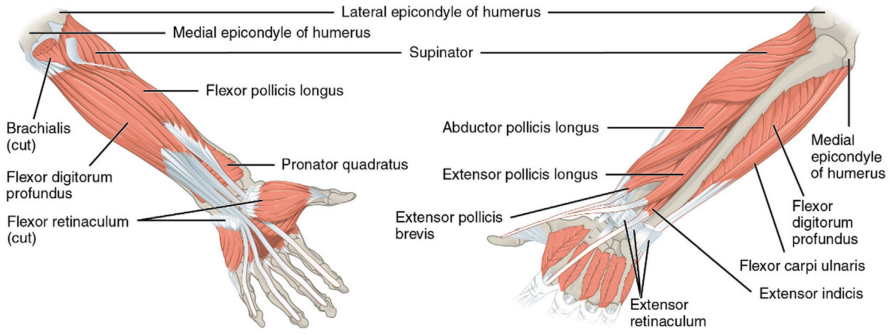

Figure 2.2: The extrinsic muscles of the human hand; displaying the left forearm deep muscles from the palmar view (left) and dorsal view (right) [15].

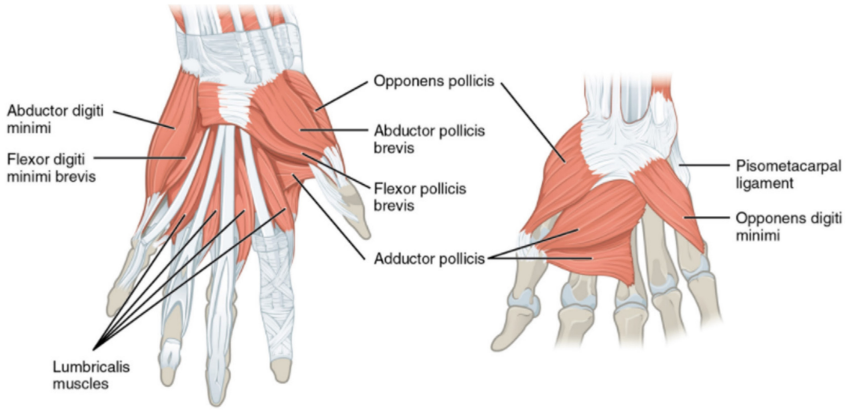

Figure 2.3: The intrinsic muscles of the human hand; displaying the left hand superficial muscles from the palmar view (left) and deep muscles from the dorsal view (right) [15].

2.2 Upper-Limb Prostheses

Significant progress has been made since the conception of upper-limb prosthetic devices, each step attempting to mimic the complex motions achieved by the hand perfectly whilst remaining cost effective. A later move to electronically powered prostheses improved user satisfaction but increased cost dramatically. Developments in actuation strategies allowed for a small reduction in price, at the cost of performance. The conception of three-dimensional (3D) printing gave significant aid to the development of prosthetic devices, introducing the first time for prostheses to be even close to reasonable for younger amputees of lower income families to afford. The prostheses outer bodies could be manufactured with ease at a significantly lower

cost than previously; this meant changes in size could be accounted for whilst conserving the motors - the notoriously expensive component when replacing electronic prostheses.

The first record of an upper-limb prosthetic device comes from Pliny the Elder in 77, who documented an artificial hand worn by Marcus Sergius which was fashioned to hold a shield after the lose of his hand in the second Punic War (218-201 B.C.) [16]. From this several similar ideas of passive prosthetics were conceived, most notably: Götz von Berlichingen in 1509 [17] and Ambroise Paré in 1564 [18]. Few changes were made until 1818, where a body powered upper-limb prostheses was introduced by Peter Bailiff [19]. The introduced prostheses utilised the shoulder motions to provide flexion and extension to the digits of the artificial hand. Body-powered devices rose quickly in popularity and are still used to this day, significantly more comfortable and practical than their first inception. Though usually unrealistic, aesthetically and in motion, many amputees show a preference to body-powered devices due to their design simplicity and robust nature, typically lasting longer and costing less than their alternatives. In 1898 Giuliano Vanghetti wrote the first document discussing the possibility of cineplastic operations, an amputation operation in which the residual muscles and tendons are used to directly control the artificial limb [20]. This technique was first performed in surgery 1905 [21] and since there have been several instances of these operations being performed [22–26]. Though pneumatics was considered as a form of powering prosthetic devices, it was implemented in few prostheses.

The first electronic hand prosthesis was published by Reinhold Reiter in the early 1948 [27]. This device employed an EMG device as the feed forward control, utilising electrical signals found from activation of residual muscles. The use of EMG signals to control upper-limb prostheses quickly developed and presented numerous variants. In 2006 Bitzer and Smagt showed how support vector machines can be used to support control inputs from surface electromyography (sEMG) readings [28]. In 2009 Castellini and Smagt utilise machine learning techniques, within an sEMG controlled hand, in order to determine the desired digit position and force [29]. Castellini and Smagt showed that this can form a reliable feed forward loop for a prosthetic hand with high potential for improving the EMG control method. Research on the application of pattern recognition in EMG prostheses aims to aid the control of the hand [30, 31]. Though found to have adequate accuracy, the real world application of this technique is questioned [32]. A study in 2019 developed an EMG sensor which was shown to be more sensitive and faster then other options for prosthetic hand control [33]. Locating useful muscle sites to collect accurate EMG signals is sparse, hence this method is typically only applied to patients with transradial amputation or wrist disarticulation.

In 1978 De Luca [34] discussed the idea of using neuroelectric signals for the feed-forward path in a prostheses. Though not proven to be an instant replacement of other techniques, De Luca showed the possibilities in the utilising the nerves of interest and argued the advantage over the common practice EMG technique. In 2005 Zhou [35] examined the possibility of using targeted muscle reinnervation (TMR) to improve the readings of intended movements, particular in areas dense in muscle sites where sEMG suffers - as is with the arm and hand. A TMR transfers residual nerves to alternative muscles, providing a biological amplifier in which the new, targeted, muscle activity can be measured using sEMG. This allowed for access to information not priorly available to sEMG devices and enabled the use of sEMG after forequarter amputation, shoulder disarticulation and transhumeral amputation. Studies since have increasingly supported the potential of TMR to improve EMG control for multiple prosthetic hands [36–39].

The use of sEMG devices have shown several issues, most notably of which is the high level of crosstalk and lack of information within superficial muscles. A study of a first-in-man of implant EMG device displayed the potential of this technique [40]. The patient, previously having used sEMG, described the device as allowing for a more natural and intuitive control. In 2021, Islam et al. [41] introduced a new, force-invariant, feature extraction method for the control of upper-limb prostheses. The method utilised the recorded amplitude changes and spatial correlation coefficients of the EMG channels to provide feature extraction. This was able to demonstrate a greater pattern recognition performance, higher accuracy, sensitivity and precision when compared to alternative feature extraction methods. Additionally, the method also exhibited a lower computational time and memory requirement over these methods.

In addition to the use of EMG signals for prostheses control, electroencephalography (EEG) devices have proven a possible control method for prostheses - measuring signals originating in the brain. In 1999 Guger et al. [42] introduced the use of a brain-computer interface with paralysed patients for controlling an external hand. It was shown that, by imagining left and right hand movements, the user was able to control a prosthetic hand with ample accuracy. Though it did not enable full digit movements (only gross opening and closing motions of the hand) this highlighted the potential of EEG control, arguing that this control method demands less attention from the user compared to alternative options. A 2007 review [43] of control strategies concludes that EEG control was not ready for practical use, though it was stated that the experimental progress made was favourable. It was also stated that more focus should be placed on the improving realism of the artificial hand joints and sensory feedback options, with EMG and TMR strategies showing the greatest potential for that time. Parr et al. [44] focus at how gaze training can

impact the use of upper-limb prostheses. Gaze training was achieved through the use of EEG and eye tracking devices, monitoring the brain and eye activity whilst the user picked up an object. The users were trained to fixate on the object to be grasped rather than the hand. After finding gaze training effectively reduces cognitive burden (reducing learning time and fatigue) Parr et al. argues that it is not the technology of prosthetic hands which requires attention but more the user interaction strategies employed. Ruhunage et al. [45] utilised the strengths of both EEG and EMG strategies in a hybrid system. This work introduced a successful hybrid system, in which EMG was used for elbow control and the gross opening and closing actions of the hand and EEG for prediction of the desired grip.

Actuation strategies for electronic devices became increasingly important - bearing great responsibility for influences on cost and comfort. The creation of taxonomies showing the common grasps performed through a typical day aids the understanding of demands the hand undergoes. Methods for actuating artificial hands can then be formed around what is discovered from these taxonomies. More effective actuation strategies help improve the lifestyle of upper-limb prostheses users and more efficient actuation strategies help reduce the costs of prosthetic devices. There have been several new actuation strategies tried and tested in the literature, particularly regarding underactuated prosthetic hands [14, 46–48].

It is typical in underactuated methods for each of the digits to be individually actuated by a single actuator [46, 48]. Massa et al. [46] introduced an underactuated prosthetic hand which mimicked the function of only three digits (the index finger, middle finger and thumb). Each of the digits is controlled by a single motor, based on the Shigeo Hirose Soft Gripper [49], to allow it to conform to any shaped object. This research aimed to use the recent developments in mechatronics design to create a simplified hand without sacrificing functionality. It was argued that the thumb-index pinch capability gave the hand high functionality whilst being able to only include few actuators controlled by a simple algorithm. More recently, Bullock and Dollar [47] created a similar, underactuated, manipulator with only the index finger and thumb. The study found the manipulator to be successful; it was able to work with objects in over 50% of the normal working volume of the human hand, with only 3 actuators used. It was remarked that future work would include the addition of more digits to increase functionality. In 2019 Jeong et al. [50] introduced a three DoF finger underactuated prostheses, demonstrating adequate control characteristics. In 2020 Abayasiri et al. [51] introduced an underactuated prosthetic hand design, aimed at improving performance in ADL. The underactuated device was able to perform extension and flexion of all digits, adduction and abduction of the four fingers and opposition and reposition of the thumb, opposed to the limited motions of other underactuated devices.

Tavakoli et al. [14] found the actuator configurations, for fixed numbers of actuators, which gave the best performance. It was argued that the results of this study could be useful when deciding upon the number of actuators and their configuration needed when designing a prosthetic hand, showing the most effective use of the actuators. Tavakoli et al. [48] argue in another paper that it is possible to have a higher level of anthropomorphism in hands with fewer actuators, supporting the research that has been undertaken in developing underactuated hand prostheses [14, 46, 47].

It is evident that there have been several upper-limb prosthesis actuation strategies suggested in the literature, many of which conclude in favour of underactuated prosthetic hands.

Research has also been prominent in prostheses for partial hand (transmetacarpal) amputations. The rise of of partial hand prostheses suffered most significantly from the fact that the EMG signals of the wrist interfered with the desired extrinsic muscle signals. Adewuyi et al. [52] studied how pattern recognition techniques could be applied to a partial prosthetic hand. The results showed that this is realisable, though the unpredictable nature of the wrist (still controlled by the user, opposed to the prosthesis) decreased system reliability and gave cause for increased training times. Earley et al. [53] explains how a classifier which switches between long and short EMG analysis window lengths could be employed to overcome these problems. It was argued that this dual window classifier had a significant positive affect. Earley et al. also highlighted that, whenever possible, benefit can be found in the utilisation of intrinsic, as well as extrinsic, muscles. Gaston et al. [54] later explained a procedure which relocates intrinsic muscles to improve accessibility. This relocation allowed for their use in the control of partial hand prostheses. Gaston et al. argued that this migration of the intrinsic muscles, to a more proximal and superficial location, improved EMG control.

Murali et al. [55] introduced a prosthetic device for partial hand loss, externally powered in order to present a more anthropomorphically correct hand. Though admitting to the need for several improvements Murali et al. argue for the potential of the introduced device. Alturkistani et al. [56] provided a 3D printed passive partial hand prosthetic for transmetacarpal amputation patients. Assessment of this prosthetic was judged on the performance of grasps given in the taxonomy presented by Feix et al. [57] and a lift test, showing sufficient grip strength with a stable grasp and preferred over active prosthetic devices due to the compactness, low weight and ease of attachment and detachment the prosthetic displayed. The use of 3D printing in upper-limb prostheses manufacture allows for easier, cheaper and quicker fabrication of devices sized precisely for varying individuals. Cuellar et

al. [58] presented a 3D printed artificial hand which required no manual assembly after printing. Aimed at developing countries, this simple and cost effective device granted a body powered prosthetic to partial hand loss amputees.

Feedback loops, as a controller exclusively within the prosthesis or including the user, have been studied to increase acceptability prosthetic hands. Controllers, not including the user, moderate the applied force from a prosthetic hand, given information of the hand and grasped object. These simple techniques aim to improve the acceptability of prosthetic hands at a low cost. A 2020 review of sensory systems with prosthetic hand devices argues that the progress made in the last 50 years is clinically limited, though it was stated that recent pushes have seen some relevance [3].

In 1998 Tufa et al. [59] presented an example of force based feedback system controlling the pressure applied by the prosthetic hand, paired with an optical detection system for preventing slipping. This feedback system was designed as a controller element within the device - the user had no feedback. In 2009 Pasluosta et al. [60] showed how a force sensing resistors, with a neural network, could allow for a cost effective force control and slippage system. Again, this was a simple controller element, not containing the user within the feedback loop.

The aforementioned feedback systems are solely controllers isolated within the device. Increasing the visual feedback, beyond the physical artificial hand, is one possible feedback method which enables the inclusion of the user within the control loop. In 2012 Engeberg and Meek [61] introduced a device utilising a two coloured light-emitting diode (LED) to indicate the gripping force, including the user visually within the feedback system. This inexpensive, lightweight and low power feedback device showed significant improvement, compared to no additional feedback, in both the results of experiential tests and the user feedback. Research has also been conducted to establish a proficient haptic feedback technique, typically employing vibrotactile or transcutaneous electrical nerve stimulation (TENS) techniques.

Studies have displayed the possible feedback options, including the user in the feedback path, with multiple feed forward controller options [62–66]. Ninu et al. [67] studied which variables show statistical importance within a closed loop feedback system. The subjects were able to estimate the grasping force when provided with closing velocity feedback alone, indicating a lower importance for force feedback. In addition to this, it was found that a vibrotactile feedback system could replace visual feedback. Christiansen et al. [68] reviews visual and vibrotactile feedback within an upper-limb prostheses. It is found that visual feedback as a greater impact on performance than vibrotactile. However, it was noted that vibrotactile provided assistance when the user could not see the target object and that the combination of

both showed no negative effect on the overall system. A previous study by Stepp and Matsuoka [69] noted an improvement when vibrotactile and visual feedback was employed, compared to the use of visual feedback alone. Witteveen et al. [65] highlighted that the inclusion of vibrotactile feedback improved grasping performance. Concluding the study, it is insisted that further work is performed to ascertain the impact of including feedback on the performance of ADL. A study in 2018, by Raveh et al., [70] measured the performance improvement seen with vibrotactile feedback on able bodies controlling an artificial hand with EMG signals. It was found that the feedback added improves time to complete and accuracy of tasks performed - concluding the importance of vibrotactile feedback when visual is not available. A study assessing the importance of vibrotactile feedback in an underactuated arm found that, though objectively visual was considered sufficient, subjectively patients preferred the additional vibrotactile feedback [62].

In 2019 Battaglia et al. [66], noting the recent trends towards underactuated prosthetic hands, aimed to asses possibility of adding proprioception to these devices. Though the single signal feedback used was unable to inform the user of positional information for each digit, it was able to provide an estimate of how open the hand was. It was concluded that this provided a simple and easy to understand feedback, giving some improvement to the quality of life for prosthetic hand users.

Upper-limb prostheses have shown significant improvements from their first inception, from passive and simple arms [16–18] to complex, dexterous, hands with feedback systems and advanced human control, with a notable desire to reduce the cost for users [39, 45, 51, 58, 66]. Open Bionics create 3D printed prosthetic arms, focusing on embracing the difference rather than viewing amputation as a burden on lives. The efforts by Open Bionics has made a significant impact and enabled children, as well as adults, to afford and use prosthetic hands with comfort. The use of 3D printing as a manufacturing method has a large influence on younger amputees as. Due to the typically rapid growth of children, many outgrow prostheses at a rate unreasonable to afford - only requiring to print the body of the arm at a low cost with growth. In 2019 Zheng et al. [71] reviews the control techniques and design of upper arm prostheses from the prospective of the users, referring to a focus group of 11 participants. The participants expressed most interest in improving the dexterity and durability of the devices. Though understanding the advantage of invasive control techniques many participants showed wariness. Zheng et al. argue the importance of educating amputees around invasive techniques, alluding to these control options as the likely next step. Despite these advancements it is still observed that modern day upper-limb prostheses are either too expensive for many consumers or have a greatly simplified choice of actions available [1–4].

2.3 Grasp Taxonomies

In the literature there are several studies that have classified the range of hand grasps performed by humans [6, 7, 57, 72–76]. These intend to aid the in the creation of devices replicating the human hand motions; though typically focused on aiding the design of manufacturing robotics, the consideration of these taxonomies during the design of upper-limb prostheses and exoskeletons may severe to provide useful information.

Schlesinger [5] was the first to attempt to organise human grasps into set categories, these were: cylindrical, top, hook, palmar, spherical and lateral. This taxonomy can be seen presented in Figure 2.4.

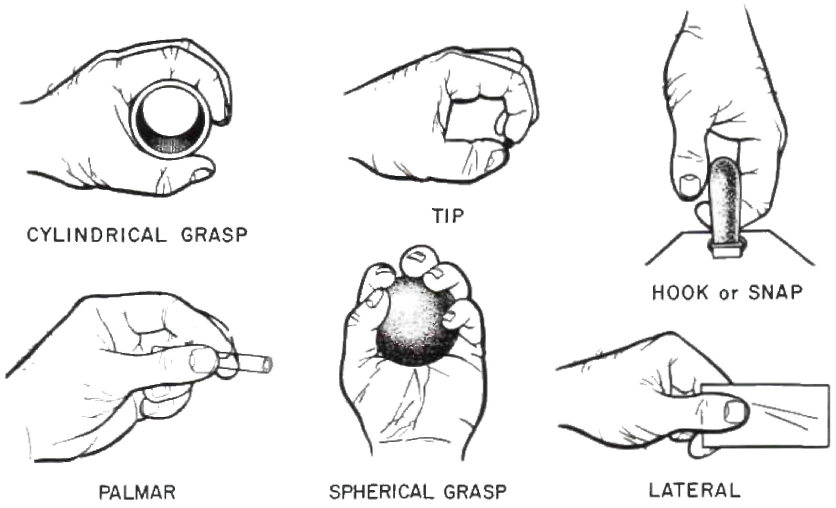

Figure 2.4: The grasp taxonomy introduced by Schlesinger [5].

Napier [6] later categorised each of the grasps into two categories, power and precision grasps. Following this Cutkosky [7] employed the same taxonomy, showcasing the possible application to robot manipulators in manufacturing processes. This taxonomy, with the divide of power and precision grasps discussed by Napier [6], is shown in Figure 2.5.

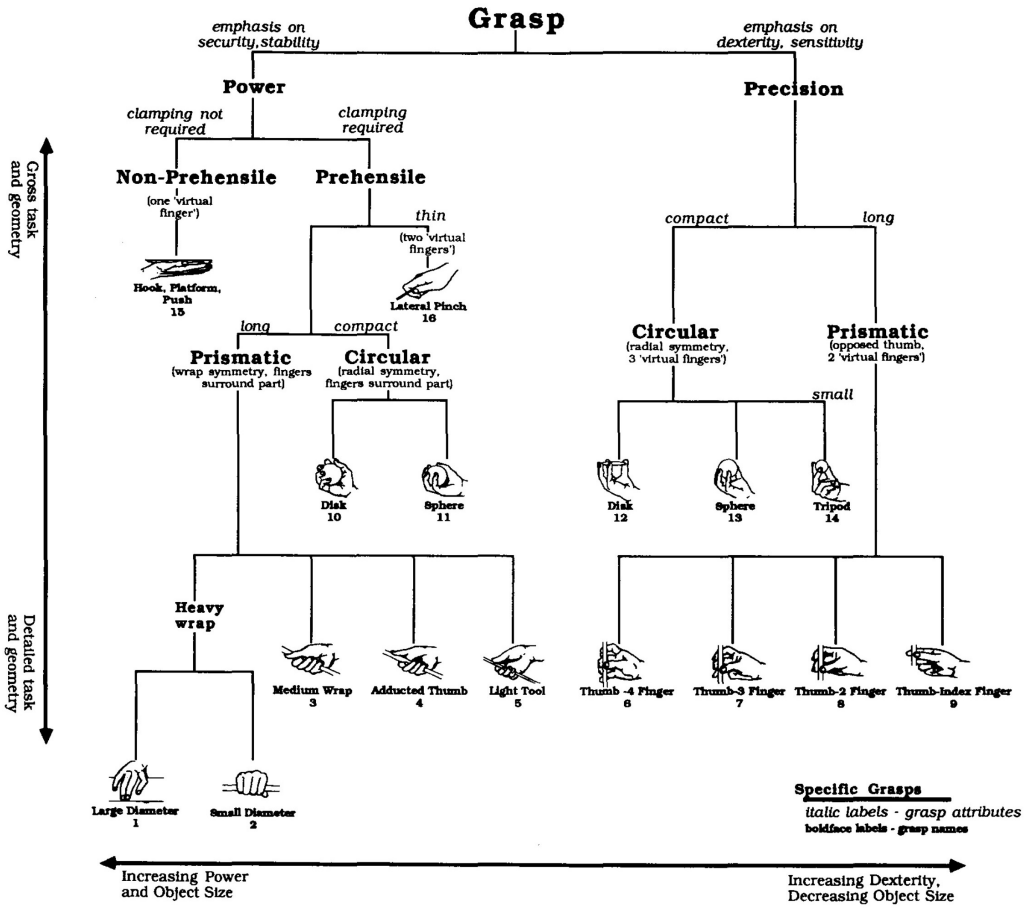

Figure 2.5: The grasp taxonomy introduced by Cutkosky [7].

More recently Feix et al. [57] reviewed the existing grasp taxonomies and gave thoughts on an updated, simplified, taxonomy. It was found that there is a possibility for 33 grasp types, given by the previous taxonomies, to be reduced to 17, more general, grasp types - arguing that each cell of the taxonomy presented previously [8] could be reduced to a standard grasp. The 33 grasps classified can be seen in Figure 2.6.

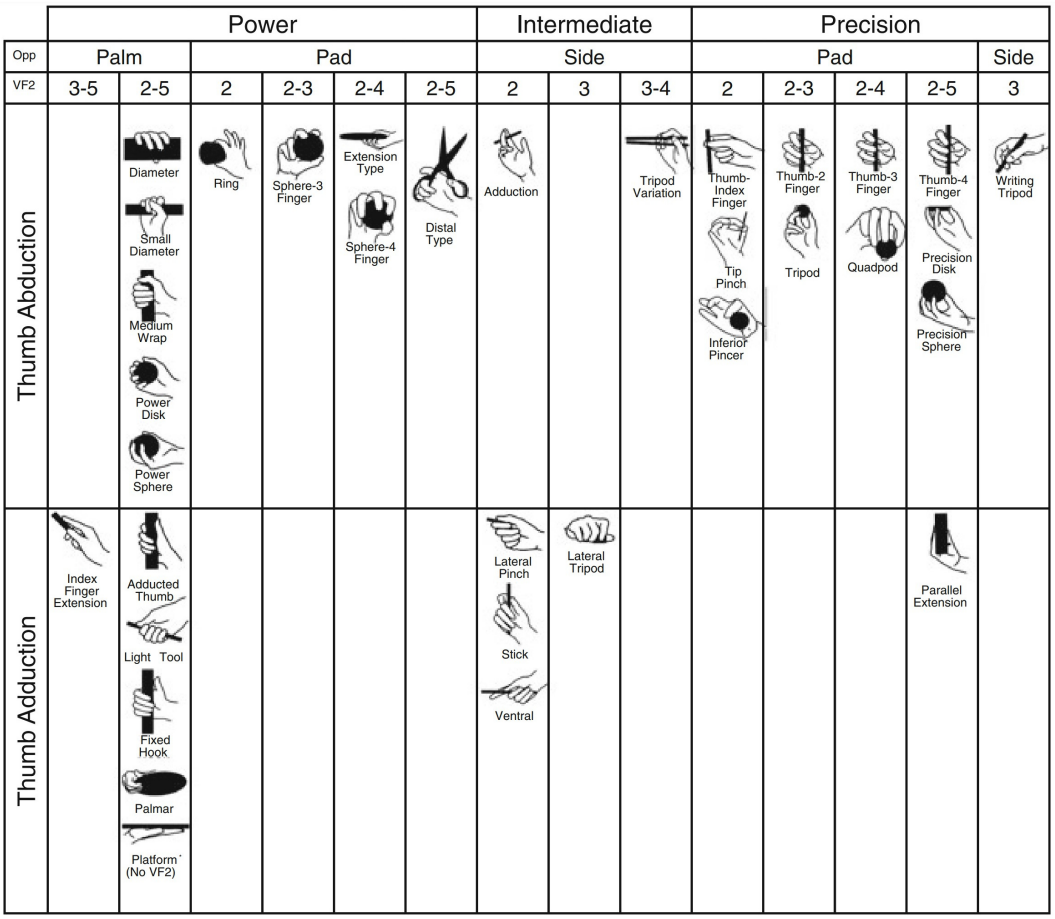

Figure 2.6: The grasp taxonomy introduced by Feix [8], as presented in [77].

It is typical in these research studies that housekeepers and machinists are chosen as subjects for the study [72, 77, 78], this is because the combination of these professions is seen to give the closest idea of the range of grasps used in normal ADL. However, Vergara et al. [75] stated that these studies, only looking at two professions, were biased, going on to study the grasps used in ADL. Vergara then used a simplified taxonomy of nine grasps (from the 24 presented by Edwards et al. [79]) to categorise grasps of ADL, arguing the needlessness of complete, more rigorous, taxonomies for ADL. A breakdown of the grasp applied in different activities was also provided, showing that not all grasps could be applied to each ADL. Liu et al. also presented a study focused on capturing the grasps performed in ADL [74]. It was found that previously established taxonomies proved insufficient for application to categorisation of grasps in ADL. Liu et al. suggested that taxonomies be written with approachability, noting the intended motion, force, and stiffness - assisting for robotics design.

Another limitation of these studies is the lack of consideration for gestures

occurring during ADL. All of the observed studies reviewing the functionality of the hand in everyday life consider grasps exclusively, yet there exists significant support for the importance of gestures in the literature [80–97].

Kita introduced the Information Packaging Hypothesis [82], which states that information is made available through gesturing - enabling access into the mind of the speaker. This hypothesis follows that more gestures will be performed with increase difficulty to conceptualise; in effect, that gesture aid the compartmentalisation aspects of speech. This leads to aid in the use of spatio-motoric concepts during speech. With this, it has been argued that gestures provide a window into the mind of the speaker [83]. It is argued that gesturing and speech should be seen as a unified system of communication, where gestures convey information in coordination with the concurrent speech [84, 85]. In a study manipulating the conceptualisation loads of picture description tasks, Melinger and Kita [86] showed that conceptualisation load increases led to increases in gesture production. Furthering this, Hostetter et al. [87] studied the amount of gestures produced in the responses of participants describing dot patterns with or without the aid of a connecting shape. The participants gestured in the exercises not including the shape, suggesting that more gestures were seen when information was difficult to conceptualise. A study by Alibali et al. [88] asked children to explain the difference between two presented items (Piagetian conservation). The experiment saw that children gestured for assistance in defining objects, with no indication that the gestures were in aid of speech production but more the conceptualisation of the images being portrayed.

An alternative hypothesis for the use of gesturing during speech production, the Lexical Retrieval Hypothesis (alternatively refereed to as Lexical Access Hypothesis) [89–91], argues that gestures are performed to provide aid to lexical retrieval. This hypothesis claims that gesturing produce linguistic stimuli, helping retrieve items from mental lexicon. Subsequently, this hypothesis argues that gestures play a significant role in the formulation of speech. One study by Chawla and Krauss [89] recorded subjects answering questions regarding personal experiences, feeling and believes, which were later recreated by actors from transcripts. It was observed that the re-enactments showed gestures occurring later than that which would be suggestive of lexical access, supporting that the gestures performed during the original recordings were to aid vocalisation of mental lexicon. Furthering this study, an included second experiment tested whether naive participants were able to discriminate between the original recordings and those reproduced by the actors. Provided with either of the audio or video recordings alone, the participants were able to predict correctly better than chance. These results suggest that gesturing adds a noticeable authenticity to comminations of a similar level to that of the spoken word. Rauscher et al. [90] found that, when the ability to gesture was removed from participants, there was an

increased difficulty to lexical access. The results of this study supported the belief that gesturing aids in the access to mental lexicon. Showing further support, Pine et al. [92] found that children were able to better formulate words when allowed to gesture; this study followed the same methodology of testing prohibited and unrestricted gesturing. A similar study by Pyers et al. [93] found that gesturing reduces the cognitive load during hard lexical retrieval - where participants with no gesturing inhibition were able to resolve more tip of the tongue word retrieval than if there was restrictions placed on gesturing ability.

Alongside these hypotheses, studies have also seen the aid that gesturing provides within learning environments. In 2019, Aussems and Kita [94] saw that watching a description with gestures helped children remember that description, arguing that the unified gesturing during task was able to facilitate the memory. In 2021, Ginns and King [95] also showed that pointing whilst being taught helped leaners retain that taught information. Lacombe et al. [96] observed that children with intellectual difficulties were aided by gesturing, showing a preference to gesturing over speech during communications. Further support for the inclusion of gesturing in daily life was shown by Chiera et al. in 2022 [97]; this study observed that gestures appeared frequently than pauses during speech, with the majority of those gestures being classified as non-communicative. This further supports that gestures accompanying speech are natural to humans and help during conversations - even if not directly supporting conceptualisation or speech production [83, 97].

The literature holds substantial support for the unnoticed aid gesturing brings to everyday life. The two hypotheses presented, the Information Packaging Hypothesis and Lexical Retrieval Hypothesis, show significant support for the consideration of gesturing during ADL. Whether they are in aid of conceptualising speech, with Information Packaging Hypothesis arguing that gesture production increases when conceptual demands increase, or formulating the speech, with Lexical Retrieval Hypothesis arguing gesture production increases when lexical demands increase, there is a clear aid brought to everyday life through the gestures performed.

This research aims to observe all of the hand shapes required for ADL. To achieve this, observations of functional hands shapes were made, comprised of: gestures and grasps. Each of these will be considered equally, though distinguishing each enables comparisons to existing knowledge. A gesture was considered as a functional hand shape not touching an object in a way to create a hold of that object, not indicative of object manipulation. A grasp was seen as a gesture physically interacting with tangible objects within the world of the user.

2.4 Motion Capture Technology

In the most current studies of the hands, motion video cameras are used to record the hands and the footage reviewed to determine the grasps performed [72, 74–76]. Typically a head-mounted video camera is placed on the subject and their hands recorded over a set period of time. After the videos had been captured trained raters would analyse each of them to determine how many times certain grasps were performed. This method can lead to unreliable results due to the reliance put on the judgements of the raters, manually labelling the data frame-by-frame. Many studies try to reduce this unreliability by comparing the judgements made by several raters, but this inherent limitation cannot be completely removed. This process is a long, slow and tedious activity which can lead to errors. However, this is not always the case and studies have also created novel methods for collecting the data.

In the study performed by Huang et al. [73] an unsupervised clustering technique was used in order to autonomously determine the grasps performed. The study showed this method to be very effective; it was stated that development should have a significant impact, across multiple disciplines, in prehensile analysis. To validate the method both choreographed and real life scenarios were used. The clusters determined by this method were compared to those from the taxonomy introduced by Cutkosky [7] and it was seen that it had created new groups as well as fitting groups in the previous taxonomy. Du [98] create a mesh for a virtual hand to be used in data collection for a virtual keyboard system.

It is typical for vision based motion capture systems to be used over other methods, such as gloves. The main reason for this is the fact that placing sensors on the hand, as is done with the motion capture gloves, encumbers movement, giving a less natural hand motion. Another study, by Qi [99], utilised EMG devices to record hand motion data and neural networks to determine the grasps performed, with the assistance of a principal component analysis (PCA) algorithm. This resulted in an accuracy of 95.1% with a recognition time of 0.19 seconds, highlighting the possibility of automatic grasp classification to speed up grasp analysis.

New developments have pushed for kinesiology recordings to be performed using motion capture technology and numerically analysed; this has resulted in faster analysis of larger amounts of data and, in turn, allowed for more data to be collected. The upcoming gaming area that is of interest to this project is virtual reality (VR) gaming; this has led to the introduction of many cheap and easily accessible motion capture devices. The devices used in VR gaming commonly differ from research focused motion capture devices due to the fact that they do not need markers. This gives a less encumbered movement and allows for a much quicker and easier set

up (providing the user with a more comfortable experience overall), however this is at the cost of the accuracy of the data collected. More recently the accuracy of these devices has greatly increased and they are becoming cheaper and more widely available alternatives to the original devices used for research.

In this project a Leap Motion controller (LMC) [100] was used for the collection of motion capture data of the hand during ADL; this is commercially available, cheap, vision based system with no markers. There have been several research papers studying the effectiveness of the LMC as a computer input device or motion capture recording device [101–103]. Bachmann et al. [101] found that the LMC is limited as an input device for everyday computer pointing tasks. Coelho and Verbeek [102] tested an LMC against a mouse in pointing tasks in a 3D virtual environment. It was seen that the mouse, again, outperformed the LMC. Guna et al. [103] argues that the LMC cannot be used as a professional tracking system due to the limited field of vision (the volume in which the LMC can capture the hands) observed and inconsistent sampling frequency.

Bizzotto et al. [104] tests the the use of the LMC in controlling imaging during live surgery. The research performed concluded that the LMC was an efficient low-cost solution to controlling imaging devices during the surgery. It had less risk of spreading infection in a surgical environment, as there would be no need to touch the equipment, and reduced surgery time, as the surgeons no longer needed to change their gloves to operate the imaging devices. In the literature the LMC has been heavily tested for teaching and learning a great range of different sign languages [105–110]. Potter et al. and Guardino et al. [105, 106] were both disappointed in the application programming interface (API) of the LMC, arguing that it limits the abilities of the controller from misleading labelling and requires further development. Guardino et al. argue that the controller is beneficial due to the much greater portability and affordability it displays, compared to alternative motion capture methods used in research (such as Cyblerglove and Microsoft Kinect). Additionally, in the study by Guardino et al. the authors found that the combination of an LMC and a webcam has the potential to become a new method for teaching and learning the American sign language. Mohandes [107] complains about field of vision and possible occlusion caused when using one LMC. It is stated that further work will be to test the use of two LMCs, one placed in front of the user and the other to their side, in order to avoid occlusion. Despite the multiple arguments in the literature against the LMC many do still support the potential of this device for research and create methods of defeating the problems encountered. The LMC will still be considered in this project due to the fact that it is a much cheaper and accessible alternative to other methods, allowing quick preliminary data collection. Arguments made against the API of the LMC have been considered but hold little value here,

as the presented error were removable during data processing. The collection and analysis of data were performed separately, meaning that the data can be correctly labelled once converted to a local co-ordinate system, with clearly identified joints, if required.

The method most commonly employed to study the human hand in use, capturing a video recording of the hand in use and then watching the video, is a time consuming process with potentially high error due to the subjective nature. For this study the use of motion capture devices to collect kinematic data of the hand is considered over the use of video cameras. The LMC is a markerless optical motion capture device which uses three infra-red (IR) cameras to determine a 22-point virtual image of the hand. The points of the hand captured by the LMC are as follows: the MCP joint, IP joint and tip of the first digit, the MCP joints, PIP joints, DIP joints and tips of the second to fifth digits, the centre point of the palm, the CMC joint and a point opposite to the CMC joint in the medial direction. The LMC is supported within the literature: proven effective for stroke rehabilitation and musculoskeletal simulation [111–114] and literature reviewing the employment of an LMC for data collection of hand kinematics provide confident support for the ability to collect clinically meaningful data [115, 116]. Though the LMC has also received some criticism in the literature [101, 103], it was used here due to the presented high portability, providing an ability to be used during the normal everyday tasks performed by the participant within comfortable environments for them, ability to work without markers, leading to unencumbered movements, and non-invasive nature, resulting in natural motions as the participant does not feel as if they are being watched in a laboratory environment.

A Vicon motion capture system [117] at University Hospitals Coventry & Warwickshire (UHCW) was used to validate the use of an LMC; this uses eight IR cameras to locate reflective markers within the laboratory space. The high level of accuracy and the fact that it suffers from occlusion far less than the LMC makes it a worthy candidate for a data collection method. However, it is not without limitations; the feeling of being watched due to the laboratory environment and the markers encumbering movements leads to less natural motions being produced by participants. This motion capture system will also be used to validate the data collected by the LMC. Preliminary testing showed that the markers used do not interfere with the data collected from LMC, allowing the use of the motion capture system for evaluating the accuracy of the LMC.

2.5 Motion Capture Analysis Techniques

Prior to analysis of large motion capture datasets, it is preferred to reduce these data. Reductions can be made either in the amount of frames observed or the dimensionality of the observations. Methods attempted and steps taken to reduce the complexity of the data collected in this study are described here, as well as any supporting use cases highlighted. Observations of the recorded data lead to the extraction of only the frames presenting the desired information, reducing the number of frame required for analysis. Reductions to the dimensionality of the data would enable faster analysis; though this may include a loss of accuracy, due to the limited information defining each observation.

In motion capture recording the dimensionality of the data is typically high, requiring three dimensions for each of the features measured. Reducing this dimensionality would allow for a simpler and quicker analysis of the data. Common methods used to achieve dimensionality reduction are: PCA, t-distributed stochastic neighbour embedding (t-SNE) and multi-dimensional scaling (MDS).

The PCA method [118] utilises singular value decomposition (SVD) [119, 120] to determine new dimensions for a given dataset, forming the new dimensions such that the high variation of the data is exhibited in a fewer number of dimensions. This provide the potential for a vast amount of the information within a high dimensionality dataset could possibly be described using three or less dimensions, a dimensionality conceivable in physical space.

An employment of PCA starts by finding the centre of each dimension (providing the centre of the dataset) - followed by a translation of the data such that these centres are placed at the origin of each dimension. Each point is projected onto a line which goes through this origin; PCA then attempts to maximise the sum of the squared distances from the project point to this new origin. The line with the highest sum of squared distances is selected as the first principal component, this sum of squared distances gives the eigenvalue of the principal component and the square root of this provides the singular value of SVD. The singular vector (eigenvector) for this component can be calculated by creating a unit length vector from the origin along this component line, the proportions of each gene which form this provide the loading scores. Each of the next principal components are found, in turn, in the same manner, remaining perpendicular to the first found principal component. The PCA score can then be created by using the principal component lines found as axes and the position of each data point along each of these axes being the position of the projected point to this axis, seen when determining the principal components. Once all of the principal components have been determined, the proportion of variation

each of the components accounts for can be calculated by taking the ratio of the eigenvalue for the component in question and sum of all eigenvalues,

$$variance_i = \frac{\lambda_i}{\lambda_1 + \lambda_2 + \ldots + \lambda_N},$$

where i is the component in question, λ is the eigenvalue for each of the components and N is the total number of components found.

Scree plot display these values to aid in the identification of the necessary principal components required to display the desired information. Observing a scree plot, the optimal number of principle components to be considered would be highlighted from a lessening in the gradient - indicating less variation change per principle component included beyond that point. This can be considered as if looking at a cross-sectional cut of a mountain, the scree of the mountain indicates a levelling out to the ground - where there is less change in altitude as you progress.

Following the performance of a PCA, a loading can be created. This plots the results of the product of the eigenvectors and square of the respective eigenvalue. From a loading plot several pieces of information retaining to the introduced principle components and original dimensions of the dataset can be observed. Reading the absolute value of a variable along the axis of one of the principle components on the loading plot provides the influence that variable has over the considered principle component. This absolute value can range from zero to one, with a higher value indicating a greater weight to that principle component. Additionally, the relative positions of the lines drawn for each original dimension can be used to determine correlations between dimensions. Lines which are within close angular proximity imply a positive correlation, a 180 degrees divide between them shows a negative correlation and dimensions 90 degrees apart are considered to have no correlation.

The uncorrelated multilinear PCA has been suggested for use with unsupervised learning for recognition tasks [121]. A MATLAB function is provided for ease of implementation. However, this technique has not been considered in this research as there exists correlations between hand joint angles and the technique has shown to provide an decreasing improvement, over PCA, past a dimensionality of 20 (the recorded Cartesian data provides a dimensionality of 60) [121].

Following recordings of hand motions in ADL, PCA was employed to attempt to aid computational complexity in analysis by reducing the dimensionality of the data. A large reason for this choice is the fact that the effect an original dimension has on the variation of the data seen by the principal components can be found. This enables the ability to identify influential joints of the hand; considered insightful information during analysis as it supports the possibility of classification from a

select number of directly recorded values. Additionally, the deterministic approach of PCA enables repeatability of the results, which was appealing when concerned with the application to different collections of hand data - enabling comparable results, without contamination.

The t-SNE method [122] attempts dimensional reduction by projecting the data onto a single axis, whilst preserving the relative clustering of the data. In an application of t-SNE the data are first placed onto the lower dimensional space in a random order. The t-SNE then pulls observations, which are closer together in the original space, together in the new space, whilst simultaneously pushing those observations further from others they are further from in the original space. It determines the similarity between points by creating a normal curve for each point, centred on the observation considered Each of the other observations are then placed on this curved, with the horizontal distance from the point representing the distance between the two points in the original space. The value of the normal distribution then provides the similarity of these observations. Once the similarities between each observation have been found, the similarities are scaled to result in a sum of one,

$$p_{j|i} = \frac{\mathrm{e}^{-|x_i - x_j|^2/2\sigma_i^2}}{\sum_{k \neq i}^{n} \mathrm{e}^{-|x_i - x_k|^2/2\sigma_i^2}},$$

where $p_{j|i}$ is the conditional probability indicating the degree in which point x_i would select point x_j if the selection was proportional to their probability density under an x_i centred Gaussian and n is the total number of data points. This allows for comparability in the results for different density of clusters within the data, explaining the variance seen in the original dimensions with a lower number of dimensions which still retain clarity of the original clusters. A binary search is used to determine the value of σ_i, which provides a probability distribution with the fixed, preset, perplexity value. The perplexity indicates the target number of neighbours to the selected point during the calculation of similarity.

Similarly for the reduced dimensional space, the similarity can be determined through the conditional probability,

$$q_{j|i} = \frac{\mathrm{e}^{-|y_i - y_j|^2}}{\sum_{k \neq i}^{n} \mathrm{e}^{-|y_i - y_k|^2}},$$

where y are the points, similarly to that seen in the original dimensional space, in the new space. This provides a matrix of similarity scores for each of the points in the original space. The steps to find the similarity matrix are then repeated for the randomly placed points in the lower dimensionality space; in this execution, however, Student t-distribution is used in place of the normal distribution. A t-distribution

is used because of the higher tail ends, resulting in a larger separation of clusters in the new dimensions. By moving each point iteratively, t-SNE converges towards a new space similarity matrix representative of that from the original space, thus preserving the information from the dataset whilst reducing the dimensions.

The t-SNE method converges towards matching similarity matrices by minimising the Kullback-Leibler [123] divergence of the dimensions P and Q,

$$KL(P||Q) = \sum_{i \neq j} p_{i|j} \log \frac{p_{i|j}}{q_{i|j}}.$$

This is minimised with a gradient descent (GD) approach. The existence of multiple local minima and nature of the GD optimisation technique leads to a relatively low reproducibility when compared to a deterministic method, such as PCA.

Due to the transformations undertaken during an application of t-SNE, the effects of the original dimensions on the variance within the data cannot be determined. For this application, knowledge of the influence of the recorded dimensions over the variation of the data would provide insightful information. The t-SNE has not been applied to the collected data does not have the repeatability of PCA and cannot display the influence of an original dimension on the variation of the results.

The MDS technique [124], also known as principal co-ordinate analysis (PCoA), is used to visually identify similarities within data points of a dataset. The application is similar to that of PCA, however, converts based on distances among the data points, rather than correlations. These distances can be measured with a range of methods, common of which include: Euclidean distance, log fold change, Manhattan distance and Hamming distance. If the Euclidean distances are used to create the distance matrix then the results of MDS would be identical to those from PCA.

The application PCA has been preferred over MDS due to indication of correlations, which could find a use in application with prosthetic hands, and known joint correlations placing confidence in the reduction capabilities of this technique.

The raw collected data provides hand motion data within the global space. For the purposes of this research, the only information of interest from these data is the shape of the hands in each frame - resulting in a benefit from transforming these data into a local co-ordinate system. To achieve this all of the joints were translated to place the wrist at the origin of the axes and then rotated such that the first digit MCP joint aligns with the positive y direction and the positive x direction axis describes the posterior to anterior of the hand. These rotational transformations were achieved through the use of 3D rotation matrices. The rotation matrices for

manipulating a vector in 3D space about the x, y and z axes by θ degrees are,

$$Rot_x(\theta) = \begin{bmatrix} 1 & 0 & 0 \\ 0 & \cos(\theta) & -\sin(\theta) \\ 0 & \sin(\theta) & \cos(\theta) \end{bmatrix}, \tag{2.1}$$

$$Rot_y(\theta) = \begin{bmatrix} \cos(\theta) & 0 & \sin(\theta) \\ 0 & 1 & 0 \\ -\sin(\theta) & 0 & \cos(\theta) \end{bmatrix}, \tag{2.2}$$

$$Rot_z(\theta) = \begin{bmatrix} \cos(\theta) & -\sin(\theta) & 0 \\ \sin(\theta) & \cos(\theta) & 0 \\ 0 & 0 & 1 \end{bmatrix}. \tag{2.3}$$

During transformation to a local co-ordinate system, the θ described the difference in the current position and local co-ordinate position for pairwise co-ordinates of selected palm feature points.

Processing and analysis of the data required calculation of the joint angles for the hand. Observations of the digit joint angles employ the vector dot product, described by,

$$\cos(\theta) = \frac{\vec{a} \cdot \vec{b}}{|\vec{a}||\vec{b}|}, \tag{2.4}$$

where θ is the angle observed between vectors $\vec{a}$ and $\vec{b}$. The joint angle of a select joint can be found by translating the joint in question, the joint next more distal and that next more proximal such that the joint in question is at the origin of the space and then calculating the angle between the more distal and more proximal joints using the vector dot product.

Validation of methods attempted and evaluation of the results included the examination of Euclidean distances between pairwise data points and correlations of datasets. During these steps the Euclidean distance, d, has been calculated in 3D Cartesian space between two points, $p_1(x_1, y_1, z_1)$ and $p_2(x_2, y_2, z_2)$, through the Pythagorean theorem,

$$d = \sqrt{(x_2 - x_1)^2 + (y_2 - y_1)^2 + (z_2 - z_1)^2}. \tag{2.5}$$

The correlation between two sets of data, in this study each representing hand shapes, has been found using the Pearson correlation coefficient [125]. For two n dimensional sets of data, x and y, with means $\bar{x}$ and $\bar{y}$, respectively, the Pearson correlation

coefficient of these samples, r_{xy} can be found using,

$$r_{x,y} = \frac{\sum_{i=1}^{n}(x_i - \bar{x})(y_i - \bar{y})}{\sqrt{\sum_{i=1}^{n}(x_i - \bar{x})^2}\sqrt{\sum_{i=1}^{n}(y_i - \bar{y})^2}}.$$

2.6 Machine Learning Techniques

The collection of numerical data to describe the hand motions observed enables the use of artificial intelligence (AI) to examine the measurements taken. These recorded hand motion data can be inputted into a machine learning or deep learning approach to provide classifications. The resultant classifications would reduce the data into a manageable size, by highlighting similar hand shapes performed. These final groupings can be manually assess and altered to form the final, presented, taxonomy of hand shapes found within modern ADL. This analysis ability is lacking from previous hand analysis research, resulting in long processing times and plausible uncertainty in the obtained results.

2.6.1 Artificial Neural Networks

Artificial neural network (ANN) classifiers are a deep learning supervised machine learning technique designed to closely share the architecture of the human neural network, within the brain [126]. Through rigorous learning the networks develops to provide knowledge from desired situations. These networks are made of neurons, each existing with a value, and synapses, connecting these nodes commonly with a weight. These are reinforcement learning techniques, typically, employed when a full model cannot be built for the system. Through an input of information from the environment and network development, ANNs can deduce an appropriate response. Commonly, these outputs of the ANNs can relate to an input to a agent within the studied environment or predictions of the scenario occurring within the environment; in this case it being a prediction of the functional hand shapes occurring.

A generalised structure of an ANN can be seen in Figure 2.7. Here, X represents the neurons for each dimension of the inputted dataset, H the neurons of a given hidden layer, Y provides each of the possible predictions which can be made, w are the weights given to each of the synapses and b the biases given to each neuron. Each neuron node value is multiplied by the weight of the connecting synapse as it passes and the biases are added to each of the values of the hidden layer neurons; these weight and biases are adjusted through reinforced training of the ANN. The input layer takes a given, unlabelled, data entry to be labelled with a predicted

category, provided by the output layer. The output layer consists of all the possible labels which can be predicted; in a pass of the network each label is given a value and the highest value proposed as the prediction for the label of the inputted data. During the design of an ANN, variations of multiple hidden layers are created and configured to improve performance.

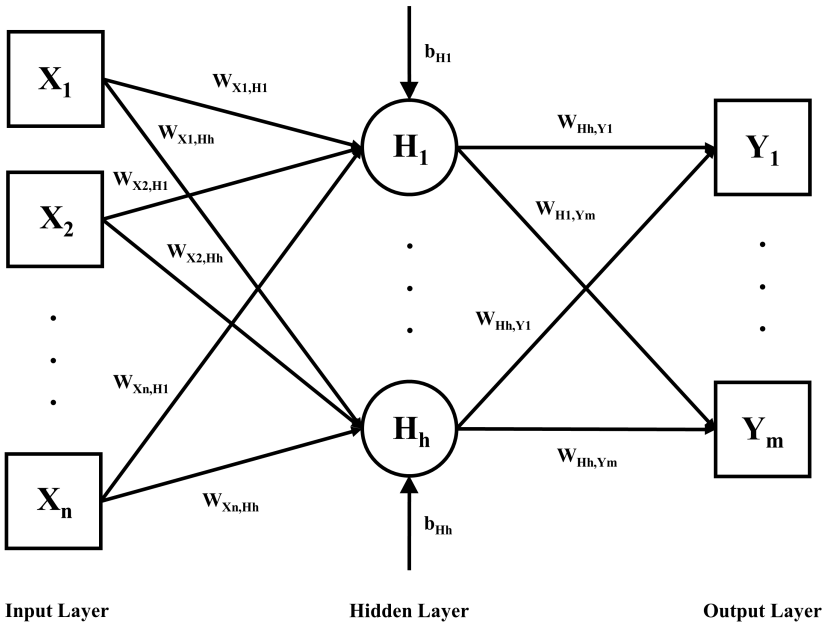

Figure 2.7: A generalised structure of a fully connected artificial neural network.

After initialising with random numbers, the network evolves through the process of continuously repeating input and outputs for one or more set scenarios, altering the neuron weights and bias value each time. An ANN attempts to reduce the cost function of the network, against a task, using backpropagation. This repetition results in a increasing accuracy, though it would not be known how exactly the final accuracy is achieved.

In an application of an ANN the inputs may be scaled to provide a consistency in values, desirable when observations exist within multiple different dimensions. During execution the output of one layer, x, is used as the input, z, to the next - influenced by the weights, w, and biases, b, of the next neuron and the synapse between. This can be mathematically represented by,

$$z = \sum_{i=1}^{n} (w_i x_i) + b.$$

An activation function is then used definite the output of a neuron, provided an

input from the previous layer. A commonly employed activation function for the output layer is the sigmoid function,

$$\hat{y} = \sigma(z),$$

where $\hat{y}$ is the predicted output value and the sigmoid function σ is defined by,

$$\sigma(x) = \frac{1}{1 + e^{-x}}.$$

Within hidden layers it is common to see the ReLU function as the chosen activation function, expressed by,

$$f(x) = \begin{cases} x, & \text{if } x > 0, \\ 0, & \text{otherwise,} \end{cases}.$$

To initiate, an ANN sets each of the weights and biases with randomised values. The first pass begins with an input of a partial training dataset, noting the difference between the predicted output labels and actual labels. Using a loss function, the network then calculates the loss of this pass. The loss function provides a numerical value to describe the averaged difference between the predicted label and known labels for an input. During learning the training dataset is divided and passed through the ANN in batches, a pass of the entire dataset is denoted as an epoch.

The aim of training a network is to minimise this loss for a provided, training, dataset; to achieve this learning a GD method is utilised. Once calculated, the gradient of the loss with respect to each weight and bias is then determined. As per the GD method, these gradients are then multiplied by the set learning rate and the results set as the new, receptive, weights and biases of the network. The repetition of this process results in a convergence toward a network with tuned weights and biases, able to provide accurate predictions for given inputs.

GoogLeNet is a highly regarded ANN developed by Google, proven to produce accurate predictions of image groupings. GoogLeNet was first introduced in September 2014 [127], as a 22 layered convolutional neural network (CNN). For this project GoogLeNet is used as an ANN attempt at classifying the collected data. In 1999 Friedrich et al. [128] applied a neural network, trained on grasps from the taxonomy introduced by Cutkosky [7], to data glove recordings, showing around 90% accuracy. Stanton et al. [129] employed an ANN to train a humanoid robot with positional data, collected from a motion capture suit. This described how a robot could be controlled, with no prior analytical or mathematical knowledge, utilising an ANN to learn the movements. Stanton et al. also stated how a change in the target robot would only require the network to be retrained, not redesigning a full descriptive

model. In 2009 Miller [130] implemented the application of an ANN on gait motion capture data. This method proved that an ANN could present autonomous and accurate detection of gait events. In 2020 Corona et al. [131] utilised a pre-trained ResNet-50 ANN to determine which grasp would be needed for object within a given image. The model takes an inputted image and locates the objects within it, then determining the shape and position of each. After which a taxonomy of 33 grasps [57] is employed to predict the most suitable grasp to approach the objects. The final stage then refines the hand shape and pose, forming the final output.

A measure taken to assess the performance of an ANN is the creation of a confusion matrix for a set of test inputs [132]. Given an input dataset with known labels, a confusion matrix can be created as a tabulated figure of the predicted labels against the known actual labels for the data. Each possible label is assigned to a row, defining the actual labels, and a column, defining the predicted labels. For each observation, with known label, passed through the classification model, the element defined by the predicted and true value of this observation is increased by one. Accuracy ratings for each are labels are given along the rows and columns assigned to each of these labels. Reviewing a plotted confusion matrix and observing the overall accuracy defines the performance of the classification model. Further details of where error has arisen can be extracted through the consideration of the individual rows and columns.

2.6.2 Classification Algorithms

Statistical classification is another respected prediction tool, a supervised machine learning technique which labels data frames with predictions from predetermined categories. Initially the classification algorithm is trained with labelled data; once trained the model can be applied to like datasets for predictions of the category of each observation.

A k-nearest neighbours (KNN) classifier is a simple and effective classifier used widely in the literature, initially arising from an armed forces technical report [133]. To provide predictions for given data the KNN classifier uses a similarity measure. First it is trained with a training dataset to identify the correlations between distances of data points and the labels of each. Once presented with an unlabelled set of data, the classifier finds the closest known label to fit each observation.

Several different measures of distance may be employed; commonly used, and implemented within this study, is the Euclidean distance. This distance can be

calculated for an n-dimensional dataset through,

$$d(x, y) = \sqrt{\sum_{i=1}^{n}(x_i - y_i)^2},$$

where $d(x, y)$ presents the distance measure between datasets x and y, x_i a component of one dataset in the i^{th} dimension and y_i a component of the other dataset in the i^{th} dimension.

One use of KNN, seen in the literature, is to create clusters of object point clouds in a working environment for obstacle avoidance in a robotic arm [134]. In 2008 Heumer et al. [135] utilised classification algorithms to determine the grasps performed whilst participants wore a data glove - an early example of the use of automatic classification for grasp analysis. The study showed positive results with the application of the taxonomy presented by Schlesinger [5]. It was also highlighted that the use of PCA gave a negligible impact on the resulting accuracy.

A confusion matrix can also be created after an application of a classifier, to visualise the accuracy between predicted and known labels in validation or testing datasets. Another measure for performance of a classification algorithm is the receiver operating characteristic (ROC) and area under the curve (AUC) [136].

The ROC is a graphical plot of the true positive rate against the false positive rate. This is used to describe the performance of a binary classifier with two classes, positive and negative. The true positive rate, also known as the sensitivity, is the proportion of positive class observations correctly classified and false positive rate, also known to be one minus the specificity, is the proportion of negative class observations incorrectly classified. These rates can be expressed as,

$$\text{TPR} = \frac{\text{TP}}{\text{TP} + \text{FN}},$$

and,

$$\text{FPR} = \frac{\text{FP}}{\text{FP} + \text{TN}} = 1 - \text{TNR},$$

where TP is the number of positive class observations correctly classified, FN is the number of positive class observations incorrectly classified, FP is the number of negative class observations incorrectly classified, TN is the number of negative class observations correctly classified and TNR is the true negative rate, describing the specificity of the model. For a non-binary classifier these rates can be simulated by aggregating the correct and incorrect prediction for each class, enabling a relative indication of classifier performance. In a binary classifier case the ROC is created by first determining the sensitivity and specificity for a classifier threshold which

classifier all observations as positive. As all positive observations would be classified correctly and all negative observations would be classified incorrectly, this gives both a true positive and false positive rate of one - indicating one end of the curve. Next the threshold is adjusted such that one observation is classified as negative, the sensitivity and specificity are calculated accordingly. This is continued until the threshold classifies all of the observations as negative. This final sensitivity and specificity, both of value zero, defines the other end of the curve.

The AUC is the area under the ROC curve, providing a comparable measure between the performance of different classifiers. The AUC can be calculated from the ROC using Simpson's Rule [137].

$$\int_a^b f(x)\mathrm{d}x \approx \frac{b-a}{6}[f(a) + 4f((a+b)/2) + f(b)],$$

where $f(x)$ is the function of the curve for predicting area under and a and b are the two points the area is to be predicted between, for the case of an ROC curve these values are zero and one respectively.

2.6.3 Decision Tree Learning

Another method for classification is the creation of a decision tree. These methods are a series of questions, aiming to propagate towards a predicted category for a given input. This method was first seen formally introduced by Belson, in 1959 [138]. Despite being a simple to create and understand method this can still provide accurate classifications to many problems.

Creation of a decision tree starts at the root node, working through the internal nodes of each branch until the creation of a leaf node. Nodes are selected one after another in the tree using an impurity measure, a common measure employed for node selection is the Gini impurity [139]. The Gini impurity, I_G, of a decision, d, can be expressed by,

$$I_G(d) = 1 - \sum_{g=1}^{J} {p_{d,g}}^2,$$

where J is total number of possible categorises the observation can be labelled under and $p_{d,g}$ is probability of an observation being categorised in decision d with, known, group g, expressed as,

$$p_{d,g} = \frac{N_{d,g}}{N_d},$$

where $N_{d,g}$ is the number of observations categorised by decision d with, known, group label g and N_d is the number of observations classified into decision d. For each node, n, the Gini impurity, I_G, is calculated using the weighted averaged of the

Gini impurities of the decision from that node, expressed as,

$$I_G(n) = \sum_{d=1}^{D_n} \frac{N_d}{N_n} I_G(d),$$

where D_n is the total number of decisions arsing from node n and N_n is the total number of observations classified with node n. Working down the tree from the root node determines each internal node, in turn, using the impurity measure; a leaf node is selected if the current node decision has a lower impurity than the impurity of another potential node applied after it. The tree creation finishes once all leaf nodes have been formed.

A confusion matrix can also be made for a classifier to visualise accuracy between predicted and known labels in a validation or testing set of data.

Decision tree classifiers are still used for a variation of classification tasks within the literature [140–144]. Zhang et al. [141] used a decision tree classifier to design a framework for gesture recognition using accelerometers and EMG sensors. In 2021, Pappalardo et al. [142] utilised a decision tree to identify causes of faults and variable importance in a lane support system. After identifying drivers reliance on lane identification systems as a cause of single vehicle and frontal crashes, this study observed the ability to identify lane lines in the road of the system under different conditions with varying parameters. Following collection, a decision tree was used to provide assessment to the performance of each setting in the set scenarios. In a study to identify cyberbullying texts, Yuvaraj et al. [143] proposed a novel deep decision tree classifier. This classifier showed a greater classification accuracy than existing classifiers and future work, extending on this, aims to employ this approach with real-life high-dimensional data. Utilising a ensemble decision tree classifier, by Fraiwan and Hassanin [144], was able to identify degenerative neuromuscular diseases from gait motion data. The proposed solution was able to achieve a classification accuracy of 99% for amyotrophic lateral sclerosis, Parkinson's disease and Huntington's disease.

2.6.4 Clustering Algorithms

Another machine learning technique often employed for the analysis of numerical data is the application of clustering algorithms. These are an unsupervised learning technique used to find clusters within the data without prior knowledge. There are four commonly used types: centroid-based, density-based, distribution-based and hierarchical.

To obtain clusters of hand motions in this study, indicative of the hand shapes performed, a k-means algorithm has been utilised. The k-means algorithm [145–147]

is a method of vector quantisation, comparing each data point to the centroids (means) of current clusters - updating the clusters with each iteration. For this reason, the k-means algorithm is labelled a centroid-based clustering algorithm. The assigned value of k in this algorithm is simply the number of clusters the algorithm creates.

In order to differentiate each of the observations into each of the k clusters the k-means looks to minimise the distance between each data point and the repetitively set cluster centre. This is achieved through optimisation of an object function, J, which provides a cost of each candidate solution,

$$J = \sum_{n=1}^{N} \sum_{k=1}^{K} r_{n,k} ||x_n - \mu_k||^2. \tag{2.6}$$

where N is the total number of dimensions to the data points, K is the total number of clusters desired, $r_{n,k}$ is a binary inductors of which cluster k data point n belongs to (where $r_{n,k} \in [0, 1]$), x_n is the dimensional co-ordinates for each data point n in a d-dimensional space ($x_n \in \mathbb{R}^d$) and μ_k is the centroid for cluster k, also belonging to the same d-dimensional space ($\mu_k \in \mathbb{R}^d$). The binary cluster indicator, $r_{n,k}$ can be expressed by,

$$r_{n,k} = \begin{cases} 1, & \text{if } k = \text{argmin}_j ||x_n - \mu_j||^2, \\ 0, & \text{otherwise.} \end{cases} \tag{2.7}$$

To determine the minimum value of the objective function, J, the derivative is taken and set to zero, as follows,

$$\nabla_{\mu_k} J = 0 = 2 \sum_{n=1}^{N} r_{n,k}(x_n - \mu_k).$$

To optimise the problem numerically this equation can be solved for μ_k to give,

$$\mu_k = \frac{\sum_{n=1}^{N} r_{n,k} x_n}{\sum_{n=1}^{N} r_{n,k}}. \tag{2.8}$$

Using the update rules for the binary cluster indicator and cluster centroids, provided by (2.7) and (2.8), receptively, the following steps are employed by the k-means algorithm in order to converge towards a solution:

1. Initialise a set of μ_k.
2. Calculate $r_{n,k}$ using (2.7), with fixed μ_k.
3. Calculate μ_k using (2.8), with fixed $r_{n,k}$.
4. Determine the new objective function, J, using (2.6).

5. Repeat steps 2 to 4 until convergence of the objective function.

This can be seen as a special case of the expectation-maximisation algorithm [148] - where the final two steps, alternated between to converge towards a final solution, can be seen as the the E step and M step. Several studies employ a k-means algorithm as a method to identify postures, described by the clusters, within whole body motions [149–152].

Thong et al. [153] discuss the use of a machine learning clustering algorithm (k-means++) for the analysis of the morphology of adolescent idiopathic scoliosis. The study aimed to find new, clinically relevant, classification groups through the use of machine learning techniques on 3D Cartesian co-ordinate data for 915 recordings of spines. From these recordings, 11 subgroups, with clinically relevant significant statistical differences, were found. This method has shown potential for simplifying complex 3D spine models. Despite the success of this study, one limitation stated was that higher quantities of data would be necessary for future development. This study has highlighted that clustering is possible for biomechanical problems and is primarily hindered by the limited amount of data that can be collected. In the study performed by Huang et al. [73] an unsupervised clustering technique was used in order to autonomously determine the grasps performed in first-person point-of-view video recordings. The study showed this method to be very effective; it was stated that the development of this should have a significant impact, across multiple disciplines, in prehensile analysis. To validate the method both choreographed and real life scenarios were used. The clusters determined by this method were compared to the taxonomy introduced by Cutkosky [7] and it was seen that it had created new groups as well as fitting the groups in this taxonomy. The results of this study have shown that it is feasible to successfully perform machine learning on typically collected hand motion data, providing meaningful results through an unsupervised clustering technique. Thus, the potential of this method for hand-object interaction and prehensile analysis has been presented.

The Calinski-Harabasz (CH) index [154] can be used to evaluate the performance of a clustering implementation, in aid of selecting the number of clusters within the data. This measure is determined by the ratio of inter- and intra-cluster dispersion. Given an inter-cluster dispersion of B_k, from (2.9), and intra-cluster dispersion of W_k, from (2.10), the CH index, CHi, can be calculated for a given number of clusters, k, using (2.11),

$$B_k = \sum_{g=1}^{k} n_g(\boldsymbol{c_g} - \boldsymbol{c})(\boldsymbol{c_g} - \boldsymbol{c})^T, \tag{2.9}$$

$$W_k = \sum_{g=1}^{k} \sum_{\boldsymbol{x} \in C_g} (\boldsymbol{x} - \boldsymbol{c_g})(\boldsymbol{x} - \boldsymbol{c_g})^T, \tag{2.10}$$

$$\text{CHi} = \frac{tr(B_k)}{k-1} \Big/ \frac{tr(W_k)}{n-k}, \tag{2.11}$$

where n_g is the number of points in cluster g, $\boldsymbol{c_g}$ is the centroid of cluster g, $\boldsymbol{c}$ is the centroid of the entire dataset and $\boldsymbol{C_g}$ represents a set of data points within cluster g. This index is quick to compute and provides a clear assessment of clustering performance - higher values indicating clusters which are internally dense and externally well separated.

Alternatively, the Davies-Bouldin (DB) index may be used to assess clustering performance [155]. The DB index provides a measure of averaged similarity between each cluster and that most similar to it. The lowest values of the DB index is zero, with a lower value representing a greater clustering performance. This index, $\overline{D}$, can be calculated through,

$$\overline{D} = \frac{1}{N} \sum_{i=1}^{N} D_i,$$

where N is the total number of clusters observed, i iterates each of these clusters and D_i, for each cluster i, is the maximum similarity measured between that cluster and each of the clusters, provided by,

$$D_i \equiv \max(D_{i,j}),$$

where $D_{i,j}$ is the similarity between clusters i and j (where $i \neq j$), calculated from,

$$D_{i,j} = \frac{S_i + S_j}{M_{i,j}},$$

where S_i is the intra-cluster dispersion for cluster i, S_j is intra-cluster dispersion for cluster j and $M_{i,j}$ is Euclidean distance between the cluster centroids for clusters i and j. The centroid distance measure, $M_{i,j}$, can be calculated using,

$$M_{i,j} = ||A_i - A_j||_2 = \sqrt{\sum_{k=1}^{N} |a_{i,k} - a_{j,k}|^2},$$

where k iterates each of the components of the data and $a_{i,k}$ and $a_{j,k}$ are each the k^{th} element of clusters A_i and A_j, receptively. The inter- and intra-cluster distance measures, S_i and S_j, can be found with,

$$S_c = \sqrt{\frac{1}{T_c} \sum_{c=1}^{T_c} |X_{c,k} - A_c|^2},$$

where T_c gives the total number of observations within cluster c, X_k is k^{th} element

of cluster c and A_c provides the centroid of cluster c.

Another evaluation method which can be employed to determine the goodness of a fit is the silhouette score [156]. This provides a value between negative and positive one to describe how dispersed and clearly distinguished each cluster is from the others. A value of negative one implies that the clusters are assigned incorrectly and positive one shows that the clusters are distributed well and distinguished clearly. Zero describes indifferent cluster, showing no significant differences between the clusters. The value for the silhouette score can be calculated by,

$$score = \frac{b - a}{\max(a, b)},$$

where b is the average inter-cluster distance (the distance between the clusters) and a is the intra-cluster distance (the distance between each point in the respective clusters).

2.7 Models of the Human Hand

There is a significant amount of work performed to capture a digital model of the human body. Though observation of the human hand is less common, there are still exists several attempts to define the kinematics, observing the digit trajectory or joint constraints, [157–163] and kinetics of the human hand, observing the resultant motion from muscle activations, [9, 164–166]. Aristotle provided the first recorded insight into understanding the bodies of animals as mechanical systems, using geometric analysis to describe the actions of the muscles [167]. Early examples of dynamical body analysis utilised photography to capture the data [168]. More recent studies typically employ marker based motion capture systems [114, 169–173]. Models describing the kinetics of the hand can be categorised as either solving an inverse dynamics or forward dynamics problem. Inverse dynamics uses external forces and the joint motions to attempt to predict the internal forces and torques which enable the exhibited motion. The kinematic data inputs can be obtained with motion capture systems and the kinetic force inputs from force plates or handheld force measuring devices. Musculoskeletal models and prediction methods are used to provide estimates of the states of the muscles. The opposite, forward dynamic modelling, uses measured muscle activities to calculate the muscle forces and joint torques, in order to formulate the joint motion that would result. In biomechanics EMGs are used to capture muscle activations and, in turn, provide the muscle forces and joint torques. Musculoskeletal models and EMG mapping scripts are used to enable forward dynamics. There are many applications for these studies, including:

myoelectric prostheses, exoskeletons, sports analysis, rehabilitation and ergonomic design [172–177].

Inverse dynamic models of the upper-limb use kinematic data to create predictions of the forces and torques acting on the joints. There have been several attempts in the literature to utilise this technique [114, 178–182]. Of these, inverse dynamic models have been used to examine upper-limb stresses during sporting activities [174–176]. Furthermore, there have been several attempts to improve the measurement techniques used during data collection for inverse dynamic models [169–171, 183]. In 1995, Happee and van der Helm [178] presented an early inverse dynamics model, investigating fast goal directed arm movements. It was seen that the 95 element muscle model could provide adequate measures in comparison to EMG recordings overall, with only some results lacking in subject dependant EMG activities. In 2003, Rasmussen et al. introduced a musculoskeletal model of the human body, AnyBody [179]. This demonstrated a versatile musculoskeletal model, intended for use in ergonomic optimisation. Later, an LMC was integrated within this system to provide a means of capturing data for the inverse dynamics of the hand [114]. Subsequent work then proceeded to fully integrate the hand within the framework of AnyBody, using anatomical data from cadaveric specimens, to include all of the intrinsic and extrinsic muscles of the hand and provide patient-specific scaling [180]. Under assessment with motion capture data, the model was able to demonstrate adequate correlations. This allowed for the later application of this model in the simulation of distal radius metaphyseal fracture healing [181]. In 2005, Tsang et al. [182] introduced a musculo-tendon model of the hand and forearm for forward and inverse dynamic simulations. This model was able to yield various correct control solutions to an inverse problem, with it also demonstrating the ability to filter to an optimal solution. The concluding notes of this study stated the possible applications of the model within a clinical environment, identifying the muscles required for unconstrained motions, and in animation, allowing for improvements to synthesised hand animations. In order to allow for the unconstrained measurement hand kinematics, Buczek et al. [169] introduced a six DoF hand model for use during motion capture. Noting the limitations imposed from the use of joints with one or two DoF, the model was created for six DoF measurements of digits. Experiments concluded that the model worked well for motion capture applications, providing results with ample accuracy for inverse dynamics. Furthering the potential effectiveness of this model, it also showed an ability to identify when there had been exposure to repetitive stress in a hand. A study by Bisseling and Hof [170] examined artefacts from the impact on force sensors during inverse dynamic analysis of the knee. The study attempted to remove these artefacts causing inaccuracies in the assessment of body torques. Within this, variations to the cutoff frequency of

a low-pass filter on the recorded positional data were explored. It was concluded that filtering the force data on impact removed these artefacts. The results of this study led to recommendations to not consider any relationship found with the peak impact force and torque during clinical studies, as these were seen as artefacts in the recordings. Though this study had focused on ground force plates and knee motion, this method could hold the potential for adaptation to force sensors in hand contact analysis. In 2022, Sterner et al. [171] introduced the possibility of using inverse dynamics with body part masses calculated using dual energy X-ray absorptiometry to predict baseball pitching arm kinetics in youths. Following the collection of upper arm, forearm and hand masses using dual energy X-ray absorptiometry, segment masses and kinetics were calculated using scaled masses. The new masses were subsequently compared via paired t-tests and regression analysis. It was found that the dual energy X-ray absorptiometry masses differed from previously used scaled masses, with arguments made that there was higher patient specific accuracy from these measurements. These new masses resulting in correlations being drawn between shoulder and elbow kinetic parameters and body measurements, supporting suggestions put forward from previous studies [174–176].

Forward dynamic models of the upper-limb use measured internal parameters and kinetics to determine the current position of the hand and digits. Within the literature there have been numerous attempts to employ this methodology in musculoskeletal modelling, to provide a greater understanding and enable control of the upper-limb [9, 172, 173, 184–186]. Alongside these, there have been attempts to improve the means of data collection for the inputs to these models [187, 188]. Forward dynamic simulations have also been used to simulate scenarios which could be dangerous or unwanted for real world experiments [177]. A musculoskeletal model introduced by Wohlman and Murray, in 2012, [184] and later in improved by McFarland et al., in 2022, [185] provided a forward simulation of the hand. The initial intent of this model was to investigate the relationship between muscle forces and thumb-tip endpoint force. This was achieved through modifications to an existing model [186], adding definitions of the muscle-tendon paths and forces generation from five intrinsic muscles. This study showed the importance of accurately defining the axes of rotation for the thumb joint when simulating the endpoint forces produced by muscle activations and highlighted the difference made to the muscle control strategies and force transmissions when the wrist muscles were surgically altered. Furthering this work, McFarland et al. [172] simulated maximum grip and pinch force through the addition of a control framework combining forward dynamic simulations with a simulated annealing optimisation. It was shown, through experimental data, that the model could accurately provide the maximum grip force, yielding further advancement of this model. In 2017, Blana et al. demonstrated control of a prosthetic

hand through a forward dynamics hand model solely employing the extrinsic muscles of the hand [9]. The model was shown to be able to operate in real time, provide accurate grasp control and respond to alterations in gripping force [173]. In aid of data collection for forward dynamic models, Nasr et al. [187] tested different regression models for the mapping of sEMG signals. Four methods were tested: ANN, recurrent neural network (RNN), CNN and region-based convolutional neural network (R-CNN). It was found that the RNN model, taking inputs of filtered sEMG and delayed kinematic data, was the most accurate for mapping estimation. This method boasted a 96.4% regression accuracy for estimations of joint angle, velocity, acceleration, torque and activation torque. Additionally, R-CNN was able to provide accurate performance with delayed kinematics and raw EMG data, displaying an average regression accuracy of 95.9% utilising these prediction measures. Conclusions from this study argued the usefulness of this method for application in the forward dynamic simulation of musculoskeletal models. In 2021, Hao and Nichols [188] tested two existing contact models for determining finger contact mechanics, arguing that finger contact mechanics are lacking in forward dynamic simulations of hand-object iterations and are key to future developments in this area. Of particular note were the alterations to friction which occurred as the contact area was changed. Both models tested displayed an ability to perform well with the forces experienced during hand-object contact, with each showcasing advantages over the other in different scenarios. It was concluded that the inclusion of either is recommended in musculoskeletal models of the hand. Several studies have used experimental testing to examine arm reactions in response to forward falling in the elderly [189–192]. Through some of these studies, it has been shown that the angle of the elbow has a high influence on the ability to absorb impact energy and control the fall [189–191]. It was also seen that muscle atrophy resulted in a lessening of the ability to arrest a forward fall without sustaining damage [191]. A study by DeGoede et al. found that the impact force on the hand was reduced by more than 40% upon decreasing the initial elbow extension and velocity of the upper-limb, relative to the impact surface - proving a link between the initial angle of the elbow and ability of the muscles to react timely during a fall [189]. In 2003, DeGoede and Miller [177] introduced simulations to examine the effects of different elbow extensions during falls. A move towards the use of forward dynamic simulations in this area would reduce the necessity for real world experiments of the unwelcome task. These forward dynamic simulations of the upper-limb during falling were able to also draw the same conclusions as the experimental studies [189–192] - showing potential of this method to replace the necessity for real world experiments.

The kinematics of hand motion has been observed in several studies. In 1991, Rijpkema [157] created an early computer animation of the hand for animating grasps -

intended for grasp planning in robotic devices. A kinematic model of the middle finger demonstrated the natural actuation of the digit could be mathematically defined [158]. Though validated with experimental data from the functional excursions of the muscles, the foundations of the analytically formed mathematical model of the hand were simplifying assumptions. More recently, in 2014, Rahman et al. [159] adopted a trajectory planning method to describe the movements of individual digits of the hand. In this model the data are recorded with FlexiForce sensors and a mathematical model of finger trajectory created using the Curve Fitting Toolbox in MATLAB. This model uses the Denavit–Hartenberg method to perform the kinematic analysis of the motion of each digit. Also of interest to the study of the hand is how the motions of the joints correlate with each other. Identifying and understanding any potential interconnected motions would aid in the design and development of simulations and devices aiming to replicate the motions of the hand. Within the literature a consensus has been formed that there exists a correlation between the DIP and PIP joints [193–195]. Hahn et al. [193] used 3D ultrasound based motion capture system to record opening and closing hand motions of 17 able bodied participants. The results showed a close relationship between the DIP and PIP joint motions, observing that one degree of PIP joint flexion caused an average 0.76 degrees of DIP joint flexion. This correlated motion was seen equally prominent in dominant and non-dominant hands. These findings were later supported by the work of Holguín et al. [194], in a study assessing hand motion video recordings of 18 healthy volunteers. Furthering the understanding of the correlated motion observed, Holguín et al. also saw that the motion was lead by the PIP joint. Understanding this correlation brings the possibility for simpler, yet amply effective, designs of simulation models and hand prostheses.

Some studies aim to understand the constraints of the joints, which dictate the possible motion seen from a kinematic study of the hand. Cobos et al. [160] studied the constraints of the hand, following on to then create a model utilising these constraints in the following year [161]. The constraints were modelled with mathematical equations describing how certain digits are naturally pulled by the motion of other digits. The kinematic model treated each of the joints in the digits, bar the metacarpophalangeal of each of the fingers and carpometacarpal, as revolute joints, the metacarpophalangeal of each of the fingers and carpometacarpal of the thumb were treated as two revolute joints with their axes of rotation placed perpendicular to each other. This model of the hand is relevant when designing and developing a prosthetic hand as similar to a human hand as possible. A few years later, Chen et al. [162] also explored the constraints of the hand and created a mathematical model from these determined constraints. Chen et al. expanded on the constraints given by Cobos et al. [160], exploring the different constraints seen

when different grasps are performed, but, overall, both showed agreement regarding the constraints and kinematic models proposed.

Additionally, studies have attempted to capture the motions exhibited by the wrists. In 2016 Rainbow et al. [196] reviewed the existing literature surrounding the kinematics of the wrist. This study focused on the early rehabilitation of radiocarpal injuries; the study resulted in ideas for a dynamical treatment of carpal injuries which can be tailored for each individual patient, based on the research performed in wrist kinematics. Murgia et al. [163] used marker-based optical motion capture to collect everyday use of the wrist in cyclical tasks. The study finds that the wrist kinematics of healthy subjects, during ADL using cyclical tasks, was able to be described by simple rotations about the axes of a co-ordinate system defined by the markers. The possible use of EMG for determining the motion of the wrist is argued by Jiang et al. [164], arguing seen effectiveness based on the fact that myoelectric control from the wrist in unilateral transradial amputess would become more intuitive. Lemay and Crago [165] employ forward dynamic modelling to provide a simulation of the forearm and wrist motions, using a Hill-type model of muscles to replicate these motion of the upper-limb. Constraints were imposed on the motion of the joints in the form of passive torques, determined from experimental results. It was commented that the model was able to correctly determine the direction of the torque vectors at the wrist; however, it was seen that it predicted much greater torques than those measured when stimulating the paralysed muscles of one tetraplegic subject.

Though limited, there exists attempts to review the kinetics of the human hand. A musculoskeletal model introduced by Blana et al. [9] showed the capability of prosthetic hand control with only extrinsic muscles in real time. Later the model was reviewed and simulations of use in prosthetic control reported [173]. The findings showed that: model provided the accuracy required for grasp control, the simulation was proven to be of an adequate speed for use in real world (with the consideration of a loop involving the hardware and a user) and demonstrated an ability to respond to alterations in the gripping force whilst the user held an object. This model employed force dynamic principles to determine the joint angles of the hand from muscle excitations measured using sEMG sensors. In 2021, Smirnov et al. [197] used a light gradient boosting machine and fully connected ANN to applied machine learning in the approximation of moment arms and muscle length relationships for provided hand postures. This technique showed low application errors for both approximations and provided confidence in the potential from applications of machine learning with musculoskeletal models of the human hand.

The musculoskeletal model of the hand presented by Blana et al. [9] has been employed within a muscle excitation prediction method presented. For application

of the model and understanding of the musculoskeletal model was required. This model is a forward dynamics model, utilising known muscle activations to determine the joint angles of the hand. As presented by van den Bogert [198], a first-order Rosenbrock method [199] is used to advance the output of the model (included in which are the digit joint angles) one time step, provide a set of muscle excitations at that next time step.

The Rosenbrock methods are stiff differential equations employed to solve ordinary differential equations. Given a vector of the musculoskeletal model state variables (the joint angles, joint angular velocities, contractile element lengths and muscle activations), x, and a vector of the muscle excitations, u, at the next time step, the musculoskeletal model [9] and Rosenbrock method can be used to calculate the joint angles for the given muscle excitations, at time step h seconds advanced from the occurrence of the current joint angle,

$$\Delta x = \left(\frac{\delta f}{\delta x} + \frac{1}{h} \cdot \frac{\delta f}{\delta \dot{x}}\right)^{-1} \left(\frac{\delta f}{\delta \dot{x}} \cdot \dot{x}_n - f(\dot{x}_n, \dot{x}_n, \dot{u}_n) - \frac{\delta f}{\delta u} \cdot (u_{n+1} - u_n)\right), \tag{2.12}$$

$$\begin{aligned} x_{n+1} &= x_n + \Delta x, \\ \dot{x}_{n+1} &= \frac{\Delta x}{h}, \end{aligned} \tag{2.13}$$

where n is the current iteration number, $f(x_n, \dot{x}_n, u_n)$ is the dynamics imbalance of the system (provided as an output from the musculoskeletal model) and $\frac{\delta f}{\delta x}$, $\frac{\delta f}{(\delta \dot{x}}$ and $\frac{\delta f}{\delta u}$ are the Jacobians of the system (also provided as an output from the musculoskeletal model). Given an initial state, x_n, derivative, $\dot{x}_n$ and muscle excitations at that time step, u_n, the model can simulate future states, h seconds away, provided the knowledge of muscle excitations at that, next, time step (u_{n+1}).

Blana et al. utilised this model to provide control of a prosthetic hand [173]. The hand begun in an equilibrium position, providing the initial x_n and u_n. The sEMG signals were recorded during the movements performed by the hand. These sEMG recordings were then normalised and mapped onto the muscle activations; this information was used to determine the each of the muscle excitations during hand motion, utilised as u_{n+1}. Inputting this obtained knowledge into (3.1) would determine x_{n+1}, from which the first 16 elements can be extracted to provide the joint angles of the hand. These joint angles were then sent to the prosthetic hand, resulting in an animation of the prosthetic hand equal to that of the observed hand. This is then repeated through several user hand movements, updating x_n, $\dot{x}_n$ and u_n every h seconds and recalculating x_{n+1} given each u_{n+1}.

2.8 Determining Muscle Excitations

Knowledge of the muscle excitations performed aids the development of upper-limb prostheses and exoskeletons; further to this, recordings of muscle excitations can be utilised to provide previously unknown information during surgeries, enable alternative options for motion capture and aid in patient assessment. A clear option for obtaining the muscle excitations performed is through direct measurements, employing EMG sensors, [29, 141, 173, 200, 201].

Intramuscular EMG readings allow for a direct measurement of the muscle activations. However, employment of this technique requires the use of invasive sensors and readings are depend on the placement of these sensors. The use of sEMG devices enables the capture of these muscle activation without need for an invasive strategy. This technique also suffers from dependencies on sensor placement and is prone to contamination from crosstalk between muscles, arising from the difficulty to isolate a single muscle observed from the skin surface.

Though limited supporting literature exists, it is feasible to make predictions of the muscle excitations from kinematic data alone [202, 203]. It is clear that a prediction method would not be able to provide the level of accuracy offered by experimental measurements; however, small increases to the accuracy of these methods would occur as musculoskeletal models of the hand and prediction techniques improve in fidelity. Vast amount of kinematic records of hand motions exist; the application of predictive models could potentially provide an indication of the muscle excitations occurring within these existing data, without the need for additional data collection. Given that hand can only take on a finite number of hand shapes, adding to a database of known muscle excitations for certain hand shapes would make future queries quicker and easier - accuracy to the desired hand shape can be provided when no existing hand shape exactly matches.

Measurements of muscle activity are acquired through invasive or sEMG recordings. Signal decomposition of these recording is then required to assign muscle activations to the appropriate motor units (MUs). There are several strategies employed to achieve this, with new methods proposed often [204, 205]. In 2006, De Luca et al., introduced a means for the decomposition of sEMG signals [204]. This utilised AI to decompose the signal into the action potentials of the constituent MUs. When compared to a needle sensor, the sEMG with autonomous decomposition achieved an accuracy ranging between 75 and 91% - this was increased to over 97% with manual intervention. Despite this high accuracy, it was observed that the MU yield was lower than that of the needle sensors; this highlights an inconsistency with the real world and would need remedying before this method is seen to be acceptable. The future

work proposed was to improve accuracy further and, more importantly, attempt to provide an increase MU yield. This study has shown success but has only been tested with orbicularis oculi, platysma and tibialis anterior muscles; there is a potential for the theory to transfer to the hand, but this is difficult to conclude without further tests - especially as the muscles which were tested are larger than those seen around the hand, making for easier placement of the sEMGs. Upon comparing high-density sEMG recordings to an invasive technique, Holobar et al. found the use of sEMGs to be a valid method for the assessment of MU behaviour during low-force contractions [205]. In this study the tibialis anterior, biceps brachii and abductor digiti minimi muscles were observed and invasive pairs of wire electrodes were used to capture the bipolar intramuscular EMG signals. The decomposition of the sEMG provided strong similarities to a state-of-the-art intramuscular EMG technique, showing further feasibility of the use of sEMG. The tibialis anterior and biceps brachii results showed adequate R-squared values, but those from the abductor digiti minimi were not able to produce similar confidence - thus this approach would need improvement and further testing before it can be confidently employed with sEMG recordings from the hand.

Aiming to aid minimally invasive spinal surgery, in 2010 Uribe et al. [206] reviewed the the possible uses of EMG for intraoperative neurophysiological monitoring. It was seen that the applications of EMG during transpsoas lateral surgical approaches reduced complication rates from 30% to less than 1%. This research concludes by arguing for the significance of EMG during minimally invasive surgical procedures, stating the additional safety provided and highlighting the importance of the safe passage granted during the minimally invasive lateral retroperitoneal approach. In 2021, Sugiarto et al. [207] proposed a means for the reduction of end-to-end latency in VR systems utilising EMG readings, inertial measurement unit (IMU) measurements and a predictive model trained through deep learning. This intervention could alleviate issues arising from the use of VR applications, most notably: motion sickness. To achieve this, pre-processed EMG and IMU readings were inputted into a trained prediction model to provide an accurate prediction of the head orientation at that time. The proposed method was found suitable for use in VR applications which exhibited high-intensity or abrupt movements on the users.

In 2009, Castellini and van der Smagt [29] noted the lacking capabilities of hand prostheses control and proposed a novel means of achieving this. Here, ANNs, support vector machines and regression algorithms were employed to provide control of a prosthetic hand using sEMG measurements. The methods used classifications of hand shapes to provide predictions of the digit joint angles and forces in a presented scenario. The proposed solution was able to provide control of a prosthetic hand to a greater degree of accuracy than the state-of-the-art, at the time, was able to provide.

Within this study only a single subject was tested, resulting in no ability to evaluate inter-subject reliability for this method. This subject was able-bodied and the study mentioned that it would be difficult to train the model on amputees, as it requires synced hand responses to the muscle activations to train the model. It was suggested that in these scenarios the desired motions could be performed with the other hand. However, this would not be the same as the tested method, leading to uncertainty in the application of this, and provides no tactile feedback from the contact, resulting in a potential for less than realistic outcomes. Though these limitations exist, the study was able to show success with the tested subject. If a way of training this control technique with amputees was found, it could be utilised but would require retraining for each individual. Though limited, this does show a possibility of this method in aiding upper-limb prosthesis control. Zhang et al. [141] utilised accelerometers and EMG sensors to provide a framework for hand gesture recognition, aiming the implementation at classification of Chinese sign language. To achieve this a decision tree and multi-stream hidden Markov model was used to classify the accelerometer and EMG readings. This work achieved a gesture recognition accuracy of 98%, finally concluding with the possible applications of this method in multiple areas of gesture study. In this study only one hand was observed, though the Chinese sign language can employ both hands. The future work highlighted understands this flaw, as well as the lack of consideration for gaze, facial expression and body posture. There was also a desire to collect more data, for a more robust gesture recognition method. In 2021, Khomami presented an algorithm for Persian sign language recognition utilising IMU and sEMG measurements [200]. Through the employment of a KNN classifier, the proposed method was able to achieve an average accuracy of 96%. However, the small dataset of 20 signs performed by inexperienced volunteers limits the conclusions of this study. These volunteers had only been taught the signs at the time of the study and provided a mixed range of habits and speeds, which influenced the accuracy of the algorithm and limited the quantity and quality of the available training data. Further testing of hand signs would be required before adoption of this method is considered, with the hope that they are performed by experienced subjects to ensure quality in the collected data. These, among other works on sign language recognition, help form a database of recorded practical hand shapes and highlight potential means of collecting gesture data [141, 200, 208, 209]. A review of ANN and linear discriminant analysis for the classification of hand motion from EMG signals [201] found both to be a feasible means of classification of EMG signals. This work aimed to aid myoelectric prostheses, providing a means to determine the desired hand shapes from EMG measurements. During collection, surface and intramuscular EMG data were recorded. The implemented ANN was proposed as the technique for classification as it was able to achieve an averaged accuracy of 95%,

across two datasets. The future work stated the desire to test more classification techniques and investigate the ability of pattern recognition methods in aiding the end accuracy. Through the presented current understanding and possible future developments, this ability to classify EMG signals shows the potential for improving upper-limb prostheses control.

The ability to predict muscle estimations would enable the utilisation of non-invasive measurement strategies, and existing kinematic data collections, to approximate muscle excitation data. The literature is sparse but there exists some attempts to achieve this. Attempts to predict muscle excitations from kinematic data in the literature are limited and typically associate with the lower-limb [202, 203]. Zaman et al. [202] aimed to provide analysis of muscle forces during heavy lifting given, exclusively, kinematic data. This was achieved through the combination of a predictive skeletal model and OpenSim modelling. The skeletal model predicts the motion, ground reaction force and centre of pressure during the motion, which are inputted into OpenSim to simulate the motion and analyse the muscle forces. The study outlined a predictive model for the analysis of lower-limb muscle forces. Though using a 3D musculoskeletal model, only the sagittal plane data were given in the predictive model; because of this, the results do not capture internal rotations, abduction or adduction. Furthermore this study lacks experimental support for the results obtained. Additionally disadvantaging, this study provided full body motion muscle predictions without the arms and hands. In spite of these limitations, this study has shown the feasibility of the application of predictive musculoskeletal modelling. Manzano and Serrancolí [203] looked at replicating EMG recordings from kinematic data alone. The correlation coefficients between the predicted and experimental EMG signals were higher than 0.7 for ten out of the 11 muscles tested, leading to the conclusion that the utilised method provides confident predictions of EMG signals. The findings support the use of this technique for real time, accurate, prediction of lower-limb EMG readings. One limitation of this, however, is that only 11 muscles of one leg were tested with one task (running). As synergies between kinematics and EMG signals have been seen to be task specific [210, 211], only testing one task limits the robustness of this method. Due to this, future work was stated as to focus on the collection of varying tasks, in order to learn the synergies of each. Though limited to the tested cases, a framework for EMG data predictions was provided within this study - showcasing feasibility for the creation of these predictions. No literature attempting to predict the muscle activations of the hand from single frames of kinematic data, exclusively, were found.

2.9 Optimisation Techniques

It was decided that a muscle excitation prediction technique developed should be focused on application with the data collected and, therefore, would be a use of an existing model with an optimisation technique to find the muscle activations, from ADL, using the collected, kinematic, data. As seen previously, little work exists in this area, with no present work for the hand. Different optimisation techniques were attempted and each are described subsequently.

2.9.1 Genetic Algorithm

The genetic algorithm (GA) method was first shown implemented by Holland in 1975 [212]. This technique was designed to solve problems by a means similar to the development of living organisms, mimicking the mechanics of evolution and natural selection. The intentions of this techniques was to solve problems where deterministic algorithms were too costly.

A GA implementation is initialised with a predetermined or randomised set (population) of initial candidate solutions (chromosomes) comprised of variable elements (genes). Each chromosome of the population is then evaluated to determine their cost. A loop is then begun, first selecting the parent members. For parent selection here a roulette wheel selection method was used. To perform a roulette wheel selection the summation of the costs of all the chromosomes is calculated and the percentage of this total which each chromosome occupies is calculated. These chromosomes are sorted in ascending order and the cumulative sum of the cost percentage for each is calculated. A uniformly distributed random number ($U(0,1)$) is then created and compared to the cumulative sum for each chromosome, the first of these above the random number generated is identified as a parent.

Following the selection of the parents ($parent_1$ and $parent_2$), children ($child_1$ and $child_2$) are created using a crossover function,

$$child_1(i) = \alpha(i)parent_1(i) + (1 - \alpha(i))parent_2(i),$$

$$child_2(i) = (1 - \alpha(i))parent_1(i) + \alpha(i)parent_2(i),$$

where $\alpha(i) \sim N(0, \sigma_c^2)$ and the index variable, i, indicates the gene of the chromosome considered. Parent selection can alter exploitation, giving influence to candidate solutions closer to the optimal value. Exploitation influences the ability of the technique to quickly converge on a known minimum, a high exploitation offers fast convergence to a prediction with lower cost but with a higher risk of the output

being a local minimum.

Gene mutation applies a random mutation to a random selection of the children. In this application,

$$flag(i) = \begin{cases} true, & \text{if } U(0,1) < \mu, \\ false, & \text{otherwise,} \end{cases}$$

$$child(flag) = child(flag) + m(flag),$$

were used to mutate the children; where μ is the preset mutation rate, m is a set of normally distributed values with a mean of zero and variance of σ_m^2 ($m \sim N(0, \sigma_m^2)$) and the index variable, i, cycles through the genes of each chromosome. Gene mutation can alter exploration, allowing random mutations to the population in order to maintain a large search region. Exploration describes the ability of the technique to find new possible minima, a high exploration results in a lower risk of convergence towards a local minimum. A balance between exploration and exploitation is key to a fast convergence to the optimal solution.

Following mutation the members are tested against the set lower and upper bounds, limited within these if they are found outside of them. The new population is then evaluated, calculating the cost of each chromosome. The population is sorted in descending order of cost and any members past the set population size are removed from the end, until the desired population size is reached. The best solution found is compared to a preset threshold after each iteration, if it found above this value then the loop continues from parent selection with the new population.

The use of GA has spread wide in the literature, displaying high levels of support for use [213–218]. In 2003, van Soest and Casius [213] showcased the abilities of GA with biomechanical engineering problems, concluding the advantage of GA in solving high-dimensional, non-smooth or discontinuous datasets. Nair et al. [214] combined a GA and non-linear finite element analysis to estimate the material parameters of intact ventricular myocardium, arguing the challenges faced with this in the fast due to the highly non-linear material behaviour. The effectiveness of this technique was demonstrated by determining the unknown material parameters of a 3D model of the heart with an exponential hyperelastic material law; the algorithm was able to converge to parameters within 5% of the true values. In a two-dimensional (2D) model, the optimised material parameters were found within 0.5% of the true values. The method was concluded to be a robust method for estimating myocardial material parameters in 2D and 3D modelling.

In 2021, Wang et al. [215] looked into the use of a GA to generate assistive torque for an ankle exoskeleton. The GA optimised torques were found superior in control and ability to adapted to muscle efficiency, when compared to a proportional assistive

torque method. You et al. [216] employed a GA to aid tendon-transfer. Noticing the aid given by a passive implanted device during ECRL-to-FDP tendon-transfer surgery, this study aimed to determine the optimal geometry and location for this device. It was seen that the optimised device provided an 11 times increase in finger kinematics, displaying only a 0.9% decrease in joint toque, when compared to biomechanical function enabled by the current suture-based surgery.

Recent studies have employed GAs for increasing the influence of individuals in social networks [217] and as aid to medical administration systems for scheduling medical treatment [218].

2.9.2 Particle Swarm Optimisation

Particle swarm optimisation (PSO) was first introduced in 1995 by Kennedy and Eberhart [219]. The PSO method was introduced as an optimisation technique for non-linear functions. The method utilises observations made of the movement of flocks of birds and schools of fish seen in social models. This method was described similarly to that of birds finding food, with no previous knowledge of the location of the food the birds work socially to determine the location. The communication and learning seen between members of a population formed the basis of the communication and learning technique employed between particles in the swarm during PSO, though individually unintelligent it is the communication which allows intelligent learning from the swarm.

Following changes, an improved version was presented by Poli et al. [220]. This paper reviewed the uses of PSO and observed growth in research, highlighting any alterations to be made highlighted by researchers. Most notable alteration was the addition of an inertial weight proposed by Shi and Eberhart in 1998 [221]. The update to the velocity of a particle were presented in terms of the previous velocity, personal best and global best. In consideration of these forces, the change in velocity, acceleration, can be written as,

$$\Delta\vec{v_i} = \vec{f_i} - (1-\omega)\vec{v_i},$$

where $\vec{v_i}$ denotes the velocity vector of particle i, $\vec{f_i}$ the force acting on it as combination of the personal and global best terms and ω the inertial weight given. This constant $1-\omega$ acts as if it is a friction coefficient and enables adjustments to the movement of particles by varying ω. The improved model was considered for implementation within this research.

A PSO implementation is initialised with a predetermined or randomise set initial candidate solutions. Each particle is tested in the function to be minimised, the

outputted result from inputting each particle provides a cost of that particle. After each iteration the results are compared to the stored personal best of each particle and the global best and updated if a new best solution is found.

Given the current position, velocity vector, personal best and global best of each particle their is then calculated using,

$$\vec{x_i}(t+1) = \vec{x_i}(t) + \vec{v_i}(t+1),$$

where $\vec{x_i}$ is the position of particle i, t denotes the current time step, $\vec{v_i}$ provides the velocity of particle i.

The velocity vector, for particle i, is calculated using,

$$\vec{v_i}(t+1) = \omega\vec{v_i}(t) + r_1c_1(\vec{p_i}(t) - \vec{x_i}(t)) + r_2c_2(\vec{g}(t) - \vec{x_i}(t)),$$

where ω the preset inertial weight used to give influence to the velocity component, r are random uniformly distributed values between zero and one ($r\ U(0,1)$), c are adjustable acceleration coefficients used to weight the effect of the personal and global best, $\vec{p}$ represents the personal best position found and $\vec{g}$ represents the global best position found. The velocity equation consists of terms referred to as: the inertia $\omega\vec{v_i}(t)$, the cognitive component $r_1c_1(\vec{p_i}(t) - \vec{x_i}(t))$ and the social component $r_2c_2(\vec{g}(t) - \vec{x_i}(t))$. It can be seen that the inertia term provides influence on the next position from the velocity of the particle, the cognitive term gives influences from the knowledge of the best solution from the particle alone and the social component that knowledge from the swarm as a collective.

Weighting can be given to the personal and global best scores to alter exploration and exploitation. Exploration describes the ability of the swarm to find new possible minima, a high exploration results in a lower risk of convergence towards a local minima. Exploitation influences the ability of the swarm to quickly converge on a known minima, a high exploitation offers fast convergence to a prediction with lower cost but with a higher risk of the output being a local minima. A balance between exploration and exploitation is key to a faster convergence to an optimal solution.

Many biomechanical studies have employed the PSO technique [222–227]. Schutte et al. [222] tested the use of optimisation algorithms in solving biomechanical based problems, arguing the difficulty of these problems due to the likely high noise, multiple local minima and possible design variable scaling that could occur. It was seen that PSO performed comparatively well in the test situation. It was also shown theoretically that PSO was insensitive to design viable scaling and proven practically - as a result PSO was argued to be more suited to biomechanical optimisation problems. A review of PSO by Saini et al. [223] found the technique to

be able to work well in a high-dimensional search space when used as human motion tracking from video sequences, a very challenging task. This work was later updated with an implementation of hierarchical multi-swarm cooperative PSO for human motion tracking [224]. Though fought with several limitation, Saini et al. argue the capabilities of this technique and possible uses in low-cost robust tracking from stroke rehabilitation in clinics.

Kwolek et al. [225] presented a method employing PSO for markerless human body tracking to provide robust and accurate results, using a Vicon system as a ground truth. Chang et al. [226] implemented PSO as part of a technique to determine key frames in human motion capture data, providing experimental results supporting the use of this method in the presented context. Rokbani [227] showed how PSO could reasonably generate the gait of a bipedal robot, showing the techniques capability to handle 3D data efficiently.

2.9.3 Gradient Descent

The GD method was first introduced by Cauchy in 1847 [228]. It was first introduced as a method for solving systems of simultaneous equations, suggested as a means of determining the movement of a star with great precision. The concept of this method is to take large steps towards an optimal solution when far away from it and then increasingly smaller steps as the method converges towards the solution.

An implementation of the GD method begins with random or pre-decided initial conditions. This method utilises the derivatives of the loss function; typically considered as the sum of the squared residuals (the difference between observed and predicted joint angles). These derivatives are used in aid of determining the lowest possible sum of squared residuals. If multiple variables exist within the problem then derivatives are taken with respect to each. If there are two or more variables to the equation considered and, therefore, derivatives of that function, these derivatives are labelled as the gradient. The gradient is used to descend to the lowest point in the loss function (commonly found by the sum of squared residuals) - providing the name gradient descent. The derivative of the sum of squared residuals is then multiplied by a learning rate to determine size of step taken; when considering multiple variables, this step is performed simultaneously for each.

In a case where the equation for the problem is not known, numerical differentiation can be applied to provide an estimate of the gradient at each iteration [229, 230]. The, commonly applied, central difference numerical method can be defined with,

$$\frac{\mathrm{d}f(x)}{\mathrm{d}x} \approx \frac{f(x+h) - f(x-h)}{2h}, \tag{2.14}$$

where $f(x)$ is the function to be differentiated with respects to variable x and h is the step size between the two observed inputs into the function (where $h \ll 1$). The stopping criteria for this method can be either a preset threshold value of the step size or a maximum number of iterations.

The following set of procedures are performed by gradient descent when implemented:

1. Determine the gradient of the loss function considered.
2. Assign initial parameters.
3. Find gradient of those parameters.
4. Calculate the step size by multiplying the learning rate by the calculated gradient, for each parameter.
5. Calculate new parameters by subtracting the step size from the current candidate solution.
6. Repeat steps 3 to 5 until the minimum step size or maximum number of steps have been reached.

The use of the GD method is prominent in the literature, showing support in biomechanics [231–233] as well as other fields of study [234, 235]. Todorov and Li [231], in a study of biological movements, utilised the GD approach to optimise the control of a two-link arm model. Desapio et al. [232] employed the GD method for minimising muscle activations of a three DoF model of the human arm, aimed to aid robotic and biomechanical design. In 2021, Wu et al. [233] applied the GD method to enable a transfer of EMG data from one patient to another, enabling an increase to the learning speeds in the control of human-machine interface (HMI) devices.

2.9.4 Brute-Force Search

An alternative method considered was the implementation of a brute-force search across all possible solutions. A brute-force search is an exhaustive search technique which systematically enumerates all possible candidate solutions to a problem. This would be quick to design but would require an excessive amount of time to execute, as it tests the output of every possible input.

The length of time can vary dramatically depending on the number of elements in the solution vector and the resolution desired. Given n as the number of elements in the solution vector, in which each element can take one of two states, then the number of combinations required in a brute-force search would be 2^n. Changes to the number of possible states for each element of this vector alters this equation to s^n, where s denotes the total number of possible states for each element. If a higher resolution is required the increments between each candidate solution tested

must be reduced. Increasing the total number of states and rewriting the previous equation in terms of the incremented value between these states, i, gives the total number of combinations as $(1 + 1/i)^n$. It can be seen that as the number of elements increases and the incremented value is reduced this total number of combinations rises exponentially.

The following steps can be used to easily create all possible combinations of the candidate solution vector, enabling an exhaustive search of all possible attempts:

1. Initialise with a candidate solution vector in which all elements are set to the minimum value.
2. Increase one of the elements by the increment value, repeating this each iteration until the maximum of that element is reached.
3. This element is then reset and the next element raised by one increment.
4. The first element to be increased is then increased again each iteration until it has reached the maximum value, where it is reset again.
5. The next element is raised by one increment again and the first element reset.
6. These steps are repeated until all of the elements of the candidate solution have reached their maximum value, implying all possible combinations have been considered.

Though it is seen as an inefficient search mechanisms, brute-force search has still found use in recent studies [236, 237]. In 2018, Alagoz [236] demonstrated use of brute-force search for the stabilisation of closed loop control systems. In 2021, Susuki et al. [237] used a greedy algorithm and brute-force search to determine the optimal amplitude and phase of transducers in an array in order to produce a desired sound field - support was shown for the application of a brute-force search due to the linear computational time and ease of implementation.

2.10 Clinical Assessment of the Human Hand

The range of motion possible by the hand joints are an important tool for assessing patient progress during rehabilitation [238]. The currently employed technique (a goniometer), however, are lacking in accuracy and repeatability; in particular the finer motions of the hand are not observed accurately by this method and it has shown limited agreement between different observers [239, 240]. There have been many attempts to improve upon the current method within the literature with new methods [241–244] and devices [116, 245–248].

The traditionally used and long standing state-of-the-art device for digit joint angle measurements is a goniometer; though the use of this device is vast, there

exists little support for this device in the literature. Lewis et al. [239] tested the use of a goniometer in measuring the range of motion for the middle finger in 20 healthy participants, each measured by seven raters. This study looked to observed the inter- and intra-rater reliability when using goniometer for digit angle measurements. It was concluded that using the same clinician to measure a patient in different visits is clinically reliable, but changing the clinician would lead to significant contamination of the measurements between recordings. McVeigh et al. [240] compared measurements taken with a goniometer, visual assessment and radiographs of the hand. The goniometer measurements and visual assessments were completed by 40 observers were used (a collection of hand surgeons and hand therapists) and the radiographs were obtained by radiographers, as control data. This found that neither of the goniometer and visual assessments measurements could reproduce the angles obtained from the radiographs within five degrees. Additionally, it was seen that the goniometer and visual assessment provided similar accuracy for the measured joints, expect for the PIP joint, where the goniometer provided a better accuracy - both were also seen to have a high level of inter-observer variability.

Attempts at rectifying any inherent issues with goniometers are prevalent in literature, aiming to increase accuracy with alternative measuring methods or introduce a new device. In 2009, Carter et al. [241], studied three different measurement techniques for using a manual wrist goniometer in a cadaveric study. A hand surgeon and hand therapist took measurements and were compared to to digitally obtained angle measurements from fluoroscopic images. The three methods tested showed similar accuracy, within seven degrees of the fluoroscopic image angles. Blonna et al, in 2012, [242] showed that, when observing the angle of the elbow, an experienced observer was able to visually estimate this high accuracy, in comparison with a goniometer measurement. This also showed the visual estimates to provide an averaged intraclass correlation coefficient (ICC) of 0.95.

In 2018, Hancock [243] compared the accuracy of knee angle measurements obtained with five differing techniques; these techniques were: a digital inclinometer, a short goniometer, a long goniometer, smartphone application and visual estimation. It was seen that the short goniometer and visual estimation provided the least accuracy (with a minimum significant difference of 14 degrees) and the digital inclinometer was found to provide the greatest accuracy (with a minimum significant difference of six degrees). The digital inclinometer also provided the benefit of contactless measurements. In 2019, Shamsi et al. [244] compared an electro-goniometer and manual goniometer in measuring the knee angle. This study showed that an electro-goniometer offered a greater ICC, when compared to a manual goniometer. From the obtained results, it was concluded that a manual goniometer is still acceptable for clinical evaluations, as it is easy to be employed, though an electro-goniometer

should be employed if a greater accuracy and reliability is required.

Given the large increase in motion capture and visual assessment technology, it is not surprising that there is a lot of literature surrounding the introduction of new computer based hand joint angle measurement devices. In 2015, Krause et al. [245] introduced a mobile application for 2D analysis of the hip, knee and ankle motions, in the sagittal plane. When compared to a Vicon 3D motion capture system, the introduced technique was found to provide clinically viable measurements - showing a mean difference across all angles measured of 5.2 degrees. In 2016, Williams et al. [246] introduced a glove able to output the angular displacement of each joint. The accuracy of this device was found compatible to currently used goniometers and the glove was proposed for clinical use in hand digit angle measurements.

In 2018, Nizamis et al. [116] investigated the use of the LMC for hand joint angle measurements with 20 healthy participants, 12 of which where also used for test-retest analysis. There was disagreement between the measurements obtained by the two methods, though the LMC showed a superior test-retest reliability and time taken. It was suggested that some of the disagreement could be due to the fact that the goniometer measures the flexion of the dorsal side of the digits, whereas the LMC measures the angle between the centres of the joints - leading to a potential difference appear due to the thicknesses of the hands measured. In the setup tested for one hand, the goniometer took 32 to 65 minutes to measure the joint angles and the LMC took seven to 22 minutes - it was noted that the LMC would also be able to measure two hands at once and that the rater was inexperienced in both setups. This study provides evidence for the support of utilising the LMC for clinical hand joint angle measurements. Utilising a Vicon marker-based motion capture setup, Reissner et al. [247] compared a goniometer and 3D motion analysis for hand joint angle measurements. Motion capture was able to show a higher test-retest agreement - demonstrating superior repeatability of results. It was argue that a goniometer had to place for every joint to complete the remeasurements, taking a significantly longer time, and this interaction with the subject could lead to contamination of the measurements - supporting the use of a motion capture based joint angle measuring system.

In 2020, Zhao et al.[248] compared the use of smartphone photography and goniometers for digit joint angle measurements. The study found that smartphone photography was a valid and reliable method, holding comparable accuracy and precision to a goniometer even when present to inexperienced users. The implementation of this method would enable home assessment, as many people have a smartphone, and shows great promise for aiding clinical assessment, providing a potential reduction to clinical visits if simply implemented alongside current therapy

routines. The presented increase in computer based patient data measurements and analysis creates a demand for methods to store these data securely and perform quick and accurate analysis to further aid patient focused treatments. Nadian-Ghomesh et al. [238] introduced a hierarchical, AI-driven, internet of things (IoT) for storage and assessment of patient data securely and reliably. The introduced, novel, machine learning technique was able to identify range of motion as a indicator for analysing patient progress during rehabilitation and provided help to clinicians when creating personalised treatment plans for patients.

There is agreement across studies within the literature that the goniometer lacks the desirable accuracy and reliability for capturing measurements of the joint angles of the hand [239, 240]. Though the consensus tends towards acceptance of the goniometer for clinical assessment, it has been shown to provide measurements of equal accuracy to visual assessment in several studies [240, 242, 243]. There have been several attempts to rectify this lack of accuracy with new measurement techniques, many offering appealing potential improvements over the current employ manual goniometers [116, 245, 246, 248]. Furthermore, movement to an electronic platform from these introduced methods offers the use of quicker and more reliable patient assessment methods [238].

Chapter 3

Methodology

In light of the weaknesses seen in previous techniques discussed within Chapter 2, a novel method for data collection has been designed. Previous studies of hand motion suffer due to a limited range of activities studied or unnatural motions arising from encumbering devices, these issues have been remedied in the introduced design. The out of sight, portable, device described here records Cartesian motion data, this enables analyse through machine learning algorithms - allowing for a larger amount of data to be collected and analysed in the same time. Each of the novel methods introduced have been validated against the state-of-the-art in the respective areas. Control hand shape data, to support the analysis performed, has been collected. The methods employed to modify existing musculoskeletal model are also discussed here. A device has been conceived for faster, easier, safer and more accurate hand joint angle measurements within clinics, named AirGo. The techniques employed for the analysis of everyday activities motion data are also discussed here. Biomedical & Scientific Research Ethics Committee (BSREC) approval has been granted for a study involving 20-30 participants to be performed using the created portable motion capture system and for the collection of choreographed hand motions in a Vicon motion capture studio (reference: REGO-2018-2210). The clinical trial of AirGo was approved by the Research Ethics Committee, for a study of up to 20 patients (reference: 18/NE/0174). The supporting documents for these ethical approvals can be seen in Appendix A. The implementation and results of these discussed methods can be seen in Chapter 4; the final output of which are accordingly distributed among Chapters 5, 6 and 7.

3.1 Proposed Solutions

Following the discussions of the previous chapter, proposed solutions to the limitations of the current state-of-the-art are introduced here. The existing methods used to capture the activities of the hand during activities of daily living (ADL) are limited in the amount of data collect and range of activities observed. The solution proposed to circumvent these issues is the application of a portable markerless motion capture system, utilising a Leap Motion controller (LMC), and analysis methods performed employing machine learning techniques.

Current research shows no existence of extracting the muscle excitations of the hand from kinematic data exclusively. The proposed solution, to introduce predictions of hand muscle excitations from kinematic data, entails the combination of an existing musculoskeletal model and optimisation techniques.

The current clinical method employed to measure the hand digit joint angles is slow and unreliable, with an uncertainty to the accuracy of the results achieved. In light of these issues, the proposed method for hand digit joint angles measurements is a markerless motion capture based system, employing the LMC. This device is able to capture more reliable data significantly quicker, within a known degree of accuracy.

3.1.1 Portable Hand Motion Capture

The method most commonly employed to study the human hand in use, capturing a video recording of the hand in use and then watching the video, is a time consuming process with potentially high error due to the subjective nature. For this study the use of motion capture devices to collect three-dimensional (3D) kinematic data of the hand is considered over the use of video cameras - enabling the deployment of machine learning techniques for the analysis of the collected data.

The LMC is a markerless optical motion capture device which uses three infra-red (IR) cameras to determine a 22-point virtual image of the hand. The points of the hand captured by the LMC are as follows: the metacarpophalangeal (MCP) joint, interphalangeal (IP) joint and tip of the first digit, the MCP joints, proximal interphalangeal (PIP) joints, distal interphalangeal (DIP) joints and tips of the second to fifth digits, the centre point of the palm, the carpometacarpal (CMC) joint and a point opposite to the CMC joint in the medial direction. The LMC is supported within the literature: proven effective for stroke rehabilitation and musculoskeletal simulation [111–114] and literature reviewing the employment of an LMC for data collection of hand kinematics provide confident support for the collection of clinically

meaningful data [115, 116]. Though the LMC has also received some criticism in the literature [101, 103], it has been used here due to the high portability potential offered, providing an ability to be used during the normal everyday tasks performed by the participants within comfortable environments for them, the fact that it captures motion data without markers, leading to unencumbered movements, and the resultant non-invasive nature of the device, resulting in natural motions as the participant does not feel as if they are being watched in a laboratory environment.

A portable motion capture system, for the collection of hand motion data in everyday activities, has been created. This system utilises an LMC, Intel i3 Next Unit of Computing (NUC), external battery (2-Power 19 V, 27 Ah), GoPro head strap, LMC GoPro mount, bespoke NUC case and small shoulder carry bag. An exploded diagram of the NUC, battery and bespoke case can be seen in Figure 3.1, with the completed system shown in Figure 3.2. The NUC is a small form factor computer, measuring just over 10 $\times$ 10 $\times$ 2.5 cm; in this study the NUC7i3DNBE model has been used. The 3D printed, bespoke case holds the NUC and battery and is placed in the small shoulder bag - to be carried by the participant. Connected to the NUC is the LMC, this is held in place on the forehead of the participant using the GoPro head strap with a bespoke 3D printed mount. To transfer the data a Kingston DataTraveler 50 16 GB universal serial bus (USB) Flash Drive was used. The total price of the items used to form the motion capture system was (at time of purchase) £521.61. Though all pieces are commercially available, the interfacing of these with one another has resulted in a portable motion capture system not previously available. The advantages this system provides over a marker-based motion capture laboratory are: the significant price reduction, portability, ability to capture natural and unencumbered movements, non-invasive and contactless nature and support seen within the literature - collectively resulting in an appealing motion capture system. The advantages this system provides over the video recordings are: a reduction in the time to analysis large collections of data, the elimination of human error during analysis, the ability to apply quantitative analysis and a wider range of available analysis techniques.

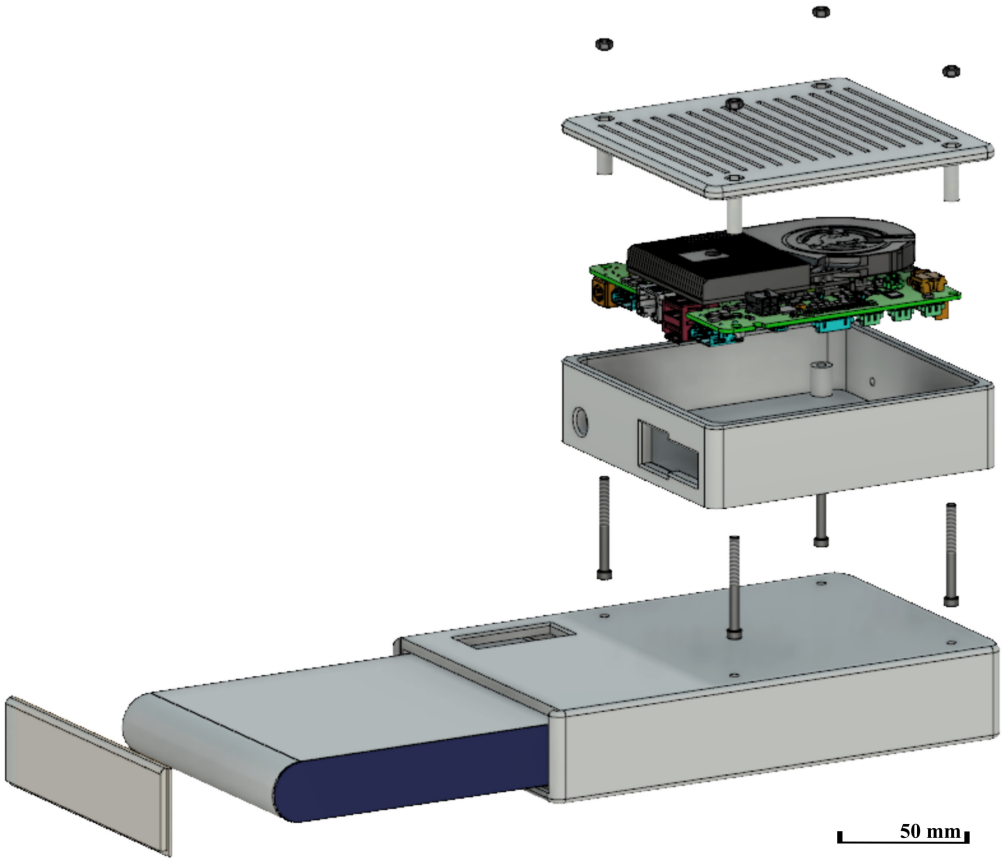

Figure 3.1: An exploded diagram of the portable data collection system, with reference scale.

Figure 3.2: The portable system components.

The LMC was chosen in the end as it provides: the ability to record without the need of placing anything on the hands of the user, a low form factor and weight allowing it to move freely and easily be made portable, the potential to last several hours with a carefully selected recording device, a USB connection which allows compatibility with most recording devices, comparatively low cost and a known clinically reliable source of hand motion data. Most importantly, the non-contact nature of the device allows the participant to perform natural and unencumbered movements throughout their day.

A GoPro head strap was chosen to fix the LMC to the forehead of the participant because the environments it is designed to operate within are far harsher than the

one this system is expected to operate within and has a standardised fixing point which is easy to 3D print a component for. The i3 NUC was chosen as it is the smallest device that was found able to meet the minimum requirements of the LMC. A 4 GB random access memory (RAM) module was used to meet the requirements of the LMC and 16 GB of storage was added to be able to store the files of the data collected. The 19 V external battery was chosen in order to be able to power the NUC whilst in use due to the predicted runtime of seven to eight hours - confirmed with real world tests. This length of time is appropriate for the environment the system is used in, a typical working day being eight hours. The NUC and battery, housed within the case, weigh approximately 1 kg and can fit in a small shoulder bag for the participant to carry during data collection. The bag chosen provides a perfect fit for the system and sits comfortably on the participant, the completed system can be seen in use in Figure 3.3. A USB flash drive must be used to transfer the data collected on the NUC to a computer for it to be analysed so that the NUC can remain disconnected from the internet, for security reasons. When compared against a Vicon motion capture system with choreographed hand shaped, the portable motion capture system was found to collect data within a mean of 14.2 mm.

Figure 3.3: The portable system, as typically worn by a participant.

A case has been 3D printed for holding the NUC during data collection, as seen in in Figure 3.2. The 3D printing of the case for data collection allowed a single structure to be accurately formed, resulting in a case that will stay together well and, with a low infill, be light weight. However, due to the fact that tall thin objects tend to not be appropriate for 3D printing, the ventilation holes for the battery case warped. Despite this error the battery case has still been considered structurally stable enough whilst in the shoulder bag. Overall, this case is perfect for protecting the NUC during data collection as it is light weight and structurally strong. Laser cutting was considered for creating a case. Though this made the case easier to produce and did not fail at the vents, the result was found to not be as sturdy as the 3D printed case.

During collect a JavaScript (JS) script within a Hypertext Markup Language (HTML) file stores a string of comma-separated numerical positional co-ordinates under the variable name `outputString`. The use of HTML allows for easy running on NUC and saving of the recorded data, it sees no draw backs for use with the LMC on this device. The data which is saved, each iteration, is as follows: a frame identification number (a global frame), an LMC frame identification number (a frame local to the LMC), the global time, the total time the device has been recording, the cumulative time each hand has been visible for in this occurrence, a confidence rating in the location and shape of the hand, the 3D Cartesian co-ordinates for the elbow and wrist and each of the joints and the tips for the digits. The final size of of `outputString` Every ten minutes `outputString` is saved as a comma-separated values (CSV) file on the i3 NUC, after which `outputString` is reset to a blank string. If the battery was to become fully depleted, or the i3 NUC crash, savings up to a window of 10 minutes before this will still be stored. If the LMC was to become unplugged the script pauses and can be resumed by plugging back in.

During early recordings with the portable motion capture system it was seen that it could not last as long as theorised (and desired), it was seen that the system would become very hot during collection. In response to this the battery was separated from the NUC and place in a separated location within the bag, creating a mild heat shield. After testing this was found to be appropriate to allow the system to collect for the theorised (and desired) time (at least six hours).

When deciding on which device to use for motion capture of the hand multiple options were considered, each being seen described in table 3.1. The table was created at time of the decision - all of the models considered, their specifications and prices are as such. The LMC was selected as the device for motion capture of the hands during ADL following comparison of the specifications of the devices listed. The LMC offers an affordable collection device with a high potential runtime and versatile data transfer method.

Table 3.1: A comparison table of potential hand motion capture devices.

Device	Resolution	Runtime	Data Transfer	Price
Leap Motion Controller	Unknown	Computer dependent	USB	£75
Vicon Motion Capture System	0.15 mm	Infinite	Ethernet cable	£100,000+
Manus VR	3 degrees	3-6 hours	2.4 GHz Wireless	£1,000
CyberGlove III	1 degree	2 hours	WiFi/USB	£10,000+
VRgluv	Unknown	Unknown	2.4 GHz Wireless	£800
Perception Neuron	0.02 degrees	3.5 hours	WiFi/USB/ Micro-SD card	£1,000
Captoglove	1 degree	10 hours	Bluetooth/ USB	£375

After concluding on the use of the LMC for data collection a device to power it and collect the recorded data was needed. For this several small computers were examined, along with the possible power sources which could be used with them. Table 3.2 shows a breakdown of all of the devices considered for this purpose. The table was created at time of the decision being made - all models considered, their specifications and prices as such. The NUC, powered with a 2-Power battery, was chosen for the: comparatively low price for an i3 processor, fact that it has an i3 processor, customisable RAM and storage options, possibility of higher voltage input (provided the battery can accommodate) and small form factor compared to alternative i3 options. In the table a NUC with 2 GB DDR3 RAM and an Intel Optane M.2 16 GB storage have been considered, as these are the desired components - though these options can be altered. Additional to this the 2-power battery provides a suitably long enough runtime for the desired application and is light weight when compared to alternative devices with similar specification. The existing knowledge that these have been tried and tested together and with the LMC provide comfort in their selection. The NUC and 2-Power battery were chosen, following a review and comparison of these listed specifications. These devices were shown offer reasonable specifications for their price and allowed for the desired collection time; additionally, it was know that the Intel i3 processor is able to support the LMC.

Table 3.2: A comparison table of potential recording devices.

Device									Battery					
Name	CPU	RAM	Operating Systems	On-Board Storage	USB Ports	Required Voltage/ Current	Size	Weight	Price	Name	Supplied Voltage/ Current	Estimated Runtime	Size	Weight	Price
Intel NUC (7i3DNBE)	Intel i3 (7100U)	2 GB (DDR3)	Linux/ Windows	16 GB	4 × USB 3.0	12-24V/ 10A	101.6 × 101.6 × 25 mm	500 g	£225	MaxOak	20V/3A, 12V/2.5A, 5V/2.1A, 5V/1A	16.5 hours (50Ah/3A)	206 × 135 × 33 mm	1.256 kg	£120
										2-Power	24V/2.5A, 19V/3.4A, 16V/4A, 5V/1A, 5V/2.1A	8 hours (27Ah/3.4A)	118 × 114 × 22 mm	620 g	£120
Jaguar One Plus	Intel Atom (Z3735F)	2 GB (DDR3L)	Linux/ Android/ Windows	16 GB	3 × USB 2.0	5V/2A	101.9 × 64.5 × 1.6 mm	54 g	£73	MaxOak	20V/3A, 12V/2.5A, 5V/2.1A, 5V/1A	25 hours (50Ah/3A)	206 × 135 × 33 mm	1.256 kg	£120
										EasyAcc	5V/4.8A	13 hours (26Ah/2A)	167 × 80 × 22 mm	454 g	£43
										Poweradd Pilot Pro2	9,12,16,19, 20V/4.5A, 5V/2.5A, 5V/1A	11.5 hours (23Ah/2A)	182.8 × 124.4 × 15.2 mm	558 g	£75
										RavPower	5V/2.4A	10 hours (20Ah/2A)	170 × 80 × 20 mm	476 g	£35
										Anker Power-Core	5V/4.8A	7.8 hours (15.6Ah/2A)	168 × 58 × 22 mm	463 g	£30
UDOO X86 ADVANCED PLUS	Intel Celeron (N3160)	4 GB (DDR3L)	Linux/ Windows	32 GB	3 × USB 3.0	12V/3A	120 × 85 × 24.5 mm	116 g	£130	Poweradd Pilot Pro2	9,12,16,19, 20V/4.5A, 5V/2.5A, 5V/1A	11.5 hours (23Ah/2A)	182.8 × 124.4 × 15.2 mm	558 g	£75
UDOO X86 ULTRA	Intel Pentium (N3710)	8 GB (DDR3L)	Linux/ Windows	32 GB	3 × USB 3.0	12V/3A	120 × 85 × 24.5 mm	116 g	£200	Poweradd Pilot Pro2	9,12,16,19, 20V/4.5A, 5V/2.5A, 5V/1A	11.5 hours (23Ah/2A)	182.8 × 124.4 × 15.2 mm	558 g	£75

LattePanda (2G/32G)	Intel Atom (Z8350)	2 GB (DDR3L)	Linux/ Windows	32 GB	1 × USB 3.0, 2 × USB 2.0	5V/2A	88 × 70 × 25 mm	55 g	£68	MaxOak	20V/3A, 12V/2.5A, 5V/2.1A, 5V/1A	25 hours (50Ah/3A)	206 × 135 × 33 mm	1.256 kg	£120
										EasyAcc	5V/4.8A	13 hours (26Ah/2A)	167 × 80 × 22 mm	454 g	£43
										Poweradd Pilot Pro2	9,12,16,19, 20V/4.5A, 5V/2.5A, 5V/1A	11.5 hours (23Ah/2A)	182.8 × 124.4 × 15.2 mm	558 g	£75
										RavPower	5V/2.4A	10 hours (20Ah/2A)	170 × 80 × 20 mm	476 g	£35
										Anker Power-Core	5V/4.8A	7.8 hours (15.6Ah/2A)	168 × 58 × 22 mm	463 g	£30
GPD Pocket	Intel Atom (X7-Z8750)	8 GB (LPDDR3)	Linux/ Windows	128 GB	1 × USB 3.0, 1 × USB Type-C	N/A	182 × 109 × 19.9 mm	503 g	£380	Internal	N/A	12 hours (7Ah)	N/A	N/A	N/A
GPD Pocket 2	Intel M3 (7Y30)	4 GB	Linux/ Windows	128 GB	2 × USB 3.0, 1 × USB Type-C	N/A	181 × 113 × 8 mm	465 g	£415	Internal	N/A	10 hours (6.8Ah)	N/A	N/A	N/A
13” Laptop	Varied	More than 4 GB	Linux/ Windows	More than 256 GB	Varied	N/A	13”	More than 1 kg	More than £500	Internal	N/A	5-10 hours	N/A	N/A	N/A

The results of the analysis on data collected with this described system can be seen in Section 4.2, with the final results achieved shown in Chapter 5.

3.1.2 Predicting Muscle Excitations from Kinematic Data

There is limited literature focusing on the estimation of muscle excitations from kinematic data alone, with none prevalent for the hand. Proposed is a combination of optimisation techniques and an existing musculoskeletal model to converge toward a prediction of the muscle excitations of the hand which reproduce the joint angles with a minimised difference to the inputted hand shape - implying the closest prediction of the muscle excitations performed to create the given hand shape. This allows for the prediction of muscle excitations of the hand from kinematic data collected, enabling further extraction of information from many existing collections of data.

In order to determine the muscle excitations from kinematic data the musculoskeletal model presented by Blana et al. [9] was implemented alongside a number of optimisation techniques. For each candidate solution, the set of muscle excitations are inputted into the musculoskeletal model and the joint angles in this scenario calculated. These joint angles are then compared to the known joint angles of the desired hand shape and an optimisation technique attempts to reduce the error between the outputted and desired joint angles. For this several different optimisation techniques were tested, as stand alone techniques and in tandem with others: genetic algorithm (GA), particle swarm optimisation (PSO), gradient descent (GD) and brute-force search. A GA technique has been selected as a well established method for optimisation. A PSO technique has been selected for the superior time performance it tends to show over a GA, with similar resultant accuracy. A GD method has been selected in aid other optimisation techniques, following application of the optimisation technique, to quickly converge closer towards a minimum more accurately. A brute-force search has been selected for the exhaustive search powers provided, though resulting in long computational time taken it does provide confidence in the results obtained.

The techniques described in Section 2.9 were implemented to utilise the equations of the musculoskeletal model for the calculation of the joint angles from the candidate solution muscle excitations. The joint angles produced by a set of muscle excitations, u, can be found by evaluating the candidate solution with the musculoskeletal model. To achieve this, (2.12) and (2.13) were combined to provide,

$$x_{n+1} = x_n + \left(\frac{\delta f}{\delta x} + \frac{1}{h} \cdot \frac{\delta f}{\delta \dot{x}}\right)^{-1} \left(\frac{\delta f}{\delta \dot{x}} \dot{x}_n - f(x_n, \dot{x}_n, u_n) - \frac{\delta f}{\delta u} \cdot (u_{n+1} - u_n)\right). \quad (3.1)$$

Candidate solutions can be inputted as u_{n+1} and the equilibrium hand shape, with

known state variables, derivatives of the state variables and muscle excitations, used as x_n, $\dot{x}_n$ and u_n. This assumes that the hand shape presented occurred h seconds after the hand was in the equilibrium. For this application, the time step, h, was selected to be 0.01 seconds, in line with the working range specified for the musculoskeletal model [9]. The found joint angles can then be compared to the recorded, desired, joint angles and the performance of the candidate solution evaluated with a cost function.

The determined hand shapes of ADL were in 3D Cartesian form. In order to be comparable to the output of the musculoskeletal model and, hence, work with the optimisation techniques these data must be converted into joint angles equivalent to those outputted by the musculoskeletal model. For each joint angle to be calculated the following were used: the joint in question, the more distal joint and that more proximal. These sets of co-ordinates were converted into a two-dimensional (2D) co-ordinate system and the desired angle found through the application of the vector dot product, found using (2.4). The 2D co-ordinate system was created by a local plane through the considered digit, formed such that the axis of flexion rotation was normal to that plane. Pictured from the medial side of the hand, the metacarpal bone of the considered digit was used to create one axis of the 2D co-ordinate system and the anterior to posterior direction through the hand was used to form the other. This can be seen visually described, for the second digit of the right hand, in Figure 3.4. In this diagram the flexion angles of the PIP and DIP joints have been depicted by θ_{PIP} and θ_{DIP}, respectively. The difference between the desired and output sets of joint angles provide a cost function to be minimised through the use of optimisation techniques.

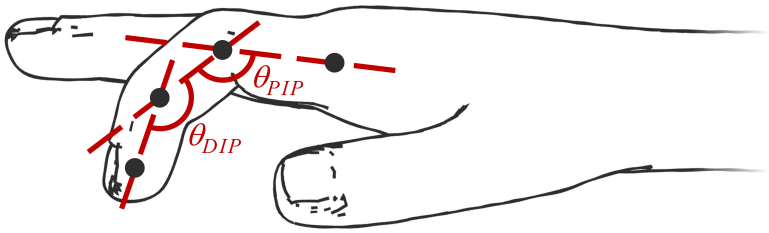

Figure 3.4: A diagrammatic representation of the calculated joint flexion angles for digits two to five.

In order to compare the candidate solutions a cost function is required. Here a function which finds the joint angles for a set of muscle excitations, from the musculoskeletal model, and compares this output to the joint angles of the desired hand shape was created. For GA, PSO and GD methods a fitness scaling technique was employed to aid convergence. Fitness scaling considers an exponential decrease in the cost as the technique converges towards a solution. This provides an increased influence of those with a lower cost. To achieve this,

$$cost_{scaled} = \sum_{i=1}^{16} \left(\boldsymbol{x_{rec}}(i) - \boldsymbol{x_{calc}}(i)\right)^2, \tag{3.2}$$

was implemented to calculate the joint angle disagreement cost for each candidate solution. In this equation, x_{rec} are the 16 joint angles determined from the recorded data and x_{calc} are the calculated joint angles, outputted from the musculoskeletal model. The further this cost reduces the greater the agreement between the angles of the predicted hand shape and the angles of the inputted hand shape becomes; in turn, the likelihood of the correct muscle excitations being obtained increases. During a brute-force search fitness scaling adds little benefit to identifying the best solution found and, therefore, the cost function for each input combination was defined to be the summation of the absolutes of the differences between the resultant and desired joint angles,

$$cost_{linear} = \sum_{i=1}^{16} \left|\boldsymbol{x_{rec}}(i) - \boldsymbol{x_{calc}}(i)\right|. \tag{3.3}$$

Alongside reducing the difference between predicted hand shape and recorded hand shape joint angles, the cost function considering the summation of the muscle excitations predicted has been implemented. This aims to provide an implementation of muscle redundancies without knowledge of the external forces acting on the inputted shapes. This cost function was defined by,

$$cost_{muscles} = \sum_{i=1}^{18} \boldsymbol{u}(i), \tag{3.4}$$

where $u(i)$ is the predicted muscle excitation for muscle i. This means of muscle redundancy implementation was not ideal but was limited by the requirement to only utilise kinematic data. The focus of this cost was to encourage the model to converge towards a solution using the minimal number of muscle excitations possible. In turn, the method is coaxed into utilising excitations only from the optimal muscles in this situation; showing little to no excitations from the redundant muscles, as would be expected in the real world.

In order to implement the functions (3.2), (3.3) and (3.4) with the optimisation techniques, a single, tunable, cost function was created. The results of these cost functions, following an iteration of the observed optimisation technique, were manipulated to form the terms of this overall cost function. To start, the costs were normalised; achieved by multiplying each element from the array of muscle excitations by the maximum of the joint angle differences. In doing this, a balance ratio of the cost components can be formed - removing the possibility of one component taking greater influence over the other due to inherently different scales of values. The weighting of this ratio was then altered in an attempt to provide the most accurate predictions of the muscle excitations. In order to obtain this knowledge, the parameters of the cost function were made tunable; here, the powers and coefficients of the components making up the cost were selected as the tuning parameters. Tuning the powers of the terms within the cost function provides control over the influence that each component has on the rate of convergence during optimisation. Tuning the coefficients to these terms enables alterations to the ratio of influence each has over the resultant cost. Hyperparameter tuning of each optimisation method has been achieved by implementing the following cost function,

$$cost = C_1 \cdot {cost_{angles}}^{P_1} + C_2 \cdot {cost_{muscles}}^{P_2}, \tag{3.5}$$

where $cost_{angles}$ is the cost function associated with the resultant joint angle error, $cost_{muscles}$ is the summation of the predicted muscle excitations and C and P are, respectively, the coefficients and powers for the $cost_{angles}$ and $cost_{muscles}$ terms, respectively denoted by 1 and 2. In this cost function, $cost_{angles}$ provided an assessment of joint angle agreement, between the inputted and the outputted hand shapes, and $cost_{muscles}$ attempted to enforce consideration of muscle redundancies. For implementation of this cost function with the optimisation techniques, $cost_{angles}$ was that defined in (3.2) for GA, PSO and GD and (3.3) for a brute-force search. For all methods, $cost_{muscles}$ was that explained by (3.4).

Upon first implementation, the ratio of the influences from the summation of the muscle excitations and summation of the joint angle differences, as well as the powers that each should be raised to, was unknown. Hyperparameter tuning of the cost functions (3.2) or (3.3), for the appropriate techniques, and (3.4) was applied in an attempt to obtain individualised cost functions for each of the tested optimisation methods. Within MATLAB, an array holding each of the coefficients and powers, C_1, C_2, P_1 and P_2, was created. This enables the use of an optimisation method to be used to modify each of these parameters in relation to each other, with respect to

a single cost function. Here, the cost function was set to be,

$$cost_{tuning} = \sum_{i=1}^{V}(1 - R_i), \tag{3.6}$$

where V is the number of validation hand shapes tested and R_i is the correlation between the known and predicted muscle excitations for the validation hand shape i. To this effect, the cost is minimised when the correlation is one - a perfect match between the predicted and known muscle excitations. By minimising this cost, the methods converge towards reasonably high muscle excitation and joint angle correlations in applications with the provided validation hand shapes.

In order to tune these parameters PSO was used, as this had provided a superior balance of speed and accuracy in testing. The time taken for this optimisation to run was of significant consideration, as within each of the passes it was required to run the tested muscle prediction optimisation script for each of the population members. Within MATLAB there are several customisable options provided for the built-in PSO function, for this implementation the following were considered: `FunctionTolerance`, `MaxIterations`, `MaxStallIterations`, `ObjectiveLimit`, `SelfAdjustmentWeight`, `SocialAdjustmentWeight` and `SwarmSize`. From these, `FunctionTolerance`, `MaxIterations`, `MaxStallIterations` and `ObjectiveLimit` are stopping criteria, each influencing the decision of whether the swarm has converged on a solution. Of these, `FunctionTolerance` provides the value which if the output is seen as lower than for `MaxStallIterations` number of iterations the PSO will stop and declare the input with the lowest found cost at that time to be the optimal solution. The `MaxIterations` gives the total number of iterations allowed before the PSO is terminated. The `ObjectiveLimit` parameter sets the value such that if the observed output of the cost function is below, then the PSO application terminates. The `SelfAdjustmentWeight` and `SocialAdjustmentWeight` give weight to the best position seen by the particle in question and that of the entire population of particles, respectively, when determining the next position vector. The `SwarmSize` value sets the number of particles which make up the population of the swarm. The following settings were used during hyperparameter tuning:

Table 3.3: The parameters selected for the optimiser hyperparameter tuning application of a particle swarm optimisation technique.

Parameter	Value
`FunctionTolerance`	`1e-10`
`MaxIterations`	50
`MaxStallIterations`	20
`ObjectiveLimit`	`1e-10`
`SelfAdjustmentWeight`	2
`SocialAdjustmentWeight`	2
`SwarmSize`	25

Here, `FunctionTolerance` and `ObjectiveLimit` were set to these extreme values to remove their influence over the termination of this tuning. Because of this, `MaxIterations` was likely to terminate the optimisation process, with testing proving 50 to be adequate for creating large accuracy improvements within a reasonable run time. A population size of 25 was chosen to allow for a large pool of particles to be tested whilst retaining an appropriate computational time for the parameter tuning. These settings were chosen to provide a balance between the time taken and the required level of accuracy of the end results.

Following the parameter optimisation using PSO, a GD method was also applied to provide a quick means of further improving the tuned parameter values. For this a learning rate of 0.01 and numerical differentiation step size of 0.4, defined as h from (2.14), were used over ten iterations. These values were selected from the results of preliminary tests with GD, showing to provide a superior balance between the speed of convergence and resultant accuracy of the tuned optimisation techniques, and on the pragmatic grounds that computational time was of great importance during this implementation. The speed of GD provided a further descent to a found minimum with a relatively lower computational time than would be required to continue with PSO, or other optimisation methods.

During validation of the LMC, it was seen that the recordings of more proximal joints showed greater agreement with the state-of-the-art motion capture system that the device was tested against. Considering this and that the end goal was to predict muscle excitations for data collected using the LMC, it was seen as preferable to give higher consideration for more proximal joints when determining the cost of a prediction. To achieve this, the results of validation of the LMC have been selected to weight the influence of each joint on the progression of the optimisation methods. The degree of influence for each joint has been calculated through the following concepts:

$$\boldsymbol{e} = \{e_{mcp}, e_{pip}, e_{dip}\},$$

$$\boldsymbol{a} = \left\{ \frac{m}{\boldsymbol{e}} \middle| \, m = \max(\boldsymbol{e}) \right\},$$

$$\boldsymbol{a}' = \left\{ \frac{\boldsymbol{a}}{\max(\boldsymbol{a})} \right\},$$

where e_{mcp}, e_{pip} and e_{dip} are the positional errors, found during validation of the LMC, of MCP, PIP and DIP joints respectively. Here, $\boldsymbol{a}$ was calculated to give the relative agreement of each joint recorded by the LMC to the state-of-the-art motion capture system. This result was normalised, to give $\boldsymbol{a}'$, for ease of compatibility with the cost function. Normalising this similarity score to the maximum value observed means that the joints which provided the most confidence during validation are able to influence the cost with no alteration, whereas joints showing lower confidence have less influence over the resultant cost. The average positional error for each joint set was used as this provides the most direct measure of confidence in the data recorded by the LMC.

Following the convergence of the employed optimisation technique, the difference between the desired and found joint angles for each hand shape were calculated and presented. Additionally, the mean difference for each hand and the overall mean difference were calculated and displayed. The the predicted joint angles were found by inputting the predicted muscle excitations into the utilised muscle model. The correlation between these predicted and desired joint angles was also observed, in an attempt to further assess ability of the technique to provide accurate muscle excitations.

To provide a visual aid, wire frame hands were plotted taking on the desired and found joint angles in a 3D grid within MATLAB. To achieve this each digit was assigned a co-ordinate along the x-axis and each bone set a length it would appear along the y-axis. The joint angles were imposed on the hands from a position with the digits extended and the thumb also adducted. The flexion of the joints (the joint angles) were used to rotate the bones about the x-axis, with the abduction of the thumb represented by a rotation of the first digit in the z-axis. To ensure these rotations did not cause a deformation of the bones, the length of each bone before and after the transformation were observed - resulting in any potential deformation being highlighted.

As an additional visual aid, providing a easily visualised comparison of the final output and the original taxonomy, Blender [249] was used to provide line art images of the hands experiencing the outputted joint angles. Comparing this to the line art image of the desired hand shape enables visual assessment of the performed. This was achieved with identical techniques to the creation the original taxonomy using Blender, described in Section 3.5.10, and, therefore, provided a visual representation of the hand shape identical to that from the original taxonomy. Additionally, the

observations of these predicted hand shapes enables the characterisation of the muscle excitations - even if these are not deemed to present the desired hand shape utilisation of the results may still be possible. Visual assessment is important as it may be that the joint angle values of two hand shapes are not close, or close, but, when observed in the real world, they could be considered to be close, or not close, enough to provide equivalent functionality.

The following steps were performed in application to determine the muscle excitations of a given frame of Cartesian data:

1. Convert the Cartesian data into joint angles of each digit.
2. Begin optimisation with random candidate solutions, recording the output as the predicted muscle excitations.
3. Input the predicted muscle excitations into muscle model to determine joint angles from this prediction.
4. Calculate difference in joint angles of the inputted and predicted hand shapes, providing the error from this application.
5. Use outputted joint angles to form Blender images, for visual assessment.

The process employed for validation and evaluation method for each technique employed can be seen in Section 3.6, with the results of which in Section 4.3. Further details on the implementation and execution of these techniques can be found in in Chapter 6.

3.1.3 AirGo

The currently employed clinical method for measuring the hand digit joint angles is a goniometer. This device has been seen to produce measurements with low repeatability and high variations across different users, with uncertain accuracy and long measurement times. Considering these limitations, a device has been created (named AirGo) which utilises the LMC to provide measurements of the angular displacement of the hand digits from markerless motion capture data. This proposed solution allows for fast collection of consistence measurements with a known accuracy.

The AirGo is an hand joint angle measuring decide, utilising the LMC; a non-contact measurement device, quicker and more accurate than current methods. A white, five millimetres thick, acrylic was laser cut and curved to create the platform for the LMC to be attached to - shown in Figure 3.5. The design includes a means to adjust the height of the LMC, so that the device can be made level with the hand of the patient; this assists the LMC in detection of the hand.

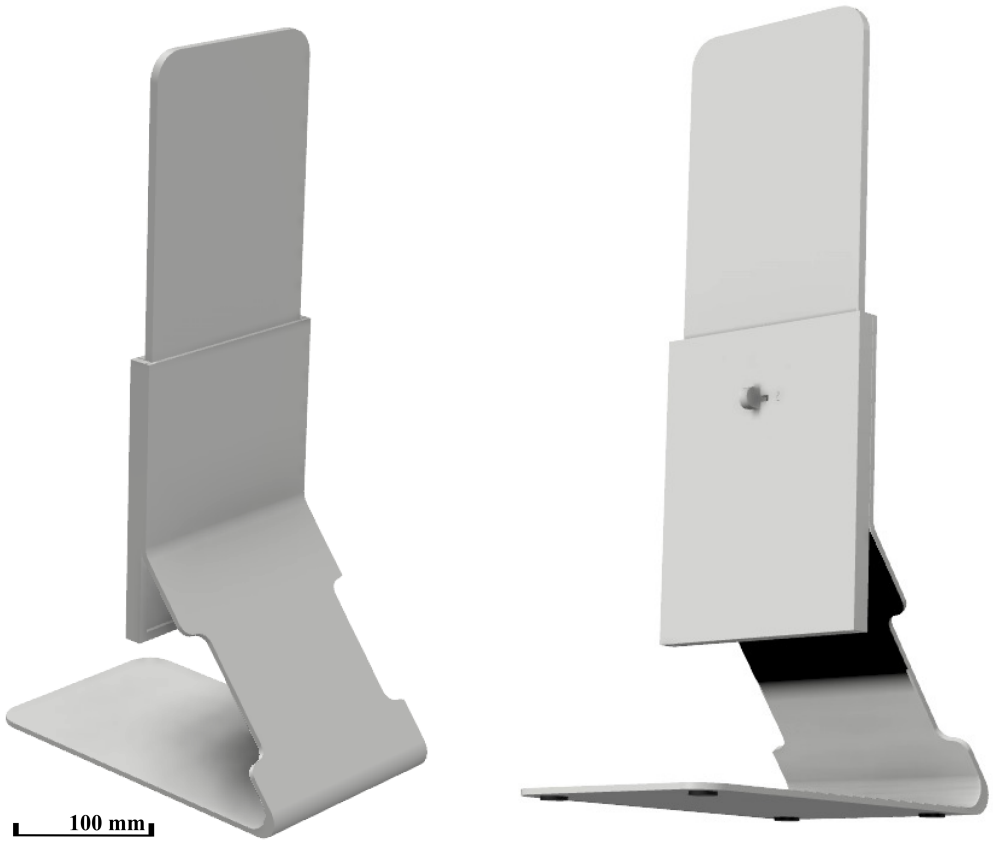

(a) The front view of the second iteration of the stand for AirGo.

(b) The rear view of the second iteration of the stand for AirGo.

Figure 3.5: The front and rear views of the second iteration of the stand for AirGo.

A HTML file with embedded JS scripts was used to extract joint positional data from LMC, perform joint angle calculations and display the relevant information. Several steps are performed with each frame of the LMC. Information is extracted from the LMC through the application programming interface (API), as with previous devices described. In the first instance the bones connecting the joint of interest are translated, such that the joint in centred at the origin of the Cartesian co-ordinate system. After which the dot product is employed to calculate the joint angle, in radians; which is later converted to degrees for easier understanding. The angle calculated is stored to be later used in a smoothing function. This function detects and removes anomalies as the data is collected (considered as three standard deviations away from the mean) and, if not, tests to see if a new maximum flexion has been reached. If there is a new maximum it replaces the previous maximum of that joint and the script continues, if not then the script simply continues. The screen displayed can be seen in Figure 3.6. A live visualisation of the presented hand

allows the users to ensure that the hand has been detected correctly by the device. Additionally to this, gauges displaying the current and maximum angle of the joints are present, enabling patient motivation. This screen includes an input box for the patient ID and "Set", "Save" and "Reset" buttons. The "Set" and "Reset" buttons set the currently viewed hand as the unaffected hand, for the affected to be compared against, and refresh the HTML file (clearing any data collected), respectively. Once the "Save" button has been pressed the date, time, patient ID and table of maximum joint angles seen is saved to a text file.

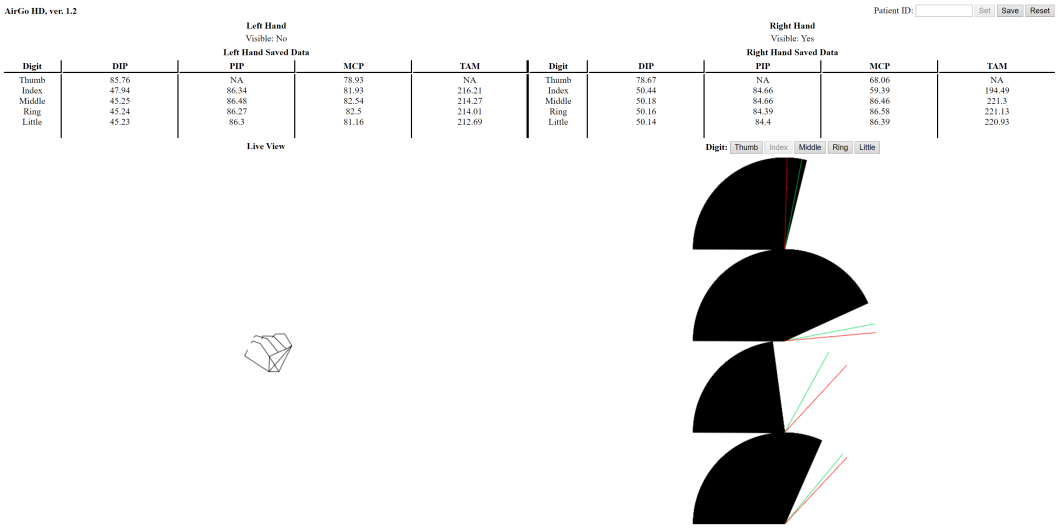

Figure 3.6: The second iteration of the display for the AirGo system.

Within a clinical environment this device would be placed on a table, with the LMC facing the patient. The height of the LMC within the device can be set so that the centre of the LMC lines up with the centre of the hand of the patient, this is not necessary but helps with LMC during collection and provides the best position for allowing any possible drifting of the hand which may occur. Once the patient is ready the AirGo can be started and the steps as described in Section 3.3.4 performed.

The methods employed to analyse the system can be seen in Section 3.7, the results of which are shown in Section 4.4. Further details of the system and a discussion of the obtained results can be found in Chapter 7.

3.2 Validation of the Portable Motion Capture System

The portable motion capture system should be validated before it is used to collect during ADL. For this a set number of choreographed hand shapes would be performed whilst measuring with both the portable motion capture system and a state-of-the-

art motion capture system, for this the Vicon motion capture studio at University Hospitals Coventry & Warwickshire (UHCW) was chosen. The control hand shapes decided to form these choreographed motions are shown in Figure 3.7. From published work by Feix et al. [57] 12 hand shapes have been selected to detail range of possibility of hand shapes. The choice was performed manually by grouping similar hand shapes with minimal visual or functional significant difference, leaving 12 groups of hand shapes, from which 12 hand shapes were decided upon to define each of these groupings. The use of predetermined grasps to train classification techniques provides confidence for the application of these techniques with the collected data. These 12 hand shapes allow for a good range of hand shapes to fit hand motion data to.

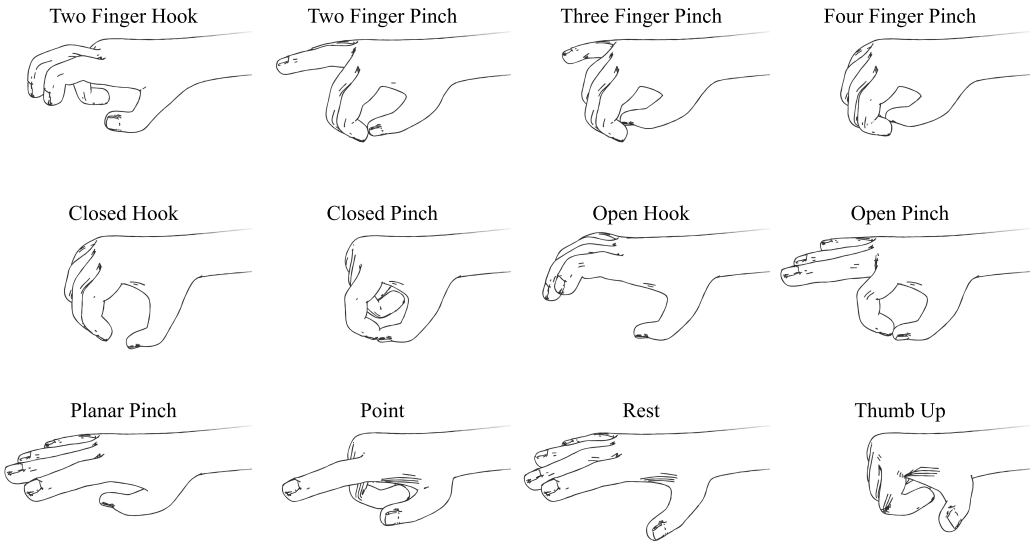

Figure 3.7: A collection of line art images of the control hand shapes.

The Vicon motion capture system at UHCW was used to collect the control hand shapes with a state-of-the-art marker based-motion capture system. Eight Vicon Vero 2.2 cameras were arranged around the subject as shown in Figure 3.8. These were moved onto a two by two by two metre frame, focusing the capture volume on the top and bottom of the area the subject was placing their hand. On each camera an array of IR light-emitting diodes (LEDs) with a 330 Hz refresh rate and resolution of 2.2 MP. These create a 3D search space and scan for reflective markers to indicate a point of interest in that space.

Figure 3.8: The capture space for hand motion capture with a Vicon motion capture system.

The reflective markers used were Vicon three millimetre hemisphere facial markers, placed on the hand to replicate the joints recorded by the LMC; this arrangement and the labelling given can be seen in Figure 3.9. These labels have been assigned in a manner such that the collected data will align with that collected with the portable motion capture system - as a result, some maybe not agree with the true joint names. A Vicon Active Wand V2 IR wand was used to calibrate the cameras in the space and provide an origin to the space. Due to the low placement of some cameras (to capture the digits when the hand is closed), the origin could not be placed on the ground; it was seen as unimportant where the origin of the captured space was, as the interest was in the hand shapes and not the hand position in space. All collected data localised to wrist during processing. A computer with Windows 10, 16 GB RAM and a Intel Xeon E5-1620 processor, running Vicon Nexus 2.11, was used to collect the data. No model was produced for the hand within the software, as only the labelled marker relative positions were of interest.

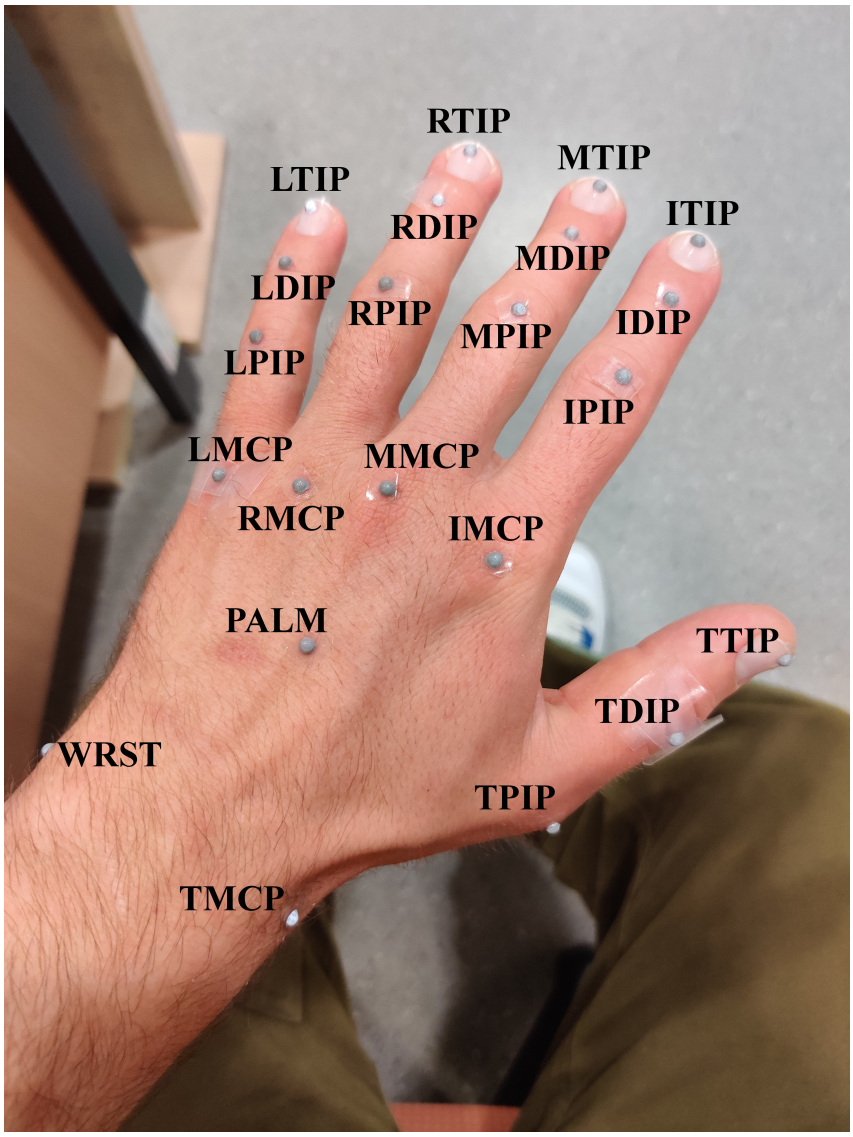

Figure 3.9: The labelled marker positions for hand motion capture with a Vicon motion capture system.

The collection of these controls has been achieved with the use of a HTML file, embedded with a JS script, and folder of hand shape images. The script is initialised with a single start button on the screen; this button removes itself from the page once pressed, displaying the hand shape, to be performed, and the hand shape label. For three seconds before each hand shape the resting position is displayed, this ensures that the LMC will have time to settle, as to not be disturbed by previous readings, and means that the transition is made from an alike hand shape each time, removing influence of the previous hand shape on the current. The script used to collect data with the portable motion capture system has been embedded within the HTML to enable the recording of the hand motion during this collection. Data are

stored as string in `outputString` during the display of each hand shape. Each hand shape is displayed twice, with each occurrence being displayed for six seconds. Before displaying the resting position `outputString` is saved with a filename congruent with the hand shape and `outputString` reset to a blank string.

Following data collection and the reduction to only including functional hand shape frames in the dataset, each frame was transformed into a pre-set local co-ordinate system. To begin with, the current frame was centred at the wrist and the second digit metacarpal bone was chosen as the y-axis. Next, the hand was rotated about the y-axis such that a positive direction along the x-axis described a lateral to medial direction across the wrist. The z-axis was then created normal to these two axes, so that a positive direction was defined by the posterior to anterior direction of the hand. The resultant local co-ordinate system can be seen in Figure 3.10. The angle differences for each of these bones, between the initial recorded frame positions and the desired axes locations, were calculated using (2.1), (2.2) and (2.3) and the subsequent rotations were achieved through applications of (2.4).

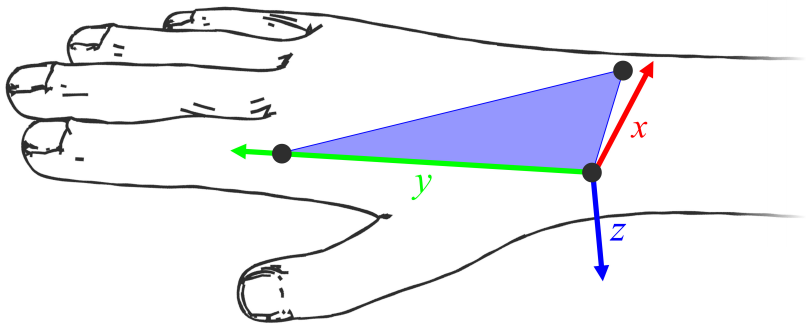

Figure 3.10: The local co-ordinate system chosen to represent the hand during data processing.

See Section 3.3.2 for steps taken to collect data and Section 3.4 for the subsequent analysis performed and results.

Additional to the validation of the portable motion capture system, these control hand shapes were used to form the training data of supervised analysis techniques. In order to perform analysis using machine learning, labelled hand shape data were needed; supplanting the necessity to inspect and manually label a large pool of data a control experiment has been designed. Two MATLAB scripts were employed to sort the control data recorded and combine each with the appropriate labels: one

allocated each recording to the correct folder of hand shape datasets and the next added each, labelled, dataset to the classifier training dataset.

3.3 Data Collection

Here, the prescribed steps followed in order to collect the control hand shapes, validate the portable motion capture system, collect hand motion data during ADL and integrate the AirGo system into a hand therapy clinic are expressed. These steps collect the data required to: train and assess analysis techniques, evaluate the accuracy of the portable motion capture system, determine the hand shapes occurring during ADL and observe the capability of the AirGo system within a clinical environment. An outlined functional hand shape definition is provided by the conclusion of rumination around the effects of definition variation on the coefficient of determination and standard deviation.

3.3.1 Control Hand Shapes

To support analysis of the data collected with the portable motion capture system, controls of known hand shapes must be captured. A large amount of labelled data would allow for the training of supervised machine learning techniques and validation of all analysis methods accuracies. The participant was asked to perform the 12 control hand shapes, shown in Figure 3.7. The set up simply requires a computer with the LMC connected and the bespoke script open.

Hand shape controls were collected through the performance of the following these steps, per participant:

1. Participant completes a practice run of each hand shape, with no timer; this is to ensure that the participant was certain about the hand shapes as they were asked to perform.
2. Participant places their hand vertically above the LMC (approximately 20 cm away from the device).
3. Press "Begin" on the file - each hand shape to be mimicked will then be displayed in turn.
4. Once complete the script stops (displaying that it has finished) and may be closed.

Following the recording of the control data, each recording were combined to make a full collection of each hand shape, using the methods aforementioned in Section 3.2. Subsequently the data became training data (for classification techniques) and validation data (for classification and clustering methods).

3.3.2 Portable Motion Capture System Validation

In order to ensure that the portable motion capture system provides the accuracy required it was validated against the current state-of-the-art in recording. For this the Vicon motion capture studio within UHCW has been chosen. The control hand shapes, introduced in Section 3.2, were used to provide choreographed hand shapes for the user to follow. The Vicon motion capture system is a marker-based motion capture system - the participant were required to wear small markers during data collection. Preliminary testing showed that these markers do not disrupt the IR sensors of the LMC. The reflective markers were placed on dorsal side of the joints recorded by the LMC, with placement to match the points recorded by the LMC. Preparation requires both systems to be initiated and the Vicon markers to be placed on the hand. Three recordings were taking in each session to improve reliability.

The following steps were performed per participant, with parallel recordings using the portable motion capture system and Vicon motion capture studio:

1. Place markers in the specified locations on the hand of the participant.
2. Fit the headband, with LMC secured to it, and i3 NUC, in the carry bag with the external battery, to the participant.
3. Start the portable motion capture system and begin recording within Vicon Nexus.
4. Ask the participant to reproduce the hand shapes presented to them.
5. Repeat the experiment three times then stop the recording and remove the equipment.

Analysis techniques performed on the collected data are described in the subsequent section, Section 3.4. The results of this analysis are presented in Section 4.1.

3.3.3 Activities of Daily Living

The capture of hand motions during everyday activities gives insight into typical hand shapes used during ADL. The results of this were used to feed data to the taxonomy of hand shape and muscle excitation prediction model, aiming to assist an everyday upper limb prostheses owner. The equipment used is designed to be as non-intrusive as possible, and for that reason the set up process is also designed to be as simple as possible. To begin data collection it is only required that the device is attached to the participant and the LMC examined and calibrated using an external monitor, there is no need for measurements to be taken or any additional items to be placed on the participant. An external monitor allows access to the vision of the LMC and enables the ability to apply adjustments to the calibration of the LMC;

such settings include the likely distance the hands would be seen at (to aid the LMC in finding the hand) and the orientation of the device.

Approval has been granted by the Biomedical & Scientific Research Ethics Committee (BSREC) at the University of Warwick for the execution of this data collection (approved on 4th October 2018 under the BSREC reference REGO-2018-2210). The decided steps for data collection are as follows:

1. Fit the headband, with the LMC secured to it, and the i3 NUC, in the carry bag with the external battery, to the participant.
2. Plug the i3 NUC into an external monitor and ask the participant to undertake a few basic tasks they would perform regularly to test the recognition of their hands.
3. Go over what is required from the participant once data collection has begun.
4. Open the HTML script, in a browser, on the i3 NUC and disconnect the external monitor.
5. Leave the participant to carry out their day, as if the LMC was not there.
6. Once the experiment has ended, stop the i3 NUC from recording further data and remove the bag and headband from the participant.

Analysis techniques performed on the collected data are described in the subsequent section, Section 3.5. The results of this analysis can be seen in Section 4.2, with the final taxonomy presented and discussed in Chapter 5.

3.3.4 AirGo Clinical Trial

A clinical trial, performed in parallel with the UHCW occupational hand therapy clinic, was established in order to collect data for real world validation of AirGo. To begin the AirGo was set up ready for the patients, as described previously - Section 3.1.3. Throughout the recording the live view of the hand is compared to the real hand to ensure recording consistency with the real world. Here the normal AirGo script was used, which saving only the final maximum value seen upon pressing "Save".

The below steps were employed, per patient, following their appointment with the occupational health therapist:

1. Patient places elbow of the unaffected arm on table, with their upper arm vertically upright.
2. Adjust the height of the LMC until centred with the hand.
3. Patient is asked to close the presented hand as far as they are comfortable with.

4. Once the angles displayed appropriately represent the behaviour of the patient press “Save”.
5. Patient places elbow of the affected arm on table, as with previous hand.
6. Adjust the height of the LMC, if necessary.
7. Patient is asked to close the presented hand as far as they are comfortable with.
8. Once the angles displayed appropriately represent the behaviour of the patient press “Save”.

Two methods were used to analyse the effectiveness of AirGo using the data collected during the clinical trial. The first method attempted was comparing the hands of each patient, to establish whether the recording provide the sensitivity required to at least detect hand injuries, and the second was testing individual patient progress, to determine whether development could be observed with AirGo. Further details of these employed methods can be found in Section 3.7. The results of the clinical trail can be found in Section 4.4.

3.4 Analysis of Portable Motion Capture System Validation Data

In order to conclude on the validity of the portable motion capture system the data collected from both this system and a state-of-the-art in hand motion tracking must be compared and their correlation examined. After collecting the data, using the methods described in Section 3.3.2 the following steps where taken to determine the validity of the LMC from these data.

The Cartesian based motion data of the hand collected with both devices was each transformed to be described within a local environment (centred at the wrist joint with the metacarpal of the index finger fixed to the y-axis in the positive direction). This local co-ordinate system is described by Figure 3.10 and was achieved by the rotations described in Section 3.2. After localisation of the data, the Vicon data were scaled such that the MCP joints matched their respective joints from the portable motion capture system data. Scaling was achieved in all axes by observing the ratio between the second digit MCP joint and the fifth digit MCP joint positions for both datasets. The differences between each of the MCP locations of the Vicon and LMC data were then observed to ensure that the scaling was applied appropriately and the relative 3D differences between each joint of the Vicon data were checked to ensure no deformation had occurred during the transformation of these data. Provided that both of these checks showed that no errors had occurred, the disagreement between

the two datasets was calculated. Frames where matched between the Vicon and portable motion capture system data by observing the time collected and filename, respectively. The data from each method was visualised and manually examined to ensure no anomalies where present in either; if required, anomalies where removed, and the remaining data averaged.

Analysis included calculating the Euclidean distances between each point of both recordings and the differences in the angles calculated for each joint of both recordings, within a local environment and with scaling applied. For each of the joints of the second to fifth digits and the IP joint of the first digit, the flexion angle was calculated in the plane depicted by Figure 3.4. This created a 2D co-ordinate system in the plane of rotation for each of the joints. In this plane, the equation (2.4) was applied to calculate the joint angles under consideration. Here, $\vec{a}$ was set to be the vector of the proximal phalanx bone for calculations of θ_{PIP} and the vector of the middle phalanx bone for calculations of θ_{DIP} and $\vec{b}$ was set to be the vector of the middle phalanx bone for calculations of θ_{PIP} and the vector of the distal phalanx bone for calculations of θ_{DIP}. The flexion and abduction angles of the first digit CMC joint were calculated in the planes shown in Figures 3.11 and 3.12, respectively. In each respective plane, the equation (2.4) was again applied to calculate the joint angle. Here, $\vec{a}$ was set to be the vector of the first digit metacarpal bone and $\vec{b}$ was set to be the vector of the second digit metacarpal bone during calculation of both θ_{fl} and θ_{ab}. Both the calculations for Euclidean distances and angle differences were performed individually for each joint. This enabled the total difference to be fond whilst also allowing for each of the joints and digits to be analysis individually. Displaying the output of this analysis would provide and average error in the distance from the portable motion capture system as well as being able to identify any of the digits or joint which results in the greatest increase in this error. This provides comfort in the results of low error digits and joints whilst highlighting those with higher error to be considered with more caution.

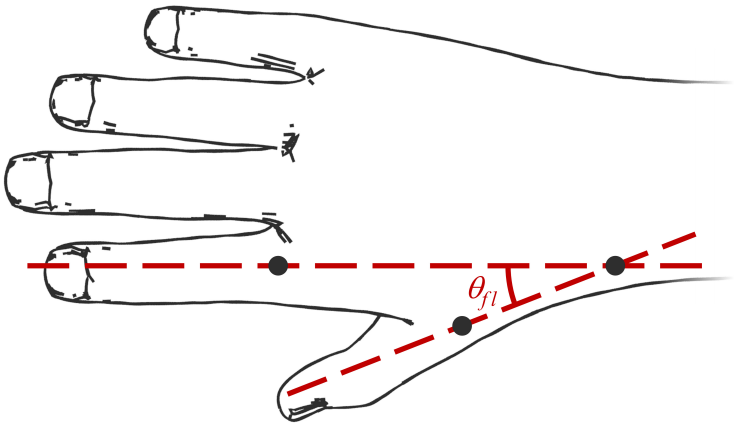

Figure 3.11: A diagrammatic representation of the calculated flexion angle of the carpometacarpal joint.

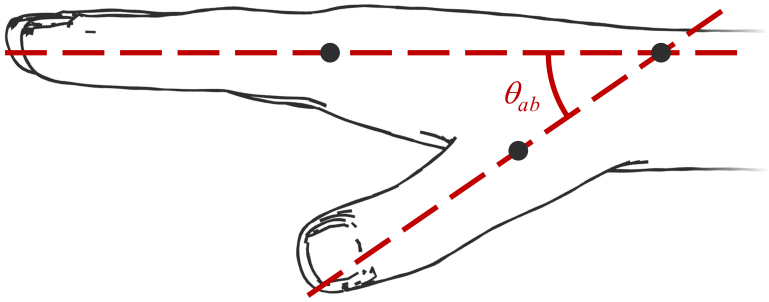

Figure 3.12: A diagrammatic representation of the calculated abduction angle of the carpometacarpal joint.

3.5 Analysis of Activities of Daily Living Recordings

Following collection, with the portable motion capture system, the data are then loaded into MATLAB and reduced to only include frames in which the hands have been recorded by the LMC. Within this, remaining, data the hands are localised, to be centred at the wrist, and the transitional frames removed - leaving, exclusively, frames in which functional hand shapes have been performed. These remaining hand shape frames become the inputs to the k-means++ algorithm; therefore, calculating the cluster centroids would effectively represent the commonly performed hand

shapes. Plotting these centroids visualises the hand shapes deemed, by the k-means algorithm, to be able to categorise each frame of the raw data. These centroids have a possibility of being merged to form the final groupings. Analysis of these final hand shape groupings found (the taxonomy) highlights the importance of the hand shapes seen in ADL by these participants - observing those most often occurring and those held, on average, for the longest period of time.

To determine capabilities to discriminate hand shapes, machine learning techniques considered were tested with recordings of the control hand shapes shown in Figure 3.7. These data were collected in the same manner as the validation of the portable motion capture system , with save file names identifying the hand shape labels. Following collection, the data were loaded into MATLAB as a `table` variable, using the file names loaded to provide the hand shape label of the final column. The recording of the hand shapes was then randomly permutated and divided into training and testing data. This provided the required labelled data for training and evaluating the performance of the machine learning techniques employed.

The supervised learning techniques were trained using these recordings of the control hand shapes, totalling 26,071 frames of hand motion data and were tested using 6,518 frames from the same dataset. The performance of the k-means++ clustering algorithm was assessed using the entire dataset of 32,589 frames - due to the fact that training is not necessary for this, unsupervised, technique.

Analysis methods considered, as well as details on the chosen clustering algorithm and subsequent merger of outputs, are given in the following sections.

3.5.1 Determining Functional Hand Shape Occurrences

In order to find the commonly occurring hand shapes within the data collected with the portable motion capture system these data must first be reduced to only contain the frames of functional hand shapes. By removing all other frames the analysis techniques used can be implemented efficiently to cluster exclusively frames of functional hand shapes, aiding in the speed and accuracy of the performed analysis.

Firstly the data are loaded into MATLAB from the recorded CSV file, after which the columns of the data are extracted into separated variables labelled with their associated joint names. For this the columns holding the x, y and z Cartesian co-ordinates of each joint are stored in a variable labelled with that hand, digit and joint as their name. Next all frame in which the hand is not seen are removed from their respective variables. To achieve this the rows (frames) of the index MCP joint are queried to see if they contain a NaN value, if so the frame is identified as empty for that hand and removed from all variables of that hand. The joint extension of

digits two to five, at each frame, were determined through the use of the vector dot product within the 3D co-ordinate system utilising the previous and next joint. To accommodate for the flexion and extension and abduction and adduction possibility of the thumb CMC the thumb CMC and MCP with the index MCP were transformed into a a local 2D co-ordinate system; for extension the y and z co-ordinates were used and for abduction the x and y co-ordinates were used. Given the set up of the hand shapes in the previous local co-ordinate system these new 2D local co-ordinates systems are set up so that implementing the vector dot product provides the desired angle in that situation. The vector dot product was found as described by (2.4).

The reduced data are the labelled as either belonging to a functional hand shape or transitional frame group, determined from the calculated joint angles. In order to categorise frames into transitional or functional hand shape frames a definition of a functional hand shape was necessary. This definition was decided to be as follows: *a position in which each joint is held within one degree for one second or longer*. A hand shape is then formed by averaging the group of frames which fall within this definition. This definition was initially decided based on pragmatic grounds and supported by numerous analysis attempts with various definitions; more relaxed rules (more than one degree or one second) resulted in a longer computational time and a higher number of anomalies appearing in the final data, though more tighter rules (less than one degree or one second) showed a loss in valid hand shapes during the reduction process. Frames that fall outside of this definition where considered transitional frames, simply transitioning to another hand shape.

Figure 3.13 displays the influences of this definition over the average R-squared value, the coefficient of determination, and standard deviation of the resulting hand shape clusters. Each plot was created from the average, between the left and right hands, of the averaged, across the clusters formed, R-squared values, between the observations of each cluster and their respective centroids, and standard deviations, of the observations within the clusters. On each plot, the changes to the degree each joint angle much stay within are described by the top x-axis and alterations to the length of time all joints must remain within this angle along the bottom. The frame numbers used defined half a second, one second and two seconds of time, derived from the average frame rate of the collected data. In Figure 3.13a the effects on the averaged R-squared, from the variations defined, are depicted. From this, support is shown for the selected degrees the joint angles must remain within, as this selection produces the greatest R-squared value. Though there exists a dramatic increase in the R-squared values as the hold length was increased, this was a result of the limited observations provided for clustering - presenting dense clusters of limited information. The effects these alterations also had on the standard deviation observed are described by Figure 3.13b. This plot supports the claim that the

high R-squared values, achieved by increases to the hold duration, are only a result of sparse observations in dense clusters. The large reduction seen in the standard deviation implies that less of the recorded variation has been captured by the clusters, indicative of a limited amount of information available. A visual examination of the resultant clusters, formed under each of the varied conditions, further supported the use of the aforementioned functional hand shape definition.

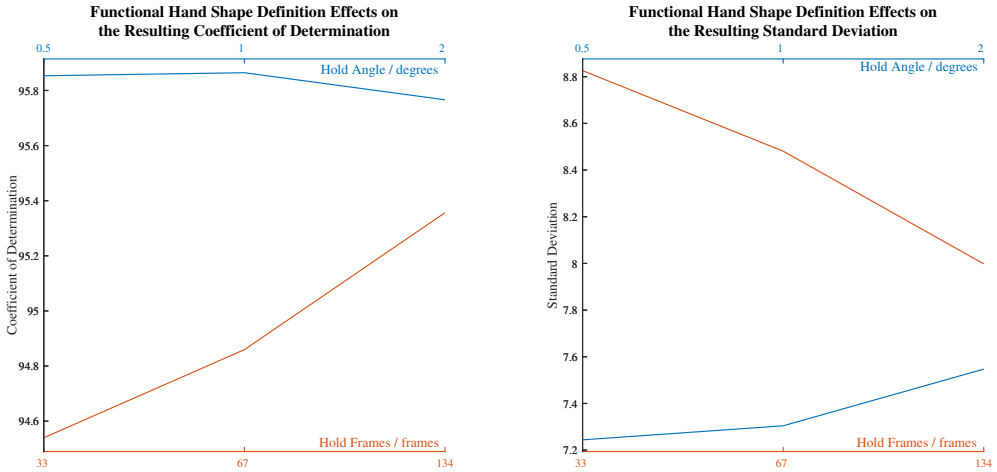

(a) The effects of definition variation on the coefficient of determination.

(b) The effects of definition variation on the standard deviation.

Figure 3.13: The effects observed from alterations to the functional hand shape definition.

As discussed in Section 2.3 these functional hand shapes can be divided into two categorises: gestures and grasps. A gesture would be considered as a functional hand shape which does hold a tangible object within space. A grasp would be considered a variant of this, physically interacting with the tangible world. Though these categorises of functional hand shapes are known to exist, the numerical kinematic data collected does not allow for a definitive answer to which hand shape belongs to either, as it would be unable to identify interactions in the world (outside of hand-on-hand contact).

The data were then transformed into a local co-ordinate system. This was done by finding the position of the wrist joint and subtracting this from all of the joints (localising the hand with the wrist as the origin) and then rotating the joints using 3D rotation matrices, described by (2.1), (2.2) and (2.3), to align the second digit MCP with the positive y direction axis and so that the positive x direction axis describes the lateral to medial direction. The z-axis was then placed normal to both of these, describing the posterior to anterior direction of the hand. The resultant local

co-ordinate system is depicted in Figure 3.10. Analysis within a local co-ordinate system is employed as the spatial location of the hand has no relevance here, it is the shape of the hand which prerequisites the desired information. This creates a local co-ordinate system with the wrist position as the origin, the index MCP along one axis, the normal to the anatomical position of the hand along another axis and the remaining axis perpendicular to both of the others.

When running multiple recordings from different participants the data are stored in a temporary MATLAB data file, the workspace cleared of the current participant specific variables and the next participant loaded, to reduce the demand on the RAM of the computer. Following the loading and reduction of all recorded data the output is then saved to reduce the time needed next time. After completing these steps the analysis was then performed to determine the information related to dataset, including: reducing the dimensions, finding possible correlations, observing joint activity, grouping commonly performed hand shapes and determining the characteristics of these grouped hand shapes.

3.5.2 Principal Component Analysis

As a means of reducing the dimensional complexity of the data principal component analysis (PCA) was considered. With a large amount of data with 60 dimensions analysis could be made fast and easier with a reduction to the dimensions. When considering joint angles the dimensionality is reduced greatly, though still containing a significant number of dimensions. Though the large reductions commonly found with PCA may lose descriptive elements needed in such vast amounts of data it was considered and assessed due to the simplicity it could provide. The PCA technique was chosen for dimension reduction over heatmaps, t-distributed stochastic neighbour embedding (t-SNE) and multi-dimensional scaling (MDS) due to the vast amount of information which can be extracted with just one application, the fact that this works well for high dimensional data, the likely high collinearity in a dataset of hand shapes and ease of implementation. Greater detailed explanations of PCA and the alternative dimension reduction methods can be seen in Section 2.5.

Within MATLAB there is a built-in function for performing PCA, `pca`. To perform PCA the angles of the joints at each frame were calculated and inputted into the built-in MATLAB PCA function. From this function the variance of each principle component (the eigenvalues of the covariance matrix of the input) can also be extracted, enabling the creation of a scree plot. A scree plot displays the eigenvalues of each of the principal components against that component number; in plotting this the ideal number of components to used would be highlighted by the plot levelling out (as would be scree at the base of a mountain). The principle component

coefficients for this PCA performed were obtained from the applied function, enabling the creation of a loading plot. Through the loading plot the influence the original dimensions have on plotted principal components can be examined. This helps identify trends in the original data (with correlations being highlighted) as well as any possible groupings formed within the reduced dimensional frame of possibly one, two or three dimensions.

Application of PCA on the collected data may provide some benefits. Following a reduction of the dataset from this, any analysis methods performed after would be quicker due to the lower number of dimensions which would need to be included. Additionally, employment of PCA would enable a means of identifying trends within the, expectedly correlated, data. Despite the appealing advantages of this technique, there are limitations which must be considered. A reduction in dimensions enables faster analysis but at the cost of a loss of information defining the data. Loss of these dimension identifiers would be a hindrance as it would limit the analysis which could be performed on interactions between the hand joints. Any reduction in dimensions could help with future time sensitive analysis, but here processing time was not of significant concern. Due to this, PCA was considered for correlation identification but not any potential dimensional reductions.

A successful reduction in dimensions would allows for more analysis techniques to be possible to employ. A large enough reduction could allow for manual analysis, or crude search algorithms, for the grouping of similar data. This reduction would also reduce the computational complexity, requiring less time to complete any analysis methods. Though it may loose accuracy this could be a good alternative analysis method for when speed is required. Additional to these, the outputs possible from a PCA could identify trends and correlations within the data otherwise not seen. Highlighting these trends will provide knowledge of how the digits of the hand comparatively interact with one another during ADL; this could lead to identifying potential possibilities in terms of complexity reductions in upper-limb prosthetic devices. Reductions in hand complexity by linking the motion of digits lessens the need for the individual actuation of each digit. This could provide a reduction in the cost of the devices and create easier means of production, with a controlled loss of accuracy during replication of hand motions. By combining the motions of only highly correlated joints, a low loss of motion replication accuracy would be ensured.

3.5.3 Joint Angle Correlations

By observing the correlations of the joint angles throughout the recordings information of aid in the development of upper-limb protheses could be obtained. Knowledge of any correlations of joint angles during ADL will allow a simplification of prosthetic

hand joints, reducing computational complexity and possibly actuation requirements. It is already known that some joints of the hand move without user input through their constraints to other joints; by observing joint angle correlations within the collected data, the joints these constrains apply to and how they move in union would be indicated. Additionally, any joints commonly activated in cohesion would be highlighted.

Upon calculating all joint angles at each frame and reducing these to only where functional hand shapes are occurring, the correlation between the joint angles can be visualised through the use of the built-in MATLAB function `plotmatrix`. This function displays scatter plots of each of the columns of the dataset (in this case set to be the joint angles) against each other. In doing this any joint which behave similarly (are correlated) would be highlighted, as well as those acting independently of others being able to be identified. Additionally, loading plots from a joint angle PCA analysis can be used to highlight any significant correlations between the recorded joint angles.

An awareness of this information during upper-limb prostheses development could enable a simplification of the devices. The knowledge could allow for the pairing of certain digits, simplifying actuation needs and computational complexity of the code used. This technique would be implemented over the complete recorded dataset and final taxonomy. A digit could be found to possess only one, two or three positions, irrespective of the other digits, or could be found to move identically to others, reducing the actuation needs of an upper-limb prostheses. This would potentially save time and money during the development and production of upper-limb prostheses whilst maintaining a similar functionality of the hand. The potential offers of the results of this method warrant application.

3.5.4 Joint and Digit Activity

From the data collected another piece of information that could be extracted is a ranking of which digits moved the most during these recordings of ADL. This would indicate an importance on certain digits, whilst highlighting an unimportance of others. Additional to the guidance provided by the taxonomy of hand shapes common to ADL, this would enforce the importance to the digits most utilised during ADL for aid with development of upper-limb prostheses.

Following the calculation of the joint angles at each frame the change in each joint angle other a set range of frames could be determined. To avoid contamination of the results minor movements, either from the hand or LMC, which are not attributed to a conscious movement by the participant were not considered. In order to achieve this

joint angles which changed by more than one degree over 20 frames were considered exclusively. The summation of these occurrences for each joint allows for the most to least active joint and digit to be determined and presented.

Using this method each joint and digit activity was observed. To display the outcomes of this analysis method the results were simply displayed as an output text, ranking the most moved digits to least moved for the left and right hands. A bar chart was also outputted for visual aid.

3.5.5 Artificial Neural Networks

An artificial neural network (ANN) is a classification algorithm designed to mimic neural networks, forming a deep learning supervised machine learning technique. An ANN consists of neurons connected by synapses, typically, over several layers, referred to as hidden layers, between the input and output layer. The input layer takes a set framework of data and the output layer assigns confidence values to each of the possible classification categories. Further details on ANNs can be found within Section 2.6.1. Here, GoogLeNet and a, created, bespoke ANN have been consider for the classification of hand shapes within recorded data. GoogLeNet has been chosen as a well establish network which has demonstrated high levels of accuracy in image classification. A bespoke ANN has been created for the collected data, in an attempt to provide high levels of classification with a faster computation time than GoogLeNet.

GoogLeNet has been chosen to use here; it is a very well establish neural network for image classification. GoogLeNet has 22 layers and takes an input image of 224-by-224 pixels; due to this input requirement, the 3D Cartesian data collected was converted into the demanded data format and size. An example of an image of a hand shape created for input into the GoogLeNet model can be seen in Figure 3.14. Despite the need to convert the data into images, GoogLenet has been chosen as a potential method for analysis due to the presented superior performance and the fact that it is already a well established network. For this reason it has been applied here for classification during preliminary assessment of the data, providing a quick test for the existence of expected hand shapes within the data, and as a means to draw comparisons between the recorded data and previous taxonomies, highlighting the rate at which hand shapes from previous taxonomies appear within the recorded data. The following steps were employed in preparation for training a network: record the hand with a note of which hand shape is being performed, group these hand shapes into the appropriate folders and then create an image for each frame from the data of the recordings. Once trained and validated, the network could be applied to the data collected using the portable motion capture system - data from

everyday activities.

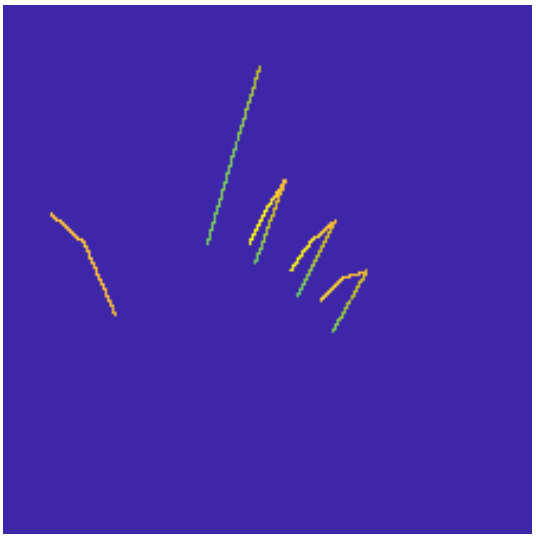

Figure 3.14: An example of a GoogLeNet input image for a point gesture.

During initial training the weights of the first ten layers were frozen (i.e. could not be altered during training) to aid training time; however, in the end all layers were trained (unfrozen). The training process of the GoogLeNet network included 10 epochs with a total of 13,036 images of the control hand shapes. One epoch describes one pass of the entire training dataset of observations through the ANN during training.

MATLAB scripts were created to handle the data conversion of the recordings (from Cartesian co-ordinates to a 224-by-224 pixel image) and training of the network. From the 3D Cartesian data a 3D binary space can be formed, in which the joints are registered as high. A bound of 224 pixels, around the hand, in all three axes is applied. From this two of the directions (in this case the x and y) can be utilised as locators for points on the image and the third (z) for alterations to the colour of the points, representing the depth into the image. This process see the creation of image describing each frame whilst retaining the information of Cartesian 3D data. Lines were constructed between points describing connected joints, forming an image of a hand skeleton, to aid edge detection during the ANN application. These were achieved by extracting the depth of and distance between the two points and plotting several points between these to fill the gap. Following the depth changes between the points ensured a line consistent with the changing colour gradient. The interval of filling was chosen to ensure that a gap did not occur along any line. Creating a fading circular pattern around each data point was attempted in preliminary analysis to assist the networks, though to no avail. A simple MATLAB script, with the

desired training settings, was then created which takes an object, containing data from the folders of images (`imageDatastore`), of the hand shapes to be studied (a collection of folders named as labels to the images within them) and inputted into GoogLeNet, as training or testing data.

Due to the high computational demand of creating images for input into GoogLeNet, a bespoke ANN was designed to input Cartesian co-ordinate hand motion data. This ANN was crated using the `feedforwardnet` function of MATLAB. This was given input characteristics to match the Cartesian co-ordinate data, specified using the `configure` function. In this implementation the network was created with ten hidden layers. The created network was then trained using the MATLAB `train` function, inputting the labelled training control hand shape data. This trained network was validated by a pass of the labelled test control hand shape data. This offers a great potential in fast implementation and execution, compared to GoogLeNet - though this approach does not offer the confidence of a well established network, such as GoogLeNet.

This was not implemented for the creation of a final analysis due to the limitations of it only grouping known hand shapes. However, this technique has been used to evaluate the ability of LMC to provide reliable data, during preliminary assessments, and to test the results of existing grasp taxonomies against the hand motion data recorded during ADL.

3.5.6 K-Nearest Neighbours Classification

Classification algorithms are supervised machine learning techniques. These techniques are trained with pre-labelled data and then provided unlabelled data to classify into the previously seen categories. The k-nearest neighbours (KNN) classifier has been used within this study; this classifier uses a similarity measure between the provided data and known labels to predict the label for the provided, unlabelled, data. Following a comparison of the inputted data to the known labels, the KNN classifier outputs predictions of the labels based on the similarity between the inputted data and the data with known labels.

The use of a classification algorithm was also attempted to label hand shapes within the collected data. As with the use of ANNs, this method allows for another means of preliminary analysis of the data collected as well as identifying trends with previous taxonomies. MATLAB classification learning app was utilised to train and export a model, which was then implemented to make predictions of hand shape occurrences within frames of data. Recordings of the control hand shape were used as training and validation data, divided as previously specified. Once validated, the

trained classifiers could be applied to the data collected with the portable motion capture system. Multiple classifiers were tested and the KNN subspace ensemble classifier selected due to the high accuracy found possible with this during testing.

The use of a classification algorithm allows for the grasps of existing taxonomies to be found with confidence in the data, supporting or arguing against their results. Once training data has been recorded it is easy to implement within MATLAB due to built-in app. Another advantage over other analysis techniques is the instant resultant accuracy available after training the algorithm. However, unlike unsupervised machine learning technique the training and validation data does need to be labelled. Considering the high dimensionality and vast number of frames from hand motion capture data an automated labelling method would be difficult to apply and manually labelling the data would be a long and tedious process. An automated approach could be applied, though this would reduce confidence in the results; anomalies are possible and can be removed, but for confidence the data would need to be checked back. Additionally this training and testing data needs to be recorded and limits the ability of the classifier, as it can only classify what it has been trained on. The purpose of this project is to update existing taxonomies with modern, new, hand shapes, so the inability to highlight new hand shapes limits the use of this method here significantly.

The classifier was trained use control train data and validated using control test data, with a 80:20 randomised split of training:testing data. During preliminary testing it was found that some hand shapes where not differentiate with the single classifier. A second classifier was run to improve prediction of the four finger pinch and closed hook, this was trained inputting only control train data of the four finger pinch and closed hook. A receiver operating characteristic (ROC) curve was used to evaluate the results.

This was not implemented for the creation of a final analysis due to the limitations of it only grouping known hand shapes, has been used to evaluated the LMC in providing reliable data and testing against existing taxonomies. Providing previously identified hand shapes as training data allows for confirmation of the findings from previous taxonomies, and potential support that the data collected with the LMC were appropriate. Additionally, this method has the potential to identify specific hand shapes in sets of data, enabling a potential reduction of a dataset to the object grasping or gesturing frames. As more data are added to the training set, it will become possible to identify more hand shapes and will enable greater customisation of the resultant groupings.

3.5.7 Decision Tree Learning

A decision tree queries an input through multiple layers to classify it into predetermined categories. A manual decision tree could be easily implemented by deciding the features of each hand shape and testing each in turn. Unlike other techniques which are formed from data obtained with the portable motion capture system, these definitions are purely what would be expected when that hand shape is performed (it assumes the system provides perfect data within the expected hand shapes. The application of a manually implemented decision tree classifier allows for categorisation into known labelled data whilst retaining control of the inner workings of the technique, enabling the customisation and addition of observed features.

This could quickly reveal comparisons between existing grasp taxonomies, where the expected hand shape is know, but would struggle with the identification of new functional hand shapes. With a manual implementation, hand shapes falling outside of the labelled categories could be highlighted, however other analysis techniques would need to be employed to provide a grouping for these. Similar to ANNs and classification algorithms, employment of this technique enables options for preliminary analysis of the collected data and the ability to test these data against previous taxonomies. Thresholds for the descriptors (open and closed) would need to be set, with limited knowledge of an ideal definition. Given labelled training data these thresholds could be learned through a learning process, training and testing the decision tree on a set of labelled control data. This would require training data to be obtained each time a hand shape is added, however refining a decision tree thresholds using this method would improve accuracy and remove a need of human judgement.

In order to form a decision tree manually the following must be determined: a structure running through the decisions, a set of characteristics able to define and differentiate the inputs and a list of hand shapes and their defining characteristics. One possible method of implementation would be to use if statements with minimal to no else statements. The script would evaluate each statement line-by-line and assign a confidence in each hand shape for every input. This would be simple to implement and expand as more hand shapes are considered. Another method, closer resembling a decision tree, would be to group hand shapes similarities and link decisions. This method could be set up to run consecutively through the possible hand shapes but would make the set up and addition of new hand shapes more complex. Joint angles were decided to be the main characteristics used to define each of the possible outcomes of the decision tree, simplified down to just defining whether a digit is open or closed. For the thumb this was found to not be enough, due to the possible flexion and extension and abduction and adduction motions, and, therefore, spatial information of the thumb tip relative to other part of the hand was used

alongside the joint extension. Though increasing the complexity of implementation it was seen as easier than defining hand shapes with the thumb abduction. Multiple methods could be used to define, allowing for vast customisation options - though with a likely increase of the complexity in the creation of the decision tree. To test the manual decision tree capability the control hand shapes were defined by the characteristic aforementioned stated. These were chosen as they closely resemble grasps found in previous taxonomies and as they were being used as controls in other analysis techniques trailed, providing a fair comparable test of the analysis techniques. Table 3.4 shows an example set of the implementation of the 12 control hand shapes within a manual decision tree. In this table the first column describes the hand shape and the following represent the descriptors for implementation of decision tree learning. The abbreviation DNM was used when the position of that digit does not matter. In the occurrence of a tip of one digit being close to another, this was is denoted by stating just the names of those digits.

Table 3.4: The suggested features for defining the previously control hand shapes within a decision tree.

Hand Shape	Thumb	Index	Middle	Ring	Little
2 finger hook	Half open	Half open	Half open	Closed	Closed
2 finger pinch	Index and middle	DNM	DNM	DNM	DNM
3 finger pinch	Index, middle and ring	DNM	DNM	DNM	DNM
4 finger pinch	Index, middle, ring and little	DNM	DNM	DNM	DNM
Closed hook	Half open	Almost closed	Almost closed	Almost closed	Almost closed
Closed pinch	Index	DNM	Closed	Closed	Closed
Open hook	Half open	Half open	Half open	Half open	Half open
Open pinch	Index	DNM	Open	Open	Open
Planar pinch	Straight under fingers	Open	Open	Open	Open
Point	DNM	Open	Closed-Half	Closed-Half	Closed-Half
Rest	Out	Open	Open	Open	Open
Thumb up	Out	Closed	Closed	Closed	Closed

The optimal value for the degrees, defining whether a digit is opened or closed, was determined through the implementation of a PSO and brute-force search. A PSO technique was chosen for fast performance and high accuracy. A brute-force search was attempted due to the known search power. The PSO application was provided lower and upper bounds of zero and 90 degrees, respectively, for both the open and closed values. The full search area was provided to the PSO as the faster computational time display by this method allows for a wider search area.

Though the brute-force search takes a considerable longer computational time, this time was reduced by implementing a two stage search method. To perform this, the brute-force search initially looks within a wide search area with large step sizes between candidate solutions. After which, the search was reduced to an area around the found best performing candidate solution with a smaller step size. This allows for a reduction in the computational time of implementation whilst retaining the search power of the brute-force search. The brute-force search first looked between zero and 45 degrees for the opened value and 45 and 90 degrees for the closed values, both with intervals of five degrees. The results of this were next used to create an input for the second application, taking five degrees above and below the found values and intervals of one degree as the next search input for the brute-force search. This style of training works similarly to a greedy algorithm, with first pass dictating choices for second. As with greedy algorithms, given the limitations imposed on the second search, there could exist a greater solution outside of this search area. This method of training, in this application, has been considered appropriate as it is unlikely that multiple minima exist within the problem.

Though offering some potential with the collected data this analysis technique was not used. The time needed to create the tree with no knowledge the ideal setting makes this method unappealing. Though use could be found as a comparison method for grasps found in existing taxonomies, classification algorithms have been a preference for their ease of implementation and reliable results. Due to the manual implementation of this classifier, customisation is high and defining hand shapes by joints characteristic, rather than the digits, could allow for more accuracy but would increase implementation time. Following an understanding of the collected data through alternative analysis methods, manually created decision trees could be employed to test future datasets or previous collections; the manual editing allows for customisation to specific desires through these assessments.

3.5.8 K-Means Clustering

Clustering algorithms are unsupervised learning techniques, employed to determine classifications within the data with no prior knowledge of potential groupings to be found. For this study a k-means++ algorithm has been utilised. This is a centroid-based clustering algorithm - providing clusters based on the proximity of data points. As the data collected was in Cartesian co-ordinate form, using a proximity measure to cluster these data provides a well suited means of determining trends within these data. The classifications would allow for observations of congruency with previously known hand shapes, validating their existence. Additionally, the aim to ascertain unfamiliar hand shapes of modern ADL from these data indicates the need for an

unsupervised learning technique.

A built-in MATLAB k-means function was used to cluster the data. The ability of this clustering methods was inspected using a collection of control hand shapes. For this, a k value of 12 was used - persuaded by the 12 types of hand shapes that would be expected within these data. Once the clusters had been formed, their centroids could be used to envision how the average hand shape of each cluster would appear. Once validated, the clustering algorithm was confidently implemented with the data collected during ADL.

A k-means++ algorithm was chosen for the computational speed and ease of implementation it demonstrates. Though this algorithm lacks a guarantee of the output accuracy, a custom test can be introduced to ensure a set accuracy is met for the results - exploiting the speed and ease of running multiple k-means++ algorithms in a single run. The k-means++ algorithm is a k-means algorithm with an improved initialisation technique to increase the speed a reliability of the algorithm. To initialise the k-mean++ algorithm randomly selects one point as a single centroid for the data, the squared Euclidean distances between this and all of the other data points are then calculated and the data point with the largest squared distance selected as an additional centroid. Once the initially inputted desired k value is reached the initialisation for a k-means algorithm has been achieved and the k-means algorithm can run. This initialisation process, compared to a randomised initialisation, can increase the computation cost of initialisation, but the subsequent application of the k-means algorithm will converge faster - reducing the overall run time. A more detailed description can be seen in Section 2.6.4. The algorithm has been set up to repeat the clustering 100,000 times, with a new initial cluster centroid each time, and output the attempt with the lowest sum of Euclidean distances between the data points in each cluster and their respective centroids.

To asses the clustering performance under variations to the number of clusters three standard measures have been tested: the Calinski-Harabasz (CH) index, Davies-Bouldin (DB) index and silhouette score. The CH index and silhouette score both provide an indication of how well dispersed and distinguished each cluster is. The DB index shows the similarity between each cluster and that within closest proximity. The combination of each of these methods serves to highlight a optimal number of clusters, to be found from a clustering algorithm implementation. Each of these methods were implemented using the built-in MATLAB function `evalclusters` - specifying the appropriate evaluation method upon each call.

A looping process was created in order to determine an optimal k value for this implementation. The mean distance from all points in cluster to their centroid (mean points-centroid distance) was used as a performance measure of each k value, found

by observing the mean of the Euclidean distance from each joint of each data point within a cluster to their respective centroid point and then taking the mean of all of these. The equation described by (2.5) was used to calculate the Euclidean distance between the pairwise data. A k value would be considered optimal if this result is below threshold of 15 mm and that of the value above it over this threshold. Once the final clustering has been completed the same method was employed to evaluated the resultant clusters.

It was found to be slow when increasing the k value by one each iteration, taking excessively long computational time as the amount of recorded data increased. In an attempt to decrease this time taken a variable k increment was applied. As the clusters were known to be, at least close to, 60 and 30 for the left and right hands, respectively, from previous attempts these where used as the starting values of k. The k increment was set to five until the clustering gave a higher than desired mean points-centroid distance, when it was reduced to two. With a k increment of two the value of k was reduced until the clustering provided a mean points-centroid distance lower than the desired value, from which k was increased by one each iteration until the optimal k value was found. When each iteration was completed the k value was stored in one of two arrays depending on whether the resultant mean points-centroid distance falls higher or lower than the desired value. Both the high and low results were stored, though only low would be necessary as it is not possible for a high variable to be repeat with this set up - storing high could later help during debugging. The changes of k increment were performed by dividing the previous increment by two and taking the floor value, once the desired mean points-centroid distance was passed with a k increment value of one it was known that the previous k value was optimal.

A flowchart depiction of the k value selection process can be seen in Figure 3.15. Within this flowchart, `inc` is the incremental step taken by `k` each iteration, `k` is the number of clusters, `distance` is the mean points-centroid distance and `threshold` preselected threshold value for the mean points-centroid distance. Utilisation of this method to determine the optimal number of clusters provides confidence that the outputted centroids will represent the original data within the set threshold value, allowing control over the information loss when creating the taxonomy of hand shapes.

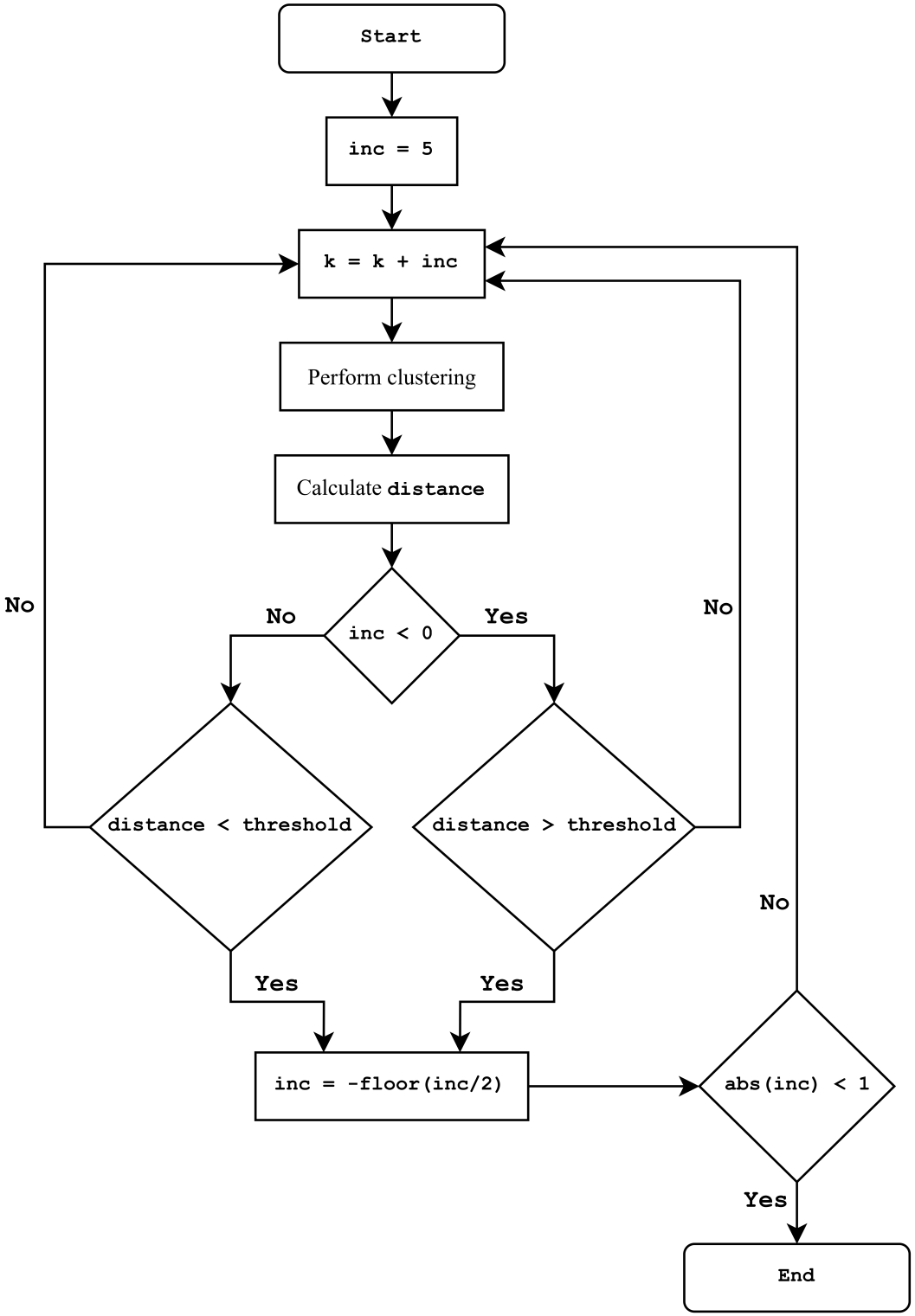

Figure 3.15: A flowchart of the process used to determine the optimal number of clusters for a k-means clustering algorithm.

This was the method used to categorise the common hand shapes found in ADL. Once a predicted hand shape had been assigned for each frame of the collected data, the results were further analysed as described in Section 3.5.10.

3.5.9 Merger of Groupings

Once a machine learning technique has been applied and the data collected grouped, the centroids of these groups provides a taxonomy of hand shapes. Though highlighting many unique functional hand shapes it was found that in reality some of these hand shapes found could be considered the same, leading to redundancies in the taxonomy. The data has been reduced greatly from the many frames collected to a manageable number, from this manual reduction could be performed if desired. To automate this process as well, allowing for the entire analysis to be automated, a merger script was made. This script calculates the Euclidean differences between all of the points for each of the cluster centroids and merges any which would likely appear similar to any observer.

A merger of similar hand shapes was performed, rather than altering the stopping credentials of the k value selection process, in order to preserve the minimal accuracy loss maintained during that procedure. Reviewing Figure 3.13 shows the selected k value, on the grounds shown, provides the best balance of the evaluation values tested. Alterations to the search definitions resulted in a lack of hand shapes being captured within each cluster or a lower explained variation in the clusters found, resulting in significant losses of information in one singular process. On pragmatic grounds, a visual observation of the results from the employed k selection method showed a variation in hand shapes with little repetition - other definitions provided an observable high repetition rate or limitations in the hand shapes captured.

The merger script utilises the calculated Euclidean norm between each point of all of the cluster centroids to assess similarities in the cluster. Initially all of the clusters are repeated using a nested for loop (repeating one to the total number of clusters in two for loops) and the Euclidean norms of each point in the two clusters calculated. If all of these Euclidean norms are found to be below a set threshold these hand shapes would be considered similar and labelled as such. When the clusters compared are the identical cluster the process is skipped to the next without consideration. The labelled clusters are stored within a cell array, with each cell holding the labels of the cluster numbers to be merged together. The merger of hand shapes considered similar would entail: the Cartesian co-ordinates of these hand shapes averaged to form a new merged hand shape, all of hand shapes labelled throughout the original data are relabelled to the new merged hand shape number, their occurrences count combined, the number of frames they occur within combined,

the percentage of functional hand shape frames the hand shape belong to combined and the average frame length recalculated.

A threshold of 30 mm was chosen to imply that two hand shapes would be considered similar, this was decided from several tests comparing the outputs of the merging script with manual reduction. Figure 3.16 shows the results of testing different merger threshold distances on the found clusters. These plots display the results for merger distances of 17 to 55 mm; these were the points at which the merger either had no effect on the founding clusters or grouped all of the hand shapes into one singular cluster, respectively.

Figure 3.16a shows how the intra-cluster distance changes with a varied threshold, calculated by the averaged distances between each data point and their respective centroid. This enables a check that the found clusters still accurately represent the data frames grouped within them, displaying the spread of the original hand shape frames from the respective centroids.

In figure 3.16b the changes of a varied merger threshold on the inter-cluster dispersion are displayed, calculated by the averaged distance of each cluster centroid from all the of the data no captured within that cluster. This measure provides an indication of variation across the clusters, ensuring clusters are unique and that there is low hand shape repetition seen in the final results.

Figure 3.16c indicates the changes in average cluster standard deviation with a varying threshold value, measured by averaging the standard deviations of each of the clusters. This provides another measure of the spread within each cluster, ensuring that the final centroids found are representative of the data within them.

Figure 3.16d displays how the coefficient of determination for the centroids and clustered points alters during threshold variation; this was calculated by taking the average of the correlation of each cluster centroid and each respective point in that cluster and then averaging these results. This highlights the agreement observed within each of the clusters, providing another measure to ensure that similar data remain within the same cluster and that no data are captured in a cluster with too high a disagreement.

The 30 mm threshold was concluded as the best balance of the studied characteristics, displaying inter- and intra-cluster characteristics. With this choice, there still remained a low variation within these resultant groupings, implying only similar hand shapes are captured within each grouping. Additionally, there were large distances across the groupings, showing that the variation of data was not diminished by these groupings and that only similar hand shapes had been grouped. As this measure identifies the amount of available information remaining following the grouping,

there was a lot of weight given to it during the selection of a merger threshold. This highlighted the performance of a 30 mm threshold value. Additionally, increases past this value saw the correlation of the classified hand shapes and respective cluster centroids decrease; the 30 mm choice was still able to keep a high agreement between the clustered data and cluster representatives. Visual analysis supported these findings, showing the removal of repeated hand shapes without unnecessary grouping of hand shapes which were not similar when the merger was applied with a 30 mm threshold value.

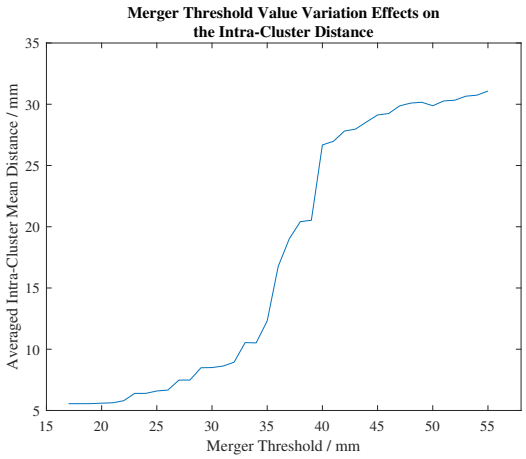

(a) The mean distance between each cluster centroid and the respectively grouped hand shapes, averaged across all clusters found, versus the merger threshold value.

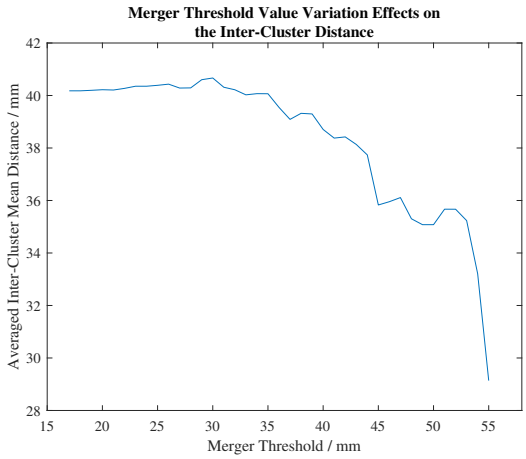

(b) The mean distance between each cluster centroid and the hand shapes of all other groupings, averaged across all clusters found, versus the merger threshold value.

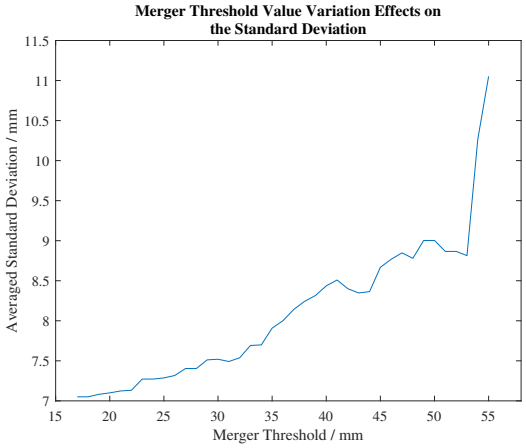

(c) The standard deviation of each cluster, averaged across all clusters found, versus the merger threshold value.

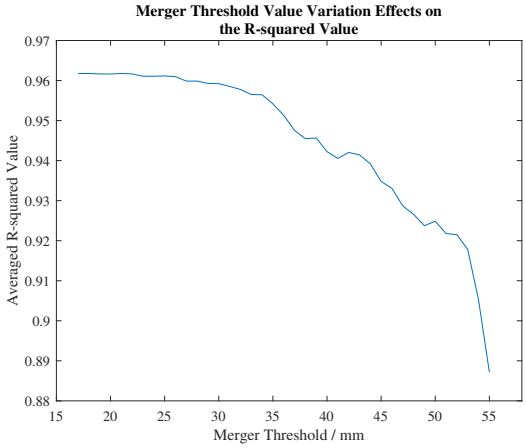

(d) The mean coefficient of determination for each cluster centroid and the respectively grouped hand shapes, averaged across all clusters found, versus the merger threshold value.

Figure 3.16: The observed effects of varying the merger threshold value on the cluster characteristics.

This technique was performed following the k-mean++ clustering of the data collected with the portable motion capture system, producing the finalised taxonomy of functional hand shapes used in ADL. As the resultant data takes an identical structure to the k-means++ output the same evaluation methods and means of displaying the results can be used. This finalised taxonomy of hand shapes would then be visually represented as described in Section 3.5.10.

3.5.10 Displaying Results

Following the application of methods determining the taxonomy it must then be visually represented in an understandable way to create the final taxonomy of hand shapes used in ADL. This was achieved by plotting each point of the centroids graphically. These centroids provided an averaged value for each of the data points for each cluster - therefore describing the common hand shapes found within the data. For each hand shape, the total number of occurrences and the total number of frames it appears for was found. The percentage of the data each hand shape occupies and the number of frames (and, hence, time) each is held for on average can be calculated. This analysis provides an understanding of the importance of each hand shape found in ADL. The amalgamation of the final groupings of hand shapes and analysis of each of these groups results in a functional hand shape taxonomy labelled with key information regarding each of the hand shapes.

The taxonomy was initially represented by wire frame images on the hand, this can be seen in Figure 3.17. This was created by connecting select points of the hand joint co-ordinates in a Cartesian system. As can be seen, in this form the hand shape is difficult to make out from a limited number of 2D images and, therefore, a different method was eventually chosen to display the final taxonomy. One advantage of this display method is the ability to add a scale to the axis, providing a further assessment of the hand shape characteristics during analysis; however, for the purposes of displaying a final taxonomy this does not add any value.

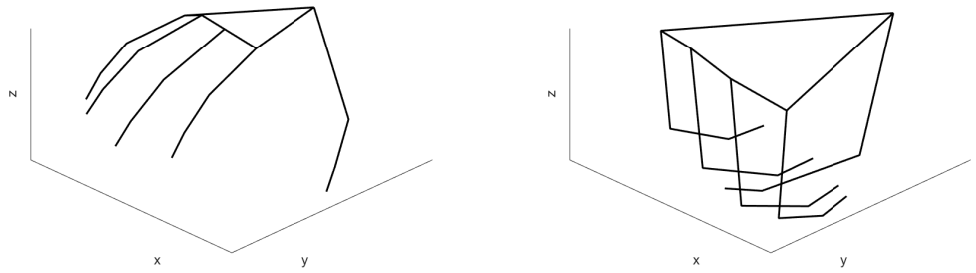

(a) A wire frame image of an opened hand. **(b)** A wire frame image of an closed hand.

Figure 3.17: The original, wire frame style, visual means to displaying the hand shapes within the taxonomy of hand shapes, plotted in MATLAB.

In order to create more visually descriptive images of the hand for the taxonomy Blender was used to render freestyle line art images from a model of the hands. An example of the style used to create the taxonomy can be seen in Figure 3.18. This showed more descriptive capabilities with just a single image and was able to distinguish all hand shapes whilst maintaining a single camera angle. The joint rotations were determined from calculations employing the vector dot product between the adjacent bones, performed using (2.4). To produce these images the joint angles were calculated from the Cartesian locations of the cluster centroids and then inputted into a Python script which rotates each bone of the armature of the Blender hand model accordingly. An image could then be rendered and used a the representing image of that cluster centroid (and, in turn, hand shape) within the final taxonomy.

(a) A line art image of an opened hand. **(b)** A line art image of an closed hand.

Figure 3.18: The final, line art style, visual means to displaying the hand shapes within the taxonomy of hand shapes, rendered in Blender.

Additional data associated with each hand shape within the taxonomy, such as the number of occurrences and average time of each occurrence, are determined

within MATLAB and display within a table.

3.5.11 Evaluation of Analysis

To ensure trust in the results of the analysis performed the outputs must be evaluated. As a k-means++ clustering algorithm, followed by an automated merger of similar hand shapes, has been chosen for the main analysis the final output of these processes was evaluated. Creation of CH, DB and silhouette graphs can be used to determine an acceptable range of k for a k-means++ algorithm prior to implementation. The steps taken to optimise the k values to have a data-centroid differences of below 15 mm ensures the resultant clusters describe the full recorded data within 15 mm. Following clustering and merge, the steps taken to find the data-centroid differences, as well as the R-squared and standard deviations, are tested on the resultant clusters.

The CH index [154], a method commonly employed to determine the optimal number of resultant clusters from an unsupervised learning algorithm, was implemented to provide confidence in the acceptable values of k. The CH index calculates the ratio of the sum of inter-cluster and intra-cluster dispersion to provide an indication of how dense the clusters are and how well separated each is from the others. Alongside this the DB index [155] has also been calculated for varied numbers of clusters. The DB index provides a measure of the similarity between clusters in close proximity, resulting in a measure inversely proportional to the performance of each clustering observed. Additionally, the silhouette score [156] has been taken for the same range of cluster numbers. This score describe how dispersed and clearly distinguished each cluster is, resulting in a measure indicative of clustering performance.

As described in Section 3.5.8, steps have been taken to ensure that a k value with data-centroid differences greater than 15 mm is not used. This keeps the clusters representing the total data within 15 mm despite the large reduction in data obtained during clustering. Following both the k-means++ clustering and merger of these resultant clusters the data-centroid differences, R-squared values and standard deviations of these groupings are found.

The differences measured are calculated identically to that for determining an optimal value of k. The data-centroid difference was calculated by taking the average of averaged pairwise distances between each observation in a cluster and the respective centroid. This provided a clear measure of how dispersed the clusters are and, in turn, how well the centroids formed represent the data collected. Reductions to this measured distance are implicit of a closer representation of all of the hand shapes seen during ADL by the centroid.

The R-squared value is a percentage measure of fit between two variables, dis-

playing how well the observed variables describe each other. Taking the average of this measure per cluster, comparing each observation in a cluster to the respective centroid, shows how well the cluster centroid describes the observations within that cluster. A higher R-squared value would indicate a better agreement between the cluster observations and their respective centroids.

Standard deviation of a dataset shows how dispersed that data are around the mean. Taking the average of the standard deviations of each clusters found provided a measure of how dispersed the observations of a clusters are around their respective centroids. A higher averaged standard deviation would imply the existence of more dispersed clusters, with centroids less representative of the observations made during ADL.

The R-squared values and standard deviations are found through the use of built-in MATLAB functions (`corrcoef` and `std`), from these functions the R-squared values can be calculated by taking the square of the correlation coefficients and the standard deviation is provided directly, respectively. The `corrcoef` function provides the linear correlation coefficients of the columns of the inputted matrices; in this case this is the cluster centroids and all of the hand shapes within that respective cluster. The results of these are then averaged and then squared to find the R-squared value for each cluster. The `std` function returns the standard deviations of the columns of the present array (in this case joint Cartesian locations), here for each frame within the cluster the standard deviation between the joint Cartesian locations and that of the cluster centroids were found and then averaged to find the overall average standard deviation for each cluster. Determining the data-centroid differences provides the knowledge of how accurately the original data are being represented by the groups outputted. The R-squared values and standard deviations, respectively, provide an indication of how closely correlated and how dispersed the clusters are.

3.6 Analysis of Muscle Excitation Techniques

The selected optimisation techniques for predicting muscle excitations from kinematic data were assessed, in order to determine the best for proposed solution. The cost function, given by (3.5), was tailored to each predictive model through alterations to the terms of this equation in order to minimise a tuning cost, set as (3.6). This hyperparameter tuning was achieve by inputting hand shapes with known muscle excitations, displayed in Figure 3.19. To assess the performance of these techniques validation and evaluation methods were employed. To validate each of the methods, for use in the prediction of muscle excitations, the resultant muscle excitations obtained by each, inputting a hand shape with known muscle excitations, were

compared to the known muscle excitations. To evaluate the capability of each method repeated applications were performed for all methods, aiming to identify the method with superior performance, across a multiple applications.

Due to an inability to collect real world data, validation data were created utilising MyoSuite [166]. Within MyoSuite two hand shapes were simulated to provide the validation data: a four finger pinch and point. These hand shapes can be seen reproduced in Figure 3.19; the four finger pinch and point hand shapes being respectively shown by Figures 3.19a and 3.19b. These hand shapes were selected in order to provide a means of validation for the predictions made - demonstrating a sufficient range of joint angle combinations when applied in conjunction with the equilibrium hand shape data. The created data contain the joint angles and muscle excitations for each hand shape, with an identical structure to the requirement from the musculoskeletal model [9].

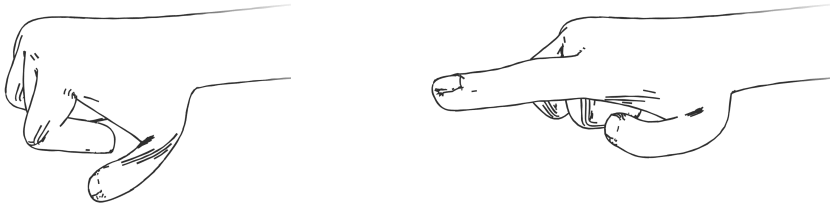

(a) The four finger pinch hand shape created by known muscle excitations within MyoSuite, for the validation of prediction methods.

(b) The pointing hand shape created by known muscle excitations within MyoSuite, for the validation of prediction methods.

Figure 3.19: The hand shapes created within MyoSuite by known muscle excitations, for the validation of prediction methods.

An equilibrium hand shape, with zero muscle excitations, was also tested; these experimental data were provided with the employed musculoskeletal model [9]. Though the zero muscle excitations reduces the complexity of this problem, these data were tested to confirm adequate performance of the predictive methods with respect to the experimental data. To ensure similarities between the simulated and experimental validation data, the equilibrium hand shape muscle excitation data were simulated within MyoSuite. The joint angles outputted from MyoSuite for this set of muscle excitations gave an exact match to those recorded in the equilibrium hand shape data provided with the musculoskeletal model, showing support for this means of simulating validation data. The equilibrium hand shapes, provided and simulated, are presented in Figure 3.20; with Figure 3.20a showing hand shape from the experimental data and Figure 3.20b showing the simulated hand shape.

(a) The hand shape for the equilibrium hand provided with the musculoskeletal model [9], for the validation of prediction methods.

(b) The hand shape for the equilibrium hand created within MyoSuite, for the validation of prediction methods.

Figure 3.20: The hand shapes of the equilibrium hand shape data used during the validation of prediction methods.

In order to determine the method to be highlighted as the proposed solution and, consequently, applied to the data recorded with the portable motion capture system, repeated applications of the same hand shapes were performed for each method. Each of the predictive methods outlined were repeated ten times with inputs of the two validation hand shapes in Figure 3.19. As indicators of performance, the average correlations between the predicted and known muscle excitations and joint angles and the time taken were observed The ranges of these measures were also recorded, in order to highlight the consistency of the predictive methods tested across these applications. By validating and evaluating these methods with data including known muscle excitations, the importance of the resultant angle correlation on the predictive ability of the method can also be observed.

The results of the validation and evaluation of the techniques employed are presented in Section 4.3.

3.7 Analysis of AirGo Clinical Data

Though the accuracy of the AirGo would mostly depend on the validity of the LMC and, hence, the results of the evaluating the portable motion capture system, the results collected during the clinical trial were analysed to assess the capability of the device.

From the clinical data collected two main pieces of information can be extracted and tested: the injured hand and whether the patient has progressed between visits. The injured hand can be predicted from the AirGo output data by comparing the motion possible by each of the joints, the lowest motion indicating the likely injured hand. Comparing this to the known injured hand would provide an indication of

the capability of the device. Progression of hand motion can be observed from patients with multiple recordings from different visits. Though largely an indication of the progression of patients, this will give comfort in using the data from AirGo in progressing sessions with patients.

In order to predict which hand was injured several methods where observed, these were: the summation of all angles, summation of all total active motions (TAMs), summation of the TAMs of the injured digits, observing only the injured joints, the summation of the MCP and PIP for the injured digits only, the MCP for the injured digits only, the summation of all MCP and PIP and the summation of all MCP. When the injured joint was known this was only used to isolate those digits from the hand, comparing that digit from both hands exclusively.

To determine whether progression was made multiple comparison methods have been considered, these were: the summation of the TAMs of the digits for each hand, the summation of TAMs of the digits for the injured digits only, the injured joints exclusively, the MCP and PIP of the injured digits, MCP of the injured digits, MCP and PIP of all digits and the MCP angle of all digits. The use of TAMs shows how the entire hand has performed, thought to indicate an injury hand if one of the hands shows lower mobility. In testing it was seen that it was not able to accurately determine an injured hand, thought to be because varying mobility from other digits masked the injured digit; because of this the injured digits, when know, was isolated and compared. Additionally during validation it was seen that the LMC provided the most accurate readings for proximal joints, for this reason the MCP and PIP joints were also isolated for analysis in both predicting the injured hand and observing progression in patients.

These prediction methods were applied to data separated by patients and trials. When considered on a trial level, simply each trial was observed, independently of the others. When considered on a patient level, the trials for patients with multiple recording were collected and the joint angles, of each recording, were averaged, producing an averaged set of measurements for that patients. If only one trial existed for a patient then only that trial was consulted.

Additional to these, the time taken to determine the joint angles of the patients, compared to the typically used alternative goniometer, can also be observed. There is no possible inter-reader difference as the device is consistently used and required no manual interference for measurements once begun. Consistency (intra-reader differences) of the LMC can be obtained from the validation of portable system.

Chapter 4

Analysis

This chapter discusses the analysis techniques performed, and the results obtained, on the data collected using the portable motion capture system, including validation of the system and evaluation of the final results. Details of the potential techniques considered can be found in Chapter 2. The main analysis technique used to extract a taxonomy of functional hand shapes from the collected data was decided to be the k-means++ algorithm, here detailed steps of the implementation can be seen. The results of the other techniques employed, all of which are outlined within Chapter 3, to extract various useful information have been also displayed and discussed here. Following implementation of the techniques selected, a modern taxonomy of hand shapes can be introduced. A significant advantage of capturing quantitative hand motion data, rather than video recordings, is that the collected data can be later analysed autonomously using machine learning algorithms. This process is quicker and, once sufficiently trained, can be more reliable than a human watching back a video to manually assign the hand shapes performed in each frame. To detect when a certain functional hand shape is performed, positional data transformed to a local co-ordinate system has been used. The data are considered only within this local co-ordinate system, as the spatial location of the hand has no relevance - it is the shape of the hand which prerequisites the desired information. The resultant taxonomy of this can be seen displayed and discussed in Chapter 5. The results of the validation and evaluation performed for the application of various optimisation techniques within a muscle excitation prediction model has been provided. Additional to this analysis, the outputs of a clinical trial performed to evaluate the performance of AirGo have been presented and reviewed. Further details on the deployment of each of these studies can be seen, respectively, in Chapters 6 and 7.

4.1 Analysis of Portable Motion Capture System Validation Data

Validation data for the portable motion capture system, utilising a Vicon motion capture studio, has been collected following the procedure outline in Section 3.4. The hand shapes observed during validation are shown in Figure 3.7. This collected data has been compared within MATLAB in order to observe any error formed from the use of the portable motion capture system and Leap Motion controller (LMC). The process undertaken to complete the validation is as shown in Section 3.2. Both the angles and distances of the two systems were compared and these comparisons can be in Tables 4.1 and 4.2, respectively. Table 4.3 shows the correlations between the joint positional co-ordinates recorded by the two systems. For each of the measurements made, the average, minimum and maximum values have been given - providing indications of the central tendency and spread of the obtained results.

The distances between the Cartesian co-ordinates was calculated by the Euclidean norm, described by (2.5), and the joint angles were found by utilising the vector dot product, shown by (2.4), of two adjacent bones. Analysis was performed in the local co-ordinate system, with data scaled to provide equivalent fixed feature points. When calculating the difference in positional distances, the metacarpophalangeal (MCP) was not considered as this was used as an anchor for local co-ordinate system and scaling and, therefore, was the same for both recordings. Though this validation was performed with the portable system, the results also validation for the LMC and, hence, can be used as validation for the AirGo device.

The overall positional difference between the two systems was calculated from the mean of the absolute of the difference between each equivalent point x, y and z value from the LMC and Vicon system. This difference was found to be 14.2 mm.

Other observed differences in the positional recordings can be seen in Table 4.1. Within this table are the pairwise distance differences between the two recording systems for the proximal interphalangeal (PIP) joint, distal interphalangeal (DIP) joint and tip of the digit and each of the digits for each of the recorded control hand shapes. The digits have been labelled one to five, one representing the thumb and five representing the little finger. Observing the average difference of the joints highlights a clear trend of the error increasing with more distal joints - indicating that more confidence should be placed on the locations of joints more proximal in data collected with this system. It can be seen that the thumb exhibits the largest error out of the digits and that the index finger showed the lowest error, this lower accuracy of the thumb positional measurements should be considered when conclusions are drawn from collected data.

Table 4.1: The positional errors, in millimetres, observed during validation of the portable motion capture system against a state-of-the-art motion capture studio.

Hand Shape	Total Difference		Joint						Digit									
			PIP		DIP		tip		1		2		3		4		5	
	Av.	Min. Max.	Av.	Min. Max.	Av.	Min. Max.	Av.	Min. Max.	Av.	Min. Max.	Av.	Min. Max.	Av.	Min. Max.	Av.	Min. Max.	Av.	Min. Max.
Two Finger Hook	11.4	11.0 11.7	8.92	8.72 9.16	10.9	9.78 11.6	14.4	14.1 14.7	21.2	19.7 24.0	5.96	4.94 7.70	13.2	12.2 14.1	8.93	8.71 9.10	7.72	7.45 7.86
Two Finger Pinch	15.2	11.6 19.1	11.7	8.43 15.1	14.8	11.0 18.7	19.2	15.4 23.4	19.5	18.8 21.0	11.1	9.52 14.1	20.8	16.1 28.3	14.8	8.42 19.0	9.77	5.13 13.0
Three Finger Pinch	14.2	12.0 18.4	10.1	8.71 12.7	14.3	11.9 18.9	18.3	15.5 23.7	19.8	18.6 20.9	10.9	8.60 13.6	15.7	11.7 22.4	17.4	11.4 27.6	7.17	5.44 8.49
Four Finger Pinch	14.3	11.9 18.1	9.93	8.00 12.9	14.1	11.7 18.3	18.8	16.1 23.0	19.9	18.5 21.0	11.5	7.25 16.0	15.4	12.2 19.6	14.8	7.86 23.3	9.78	5.11 16.1
Closed Hook	13.4	12.2 14.2	9.51	8.81 10.2	13.9	12.5 14.8	16.8	14.7 17.9	23.7	21.4 27.7	12.7	10.5 14.8	12.0	9.50 13.8	10.1	7.90 12.7	8.56	6.83 10.4
Closed Pinch	14.4	13.8 15.0	12.9	12.5 13.6	14.9	14.1 15.6	15.5	14.7 16.3	17.8	17.4 18.1	9.42	8.20 11.3	15.8	14.5 17.0	14.6	13.8 15.9	14.5	13.4 16.1
Open Hook	17.1	15.0 18.7	10.9	10.1 11.5	17.0	14.5 18.9	23.3	20.2 25.8	22.6	21.2 23.7	10.9	10.2 12.1	17.6	14.3 20.5	19.2	15.4 22.5	15.0	11.0 17.3
Open Pinch	15.8	14.9 17.4	11.7	10.9 12.9	15.9	15.0 17.7	19.8	18.9 21.5	20.3	18.2 23.5	11.5	7.42 14.6	21.1	20.5 22.2	15.9	14.2 17.2	10.3	9.59 11.1
Planar Pinch	9.79	7.62 11.7	8.24	7.06 9.08	9.41	6.92 11.4	11.7	8.89 14.5	15.3	14.7 15.8	4.75	2.99 6.17	10.9	5.99 14.9	11.1	6.72 14.4	6.88	3.91 9.19
Point	11.9	10.9 13.3	10.8	10.2 12.0	11.7	9.74 13.6	13.1	12.4 14.3	22.7	21.0 26.0	4.33	3.33 5.77	10.5	9.61 12.0	9.40	8.99 9.91	12.5	10.5 14.9
Rest	11.5	9.87 13.1	8.37	7.79 8.70	11.2	9.47 12.8	14.9	12.3 17.8	15.7	12.9 19.9	7.10	3.82 10.2	13.3	11.2 15.1	11.8	10.6 12.8	9.57	9.48 9.71
Thumb Up	21.7	15.3 32.3	14.9	12.0 20.9	22.4	15.3 33.7	27.9	18.8 42.2	22.0	19.2 23.5	18.7	11.8 31.2	25.0	15.1 39.0	23.9	14.9 37.5	19.2	11.7 30.1
Average	14.2		10.7		14.2		17.8		20.0		9.91		15.9		14.3		10.9	

The overall angular difference between the two systems was calculated from the mean of the absolute of the difference in the angles of each equivalent point from the LMC and Vicon. This difference was found to be 18.4 degrees.

The observed differences in the angles measured can be seen in Table 4.2. Within this table are the pairwise angular differences between the two recording systems for the MCP, PIP and DIP joints of the digit and each of the digits for each of the control hand shapes. The digits have been labelled with one to five, one representing the thumb and five representing the little finger. Despite the lower error observed in joints more proximal during consideration of the error in the Cartesian locations, measurements of the joint angles indicated a superior performance from the PIP joints over the MCP joints. This greater error displayed by the MCP jointed could be argued to be a result of the greater degrees of freedom (DoF) this joint exhibits - positional measurements would have been affected by abduction and adduction, whereas the observed joint angle only considered the flexion and extension of the joints. Similarly to the Cartesian differences analysis, the index finger was the digit which exhibited the lowest error. Though there was little range in the errors of the other digits it should be noted that the thumb showed the second lowest error when the joint angles were measured. These results should be consulted when joint angles measurements are taken with an LMC.

Table 4.2: The joint angle errors, in degrees, observed during validation of the portable motion capture system against a state-of-the-art motion capture studio.

Hand Shape	Total Difference		Joint						Digit									
			MCP		PIP		DIP		1		2		3		4		5	
	Av.	Min. Max.	Av.	Min. Max.	Av.	Min. Max.	Av.	Min. Max.	Av.	Min. Max.	Av.	Min. Max.	Av.	Min. Max.	Av.	Min. Max.	Av.	Min. Max.
Two Finger Hook	13.8	12.2 15.3	9.03	7.43 11.0	14.8	12.4 19.7	17.4	16.8 17.9	11.3	10.4 12.3	13.0	10.6 17.3	10.5	9.55 12.0	15.1	11.9 20.3	18.9	15.9 24.3
Two Finger Pinch	20.6	13.0 27.8	22.3	10.6 32.9	19.3	14.8 23.5	20.6	13.9 28.4	10.3	7.72 12.9	22.3	14.6 31.5	31.0	23.3 40.0	21.0	10.7 27.9	18.5	6.40 27.7
Three Finger Pinch	12.7	10.4 16.7	15.5	11.1 23.0	11.9	9.48 15.1	10.7	9.08 12.1	15.4	15.2 15.8	10.8	7.86 14.9	13.2	8.46 19.8	15.1	9.09 24.0	9.17	6.82 11.2
Four Finger Pinch	18.6	15.1 22.8	16.0	9.32 27.4	21.7	18.1 26.3	18.1	15.4 22.7	18.9	17.1 21.0	16.6	10.9 20.0	16.3	8.00 25.8	20.0	9.19 27.6	21.4	14.1 26.3
Closed Hook	20.1	19.0 22.2	12.4	11.3 14.4	21.3	19.6 22.6	26.4	23.1 32.5	34.1	25.0 43.0	15.4	11.5 20.9	13.8	12.5 16.4	18.7	15.6 24.5	18.6	14.2 22.3
Closed Pinch	20.3	20.0 20.5	23.5	22.7 24.3	12.0	11.2 12.9	25.1	23.6 26.5	11.4	11.2 11.6	14.6	12.6 16.9	22.0	20.1 24.1	23.6	22.5 25.2	29.1	28.3 29.8
Open Hook	19.5	19.2 20.2	24.3	21.2 26.3	13.7	12.9 14.9	20.4	15.4 23.8	10.8	10.0 11.3	23.3	18.2 26.9	21.5	19.9 22.4	21.0	19.9 22.3	21.0	15.6 25.5
Open Pinch	19.5	17.2 21.9	29.7	27.7 32.9	12.9	10.1 15.7	16.0	13.9 17.2	18.8	17.1 21.5	16.0	10.8 19.3	27.9	22.6 33.2	19.5	17.9 22.5	15.4	14.7 16.9
Planar Pinch	15.3	12.0 19.5	17.2	11.9 21.8	14.4	13.0 15.8	14.7	4.96 30.7	31.9	19.2 55.6	9.10	7.02 12.7	11.6	7.67 16.2	13.3	11.4 16.6	10.9	9.34 13.4
Point	17.6	15.8 19.5	14.1	12.4 16.6	16.3	14.5 19.5	22.4	19.5 26.7	19.3	17.8 21.8	7.18	5.69 8.86	22.4	18.3 29.5	20.5	16.3 27.7	18.4	16.2 20.9
Rest	16.4	15.2 18.2	22.5	19.9 24.1	13.3	9.44 16.0	13.3	7.42 20.0	20.3	19.2 22.4	11.9	9.84 14.3	19.1	14.0 24.1	16.0	14.4 18.5	14.2	12.7 15.3
Thumb Up	26.4	21.8 35.4	31.1	18.8 52.9	32.5	29.3 37.3	15.4	13.4 17.0	23.1	20.9 24.8	19.7	9.42 35.5	24.2	15.3 38.4	32.4	27.7 39.7	31.1	27.2 36.6
Average	18.4		19.8		17.0		18.4		18.8		15.0		19.5		19.7		18.9	

The overall correlation between the two systems was calculated from the mean of the correlations found between each recorded joint location from the LMC and Vicon. This correlation was found to be 0.92.

The observed correlations between both capture systems can be seen in Table 4.3. Within this table are the correlations between the two recording systems for the PIP and DIP joints and tip of the digit and each of the digits for each of the control hand shapes. The digits have been labelled with one to five, one representing the thumb and five representing the little finger. As would be expected, the majority of the correlations exhibited the same patterns as was seen in the Cartesian errors; more proximal joint displayed a higher correlation and the index finger exhibited the highest correlation of the digits. One difference was the high correlation calculated for the thumb, contrasting the high error seen when observing the Cartesian distance error but agreeing with the results of joint angle comparisons.

Table 4.3: The correlations observed during validation of the portable motion capture system against a state-of-the-art motion capture studio.

Hand Shape	Total Difference		Joint						Digit									
			PIP		DIP		tip		1		2		3		4		5	
	Av.	Min. Max.	Av.	Min. Max.	Av.	Min. Max.	Av.	Min. Max.	Av.	Min. Max.	Av.	Min. Max.	Av.	Min. Max.	Av.	Min. Max.	Av.	Min. Max.
Two Finger Hook	0.95	0.95 0.96	0.97	0.97 0.97	0.96	0.96 0.97	0.91	0.91 0.92	0.96	0.96 0.97	1.00	0.99 1.00	0.97	0.97 0.98	0.79	0.77 0.82	0.68	0.57 0.77
Two Finger Pinch	0.90	0.84 0.94	0.93	0.89 0.95	0.87	0.79 0.92	0.80	0.68 0.87	0.95	0.93 0.96	0.96	0.92 0.99	0.67	0.47 0.80	0.88	0.84 0.94	0.96	0.91 0.99
Three Finger Pinch	0.90	0.84 0.93	0.94	0.92 0.95	0.87	0.79 0.92	0.78	0.64 0.85	0.91	0.88 0.95	0.98	0.96 0.99	0.83	0.69 0.91	0.63	0.54 0.72	0.99	0.99 1.00
Four Finger Pinch	0.89	0.85 0.93	0.95	0.93 0.95	0.87	0.78 0.92	0.64	0.50 0.77	0.88	0.85 0.90	0.97	0.96 0.99	0.86	0.78 0.93	0.68	0.47 0.85	0.82	0.74 0.89
Closed Hook	0.89	0.88 0.91	0.94	0.93 0.95	0.86	0.84 0.88	0.65	0.59 0.73	0.89	0.89 0.91	0.98	0.96 0.99	0.90	0.85 0.95	0.75	0.65 0.83	0.58	0.47 0.67
Closed Pinch	0.93	0.92 0.94	0.90	0.89 0.91	0.95	0.93 0.95	0.94	0.90 0.97	0.98	0.98 0.98	0.98	0.97 0.99	0.91	0.87 0.94	0.77	0.76 0.78	0.57	0.54 0.61
Open Hook	0.92	0.90 0.94	0.97	0.96 0.97	0.92	0.90 0.95	0.81	0.77 0.85	0.97	0.96 0.97	0.99	0.97 0.99	0.93	0.90 0.95	0.83	0.79 0.86	0.87	0.85 0.91
Open Pinch	0.92	0.91 0.94	0.95	0.95 0.96	0.94	0.93 0.95	0.93	0.91 0.95	0.94	0.92 0.95	0.95	0.94 0.98	0.93	0.92 0.94	0.96	0.95 0.97	0.97	0.96 0.98
Planar Pinch	0.97	0.96 0.98	0.97	0.96 0.97	0.97	0.97 0.98	0.97	0.96 0.97	0.94	0.94 0.95	0.99	0.99 1.00	0.99	0.97 1.00	0.98	0.97 0.99	0.99	0.99 1.00
Point	0.95	0.94 0.96	0.95	0.93 0.96	0.96	0.96 0.96	0.94	0.93 0.95	0.98	0.97 0.99	0.99	0.98 1.00	0.94	0.92 0.96	0.86	0.78 0.91	0.61	0.60 0.62
Rest	0.97	0.96 0.98	0.98	0.98 0.98	0.98	0.98 0.98	0.97	0.97 0.98	0.98	0.98 0.98	0.99	0.98 1.00	0.98	0.98 0.99	0.98	0.97 0.99	0.98	0.98 0.99
Thumb Up	0.78	0.63 0.88	0.88	0.79 0.92	0.73	0.55 0.85	0.72	0.67 0.77	0.97	0.96 0.98	0.87	0.68 0.98	0.72	0.56 0.84	0.52	0.24 0.74	0.17	0.03 0.29
Average	0.92		0.94		0.91		0.84		0.95		0.97		0.88		0.80		0.77	

The observed errors highlight the limitations of the LMC, but the results are able to support the claims of many authors [104, 111–116] that the LMC can provide clinically viable data. Across all of the adopted hand shapes, the system was able to provide a high correlation; this establishes confidence in this data collection method. The performed validation highlights digits and joints to be taken with confidence or avoided to maintain a high accuracy of results. Caution should be exercised when assessing the joint angles of distal joint and the thumb joint positions following collection with this system.

The evaluated system, an Intel Next Unit of Computing (NUC) powered by an external battery, does not provide the ideal conditions for the LMC. It is assumed that if this experiment was to be repeated with LMC data extracted employing a desktop computer, then greater agreement between the two collection methods would be found. Though efforts were taken to match the marker positions of the Vicon system with the recorded points of the LMC, this has likely been a source of error, particularly as the physical markers could drift throughout the recordings. Several recordings were taken and the markers were checked and, if needed, realigned between recordings to reduce this influence as much as possible.

4.2 Analysis of Activities of Daily Living Recordings

Following the collection of hand motions during activities of daily living (ADL), analysis was performed to filter and segregate functional hand shape occurrences and transitional frames, determine correlations in joint angles, observe variation in activity from the joints, determine hand shapes commonly found within these recordings and evaluate these found hand shapes. A significant advantage of a data collection method which captures the 3D positional data of the hand, rather than a video recording, is that the numerical data recorded can be later analysed autonomously using basic machine learning techniques. This process is quicker and more reliable than a human watching back a video to decide when specific hand shapes are used.

To determine the capabilities to discriminate hand shapes, machine learning techniques considered were tested with recordings of the control hand shapes shown in Figure 3.7. Recordings of the control hand shapes were randomly permutated and divided into training and testing data (with a 80:20 training:testing ratio). This collated data contained 32,589 performed hand shapes - providing 26,071 training hand shapes and 6,518 testing hand shapes. All of the analysis of the portable motion capture system collected data was performed using MATLAB R2020b (9.9.0.1467703) on a computer with Windows 10, 32 GB random access memory (RAM) and an Intel

Core i7-7700 processor and as described in Section 3.5.

A preliminary analysis was performed after recording hand motions for 13 participants and used to support analysis choices going forward. The results of the preliminary analysis, including the patient data, resultant taxonomy of hand shapes and hand shape characteristics, can be seen in Appendix B.

4.2.1 Determining Functional Hand Shape Occurrences

Data were reduced following the steps explained in Section 3.5.1. From the initial collection of 20,188,273 frames, 1,877,430 and 1,353,969 frames were considered functional hand shape frames, for the left and right hands respectively. Following the averaging of each occurrence of a functional hand shape, the functional hand shape frames where reduced to 1,237 and 662 averaged hand shape frames, prepared as an input for clustering, for the left and right hands respectively.

A total time of 22 hours 53 minutes and ten seconds was taken to load and process the 111 hours and 20 minutes of recordings. This time was comprised of, per hand per recording: loading the data into MATLAB, removing the frames which the hand of interest is not seen in, labelling each of the remaining frames as a functional hand shape or transition frame, transforming these functional hand shapes into a local reference frame and calculating the averaged Cartesian joint locations for each of the functional hand shape occurrences. It should be noted that a large amount of this time was taken loading the data; once the raw data had been loaded and processed they were saved as MATLAB variables, to later be loaded in more rapidly for analysis. The analysis of the data, exclusively, took 52 seconds; this was considered as reloading the variables, clustering the data, merging the data and determining characteristics of the data. This was all performed on a computer with Windows 10, 32 GB RAM and an Intel Core i7-7700 processor running MATLAB R2020b (9.9.0.1467703). It should also be noted that this can be executed without the need of a human present, once told the data location the script performs the aforementioned tasks independently.

4.2.2 Principal Component Analysis

A principal component analysis (PCA) was applied in an attempt to reduce the number of dimensions of the collected data. After centring the data on the origin, PCA determines perpendicular axes through the data which provide the largest sum of squared distances of the data point projected onto the created axes - these axes become the principle components. For the collected data PCA was applied to the recorded Cartesian positions and calculated joint angles. The steps taken

were as described in Section 3.5.2. To asses the reductions, reasonably, possible with the application of PCA a scree plot and loading plot were created. Scree plots visualise the eigenvalues of the principle components in order to indicate the number of principle components needed. Loading plots display the loadings of each original variable along the principle components. The loading for each of the original dimension is calculated from the product of the eigenvectors and square of eigenvalue for that dimension. A loading plot highlights trends within the data and conveys the influence of original dimensions on the principle components. Further description around the techniques used is given within Section 2.5.

The resultant scree plots for the both hands, following the implementation of a PCA with the joint angles of the collect hand motions can be seen in Figure 4.1. The loading plots for this implementation are shown in Figure 4.2. This same analysis applied to the Cartesian data is provided within Appendix C. The score plots of both datasets, of Cartesian and joint angle data, were unable to present clear information due to the vast amount of continuous observations collected.

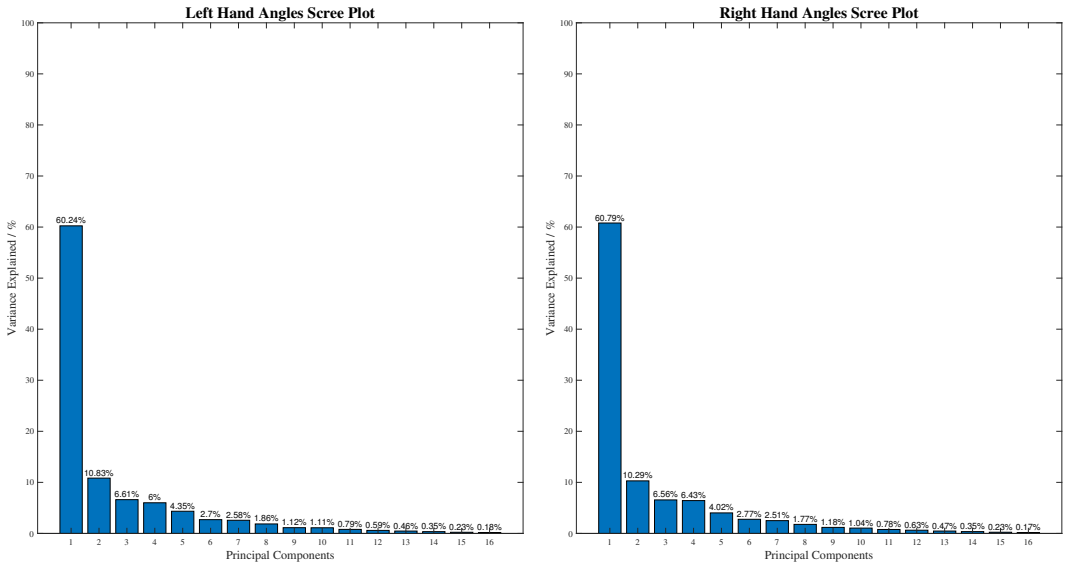

(a) A scree plot for the joint angles of the left hand.

(b) A scree plot for the joint angles of the right hand.

Figure 4.1: The scree plots from a principal component analysis evaluation of the joint angles from the collected data.

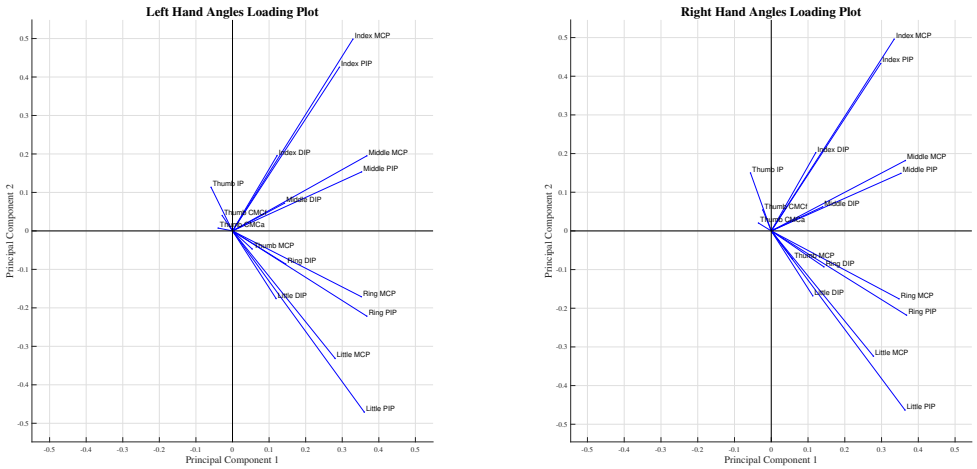

(a) A loading plot for the joint angles of the left hand.

(b) A loading plot for the joint angles of the right hand.

Figure 4.2: The loading plots from a principal component analysis evaluation of the joint angles from the collected data.

The first principle component provided 60.2% and 60.8% of the variation of the collected data, an unsuitable signifiant loss of data, for the left and right hand respectively. Observing the scree plot identifies that three principle component were able to retain 77.7% and 77.6% variation of the data, for the left and right hand respectively. Employment of this ascertained information could aid in the reduction of computational complexity during analysis, though result in a partial loss in recorded information. From the loading plots presented for each hand, it can be seen that all of the joints on each digit, bar the thumb, tend to show a positive correlation to each other. Furthering this it can be deduced that the index and middle and ring and little digits show a positive correlation to each other but exhibit a low correlation between these two groups. Though the score plots were unable to present any relevant data, the scree and loading plots still provided an insight into possible reductions for clustering and the correlations of the hand joint angles.

4.2.3 Joint Angle Correlations

Determining any correlations in the joints as they move during ADL would aid the design of upper-limb prostheses, highlighting any possible linkages in actuation strategies. If two or more joints were seen to move in cohesion then their actuation could be linked, saving the cost of components and the complexity in the actuation script. The recordings of the control hand shapes shown in Figure 3.7 were used to validate the possible application of this method. Following confirmation in the

potential of this method, it was applied to the hand motion recordings from ADL. The steps taken were as described in Section 3.5.4. Further description around the techniques used given in Section 2.5.

Matrices of scatter plots drawing comparisons of each joint from the recorded data collected during ADL can be seen in Figures 4.3 and 4.4. From these plots the the correlations between hand joints during ADL are displayed. This was achieved through the MATLAB function `plotmatrix`. This function creates a matrix of subplots containing scatter plots of each of the dimensions against one another; this additionally place histogram plots for each of the dimensions in the respective columns along the matrix diagonal. Along the rows and columns are the hand joints, with each matrix element displaying a plot of the recorded respective joint angles; a single point on a plot representing the angle of each joint at a given frame.

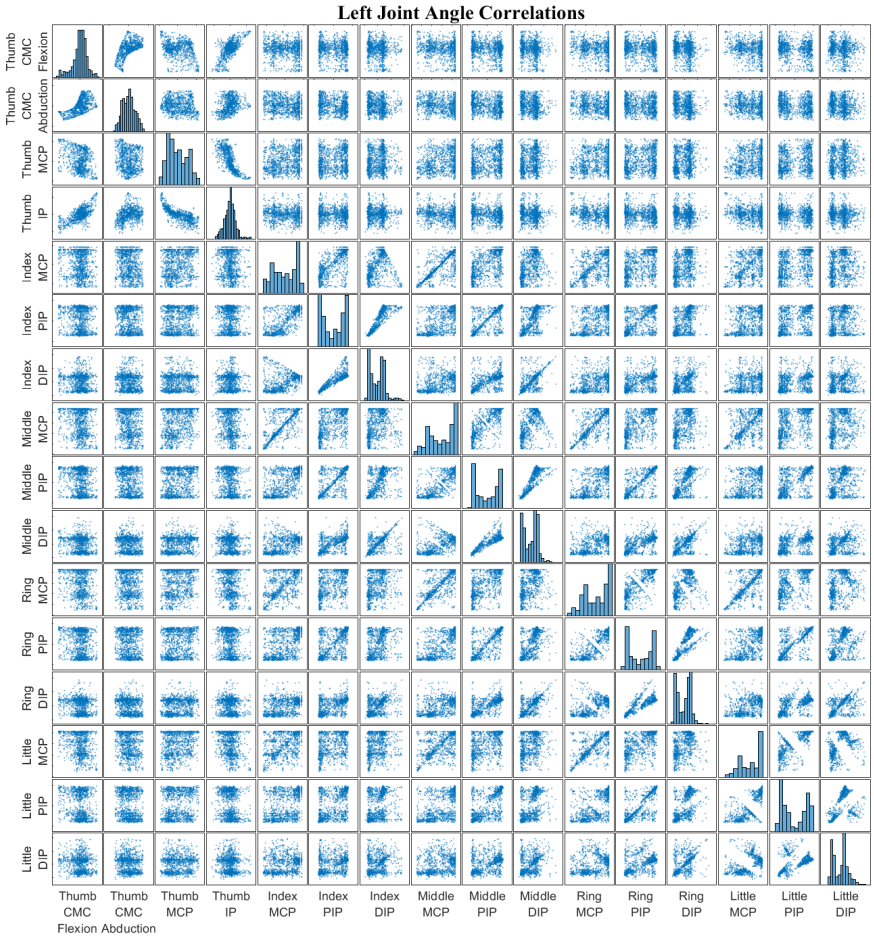

Figure 4.3: The joint angles correlations for the left hand from the collected data.

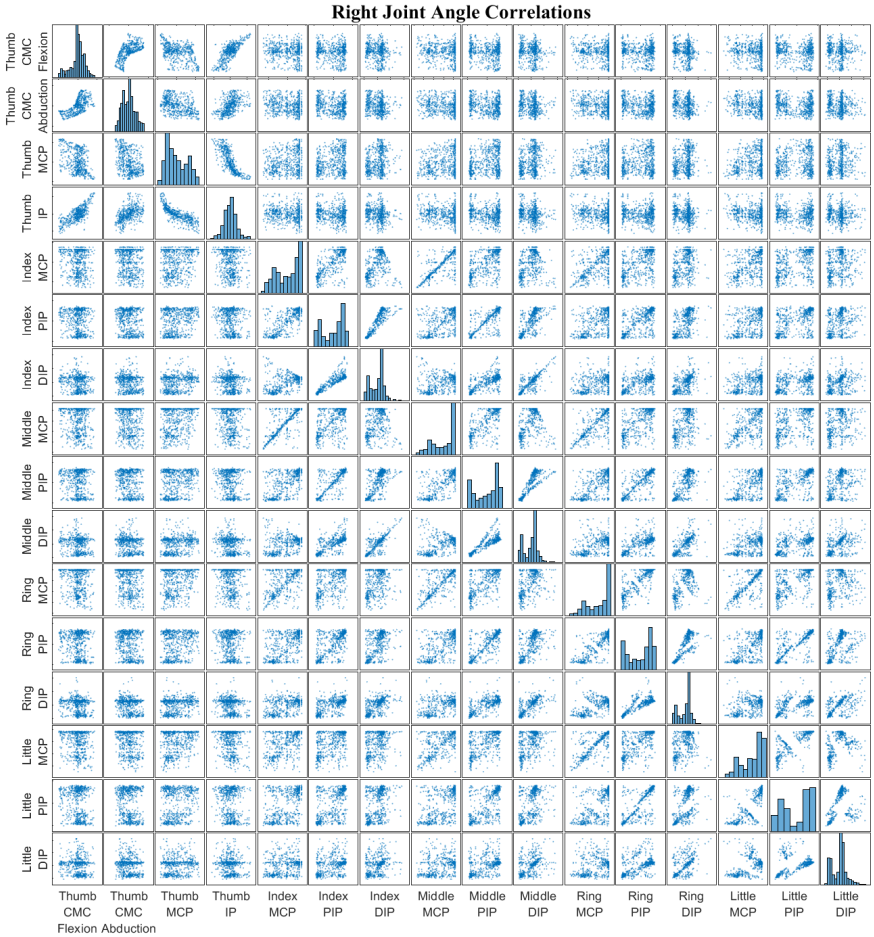

Figure 4.4: The joint angles correlations for the right hand from the collected data.

Of significant note from the left hand is the correlations between the MCP and PIP for the middle, ring and little fingers, which all displayed a correlation coefficient greater than 0.8. These positive extremities of correlation coefficients is likely to be indicative of a common motion exhibited between these joints. The MCP and PIP joints of index finger displayed a close to 0.8 positive correlation for the left hand and over 0.8 for the right hand, implying this high correlation exists between the MCP and PIP joints in motion. Additional to these high positive correlations, on the right hand both the PIP and MCP joint for the ring and little finger each displayed a correlation greater than 0.8. It is arguable that this high positive correlation is implicit of a constraint between these joints. From these plots, it can also be seen that there is a strong relationship between the DIP and PIP joints. This can be seen on both hands and is more pronounced in the first and second digits. These findings agree with the claims that there exists correlations between the DIP and PIP joints, widely supported within the literature [193–195]. This analysis highlights correlations of the hand digits, for consideration in attempts to replicate the hand motions.

4.2.4 Joint and Digit Activity

A practically useful piece of information that could be extracted from the collected data is the comparative activity exhibited by each of the joint during ADL. This has the potential to highlight any possible redundancies to actuation strategies. If a joint is found to have not moved or moved very little it could be made redundant in actuation, removing a need of a component to actuate it and the extra computational complexity of the inclusion. Oppositely, if a joint is shown to experience an abundance of activations during ADL, support for a greater focus to be given to this joint would be provided. This exploration of joint activity was applied the entirety of the data collected during ADL, in order to provide information for the development of upper-limb prostheses. The steps taken were as described in Section 3.5.4. Further description around the techniques used has been provided within Section 2.5.

The extracted joint activities, from the raw data collected during ADL, can be observed in Figures 4.5 and 4.6. A threshold was selected to provide clarity to joint activities, enabling a clear identification of joint which are more active through ADL. Reducing the threshold such that the activity of the thumb carpometacarpal (CMC) and MCP was registered resulted in saturation of the other joint activities. However, observing the thumb CMC and MCP joints activities would provide insightful information. For this reason, bar chart presenting joint activity calculations with a lower threshold have been included within Appendix C.

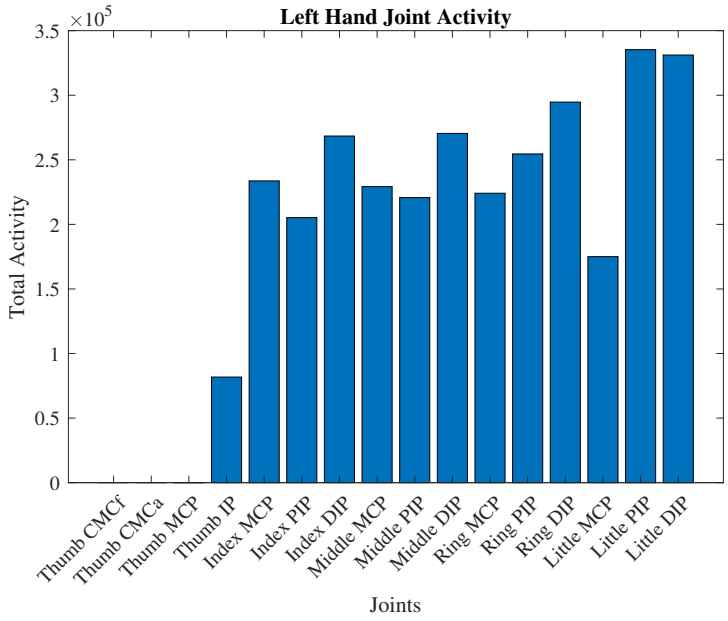

Figure 4.5: The joint activity seen for each joint on the left during data collection.

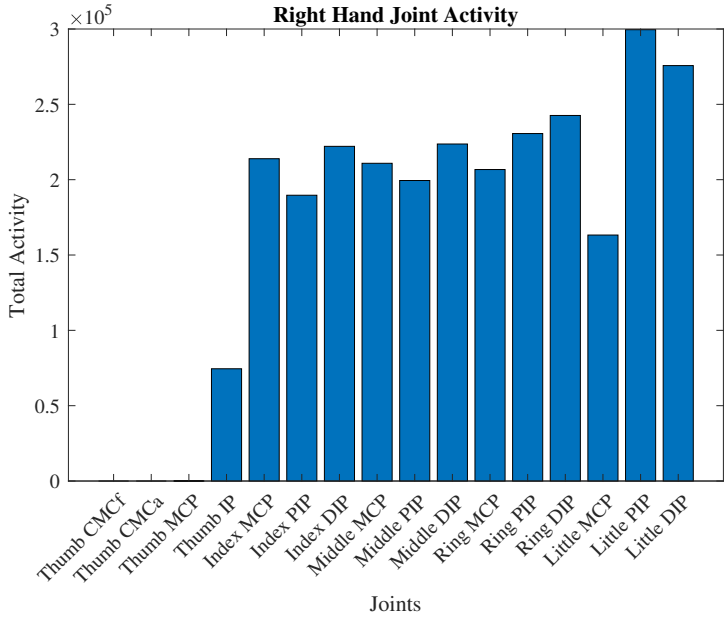

Figure 4.6: The joint activity seen for each joint on the right during data collection.

Immediately from the presented figures, it can be seen that the thumb exhibits comparatively little motion throughout ADL. This suggests a possible redundancy of the actuation of thumb joints. Of the other joints, there was no significant difference

across the activity of each joint, though the MCP little finger did display a noticeable lower activity than the others. It can been seen that both hands present identical patterns in the activities of their joints, suggesting that an actuation strategy for either hand would present the same results if applied to the other.

During validation of the portable system it was observed that the thumb typically exhibited a greater positional error than the other digits. This error could contribute to the lower activity seen though is unlikely to have a significant effect, as this error was not considerably higher than that of the other digits. For the selected threshold for activity, slight activity was seen in the thumb interphalangeal (IP) joint, supporting the influence of the error due to proximal joints typically displaying a lower positional error during validation. It could be argued that the lower activity and greater error seen by the distal joint of the thumb, during observations of joint activity and validation, could be caused by the LMC not registering the motion of the thumb CMC and MCP joints as effectively, resulting in the device assuming they remain stationary.

4.2.5 Artificial Neural Networks

An artificial neural network (ANN) is a, supervised, reinforced learning technique which learn through methods mimicking neural behaviour. They are a supervised learning technique, trained with labelled data to predict classifications of unlabelled data. The exact inner workings of this predictive model are typically not known, evolved through repetitive modification made by reinforcement learning. An ANN is made up of, typically, several layers of neurons connected by synapses and learn through adjustments to weights along the synapses and bias designed in into the neurons. The steps taken to implement this with hand motion data were as described in Section 3.5.5. In order to evaluate the performance of this method confusion matrices were used. A confusion matrix shows the predicted against the actual categories for labelled data within a matrix plot; the diagonal presents the correct predictions, with any data outside of this highlighting misclassification of observations. Further description around the techniques used has been given in Section 2.6.1.

GoogLeNet is a complex, well established and highly accurate ANN for image classification. In an attempt to capture this accuracy for the classification of hand shapes in motion capture data, GoogLeNet has been employed. For this the training data were converted into images and divided 70%:30% (train:validate). Within the first epoch the network achieved a prediction accuracy close to 100% and maintains this high level of accuracy for the remainder of the training. The resultant confusion matrix from the application of GoogLeNet with the test images of the control hand shapes can be seen in Figure 4.7. It took 45 hours and 39 minutes to create the

32,589 images for training and testing. After data conversion, it took 51 minutes to train the network and one minute and 40 seconds to then make the predictions for the test dataset.

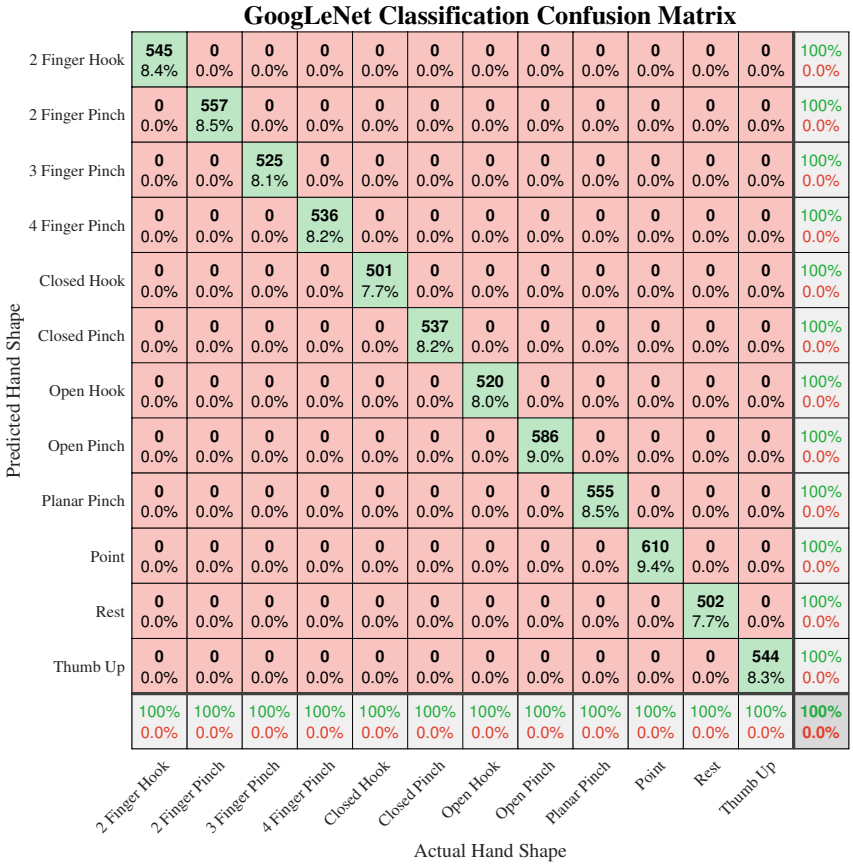

Figure 4.7: A confusion matrix from the implementation of GoogLeNet with images of the control hand shapes.

A bespoke ANN, designed to receive an input of the Cartesian hand motion data, was also trained and tested with these same datasets. This was created using the `feedforwardnet` function in MATLAB and, subsequently, trained with `train`, in an attempt to provide faster classifications than GoogLeNet with a similar level of accuracy. The confusion matrix from inputting the test dataset into this ANN can be seen in Figure 4.8. This network did not require any conversion to be applied to the data before application and took only eight seconds to train and 16 milliseconds to make the predictions, as a result of this.

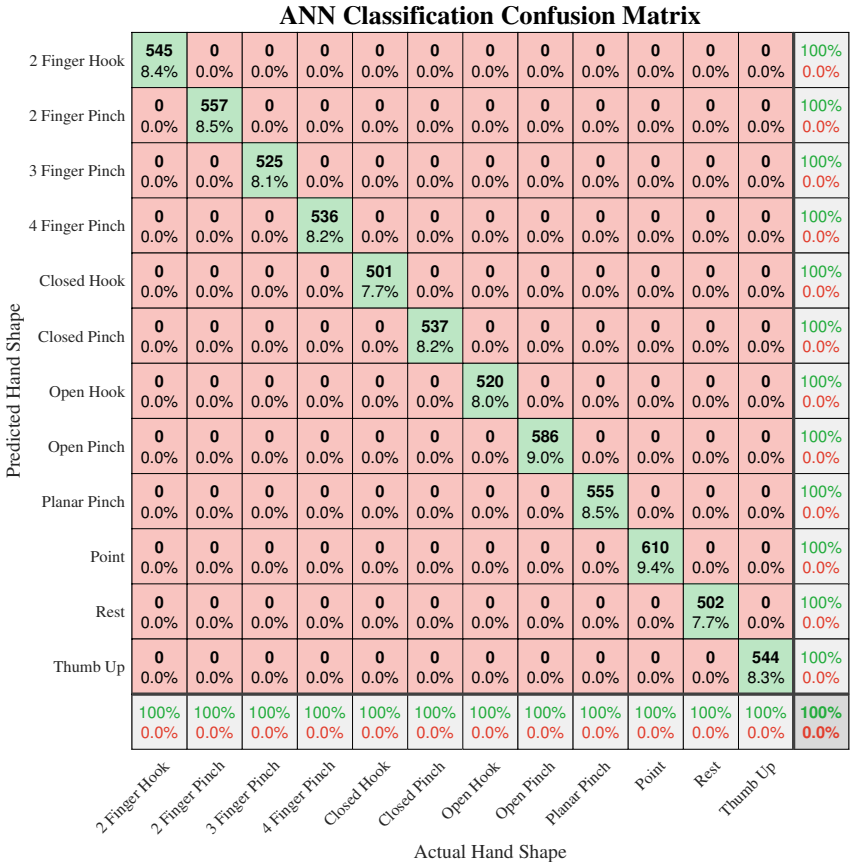

Figure 4.8: A confusion matrix from the implementation of a purpose built artificial neural network with Cartesian co-ordinates of the control hand shapes.

GoogLeNet was able to offer a perfect accuracy score with the test dataset and provides confidences as a well established network. However, it took a considerable amount of time to convert the hand motion data into appropriate images for input into this network. Applying this method to collection of hand shapes recorded over several hours would take an unpractical amount of time. The bespoke ANN was able to hold the same accuracy as GoogLeNet, when provided the test dataset, in a significant reduced time for both training and testing. This low application time enables use with larger collections of hand motion data. Both of the considered ANN methods displayed high accuracy with the control hand shapes; however, these will not be applied to the collected data as they are unable to identify new hand shapes and allow for no manual customisation of the categories. If a bin for unclassified hand shapes was created, hand shaped categorised here could then be manually labelled - providing identification of new hand shapes within the data. Though predictions with low confidence from the ANN could be identified as unclassified, it was uncertain that this would present reasonable results and still requires a, likely, significant amount of manual intervention.

4.2.6 K-Nearest Neighbours Classification

Another supervised learning approach which can be implemented with the collected data is classification algorithms. Classification algorithms observe properties of the data in order to label individual readings of a dataset into predetermined categories. The properties used to classify the data vary depending on the dataset in question and technique applied, these can be: categorical, ordinal, integer-values or real-values. Here, the co-ordinate values of hand motion data collected were classified. The steps taken were as described in Section 2.10.

The training of a classification algorithm, to be able to label data accuracy, requires labelled training data, with also labelled testing data if validation is desired. Here, the control hand shapes recorded, represented in Figure 3.7, were used as train and test data. The MATLAB Classification Leaner application was used quickly explore the performance of the possible classification algorithms which could be applied to the recorded data. A k-nearest neighbours (KNN) subspace ensemble classifier provided the highest accuracy score among the tested classifiers and was subsequently chosen to asses the performance of classification algorithms with hand motion data. This classifier predicts observation labels based on a similarity measure to trained groups of labelled observations.

Confusion matrices and receiver operating characteristic (ROC) curves were created in order to visually evaluate the performance of the implemented technique. A ROC curve provides a graphical plot comparing the true positive rate against the false positive rate for a classification algorithm. The true positive rate defines the sensitivity of the system and the specificity can be found by subtracting the false positive rate from one. The area under the curve (AUC) was also calculated to assess the performance of the algorithm; calculated from the area under the ROC curve. A higher AUC value indicates a superior performance of the compared algorithm. Further description of the techniques employed is provided in Section 2.6.2.

A KNN subspace ensemble classifier was found to achieve an accuracy for both the training data and testing data of 100%. The classifier was trained in 16.8 seconds and was able to classify the test hand shapes collection in 0.805 seconds. Figure 4.9 shows the confusion matrix from inputting the testing data into a trained KNN subspace ensemble classifier. This highlights the ability of the classifier to correctly predict all of the testing, control, hand shapes. Additionally, Figure 4.10 displays the ROC curve. This presents an AUC of one, due to the perfect predictions.

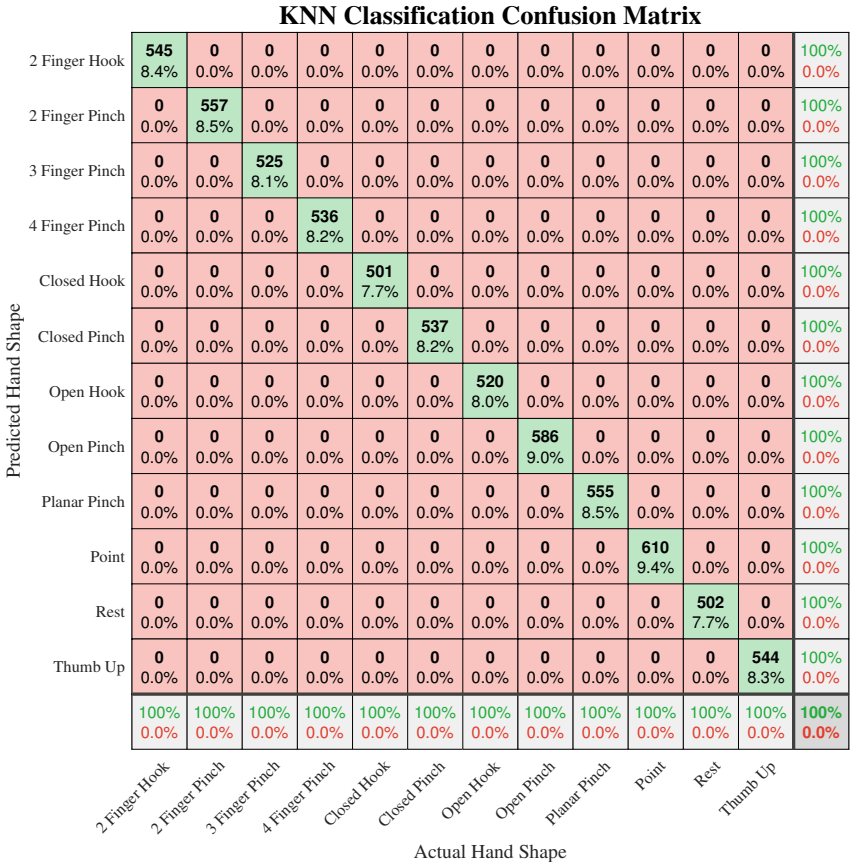

Figure 4.9: A confusion matrix from the implementation of a k-nearest neighbours classifier with Cartesian co-ordinates of the control hand shapes.

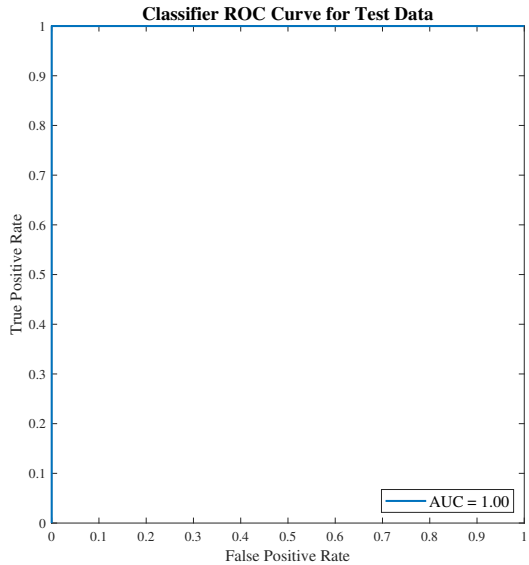

Figure 4.10: The receiver operating characteristic curve from the implementation of a k-nearest neighbours classifier with Cartesian co-ordinates of the control hand shapes.

This classification method has been shown to be capable, predicting control hand shapes perfectly and taking relativity little time to do so. Implementation of this method could identify expected hand shapes within collected data, enabling a possibility to evaluate existing grasp taxonomies with data collected during modern ADL. However, the limitations it imposes (as with ANNs) make it not worth application for the creation of a novel taxonomy of hand shapes. For this reason, it will not be employed to create the final modern taxonomy of hand shapes found in ADL.

4.2.7 Decision Tree Learning

Decision tree analysis is a predictive modelling technique used to categorise similar occurrences within dataset. The similarity between hand joints in observed hand shapes suggested the use of decision tree learning as a potentially superior supervised learning technique. A typical implementation of this method would be similar to that of classification algorithms, training on a set amount of data and validating this on another - to then be applied to unlabelled data. Here, similar approaches to the underlining philosophy of decision tree learning have been taken to create a manual decision tree, aimed at categorising similar hand shapes observed. This manual implementation allows for high customisation during the build of a tree; one element which could also be added, which is not available in normal employment or other supervised learning techniques, is a category for hand shapes not fitting the provided definitions. An unknown category would be beneficial in this research for the extraction of new hand shapes seen during ADL. Any found hand shapes deemed to be appropriate to add could be added to later developments of the tree; the addition of new classifications is possible but grows increasingly demanding in comparison to other considered classification techniques. The closed and opened values were determined through trained using particle swarm optimisation (PSO) and brute-force search optimisation techniques. During training the same divide, as with other classification methods, of the control hand shape data was used - a train:test split of 80:20. The steps taken to implement the manual decision tree were as described in Section 3.5.7. Further description around the techniques used is given in Section 2.6.3.

Both a PSO and binary-brute force search were used to train the decision tree with the selected training data, of labelled control hand shapes. The PSO technique was able to provide an accuracy of 44.8% - taking four minutes and 42 seconds to converge towards this result. This training suggested an opened value of 16.9 degrees and a closed value of 47.5 degrees. The brute-force search was able to achieve 44.9% accuracy with this training dataset and 44.5% with the test data - taking five hours

four minutes and 36 seconds to determine this. This accuracy was obtained from an opened threshold value of 17 degrees and closed of 46 degrees; these value were refined from 20 degrees and 45 degrees, found by the first pass to present an accuracy of 44.6%. The brute-force search results were in agreement with that found from the PSO method, supporting the use of these values. The values found with the brute-force search were used due to the confidence provided by the exhaustive search.

To predict the hand shapes of the test data the decision tree classifier took 18 seconds. The results of this application can be seen in Figure 4.11.

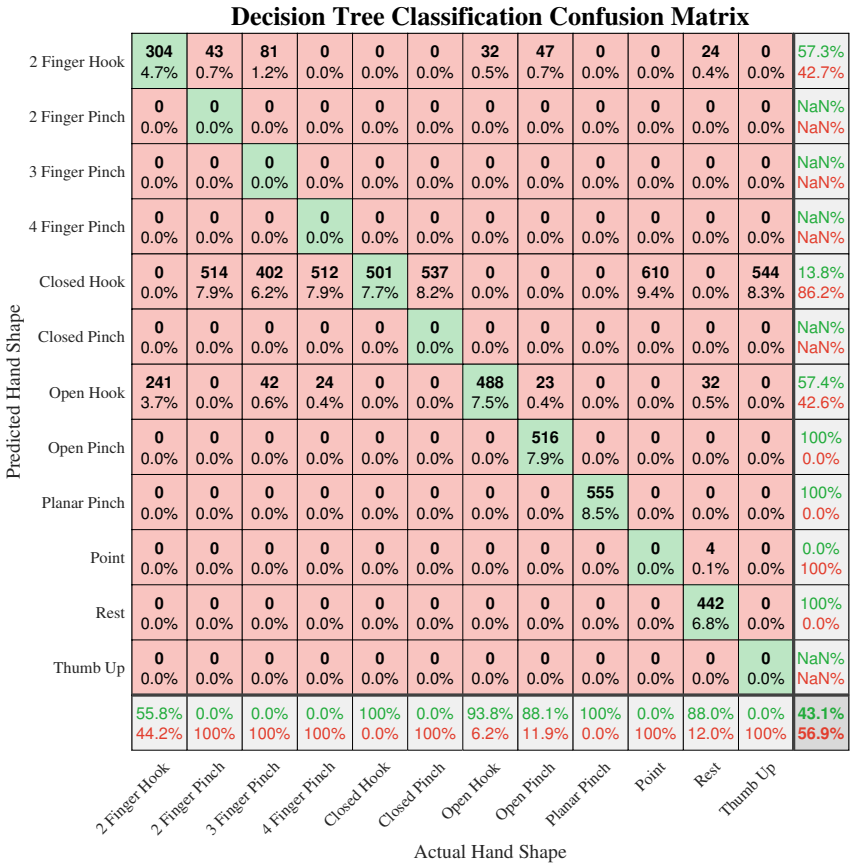

Figure 4.11: A confusion matrix from the implementation of a decision tree classifier with Cartesian co-ordinates of the control hand shapes.

The decision tree classification method provided a fast application but lacked the desired accuracy for hand motion classifications. The employed PSO provided similar accuracy to the brute-force search with a reduced time of convergence. When a brute-force search was applied it was found to give results within the proximity of the PSO technique, providing confidence in the quicker application of the PSO technique. Due to the close proximity of the resultant trained values, those achieved by the brute-force search were selected because of the exhaustive power of this

technique. Though the brute-force search gives an exhaustive search through the possible solutions a PSO technique could be employed were computation speed is of importance.

The manual implementation of this technique suggested the definitions provided could be causing the error - if taken further, methods should be employed to optimise the set definitions for the tree. However, this application was able to provide a framework for the classification of hand shapes in a decision tree; this shows potential for future applications, provided the definitions were improved. Despite the promise it is, again, unreasonable to assume a supervised classification technique could provide useful data for the creation of a modern taxonomy present new hand shapes of ADL. The manual implementation does offer the creation of a bin for hand shapes which do not fit any previously defined categories, though this would require manual labelling of hand motion data post application.

4.2.8 K-Means Clustering

Clustering algorithms are unsupervised machine learning techniques. The use of an unsupervised learning technique has been seen to be more fitting for the collected data, providing the possibility go indicate unexpected functional hand shapes within the modern ADL. Clustering algorithms attempt to find clusters of observations within the data which are similar, typical determined by the Euclidean distance between those points. They does not require training data, but evaluation techniques can be employed after implementation to assess the obtained results. Supervised learning evaluation method can be enforced onto results obtained from labelled data, though cluster evaluation methods provide feasible means of assessing the performance of a cluster analysis application. The clustering algorithm chosen for analysis here is the k-means++ algorithm. The k-means algorithm is a centroid-based clustering algorithm, determining cluster based on proximity of the data points within their dimensions - selected due to the nature of Cartesian hand motion data. The k-means++ algorithm offers an improved method for the selection of initial condition, over the original k-means algorithm. The steps taken were as described in Section 3.5.8. Further description around the techniques used is given in Section 2.6.4.

The k-means++ clustering algorithm needs to be provided with a number of clusters to find within the data. Due to the vast and complex nature of the hand motion data collected it is unfeasible to assert a priori assumptions of this value. To aid in the selection of the number of clusters to be achieved there exists several methods. Most commonly used are, the Calinski-Harabasz (CH) index, Davies-Bouldin (DB) index and silhouette score. The theory behind each of these methods can be seen in Section 2.6.4. Each of these methods were first attempted on the control hand

shapes recorded, observing whether they can each determine the optimal number of clusters as 12 (the known amount of identifiable hand shapes). The application of each method can be seen in Figures 4.12, 4.13 and 4.14. Though the CH index plot provides a less clear conclusion than the other methods, it was stated by Calinksi and Harabasz [154] that if there are several local maxima then it is most economical to select the lowest value of k providing a local maxima. After the application of these methods with the control hand shapes, all were able to deem 12 as the optimal number of clusters. These applications have shown promise in these evaluation methods and provided confidence in their application with the collected data.

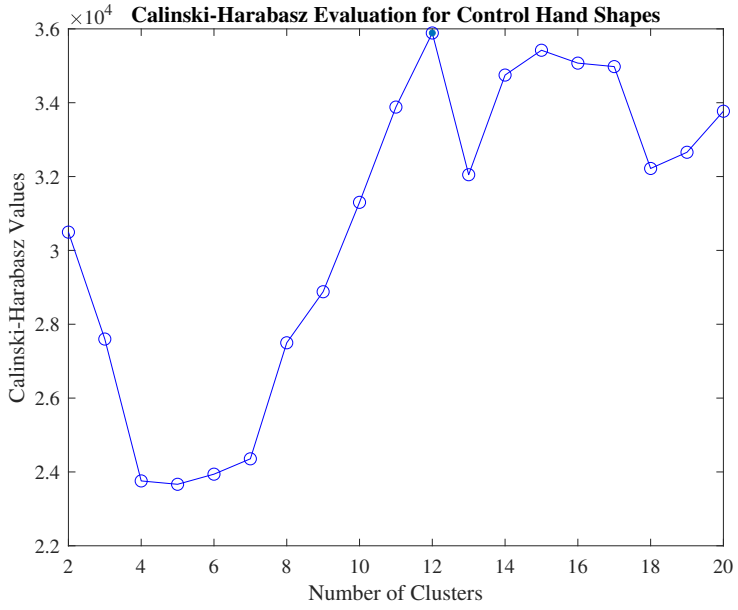

Figure 4.12: A plot of the Calinski-Harabasz index values for the control hand shapes for a k-means clustering algorithm.

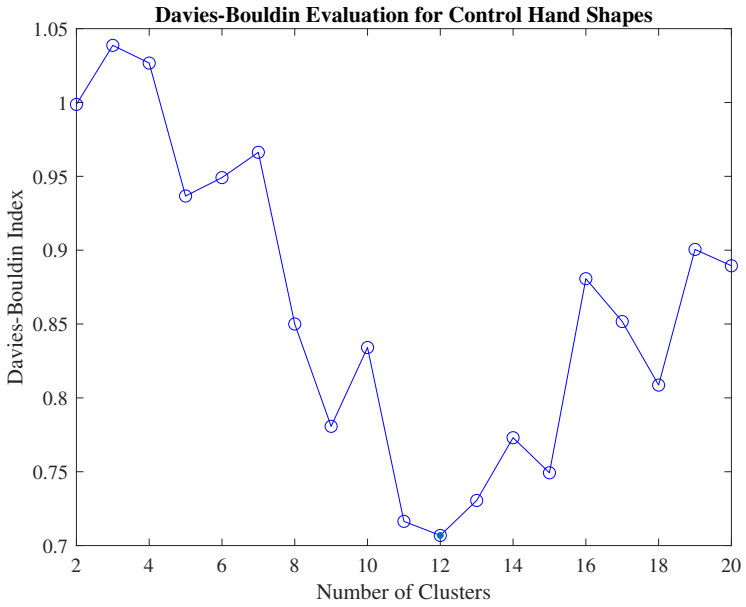

Figure 4.13: A plot of the Davies-Bouldin index values for the control hand shapes for a k-means clustering algorithm.

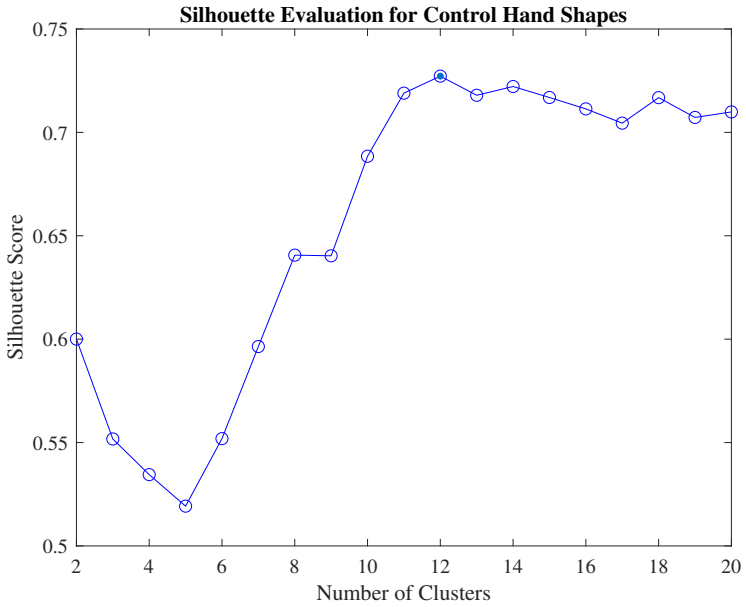

Figure 4.14: A plot of the silhouette scores for the control hand shapes for a k-means clustering algorithm.

The control hand shapes recorded were inputted into a k-means++ algorithm to confirm competency to output clusters correlated with the known hand shapes. The similarity between the resultant centroids and original 12 hand shapes shows

that the classifier is able to determine congruent clusters without prior information. Figure 4.15 shows the centroids of each cluster, each representing a hand shape averaged from the cluster. Comparing these centroids to the ideal control hand shapes in Figure 3.7 provides a visual evaluation of clustering performance.

The clusters were numerically evaluated by observing the number of correctly labelled observations within a single cluster. Taking the most occurring label within each cluster as the predicted label for that cluster and, ergo, the observations within it enables the creation of a confusion matrix for the k-means++ algorithm. This created confusion matrix can be seen in Figure 4.16.

The confusion matrix displays a lower accuracy than what was seen by alternative classification methods; however, upon inspecting the hand shapes drawn from the centroids of this clustering it can be seen that this method was able to identify the desired hand shapes with clarity. The four finger pinch hand shape displays a lower flexion of the digits than would be expected, this is reflected by the inaccuracy highlighted by the confusion matrix. The other drawn hands shapes accurately depicted the desired hand shape, even when a lower accuracy is exhibited in the confusion matrix. This suggests that some of the control hand shapes could have been grouped, as they display little significant difference from each other. Despite the lower accuracy seen, the k-means++ clustering algorithm was applied to the collected data, as it was able to reproduce the hand shapes within the given data with visual accuracy, a desirable trait of the final taxonomy, and is not limited to previously known hand shapes, enabling the identification of new hand shapes within ADL.

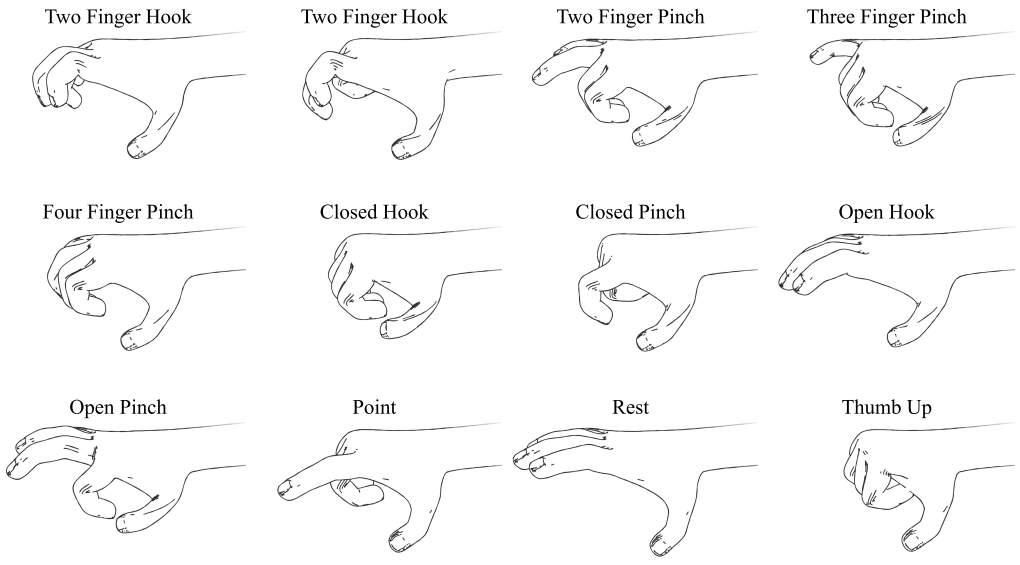

Figure 4.15: The centroids found for the control hand shapes using k-means, presented by line art images.

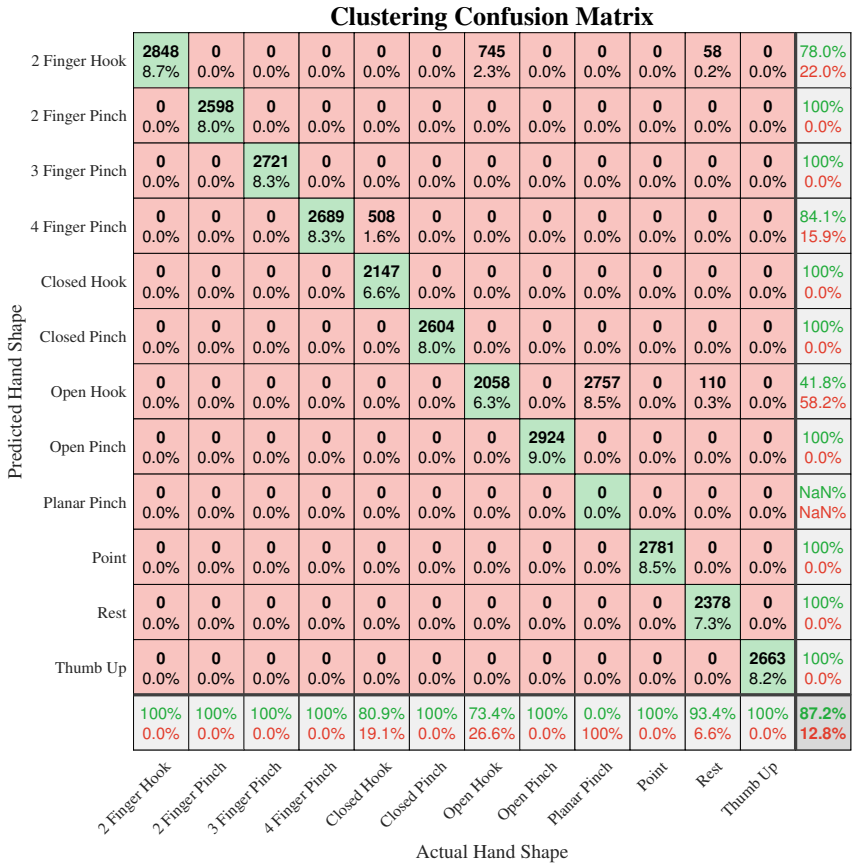

Figure 4.16: A confusion matrix from the implementation of a k-means clustering algorithm with Cartesian co-ordinates of the control hand shapes.

Preliminary analysis performed after the collection of 13 participants, totalling 62 hours and ten minutes of data, showed promising results and confidence in the future data collected. The results of this analysis can be seen in Appendix B. The clusters showed a good spread of hand shapes, with some agreement with previous taxonomies and introducing some, valid, new hand shapes.

Once seen to be capable at extracting the expected hand shapes as clusters from the control data, the k-means++ was applied to the data recorded during ADL. This provided an initial grouping of the functional hand shapes within the data, with the possibility of further analysis refining this to the final taxonomy. Each average hand shape was defined with 60 values (inputted into the algorithm): the x, y and z Cartesian localised co-ordinates for each of the hand joints recorded by the LMC. The clusters were determined through the use of squared Euclidean distances, with the algorithm repeating the clustering 100,000 times and selecting the attempt with the lowest sum of squared Euclidean distances.

The promising results, for the control hand shapes, obtained from each of the

techniques to identify the ideal number of clusters in a dataset (the CH index, DB index and silhouette score) justified the applications of these with the collected data. However, despite this performance shown with the control hand shapes, the evaluation methods employed provided no clear identification of an optimal k values for either hand. The graphical representation of each of these measures for k values between two and 100 can be seen in Figures 4.17, 4.18 and 4.19, respectively. It can be seen that, despite their confident applications during analysis of the control hand shapes, these cluster evaluation methods provide no clear indication of an optimal number of clusters. Though these cannot identify the optimal number, there is potential to use the provided information to support a cluster number value chosen through an alternative means.

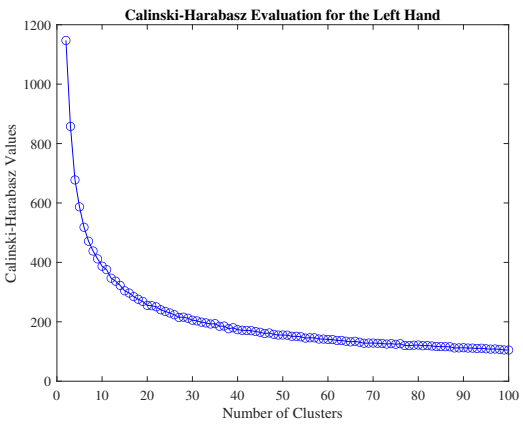

(a) A plot of the Calinski-Harabasz index values for the left hand, using k values of 2 to 100.

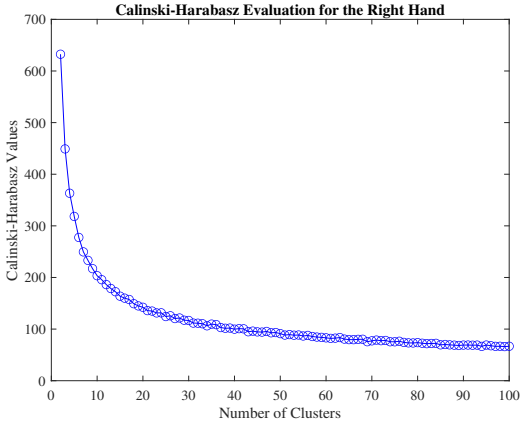

(b) A plot of the Calinski-Harabasz index values for the right hand, using k values of 2 to 100.

Figure 4.17: The plots of the Calinski-Harabasz index values for the data collected within activities of daily living for a k-means clustering algorithm.

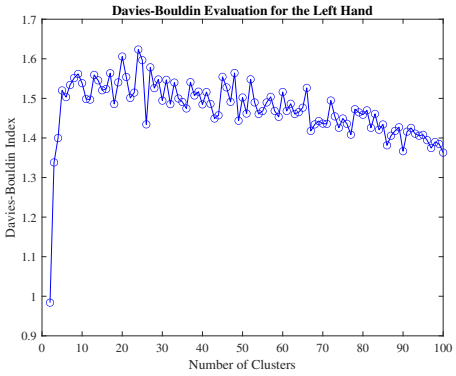

(a) A plot of the Davies-Bouldin index values for the left hand, using k values of 2 to 100.

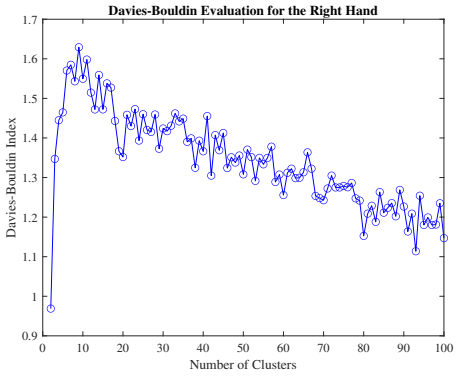

(b) A plot of the Davies-Bouldin index values for the right hand, using k values of 2 to 100.

Figure 4.18: The plots of the Davies-Bouldin index values for the data collected within activities of daily living for a k-means clustering algorithm.

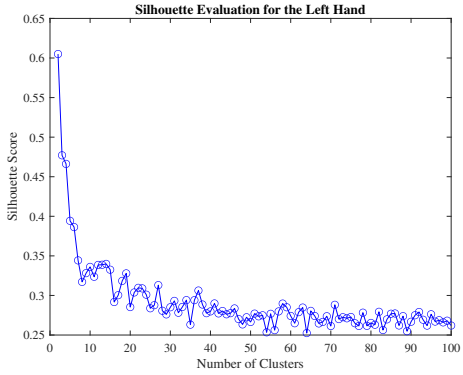

(a) A plot of the silhouette scores for the left hand, using k values of 2 to 100.

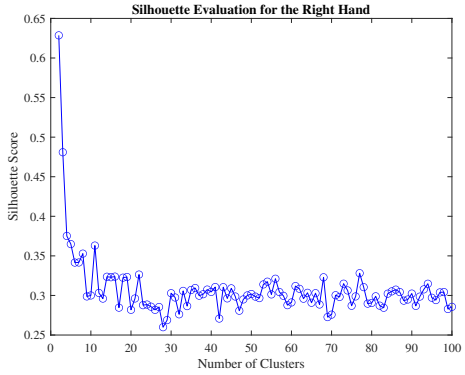

(b) A plot of the silhouette scores for the right hand, using k values of 2 to 100.

Figure 4.19: The plots of the silhouette scores for the data collected within activities of daily living for a k-means clustering algorithm.

The low confidence in the assessed cluster evaluation methods results in a need for another measure of clustering performance. The optimal value for k was determined through observations of the mean points-centroid distance, following applications of the k-means++ algorithm with differing values of k. The value of k providing clustering with a mean points-centroid Euclidean norm distance below a set threshold, with the next integer increase of k providing a mean points-centroid distance above the set threshold, would be considered optimal. Further details of the process applied can be seen in Section 3.5.8 - with a flowchart of the process undertaken shown in Figure 3.15. Any value of k found which produces clusters of data with distances between the clustered functional hand shape frames and their centroid below the set threshold distance would be accepted.

The performance of the k-means++ algorithm results in a reduction in the number of hand shapes which need to be displayed to visualise the hand shapes occurring within the collected data. This collection allows for manual intervention, if desired, and can be brought to a final solution through the combination of similar clusters. To calculate the mean points-centroid distances for each application of k-means++ the averaged means of the Euclidean distances from each joint of each data points within each of the clusters to their respective centroid points were taken. For this analysis a threshold value of 15 mm was used to deem an appropriate performance of a k value. This threshold value was selected for pragmatic reasons, then assessed through rigorous testing of the preliminary data with altered threshold values. This selected value was found to be the value able to provide an ample number of descriptive hand shapes.

During preliminary analysis, a script running through all of the values one by one was possible. With the full collection this took too long and was reduced to only looking around the area found during preliminary experiments, as this was deemed to be suitable and provided clusters with the predefined desired characteristics. For the preliminary data k values of 60 and 30 were deemed appropriate for clustering, further information of these clusters can be seen in Appendix B. Following attainment of this knowledge, k values ranging by 20 either side of these in intervals of 5 were tested. Tables 4.4a and 4.4b show the results of the k values tested around this area. The optimal values of k decided for the left and right hands, respectively, were 30 and 60, providing a mean points-centroid distance of 9.81 and 10.5 mm, receptively. Upon observing the application of these values alongside alternative values it was seen that these values were able to retain an apt amount of information of the collected data and, hence, were selected. This was further supported by the confidence in the results obtained from these k values during preliminary analysis.

Table 4.4: The results from varied clustering k values, selected within proximity to the results of preliminary clustering.

(a) The results of varying the clustering k value for the left hand.

k value	Distance / mm	R-squared
40	10.7	0.96
50	10.4	0.96
55	10.1	0.96
60	9.81	0.96
65	9.66	0.96
70	9.53	0.96
80	9.35	0.96

(b) The results of varying the clustering k value for the right hand.

k value	Distance / mm	R-squared
10	11.9	0.95
20	11.1	0.95
25	10.8	0.95
30	10.5	0.96
35	10.4	0.96
40	10.2	0.96
50	9.90	0.96

The k-means++ clustering algorithm has been used, to reduce the processed data into a manageable number of hand shapes; in turn, leading to the creation of the final taxonomy of the hand shape observed within modern ADL. The final taxonomy is presented in Section 5.2.

4.2.9 Merger of Groupings

After the initial clusters are formed a merge script is then run, which indicates whether any of the clusters could be combined - leading to a final solution. This looks at reducing the number of groups formed from the data using features specific to the data, in this case the pairwise Euclidean norms between each of the points of the group centroids was chosen. Each of the cluster centroids are compared to each of the others; the x, y and z values of each point from one centroid are subtracted from those of the other considered centroid and the norm of this distance vector found. If this norm is below a set threshold then the hand shapes are considered, by the script, similar enough to be combined. Visual inspection could then be performed to determine whether it is reasonable for these highlighted clusters to be combined; alternatively, the script can be set to continue with the merger autonomously. The steps taken were as described in Section 3.5.9.

Preliminary analysis of collected data showed a need for this merger. The obtained results of the k-means++ application contained redundant information and it was found manual intervention was required to provide a concise taxonomy of hand shapes. The merger script was executed to remove these redundancies and display the desired concise taxonomy of hand shapes for modern ADL. The final results of the k-means++ clustering algorithm and subsequent merger of clusters can be seen in Section 5.2. It can be seen, by comparing the pre- and post-merger taxonomies presented, that the merger simply removed any redundant information from the results of clustering.

4.2.10 Displaying Results

Following the discovery of the common hand shapes of modern ADL, the centroids of the final groupings were visualised to provide an updated taxonomy of hand shapes. This was achieved by the steps shown in Section 3.5.10, using Blender to form a three-dimensional (3D) image of the hand and, subsequently, render the model as line art. These images were then consolidated to form a modern taxonomy of hand shapes. The joint angles used as inputs for the rotations in Blender were calculated using the vector dot product, as presented by (2.4). The movement of the joints in Blender, rendering of the images and concatenation of these images employed

the Python scripts within Blender. Inputting the results of analysis on preliminary collected data showed this to be capable method with promise to display the final taxonomy clearly. The results of the performed preliminary analysis can be seen demonstrated within Appendix B. This final taxonomy of the hand shapes observed within ADL can be seen in Section 5.2.

4.2.11 Evaluation of Analysis

After a set of hand shapes were identified as the common hand shapes of ADL they were evaluated to ensure confidence in the results. As cluster analysis, an unsupervised machine learning technique, has been employed for the process of categorising the hand shapes found in the recorded data, there exists no native evaluation of the results. Furthermore, the large amounts of complex motion data results in no abundance of labelled data. Alternative methods for evaluation of these results have been considered. The method employed to deem an optimal k value, with clusters centroids which represent the data of that cluster within an acceptable bound, the mean points-centroid distance, were additionally used as an evaluation method. Alongside this, the standard deviation and correlations have been taken; these measures were both taken for each of the clusters of data and averaged to provide a value for the entire data. Both groupings found pre- and post-merge have been evaluated - this ensures that the automated merger of hand shapes does not result in a significant loss of accuracy. The steps taken to evaluate the results were as described in Section 3.5.11.

The results of the k-means++ algorithm gave a cluster mean distance of 5.36 mm and standard deviation of 6.67 mm for the left hand and a cluster mean distance of 5.95 mm and with a standard deviation of 7.33 mm for the right hand. This indicates that the clusters generated represent all of the functional hand shapes occurring during the 111 hours and 20 minutes of collected data to within 6.70 mm for both hands using 60 and 30 hand shapes. Standard deviations were calculated by observing the variation of the joint positions across all of the hand shapes which formed each cluster. These clusters showed R-squared values of 96.6% and 95.9%, for the left and right respectively - observing the correlation of each hand shape inputted into the k-means algorithm with the cluster centres. All of these statistical values were calculated omitting fixed points (the wrist and MCP joints). The final resultant groupings of hand shapes (the output of the k-means++ algorithm followed by a merger of similar clusters) gave average R-squared values of 96.0% and 95.6% for the left and right hand, respectively. These groupings provided cluster mean distances of 11.7 mm and 8.36 mm with standard deviations of 7.20 mm and 7.72 mm, for the left and right hand respectively. This implies that the collections of 40 and 24 hand

shapes presented in Section 5.2 resemble the functional hand shapes seen in ADL within 12.0 mm, for both the left and right hand.

The selected analysis techniques, k-means++ clustering and a merger of similar hand shapes, were proven to cluster the data with centroids representing the original recorded data within an acceptable error. The overall average distance between the collected data and found centroids, of 12.0 mm, implies that these hand shapes, presented as the hand shapes of ADL, are able to display the functional hand motions performed in everyday life with ample accuracy. Additionally, the average R-squared value, between both hands, of 95.8% shows a high level of agreement between the cluster centroids obtained and the data categorised within each respective cluster. The standard deviation of the found clusters, averaged at 7.46 mm, indicates that the observations within the clusters formed remain within reasonable proximity to their means - highlighting confidence in the representation of the collected data by the presented taxonomy.

4.3 Analysis of Muscle Excitation Techniques

Optimisation techniques have been employed alongside an existing musculoskeletal model in order to provide predictions of muscle excitations occurring within a single frame of kinematic data of the hand. The selected optimisation techniques chosen to form prediction methods were the: genetic algorithm (GA), PSO, gradient descent (GD) and brute-force search techniques. The cost function for each method was tailored through optimisations of the tunable cost function, (3.5), using inputs of simulated muscle excitations; these hand shapes with simulated muscle excitations can be seen in Figure 3.19. To validate each method, these two hand shapes were inputted and the resultant predictions compared to the known muscle excitations of each hand shape. In addition, the equilibrium hand shape, shown in Figure 3.20a, was inputted into each of the methods; this provided an additional validation test and performance evaluation with experimental data. In the repeated applications, the two validation hand shapes were passed into each method ten times and characteristics of interest are recorded. These characteristics were: the accuracy, reliability and time taken. The method found to perform with the desired characteristics was selected as proposed solution for the prediction of muscle excitations from kinematic data. Acquisition of the muscle excitations seen during modern ADL was then achieved by the application of the proposed prediction method with the hand shapes found within modern ADL. The results of the validation and repeated applications of each methods are showcased within this section. Further details of these methods can be seen in Section 2.9, with the chosen implementations for this research described in

Section 6.2.

Hyperparameter tuning was applied to balance the influence of the two elements of the cost function utilised - attempting to minimise the joint angle error, through (3.2) or (3.3), and the summation of muscle excitations, through (3.4). These cost terms were balanced by altering the parameters of (3.5) through inputs of hand shapes in Figure 3.19. Tuning each method with hand shape data containing known muscle excitations enables confidence in these methods, before the application of solely kinematic data. These resultant, individualised, cost functions were then used for the application of each method during validation and evaluation.

Repeated applications of each of the methods were performed in order to provide comparable evaluation measures for the selection process. This involved applying each of the methods ten times with the same hand shapes and recording the correlations between the calculated and desired muscle excitations and joint angles and the time taken. For each of these measures, the average value and variation from this were recorded. This evaluation was performed following hyperparameter tuning on hand shapes with known muscle excitations to ensure that the methods perform adequately in a controlled situation. This provided an evaluation of the results obtained by the selected techniques, enabling comparisons to be drawn and a superior method to be highlighted. Line art of the hand shapes used as an input during these repeated applications can be seen in Figure 3.19. The results of applying the selected optimisation methods can be seen in Table 4.5, this table shows the results of ten repeated applications of the validation hand shapes with the tuned cost parameters for each method. Within this table, the muscle excitation correlation shows the correlations between the known hand shape muscle excitations and the predicted muscle excitations and the joint angle correlation gives the correlations between the known hand shape joint angles and the joint angles resulting from inputting the predicted muscle excitations into the musculoskeletal model. The time taken shows, in seconds, the length of time taken to predict the muscle excitations for one hand shape. The values for each of the ten applications were calculated with the average values from the results obtained by inputting the two validation hand shape joint angles. For each of the performance measures, the average, minimum and maximum values seen across the ten applications have been given. Each test was executed on a PC with Windows 10, 16 GB RAM, Intel Core i7-7700 processor and MATLAB 2020b (9.9.0.1570001).

Table 4.5: The results from the repeated applications of the different optimisation techniques considered.

Method	Muscle Excitation Correlation		Joint Angle Correlation		Time taken / seconds	
	Av.	Min. Max.	Av.	Min. Max.	Av.	Min. Max.
GA	0.67	0.67 0.67	0.76	0.76 0.76	63	40 81
PSO	0.69	0.69 0.69	0.76	0.76 0.76	158	154 176
Binary Brute-Force Search	0.46	0.46 0.46	0.74	0.74 0.74	114	113 115
GD	0.22	0.05 0.36	0.71	0.69 0.74	21	20 22
GA into GD	0.68	0.68 0.68	0.74	0.74 0.74	83	59 99
Brute-Force Search into GA	0.64	0.64 0.64	0.72	0.72 0.72	115	102 145
Brute-Force Search into GA into GD	0.67	0.67 0.67	0.74	0.74 0.74	140	127 165
PSO into GD	0.74	0.74 0.74	0.74	0.74 0.74	173	171 176
Brute-Force Search into PSO	0.64	0.64 0.64	0.74	0.74 0.74	144	142 146
Brute-Force Search into PSO into GD	0.70	0.70 0.70	0.74	0.74 0.74	193	167 271

Though solving the equilibrium hand shape can be viewed as a trivial problem, this does provide an additional indication of the abilities of the selected methods. A recording of a hand in the rest, equilibrium, position was provided with the employed musculoskeletal model [9]; these data included the joint angles and muscle excitations of the recorded hand shape. Table 4.6 displays the results of an application of each method with the data of a hand held in an equilibrium position, with zero muscle excitations. Simulating zero muscle excitations from all muscles (a hand held in equilibrium) within MyoSuite resulted in identical angles to those for the recorded equilibrium hand data. As a result, the muscle predictions found were equal for all of the methods considered. Both of the hand shapes, provided with the model and simulated within MyoSuite, can be seen in Figure 3.20.

Table 4.6: The results of applying each of the tested optimisation methods with the joint angles of the equilibrium hand shape.

Method	Muscle																	
	FDSL	FDSR	FDSM	FDSI	FDPL	FDPR	FDPM	FDPI	EDCL	EDCR	EDCM	EDCI	EDM	EIP	EPL	EPB	FPL	APL
GA	0.01	0.00	0.00	0.73	0.00	0.00	0.00	0.32	0.00	0.00	0.01	0.07	0.00	0.33	0.00	0.00	0.00	0.00
PSO	0.00	0.00	0.00	0.00	0.00	0.00	0.00	0.00	0.00	0.00	0.00	0.00	0.00	0.00	0.00	0.00	0.00	0.00
Binary Brute-Force Search	1.00	0.00	0.00	0.00	0.00	0.00	0.00	0.00	1.00	0.00	0.00	0.00	0.00	0.00	0.00	0.00	0.00	0.00
GD	0.01	0.00	0.00	0.73	0.00	0.00	0.00	0.32	0.00	0.00	0.01	0.07	0.00	0.33	0.00	0.00	0.00	0.00
GA into GD	0.01	0.00	0.00	0.73	0.00	0.00	0.00	0.32	0.00	0.00	0.01	0.06	0.00	0.33	0.00	0.00	0.00	0.00
Brute-Force Search into GA	0.00	0.00	0.00	0.00	0.13	0.00	0.00	0.00	0.14	0.00	0.00	0.00	0.00	0.00	0.00	0.54	0.00	0.00
Brute-Force Search into GA into GD	0.00	0.00	0.00	0.00	0.12	0.00	0.00	0.00	0.15	0.00	0.00	0.00	0.00	0.00	0.00	0.54	0.00	0.00
PSO into GD	0.00	0.00	0.00	0.00	0.00	0.00	0.00	0.00	0.00	0.00	0.00	0.00	0.00	0.00	0.00	0.00	0.00	0.00
Brute-Force Search into PSO	1.00	0.00	0.00	0.00	0.21	0.00	0.00	0.00	1.00	0.00	0.00	0.00	0.00	0.00	0.00	0.00	0.00	0.00
Brute-Force Search into PSO into GD	1.00	0.00	0.00	0.00	0.21	0.00	0.00	0.00	1.00	0.00	0.00	0.00	0.00	0.00	0.00	0.00	0.00	0.00

This collected data shows the use of optimisation techniques with a musculoskeletal model to be a plausible method for the determination of hand muscle excitation. The applied GA technique showed an adequate average muscle excitation correlation, with a comparatively strong average joint angle correlation. Both of these measured correlations showed consistent results for this technique. Applications of this method were relatively quick to complete but did show a relatively low consistency in the time taken. The PSO technique took nearly three times longer to perform than GA but presented a slight improvement in muscle excitation correlation, with no difference in the joint angle correlation. Additionally, the time elapsed for the PSO technique was able to display a higher consistency. Both of the measured correlations for the GA and PSO methods showed highly competitive consistencies.

The brute-force search gave consistent but low muscle excitation correlations; these results were expected as an exhaustive search would result in identical predictions being made each time, leading to a high consistency in the results, and this search was restricted to binary cases of muscle excitations, limiting the possible accuracy of these predictions. Despite this, the method was able to exhibit a comparatively high joint angle correlation. This method took a relatively long time to complete but was able to provide results quicker than a singular application of PSO. The use of a brute-force search prior to applications of GA and PSO showed worse performance than the original applications of GA and PSO, for all measures. Within this hybrid method it appeared that the brute-force search takes a considerable amount of the time to provide worse initial conditions. With the brute-force search limited to only exploring binary cases of muscle excitations, some of these excitations may be too far away from the truth for the current implementation of this method to obtain a close to correct solution. Additionally, the muscle excitation cost term attempts to keep any zero excitations obtained, which may not be true in reality. Though with time the GA and PSO method can correct for this, the current implementation does not appear to provide the time required for this to occur.

The standalone application of a GD showed relatively poor correlations for both the muscle excitations and joint angles. Furthermore, these measures exhibited low consistency across the applications. Though the correlation results were relatively poor this did display the lowest average time taken, with high consistency to the times recorded. These results highlight the inabilities of this technique when applied outside of a region close to the minimum of a problem, though it was able to show that there would be limited influence on the time taken from tandem applications with this method. The tandem application of GA and PSO with GD displayed the highest correlation between the desired and predicted muscle excitation correlations. Despite this performance, the joint angle correlation observed was lower than individual applications of the GA and PSO methods. A slight increase in the average time

taken was observed, with variations to this time being similar to those of the original applications of these methods. These results follow the expected outcomes for applications of the GD method subsequent to another optimisation technique. Applying a brute-force search before applications of a GA or PSO with GD showed little to no improvements in terms of muscle excitation correlations. Additionally, this method proved to show lower angle correlations when compared to standalone applications of GA or PSO techniques. For both of the GA and PSO techniques, this hybrid application took the greatest amount of time. The use of GD showed aid in improving the correlations but was unable to provide appropriate results when employed as a standalone application.

Examination of the binary brute-force search shows this application would require a total number of combinations of 262,144 (2^{18}) and, therefore, the average time taken for each combination was 0.435 milliseconds. If a brute-force search was to be implemented with a more appropriate increment between increases in muscle excitations of 0.01 there would be a total number of combinations of $(1 + 1/0.01)^{18} \approx 1.2 \times 10^{36}$. In this application it would take approximately 1.7×10^{25} years to complete. This is, clearly, not feasible; however, the binary variant was able to provide the GA and PSO optimisation techniques with improved initial candidate solutions. Given enough time the shown brute-force search would be able to find a close replication of the desired hand shapes, with knowledge of the required muscle excitations. One possible alternative implementation is to run a brute-force search after the application of PSO, exhaustively searching the surrounding area within set bounds to further improve the acquired accuracy.

When applied as a standalone method the GD was not able to produce results of ample accuracy. However, utilising GD following applications of GA and PSO showed the capability of this method in further increase the observed muscle correlation - increasing the accuracy of these results. This method was able to also provide muscle excitation correlation improvements to the hybrid techniques applying GA and PSO following a brute-force search. Utilised following applications of other techniques this did not increase the computational time dramatically, showing an average 27.3 seconds increase over the original application of these techniques.

Due to the superior performance displayed when tested with the validation hand shape data and proven ability to accurately predict the equilibrium muscle excitations, the PSO followed GD method was selected as the most appropriate method for predicting the muscle excitations from kinematic hand data. The correlation between the inputted and outputted joint angles was not the best seen (coming second to the lone implementations of PSO and GA); however, this method provided the best muscle excitation correlation. Among the best performing methods, the PSO

with GD method provided the same level of consistency in the correlations of the muscle excitations and joint angles - as seen in Table 4.5. Though this method was among the slowest, the recorded time taken had one of the highest consistencies; the minimum and maximum times taken showed only a 1.15% and 1.44% difference from the mean value, respectively. Furthering the case for this selection, this method and a standalone PSO were the only methods that were able to predict the equilibrium hand shape muscle excitations with 100% accuracy.

After hyperparameter tuning, the following parameter values were used in the cost function for the PSO:

$$P_1 = 0.11, P_2 = 1.67, C_1 = 0.10, C_2 = 0.10,$$

and the following values for GD cost function:

$$P_1 = 18.3, P_2 = 15.3, C_1 = 2.76, C_2 = 10.7.$$

Each set of parameters has been quoted with respect to (3.5).

Table 4.7 shows the known muscle excitations of the validation hand shape muscles, with Table 4.8 showing the results of using PSO followed GD to predict these muscle excitations.

Table 4.7: The recorded muscle excitations for the validation hand shapes used, found within MyoSuite.

Hand Shape	Muscle																	
	FDSL	FDSR	FDSM	FDSI	FDPL	FDPR	FDPM	FDPI	EDCL	EDCR	EDCM	EDCI	EDM	EIP	EPL	EPB	FPL	APL
Hand Shape 1	0.34	0.15	0.19	0.22	0.13	0.49	0.10	0.09	0.09	0.24	0.31	0.26	0.37	0.26	0.41	0.26	0.70	0.35
Hand Shape 2	0.82	0.17	0.32	0.09	0.87	0.20	0.77	0.01	0.09	0.29	0.41	0.83	0.80	0.08	0.23	0.24	0.87	0.75

Table 4.8: The predicted muscle excitations for the validation hand shapes used, provided by using a composite method of particle swarm optimisation and gradient descent.

Hand Shape	Muscle																	
	FDSL	FDSR	FDSM	FDSI	FDPL	FDPR	FDPM	FDPI	EDCL	EDCR	EDCM	EDCI	EDM	EIP	EPL	EPB	FPL	APL
Hand Shape 1	0.36	0.00	0.03	0.01	0.10	0.71	0.00	0.00	0.00	0.00	0.00	0.00	0.00	0.00	0.00	0.04	1.00	0.40
Hand Shape 2	0.25	0.00	0.06	0.00	0.41	0.33	0.77	0.00	0.00	0.00	0.00	0.20	0.04	0.07	0.00	0.00	1.00	0.71

The results and analysis following implementation of the PSO into GD hybrid method can be seen in Chapter 6.

4.4 Analysis of AirGo Clinical Data

The validation performed with the LMC has provided validation fro the AirGo system, with a known measurement accuracy of 18.4 degrees. In addition to the validation of the LMC, further tests were carried out to understand how AirGo performed in a clinical environment. For this the ability to predict injured hands and show progress made by patients from the collected data was observed. These observations were made to provide an indication of the capability of AirGo to provide adequately sensitive information during clinical application. Eight different methods were employed to determine these, these were: the summation of all angles, summation of all total active motions (TAMs), summation of the TAMs of the injured digits, observing only the injured joints, the summation of the MCP and PIP for the injured digits only, the MCP for the injured digits only, the summation of all MCP and PIP and the summation of all MCP. Further details of these methods are provided in Section 3.7. Though subjective to how the patients performed it is an indication of the capability of the measurements made with the AirGo device.

A total of 11 patients, over 16 trials, have been measured with this system, with four of the patients returning at least once. This study took place during a hand therapy clinic at University Hospitals Coventry & Warwickshire (UHCW).

Table 4.9 shows the results of the analysis performed on the data recorded using AirGo. With reference to this table, the presented methods used to review the data, in order, are: the summation of all angles (1), summation of all TAMs (2), summation of the TAMs for the injured digits (3), observing only the injured joints (4), the summation of the MCP and PIP for the injured digits only (5), the MCP for the injured digits only (6), the summation of all MCP and PIP (7) and the summation of all MCP (8). The patients correctly predicted column shows the fraction of patient recordings in which the injured hand was able to be correctly predicted and the trials correctly predicted column shows the fraction of trails in which the injured hand was able to be correctly identified using the data. The progress seen in patients shows the fraction of patients which showed improvement between recordings, when multiple recordings of a patient were available. Each of the differing methods employed to review the results are labelled one to eight and their performance in the prediction of the injured hand and observation of patient progress has been presented.

From these methods run eight out of 11 patient injuries were correctly predicted using only the injured MCP (method six). This method was also able to predict

11 out of 16 trials correctly and showed the most progress amongst the patients, showing progress for two out of the four patients with multiple visits. If the injury was not know, then the best predictor was seen to be only utilisation of the MCP measurements, which also displayed one of the highest rates for identification of patient progress. During validation of the angles collected by the LMC using the portable motion capture system, displayed in Table 4.2, it was seen that all joints tended to present the same degree of error in angular measurements; however, the index finger showed a significantly lower error when compared to the other digits. If the injured joint was not known prior to analysis, using the summation of all MCP joint angles was found to perform the best; this predicted the injured hand correctly for seven out of 11 patients, with 11 out of 16 of the trials correctly predicted and two of four patients deemed to show progress. Other methods considered did not hold as great performance with patient data but were found generally acceptable with trail wide data, with some only suggesting progress in one patient out of the four with multiple recordings.

Table 4.9: The results of the analysis performed with the data collected using AirGo.

Method	Patients Correctly Predicted	Trials Correctly Predicted	Progress Seen in Patients
1	5/11	8/16	1/4
2	5/11	8/16	1/4
3	7/11	10/16	1/4
4	5/11	9/16	1/4
5	8/11	9/16	2/4
6	8/11	11/16	2/4
7	7/11	10/16	2/4
8	7/11	11/16	2/4

With no true readings for the collected data, analysis of these data is difficult - the results are subject to the performance of the patients. However, from this, the practicality of the data collected was observed, exposing the ability of the data collected with AirGo. Additionally, it highlights the best method for analysis of data in a clinical setting, for implementation of AirGo in clinics.

The best performance was seen using the MCP joint of the injured hand, though with no prior knowledge the summation of all MCP joint angles present a close results to this. With the MCP joint angle of the inured digit, eight out of 11 patients were correctly predicted and 11 out of 16 trials. Observing the summation of the MCP joint angles for all digits provided correct predictions for seven out of the 11

patients (only one worse than when the injury was known) and 11 of the 16 trials (identical to that achieved with knowledge of the injury). Both of these methods showed progress in two out of the four patients.

The fact that observations of the MCP joint only was able to perform comparatively well implies that the inaccuracies may exist within the other joints considered. Due to the lack of measurements with alternative devices, it could be argued that this is a result of performance from recorded patients; however, it was also seen that more distal joints performed worse when validating the portable motion capture system, which also employed an LMC for data collection. This does not give rise to significant issues but encourages the use of the MCP joint measurements, if AirGo was to be clinically utilised for the analysis of patient data. Both methods outlined by the MCP summation showed progress in the same patients, regardless of prior knowledge of the injured digit. This implies that the summation of the recorded MCP joint angles, alone, could be employed for the quick assessment of progress in patients.

A possible alternative measure for the performance of AirGo is a comparison between the measurements obtained with AirGo and that collected using a goniometer. Collecting data with both techniques in the same session would enable the possibility of comparisons between the data. However, due to the inaccuracy in measurements collected with a goniometer this validation process is likely to not hold significant confidence. As it stands, the validation of the portable motion capture system provides a good view of the capability of the LMC and, therefore, AirGo. To ensure confident validation of the AirGo system, recordings with both AirGo and a state-of-the-art motion capture device under equivalent conditions AirGo should be undertaken. This would provide assurance in the clinical application of the AirGo system.

Chapter 5

Taxonomy of Functional Hand Shapes

Following the discussion, presented in Chapter 2, of grasp taxonomies described in the literature, the taxonomy of the functional hand shapes observed within modern activities of daily living (ADL) is presented. The data have been recorded and analysed following the procedures laid out in Chapter 3 and the taxonomy has been explicated following the results obtained in Chapter 4. All obtainable information surrounding each hand shape is provided. A means in which the final output can be manually modified to suit set desires, employing the information of each hand shape, is explained. Comparisons are then drawn between the presented taxonomy and current state-of-the-art, observing any differences and deducing possible reasoning for each of these.

5.1 Introduction

There have been several attempts to produce a taxonomy of the hand grasps used in activities of daily living (ADL), these can be seen described in Section 2.3. However, the current understanding of hand motion still remains limited; within studies it is common for only one or two professions to be observed [7, 72] and there is little research focused on monitoring the hand shape used in everyday activities [74, 75]. The majority of studies are limited by their use of video cameras for recording and low selection of subjects and tasks. Though recent attempts have moved towards the use of machine learning for their analysis and, some, implement motion capture for data collection, these are still limited. The most recent development in grasp taxonomies was that introduced by Feix et al. [8], from which this work aims to further update this to modern ADL.

The portable motion capture system has been used to collect which can be used as a base for the updated taxonomy of hand shapes. From this system and the analyse methods chosen a greater length of data has been possible to collect and analyse. The final output of the analyse offers an update to the current grasp taxonomies, including the motions used in modern ADL.

Within this chapter the results of the analysis performed on the data collected during modern ADL, employing the introduced portable motion capture system, are displayed and discussed. Details of the participants recorded during ADL, including their recorded time, is provided. The updated taxonomy of hand shapes seen in modern ADL is presented. From this taxonomy, the characteristics of each of the hand shapes has been determined, displaying the number of occurrences of each during collection and the average time each is held for. A discussion of results, including comparison to existing taxonomies, provides an insight into the agreement with existing taxonomies and highlights the new hand shapes introduced by the presented taxonomy.

5.2 Modern Taxonomy

With the portable motion capture system a total of 111 hours and 20 minutes of data were collected, an individual breakdown of the participants is shown in Table 5.1. Recordings were taken over the whole week, collecting various activities in working and recreational environments with healthy participants. Each recording session lasted until the participant was no longer willing to continue or the battery fully depleted. Recorded tasks include: working at a computer, housework, cooking, shopping, car repairs and playing violin.

Table 5.1: The anonymised participant information.

Participant	Recorded Time	Age	Dominant Hand	Gender
01	8 hours 10 minutes	45	Right	Female
02	5 hours 20 minutes	72	Right	Male
03	2 hours 30 minutes	30	Right	Female
04	2 hours 50 minutes	24	Left	Male
05	4 hours 50 minutes	24	Right	Female
06	6 hours 20 minutes	54	Right	Female
07	2 hours 10 minutes	22	Right	Female
08	6 hours 0 minutes	53	Right	Female
09	5 hours 20 minutes	47	Right	Female
10	2 hours 10 minutes	46	Right	Female
11	3 hours 20 minutes	75	Right	Female
12	3 hours 20 minutes	28	Right	Female
13	9 hours 50 minutes	26	Right	Male
14	5 hours 30 minutes	21	Right	Female
15	5 hours 10 minutes	23	Right	Female
16	6 hours 50 minutes	22	Left	Female
17	3 hours 20 minutes	21	Right	Male
18	4 hours 40 minutes	24	Right	Male
19	7 hours 30 minutes	50	Right	Male
20	2 hours 20 minutes	26	Right	Female
21	6 hours 0 minutes	49	Right	Male
22	7 hours 50 minutes	52	Right	Male

The final centroids, to visually display the common hand shapes performed in ADL, for the left and right hand are shown in Figures 5.1 and 5.2, respectively. The script to decide the value of k, for application of a k-means++ algorithm, outputted optimal k values of 60 and 30 for the left and right hand, respectively - which were reduced to 40 and 24 unique hand shapes with the execution of the merging script.

Figures 5.3 and 5.4 present the initial clustering, prior to the merger of similar hand shapes, for the left and right hand respectively. The number of occurrences of each of these hand shapes and the total number of frames each occurs in for the left and right hand, respectively, can be seen in Figures 5.5, 5.6, 5.7 and 5.8.

Additionally, further information for each of the clusters presented can be found in Tables 5.2 and 5.3. Within these tables the first column provides the label of the cluster, the second the percentage of the data which this hand shape exists within,

the third and fourth columns show the total number of times the hand shape occurs within the data and the total number of frames it is seen within, respectively and the fifth column provides the average number of frames each hand shape is held for each time, this has been rounded to a whole integer. As evaluated in Section 4.2.11, these clusters represent the recorded data 12 mm.

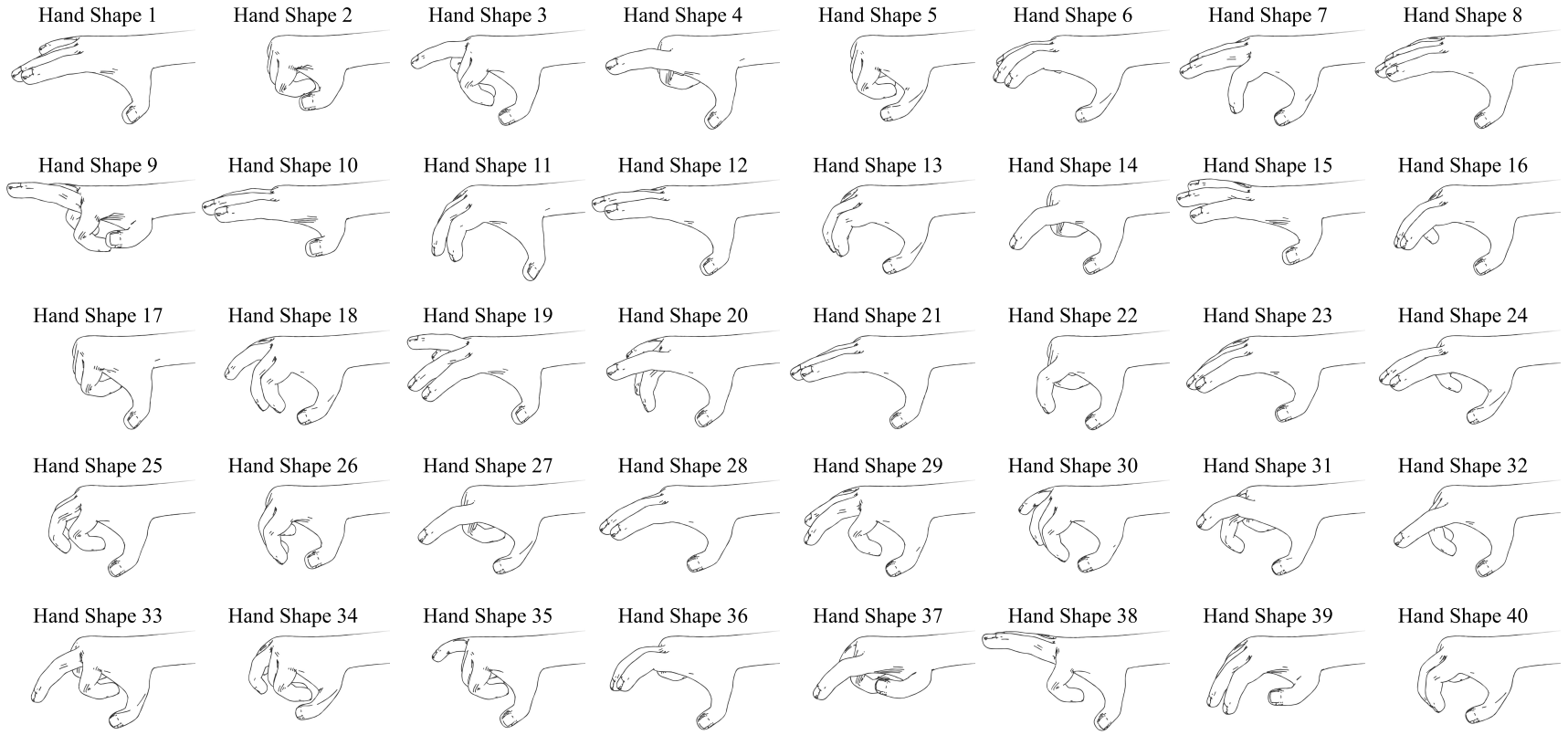

Figure 5.1: The taxonomy of hand shapes for the left hand, provided by line art of the 40 cluster centroids.

Figure 5.2: The taxonomy of hand shapes for the right hand, provided by line art of the 22 cluster centroids.

Figure 5.3: The hand shape representations for the initial k-means cluster centroid of the left hand, provided by line art of the 60 cluster centroids.

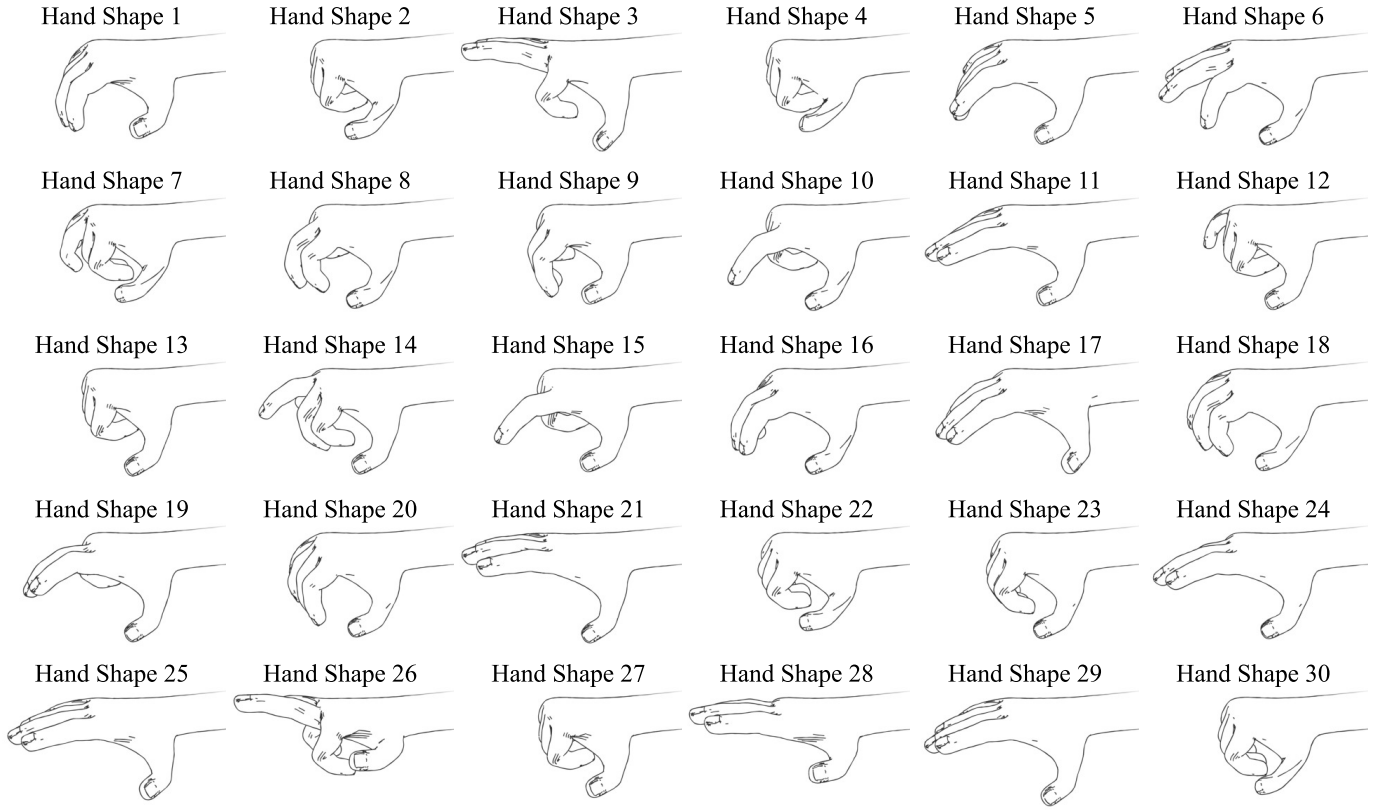

Figure 5.4: The hand shape representations for the initial k-means cluster centroids of the right hand, provided by line art of the 30 cluster centroids.

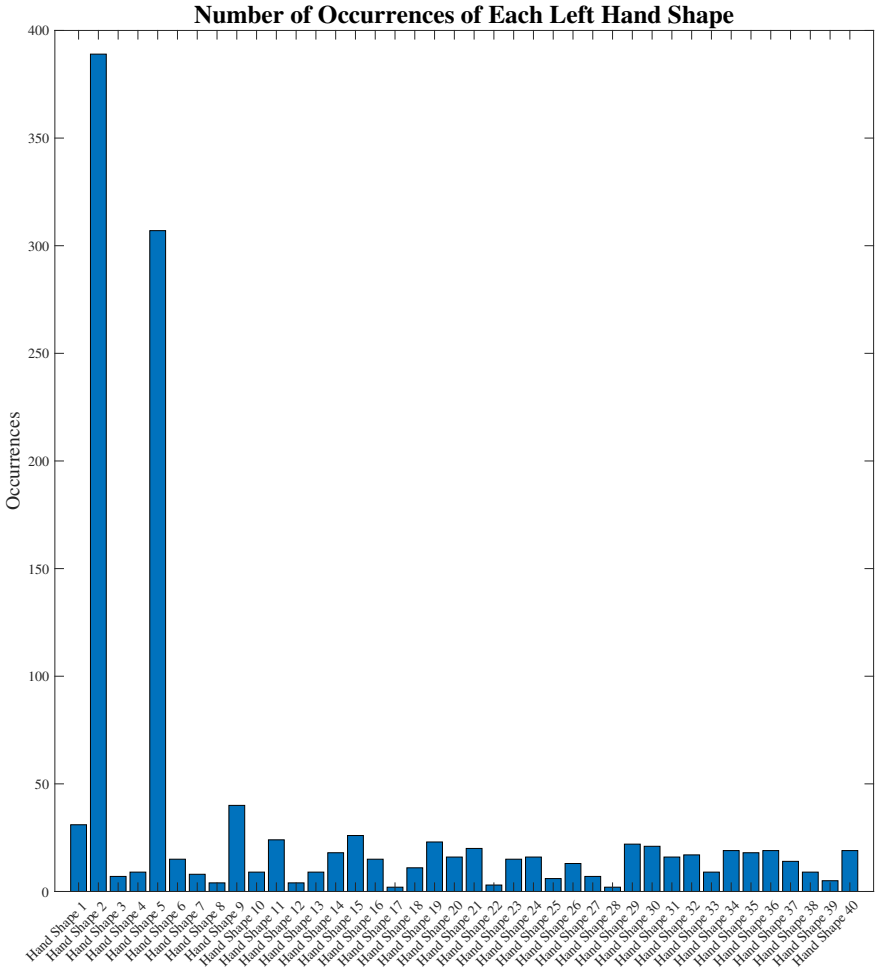

Figure 5.5: A bar chart displaying the total number of occurrences of each hand shape for the left hand.

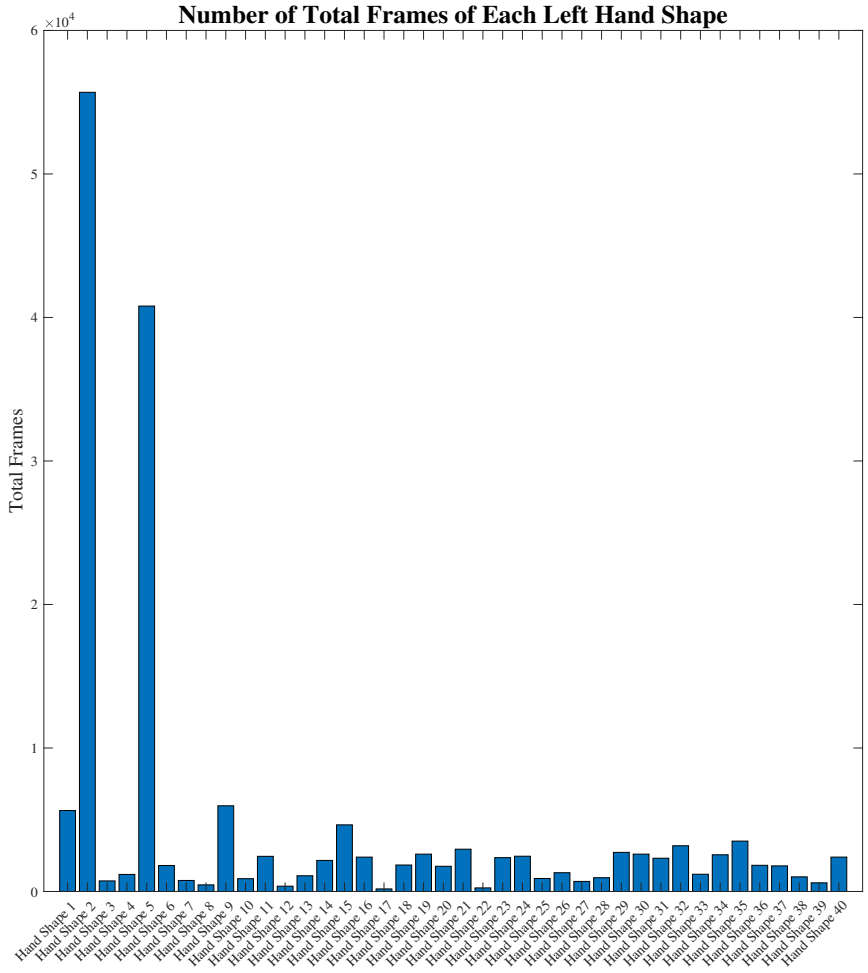

Figure 5.6: A bar chart displaying the total number of frames each hand shape is seen within for the left hand.

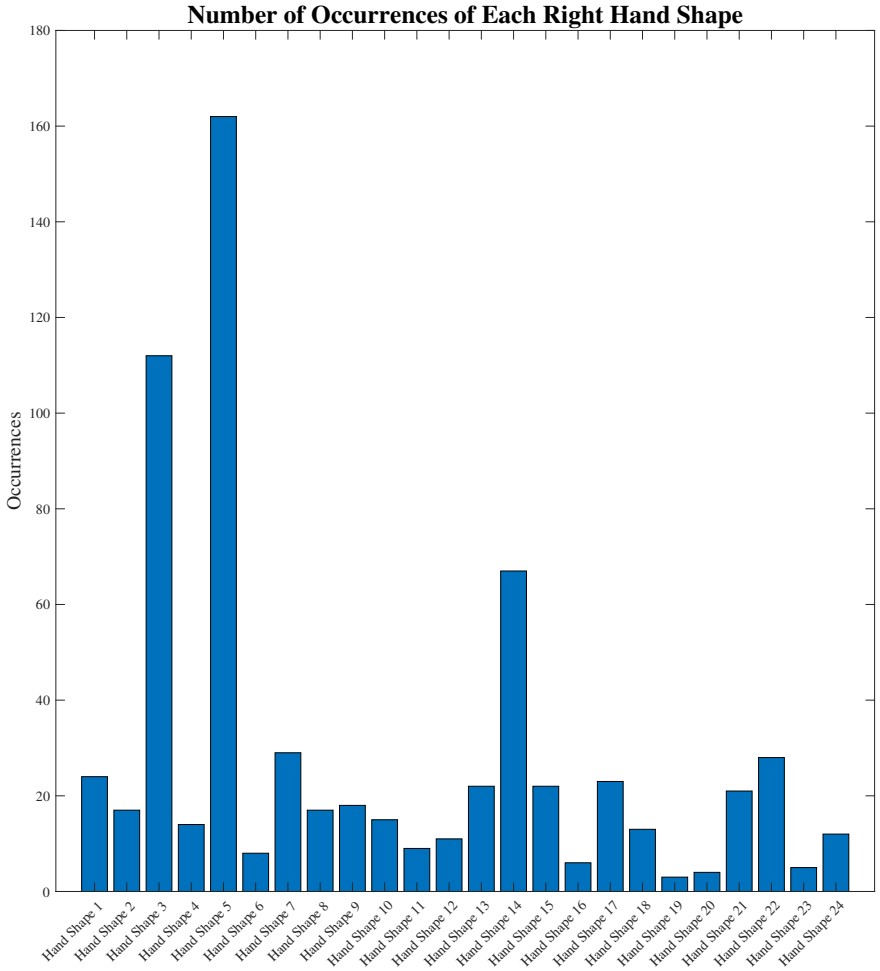

Figure 5.7: A bar chart displaying the total number of occurrences of each hand shape for the right hand.

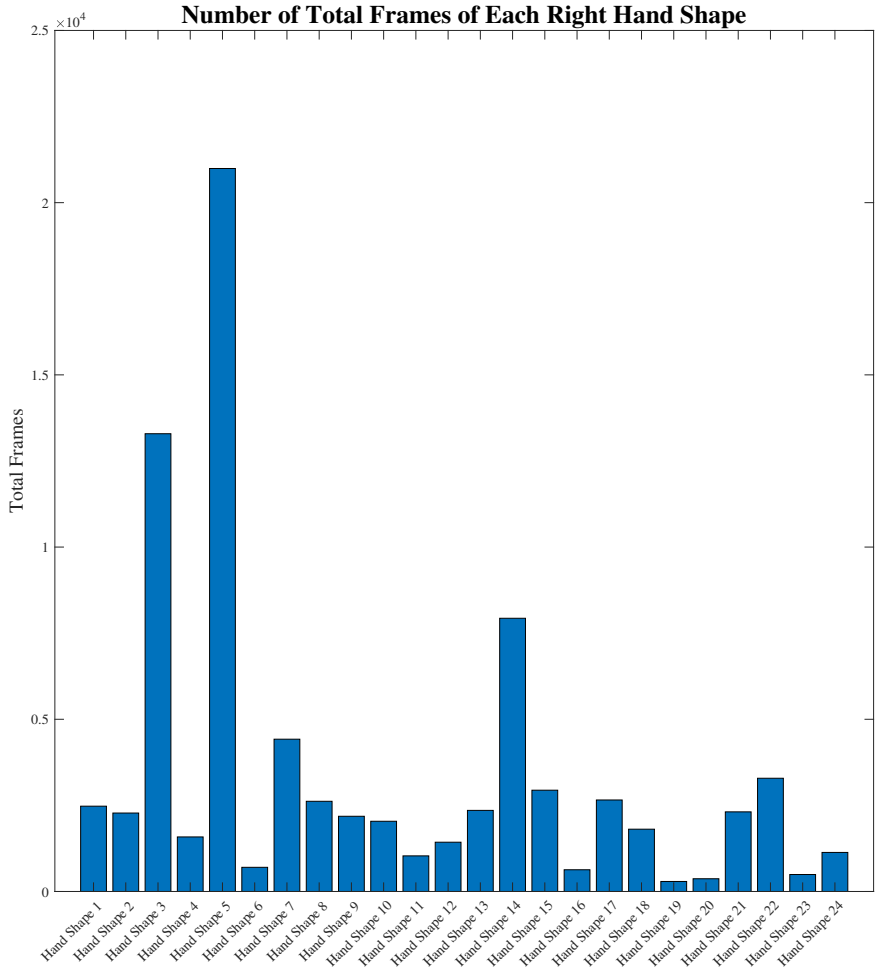

Figure 5.8: A bar chart displaying the total number of frames each hand shape is seen within for the right hand.

Table 5.2: The further hand shape cluster characteristics for the left hand.

Hand Shape	Percentage of Data / %	Total occurrences	Total Frames	Average Frames
1	0.30	31	5641	182
2	2.97	389	55689	143
3	0.04	7	737	105
4	0.06	9	1190	132
5	2.17	307	40794	133
6	0.10	15	1812	121
7	0.04	8	769	96
8	0.02	4	462	116
9	0.32	40	5972	149
10	0.05	9	892	99
11	0.13	24	2450	102
12	0.02	4	370	93
13	0.06	9	1096	122
14	0.12	18	2165	120
15	0.25	26	4643	179
16	0.13	15	2395	160
17	0.01	2	179	90
18	0.10	11	1845	168
19	0.14	23	2603	113
20	0.09	16	1757	110
21	0.16	20	2947	147
22	0.01	3	250	83
23	0.13	15	2359	157
24	0.13	16	2458	154
25	0.05	6	906	151
26	0.07	13	1308	101
27	0.04	7	702	100
28	0.05	2	960	480
29	0.15	22	2727	124
30	0.14	21	2604	124
31	0.12	16	2319	145
32	0.17	17	3187	187
33	0.06	9	1202	134
34	0.14	19	2558	135
35	0.19	18	3511	195
36	0.10	19	1825	96
37	0.10	14	1784	127
38	0.05	9	1020	113
39	0.03	5	604	121
40	0.13	19	2397	126

Table 5.3: The further hand shape cluster characteristics for the right hand.

Hand Shape	Percentage of Data / %	Total occurrences	Total Frames	Average Frames
1	0.18	24	2477	103
2	0.17	17	2278	134
3	0.98	112	13291	119
4	0.12	14	1584	113
5	1.55	162	20992	130
6	0.05	8	702	88
7	0.33	29	4422	152
8	0.19	17	2619	154
9	0.16	18	2184	121
10	0.15	15	2039	136
11	0.08	9	1034	115
12	0.11	11	1431	130
13	0.17	22	2355	107
14	0.59	67	7933	118
15	0.22	22	2941	134
16	0.05	6	631	105
17	0.20	23	2657	116
18	0.13	13	1809	139
19	0.02	3	291	97
20	0.03	4	370	93
21	0.17	21	2312	110
22	0.24	28	3288	117
23	0.04	5	493	99
24	0.08	12	1134	95

As highlighted in Section 4.2.1, the loading and processing of the data took 22 hours 53 minutes and ten seconds and the analysis of this processed data took 52 seconds. Though processing take an undesirable computational time it can all be completed without the need of a human present. These timings were collected on a computer with Windows 10, 32 GB random access memory (RAM) and an Intel Core i7-7700 processor, running MATLAB R2020b (9.9.0.1467703).

After reviewing the images of the hand shapes it appears that a few could be considered anomalies (hand shapes 3, 20 and 25 for the left hand and 6 and 11 for the right). However, their appearances within the data are scarce and they are typically removed when considering hand shapes which occur above a set threshold. Extracting hand shapes based on the number of occurrences for each hand is a quick and simple reduction technique, employing a crudeness maybe not ideal for some situations. For example, a reduction to the ten most commonly occurring hand

shapes provides a quick reduction in data and removal of possible anomalies. Despite the simplicity, however, the tenth most commonly occurring hand shapes only occur for 1.62% and 3.17%, for the left and right hand respectfully, and the combined percentage of the time for these ten hand shapes is 73.0% and 77.0% of the time spent performing functional hand shapes, for the left and right hand respectfully. From a quick and simple reduction there is still a high representation of the hand shapes occurring within the data. As the data consists of a total of only 60 hand shapes between both hands manual analysis would be feasible. From the present hand shape taxonomy, specific hand shapes could be manually favoured over others (for example, selecting either those considered gestures or hand shapes) - supported by the data available in Tables 5.2 and 5.3.

With the intention to further simplify the presented taxonomies of functional hand shapes, similar hand shapes seen across both taxonomies were merged into a single taxonomy of functional hand shapes. The resultant taxonomy of this can be seen in Figure 5.9. The previously observed results strongly advise that focus is given to the separated taxonomies introduced, as it was seen that each hand presented different hand shapes and occurrence rates - indicating a need for individual consideration of each hand. However, this simplified taxonomy provides an easier means of consideration and implementation of the results obtained from ADL hand motion data, if a quick overview is desired.

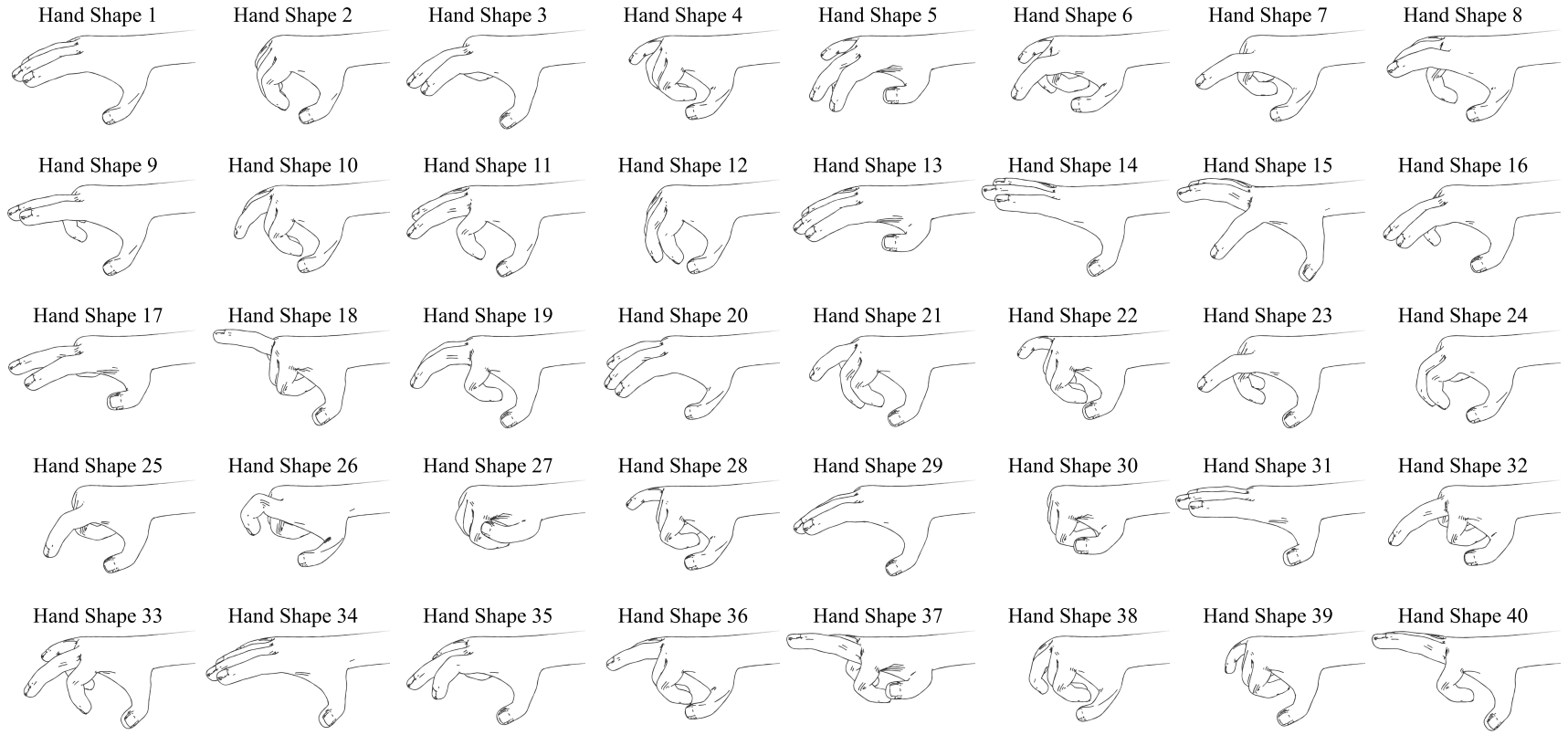

Figure 5.9: The simplified, singular, taxonomy of hand shapes.

5.3 Discussion

It has been shown that large amounts of data can be obtained from a variety of common ADL and locations and processed quickly and reliably using the measurement approach presented. The data collection system gave no issues and was able to record natural hand movements, not encumbered by markers and within a normal, comfortable, environment for the participants. It could be used in all situations it was presented with, with no complaints from the participants, and gave no hindrance during the normal daily tasks performed.

Following collection, the data were successfully aggregated into the hand shapes of ADL through quantitative analysis. It can be seen that the hand shape which occurs the most times throughout the recordings, and therefore in ADL, is, for the left hand, hand shape 2 and, for the right hand, hand shape 5; which displays a closed fist shape for the left hand and close to an open pinch for the right hand. These hand shape form 31.4% and 24.5% of hand shapes seen for each hand, respectively. Further extending this search shows the left hand to produce hand shapes close to a closed fist and the right hand to present variations of pinching actions. It is arguable that the prosthetic devices which allow, exclusively, open and close functionality provide acceptable functionality, but these omit hand shapes which have been seen to be required for large amounts of time during ADL.

Given the higher number of right hand dominate participants, the nature of the grasps and the motion capture setup it could be argued that this greater grasping time for the left hand is due to the right hand being obscured in some frames. Additionally, in some circumstances it would be expected that the non-dominate hand holds an object whilst the dominate hand interacts with it (e.g. using a phone). Given the higher number of right hand dominate participants and the requirement for a collection of frames to be considered functional hand shape frames only when the hand joints remain close to stationary for a period of time, it is arguable that this is a large reason for the greater number of functional hand shape performances from the left hand. Observing the percentage of the frames in which the hands were seen for, across all of the participants, showed a greater percentage of functional hand shape frames for the left hand; however, for the left hand dominate participant alone this was shown to be greater for the right hand. This suggests that hand dominance had an effect on the collected data.

Further, manual, reductions can be taken, given information determined about each of the hand shapes - which would provide a concise display of the desired hand shapes from ADL. The previously discussed clustering evaluation methods, the Calinski-Harabasz (CH) index, Davies-Bouldin (DB) index and silhouette score, have

not been used due to the poor performance observed when applied to the collected data, as has been shown in Figures 4.17, 4.18 and 4.19.

The classification of a functional hand shape being a position in which each joint is held within one degree for one second or longer results in the data reflecting several hand gestures as well as grasps. Previous taxonomies have only considered grasps, occurring whilst an object is held. For example, hand shape 4 for the left hand resembles an index pointing gesture - not displayed within previous taxonomies. In addition to this, various grasps displayed in this taxonomy may appear similar to those found within previous taxonomies though it could be argued that, in some cases, these are being used as gestures (for example, a closed fist or flat hand). Gestures are also of significant value to ADL and should not be omitted from a final taxonomy. As examined in Section 2.3, there has been considerable support expressed in the literature for the aid gesturing provides to daily living [80–97]. Gesturing has been observed to help with: conceptualising speech and accessing the speakers mind [82–88], problem solving [89], accessing mental lexicon and formulating speech [90–93], memory-based tasks [94, 95] and communication for children with intellectual difficulty [96]. Among these studies, it has been shown that pointing helps retain taught knowledge [95] - highlighting the significance of a pointing gesture being observed within the final taxonomy for ADL. In consideration of the aid gesturing has been shown to bring to everyday life, it was seen as of significant importance that gestures were able to be extracted from the collected data during the performed analysis.

Comparing the new taxonomy to those previously defined in the literature reveals several novel hand shapes which have been identified, by this taxonomy, as relevant for ADL. The additional hand shapes seen were: index finger point (with thumb abduction and adduction), inferior pincer with index and middle finger, peace sign, relaxed hand, fully closed fist, thumb-little finger opposition, thumb up and middle finger pinch. Similarly, there are some grasps that exist in the previous taxonomies which the new taxonomy does not deem relevant. These grasps were, when compared to the taxonomy introduced by Feix et al. [8]: parallel extension, thumb-3 finger and extension type. The analysis of the data collected resulted in 16 more groupings of hand shapes for the left hand, compared to the right; these additional hand shapes seen on the left hand included: index and middle hook, light tool with little finger extension, small diameter with index point and sphere-3 finger with extended ring and little finger, with reference to the taxonomy by Feix et al. [8]. Despite the lower number of hand shapes, the right hand also highlighted some hand shapes which were not seen from the left hand, including: platform and medium wrap with ring finger extension, with reference to the taxonomy by Feix et al. [8]. This dissimilarity between the two hands implies a requirement to develop upper-limb

prosthetic devices for each hand, individually - accounting for the differences seen within the taxonomy.

It can be observed from the taxonomy that there is little difference in the thumb position across all of the presented hand shapes, this is further supported by the lack of activity shown by the thumb in Figures 4.5 and 4.6. The thumb is considered to only act as a stabilising post for the other digits to work against, implicated by the limited motion provided by the metacarpophalangeal (MCP) joint of the thumb. Consideration of this limited motion when replicating the hand motions would aid in the reduction of complexity of the device.

The taxonomy shown here provides a confident display of the hand shapes relevant to ADL; highlighting both grasps and gestures performed throughout a typical working day, introducing new hand shapes to those seen in previously defined taxonomies of grasps and providing a distinction between the everyday needs of the left and right hands. The obtained knowledge, through this collection of hand shapes found in modern ADL, offers the potential of refinement to upper-limb prostheses. The presented taxonomy offers a convergence of human hand replicas towards an exact reproduction of the human hand motions required for ADL. The data seen here has shown support for many of the grasps presented in previously introduced taxonomies, with only a few grasps form previous taxonomies not being represented. However, here there are several hand shapes presented in addition to those seen from previous taxonomies; many of which could be argued to represent gestures, not considered during the creation of previous taxonomies. This highlights the importance of gestures in everyday modern life. Support is seen for the creation of an upper-limb prostheses only providing an open and close function. However, it has been seen that these devices are greatly limited and do not allow for many of the hand shapes performed during ADL. The taxonomy presented here has indicated a difference in the left and right hand, providing a useful note for the design of upper-limb prostheses for each hand. This newly found information will aid in the development of upper-limb prostheses, enabling an improvement to the quality of life of recipients and a reduction in the cost of these devices.

Chapter 6

Predicting Hand Muscle Excitations

This chapter looks at existing mathematical models of the human hand, initially highlighted in Chapter 2, and the possible next steps to these. An existing musculoskeletal model of the human hand is reviewed, focusing on the potential implementation alongside optimisation techniques to determine muscle excitations from kinematic data. The optimisation techniques employed can be found discussed in Chapter 2, with the methods taken to implement these with the existing musculoskeletal model shown in Chapter 3. The results of this development, implemented with the hand shapes of the taxonomy presented in Chapter 5, are then displayed. Finally, the technique proposed as a solution for predicting muscle excitations and the obtained results are discussed.

6.1 Introduction

Several varying models of the human hand exist within the literature; these attempt to understand the kinematic motions of the hand [157–159], define the constraints limiting digit motion [160–162], explain the motion made possible by the wrist [163–165, 196] or examine the kinetic properties of the human hand [9, 197]. Utilising a musculoskeletal model of the hand to provide the muscle excitations from a single frame of kinematic data would present many opportunities. From the data collected with the portable motion capture system, this ability would enable the determination of muscle excitations performed during activities of daily living (ADL). This could present great aid to the development of myoelectric upper-limb prostheses.

Predictive models for muscle excitations, exclusively inputting a single frame of kinematic data, are sparse within the literature, with none presented for the hand. For this reason, a predictive model has been proposed - designed to provide prediction from the data collected during ADL. For this the musculoskeletal model proposed by Blana et al. [9] has been selected for implementation with optimisation techniques, to achieve a prediction of the muscle excitations occurring within select single frames of hand kinematic data. After the optimisation has completed, the output provides a close approximation to exact representation of the desired joint angles and, therefore, the knowledge of the muscle excitations which result in this. The outputted joint angles can be visualised alongside the the desired joint angles to visually evaluate the results. Numerical assessment can also be provided by comparing the differences in the joint angle values.

The existing musculoskeletal model chosen to support this muscle excitation prediction method uses muscle excitations to determine the joint angles of the hand. In this application, the optimisation techniques select proposed candidate solutions of muscle excitations aimed to result in an inputted set of hand joint angles. By repeatedly inputting these candidate sets of muscle excitations into the model and determining the cost of each solution proposed, the applied optimisation technique converges towards a solution - a set of muscle excitations which result in the inputted hand joint angles (implicit of the muscle excitations for this hand shape being found). This model has been selected as it is openly available and has a desirable input and output characteristics for the intended application and data collected during ADL.

In this chapter, the implementation of the selected optimisation methods, applied alongside the musculoskeletal model, has been described. The methods used to create an input from Cartesian co-ordinate data, the cost function applied and how each method was validated and evaluated are also presented. Following assessment of the selected methods, one is highlighted as the proposed solution and implemented to

determine the muscle excitations of ADL using the data collected with the portable motion capture system, presented in Figures 5.1 and 5.2. The chapter concludes with a discussion around the implementation of each technique and the final results obtained.

6.2 Proposed Techniques

The proposed solution, as aforementioned, utilises the musculoskeletal model introduced by Blana et al. [9] and a selected optimisation technique. Several optimisation techniques were attempted to enable the desired balance of accuracy, reliability and speed. The Cartesian data collected with the portable motion capture system was used as an input to this method. As the musculoskeletal model employed provides the joint angles, these Cartesian data were transformed into joint angles prior to application. As the optimisation techniques reduce a given function, a cost function was created such that lower outputted minimised the difference between the joint angles found from the predicted muscle excitations and the desired, inputted, joint angles. Each method was validated with control data, with known muscle excitations, and assessed from repeated applications of identical inputs. The outline of the designed prediction technique can be seen in Section 3.1.2 and the a full description of the means employed to assess the ability of the selected optimisation techniques can be seen in Section 3.6.

The musculoskeletal model selected to create the proposed muscle prediction method was that presented by Blana et al. [9]. The model takes an input of the current muscle excitations of the hand, determined through electromyography (EMG) readings in a typical implementation, to provide the current joint angles of the hand. It was proposed as a technique for the control of a robotic hand - providing the joint angles to be performed following acquisition of muscle excitations from an EMG sensor.

This model only considers the extrinsic muscles of the hands but has been selected for several reasons. The open availability, with support readily available, and the MATLAB integration provided results in an appealing model. The MATLAB support allows for muscle excitations to be performed directly after data process and analysis, autonomously - performed also within the MATLAB space. Though timing is not of significant value in this application, the model was demonstrated to be capable of performing real time - promising fast predictions of muscle excitations. The clearly defined inputs and outputs provides easy implementation and alternative uses. Further to this, the use of joint angles as an output means that this could easily be integrated with the collected data within ADL - which had been converted

into joint angles during the analysis process. Using this model, the hand joint angles performed by a set of muscle excitations can be determined using (3.1). Inputting the best solution found, from the applied optimisation techniques, each iteration into this equation provides the joint angles for that best solution. Repeatedly proposing candidate solutions of muscle excitations, altered iteratively by the optimisation techniques, to be inputted into this equation provides a cost of each iteration and enables comparisons of candidate solutions.

The selected techniques, for application as strand alone methods and in tandem, are: genetic algorithm (GA), particle swarm optimisation (PSO), gradient descent (GD) and brute-force search. These were selected to provide a range of approaches for solving the problem of predicting muscle excitations from kinematic data. The GA technique is a well established method for optimisation of a problem, shown applicable in numerous situations. The PSO technique has shown superior performance to other optimisation techniques within several applications. The GD method has been seen to provide support to other optimisation techniques by converging closer towards a found minimum. The brute-force search is an exhaustive search strategy which, given enough time, assure the global minimum to a presented problem.

The determined hand shapes of ADL were in three-dimensional (3D) Cartesian form. In order to be comparable to the output of the musculoskeletal model and, hence, work with the optimisation techniques these data must be converted into joint angles equivalent to those outputted by the musculoskeletal model. For each joint angle to be calculated the following were used: the joint in question, the more distal joint and that more proximal. These sets of co-ordinates were converted into a two-dimensional (2D) co-ordinate system and the desired angle found through the application of the vector dot product, as described by (2.4). Only the flexion angle of the joints was required and, hence, the angle was calculated in the 2D co-ordinate system - the transformations applied ensured alignment with the desired axes.

In order to compare the candidate solutions a cost function is required. Here a function which finds the joint angles for a set of muscle excitations, from the musculoskeletal model, and compares this output to the joint angles of the desired hand shape was created. For the GA and PSO implementations a fitness scaling technique was employed to aid convergence. Fitness scaling considers an exponential decrease in the cost as the technique converges towards a solution. This provides an increased influence of those with a lower cost. To achieve this (3.2) was implemented to calculate the cost of each candidate solution. Several similar cost functions were implemented and tested, though this was found to best aid the convergence of the PSO. During a brute-force search fitness scaling adds no benefit and, therefore, the cost function for each input combination was defined to be the summation of the

absolutes of the differences between the resultant and desired joint angles, as shown in (3.3).

The steps taken during an application of this prediction method can be seen described within Section 3.1.2. From the Cartesian data of the hand, joint angles of each observed hand shape were calculated and inputted into the predictive model. The applied optimisation method was then initiated with a random candidate solution and begun. Once a prediction had been made of the muscle excitations, these values were inputted into he musculoskeletal model to determine the joint angles these excitations create. Next the difference between these, found, joint angles and those desired, from the inputted hand shape, was taken to calculate the cost of this application. The final outputted joint angles were also used to create a render of the hand taking up this position, to provide a visual assessment of performance.

Each of the selected techniques were validated by assessing the results of inputting hand shapes with known muscle excitations; the performance of each was then determined through repeated applications inputting these validation hand shapes. The final output of the implemented technique was assessed numerically; comparing the absolute difference between the predicted joint angles, found using the predicted muscle excitations, and inputted joint angles. Additional visual assessment was carried out through comparisons of the predicted and inputted hand shapes. The predicted joint angles, to form the hand shape from the predicted muscle excitations, were calculated by inputting the outputted muscle excitations into the musculoskeletal model.

The optimisation techniques selected are described fully in Section 2.9.

6.2.1 Genetic Algorithm

The GA technique attempts to mimic the natural learning behaviour of living organisms. The optimal solution to a provided problem is found by improvements made through generations of a population of candidate solutions. Exploitation of a current best solution and exploration of the possible solutions are tunable through alterations to the parent selection and child mutation techniques. This method has been chosen as it is a well established, effective, optimisation algorithm.

A built-in MATLAB function was utilised for the employment of a GA technique. A population of 200 chromosomes was used; the collection of extrinsic muscle excitations, the candidate solution, was considered a chromosome, with each muscle excitation considered a gene. The cost function (3.2) was implemented. Parent selection was completed using a roulette wheel selection method. A scattered crossover function was implemented to generate children, from the selected parents. A uniform

mutation function was utilised to mutate a random selection of the generated children. The following options altered and tested to optimise the employment of GA: `FunctionTolerance`, `MaxGenerations` and `MaxStallGenerations`. These are stopping criteria, each influencing the decision of whether the technique has converged to a solution. `FunctionTolerance` provides the value which, if the output is seen as lower than for `MaxStallGenerations` number of iterations, then the GA will stop and declare the input with the lowest found cost at that time to be the optimal solution. `MaxGenerations` gives the total number of iterations allowed before the GA is terminated.

6.2.2 Particle Swarm Optimisation

The PSO technique mimics the behaviour seen in swarms of animals, aimed to replicate the communication and learning behaviour to converge towards a set of inputs which result in the smallest possible output of a given function. Using a cost function, observing the difference between the calculated and desired joint angles, as this function results in PSO being able to be used to converge on the solution of the muscle excitations used to achieve these desired joint angles. This results in the knowledge of the muscle excitations used to create the given hand shape. To achieve this a swarm of particles, initiated with varying conditions, are inputted into the function and result of each input found. These results highlight a personal best for each particle and global best of the swarm, updated upon acquisition of superior results. In each iteration the position, velocity and personal best for each particle in the swarm and the global best are considered to form the next step of that particle. This communication and learning of each particle through the iterations results in convergence towards the optimal solution. The PSO technique was considered for the displayed comparatively fast convergence and high accuracy.

A PSO technique was implemented through the use of a built-in MATLAB function. For this, a function which is to be optimised must be provided; here, a function inputting the muscle excitations and outputting the cost of that candidate solution was selected. Provided with a set of muscle excitations this function would employ the musculoskeletal model to calculate the joint angles this combination achieves. The cost for this set of muscle excitations is then calculated, which becomes the output of the function to be minimised. As this resultant cost is minimised by the PSO technique, the muscle excitations of the presented hand shape are converged toward with each iteration. Within MATLAB there are several customisable options provided for the built-in PSO function, for this implementation the following were considered: `FunctionTolerance`, `MaxIterations`, `MaxStallIterations`, `ObjectiveLimit`, `SelfAdjustmentWeight`, `SocialAdjustmentWeight` and `SwarmSize`. These para-

meters can be seen described in Section 3.1.2. Each of these options were altered and tested to optimise the employment of PSO. The PSO employed took on the following settings:

Table 6.1: The parameters selected for the muscle excitation predicting application of a particle swarm optimisation technique.

Parameter	Value
`FunctionTolerance`	`1e-10`
`MaxIterations`	`inf`
`MaxStallIterations`	100
`ObjectiveLimit`	`1e-10`
`SelfAdjustmentWeight`	2
`SocialAdjustmentWeight`	2
`SwarmSize`	200

Here, `FunctionTolerance`, `MaxIterations` and `ObjectiveLimit` were set to these extreme values to remove any influence over the termination of the algorithm. This resulted in the sole use of `MaxStallIterations` as the indicator that a solution had been found. Other settings were determined through testing, found to accuracy converge on a solution with minimal computational time.

6.2.3 Gradient Descent

The GD method utilises the gradient of the equation being minimised to converge towards a minimum. After the gradient of the current candidate solution has been determined, it is multiplied by a set constant and subtracted from the current candidate solution - providing the new candidate solution. This results in the ability to take larger steps towards a minimum when at a greater distance from it and smaller steps as the process converges closer to one of the minima. For this implementation, the gradient was determined each step using numerical differentiation. One weakness of the GD method is the tendency to converge towards local minima, a problem arising if the selected initial candidate solution is not in proximity of the global minimum. Due to this limitation, the GD method is typically applied after an optimisation technique, to converge further towards the solution - in this study the GD method has been considered to aid the convergence of the other techniques applied.

A GD optimisation algorithm was created within MATLAB, implementing the steps pictorially outlined by Figure 6.1. The gradient of each attempt was calculated through numerical differentiation, using the central difference formula with a step of 0.2 for each muscle excitation above and below the currently considered set of

muscle excitations. The applied central difference numerical method followed the formula (2.14) to provide an estimate of the gradient of each iteration. The learning rate was set to 0.01, due to the fine detail of the problem, and the total number of iterations allowed was 2,000. No stopping criterion was implemented for reaching a low enough cost, in each implementation the total number of iterations must be reached. The lower (zero) and upper (one) bounds were tested after each iteration to keep values within practical bounds. These set values for an implementation of GD were all found to be optimal through testing.

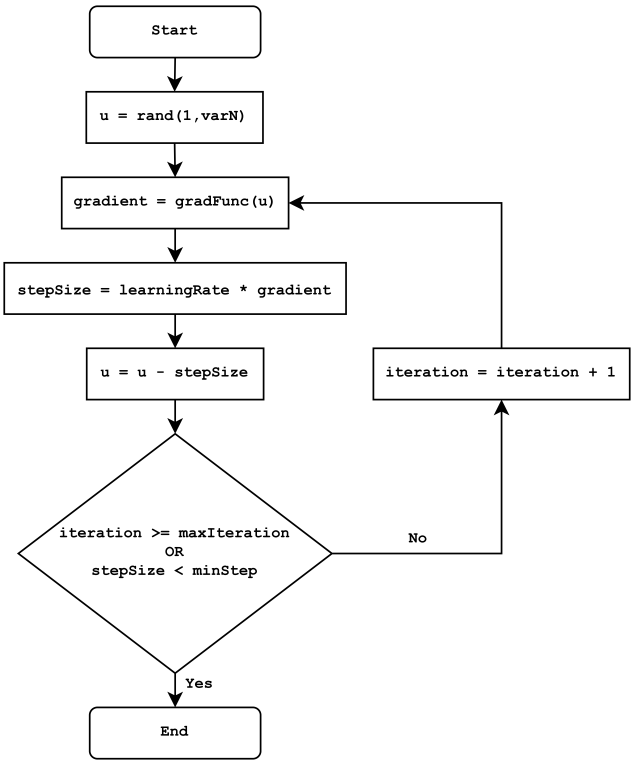

Figure 6.1: A flowchart representation of the implementation of a gradient descent method within MATLAB.

6.2.4 Brute-Force Search

A brute-force search has been consider in an attempt to observe vast amounts of varying all possible solutions. Though likely to converge on an accurate solution with enough time this method takes a considerably long time and has only been considered due to the ease of implementation it offers. A binary brute-force search was initially implemented and found to perform well, once increased to a finer range of real numbers, between zero and one, the computational complexity increased dramatically. As detail was added to the search range the number of iterations

required increases exponentially, becoming increasingly demanding on computational time with the musculoskeletal model being run each iteration.

A binary brute-force search was implemented within MATLAB following the process described Figure 6.2. This generates all possible combinations of the candidate solution vector, enabling an exhaustive search of all possible solutions. Here, `n` represents the number of elements in the solution vector, `increment` is a predefined value which provides the resolution of the brute-force search and `minU` and `maxU` are the minimum and maximum values of muscle excitations, receptively. As this was a binary search, the increment was set to one and the minimum and maximum values of muscles excitations searched were set to zero and one, receptively. To initialise, all muscle excitations of the candidate solution vector were set to zero. Here `n` represents the number of elements in the solution vector, `increment` is a predefined value which provides the resolution of the brute-force search and `minU` and `maxU` are the minimum and maximum values of muscle excitations (zero and one), receptively. To initialise, all muscle excitations of the candidate solution vector are set to zero. To initialise, all muscle excitations are set to zero and one iteration completed. The position of the last element in the candidate solution vector is then selected as the `increaseValue`. In the next iteration, as the element at position `increaseValue` has not reached the maximum possible value of this element (one), it is increased by the set incremental value. Once the maximum value has been reached by the element at position `increaseValue`, the value of this element is reset to zero in the following iteration and `increaseValue` decreased by one. Following this the element at the position of the, now decreased, `increaseValue` is increased by one increment. Then all of the elements before the `increaseValue` position are queried against the maximum possible value (one); the first position found to have a value not be equal to the maximum value is set as the `increaseValue` and the cycle continued. Once all elements have reached the maximum value the brute-force search is known to have finished. In the case of a binary brute search this increment was set to one; however, the process has been programmed in the way described to allow for the increment to be altered if desired. During each iteration the model is executed with the muscle excitations of that iteration. The cost of each combination is found by the summation of the absolute differences between the fond and desired joint angles. fitness scaling is not required as each possible combination is being tested and this cost function will provide enough detail to highlight the best. The muscle excitations with the lowest cost are stored separately in a vector, as well as their cost and output. Once complete the muscle excitations of best found solution are set as the initial conditions for the implementation of PSO.

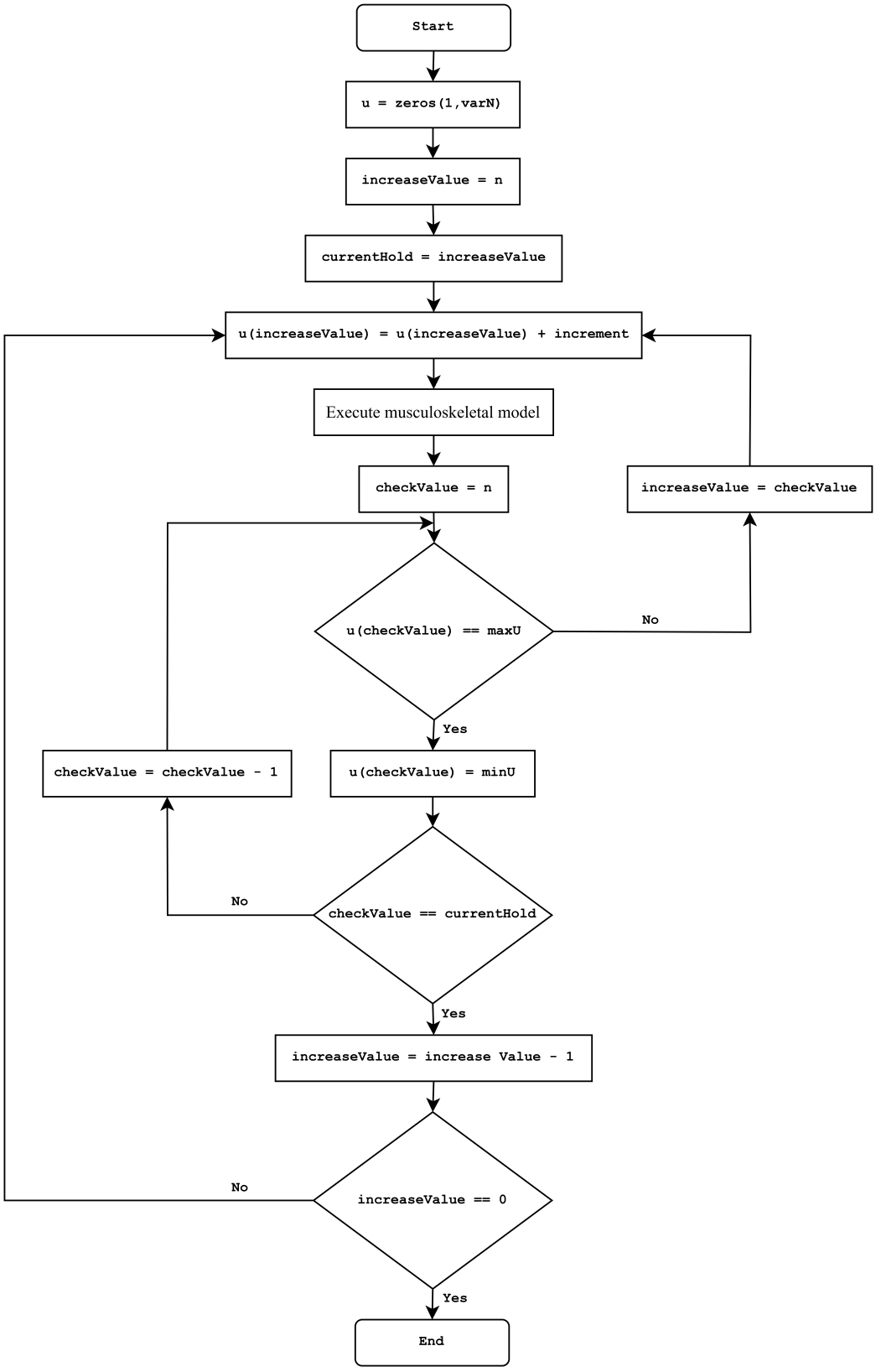

Figure 6.2: A flowchart representation of the implementation of a brute-force search algorithm within MATLAB.

In a brute search the total number of combinations are given by the possible values one element could take on raised to the power of the total number of elements. Mathematical expressed by $c = v^e$, where c denoted the total number of combinations, v is the number of possible values each element can be and e is the total number of elements considered. In this application there are 12 elements to the muscle excitation vector. Considering a binary brute-force search, with be two possible values for each element, results in a total of 4,096 (2^{12}) combinations.

Moving from a binary search to continuous, the increments between possible values can be substituted into this equation to quickly determine the effect of increasing the fineness of the search. As the values lay between, and including, zero and one the possible values are given by $1 + 1/i$, where i is the the value of the increment used. Substituting this into the equation for the total number of combinations gives $c = (1 + 1/i)^e$. As can be seen, a decrease in the increment used results in and increase in the possible values which an element can experience and, in turn, the total combinations. Decreasing this increment, and in turn improving the fineness of the search, as little as one step to 0.5 results in a total number of combinations of 531,441 ($(1 + 1/0.5)^{12}$). If this was to be decreased to a value more fitting to the situation and sensitivity of the musculoskeletal model, 0.01, it would require 1.13e24 ($(1 + 1/0.01)^{12}$) total combinations. Ideally this step size would be further decreased, though it can be seen this would result in an unreasonably large number of combinations.

This approach can be seen to be simple to implement and, given a fine enough interment, would accurately determine the correct muscle excitations for a presented hand shape. However, as has been shown, decreasing this increment results in a dramatic increase in he total number of combinations needed to be tested and, as a result, the computational complexity of this algorithm. Though easy to implement, it is unlikely that this search method would be a practical application for determining the muscle excitations of hand shapes from kinematic data. Due to the superior efficiency, a converging algorithm is more desirable.

6.2.5 Hybrid Methods

Additional to the implementation of the described techniques individually, a selection of these methods where implemented in tandem with one another. This fusion was performed in an attempt to provide a balanced performance of the techniques. The GA and PSO methods showed superior results during preliminary testing, for this reason they have been the focus of the hybrid method - using the other techniques to further their abilities. The techniques chosen to aid these were a binary brute-force search and GD, aiming to utilise the search power of the brute-force search and

speed of GD. All of the methods chosen were implemented with the aforementioned settings.

One hybrid method attempted was the implementation of a GD following an application of GA and PSO. This is a typical application of GD, used to converge further towards a solution following an approximation of the global minimum to a problem. Following the GA and PSO, the GD method is then applied to converge to a final solution - improving the accuracy of the results with little cost of the computational time.

Another method which attempted was the application of a binary brute-force search prior to the execution of the GA and PSO methods. A binary brute-force search was chosen, compared to a finer search interval, in the interest of time; a binary search required 4,096 iterations, compared to the next finest search (increments of 0.5) requiring 531,441 iterations. The applications of the GA and PSO techniques following the search resulted in the conclusion that this search did not require a high accuracy. It was decided that reducing the computational complexity of the overall method was sought after more than the initial pass accuracy. Using a brute-force search to initialise the GA and PSO applications allowed for a faster convergence promised by both, with an increase in accuracy as a result of these improved initial conditions. The binary brute-force search attempts each binary combination of muscle excitations with the musculoskeletal model and calculates the resultant cost of each, selecting the set of muscle excitations displaying the lowest cost as the initial conditions for the next technique. A GA or PSO is then performed, converging towards the solution from these given initial conditions.

In an attempt to utilise the favourable properties of each algorithm, methods employing the results of a brute-force search with either a GA or PSO optimisation method, to then be reduced by GD, were trialled. This was trialled due to the initial capable performance of the brute-force search into GA and PSO combinations and the improvements seen of following the GA and PSO methods with GD. The exhaustive exploration of a brute-force search, into the balanced exploration and exploitation of the GA and PSO methods, with the exploitation from GD, through the quick descent on a minimum, makes this combination appealing. To initialise, these hybrid methods performed a brute-force search across an exhaustive collection of binary muscle excitations to find the closest match to the solution. The muscle excitation set with the lowest cost from this search was then inputted to either a GA or PSO technique, to minimise the cost of this set. A GD method was then implemented to further reduce this cost, in attempt to find the global minimum cost for the problem - the optimal set of muscle excitations creating the inputted hand shape.

6.3 Proposed Solution Selection

To assess the ability of the collection of suggested optimisation techniques, validation and evaluation of each was conducted. The cost function was tailored to each of the optimisation technique through tuning based on the results of inputting two hand shapes with known muscle excitations, shown in Figure 3.19. To evaluate the effectiveness of each method, these hand shapes with known muscle excitations were then inputted into each method ten times. The muscle excitation and joint angle correlations and time taken of each application was recorded to determine an average performance of each method. Following this, each method was then tested with an input of a recorded equilibrium hand shape, seen in Figure 3.20, to ensure adequate performance with experimental data. Selection of a proposed technique was completed from a review of the results from each assessment method to deem the best overall performing method. These chosen assessment methods are described in Section 3.6, with the results of which in Section 4.3.

The parameters of the cost function for each method were tuned prior to validation and evaluation. The optimisation methods underwent hyperparameter tuning through parameter variations over multiple applications of the hand shapes in given in Figure 3.19. Utilising (3.5), the components of the cost function for each method were coaxed towards those providing the best performance using PSO and GD optimisers. Through each iteration the correlation between the known and predicted muscle excitations was tested and the parameters altered, in an attempt to minimise the difference between the recorded data and predictions made - resulting in convergence towards the best possible predictive performance for each technique. This minimisation was achieved by implementing equation (3.6) as the cost function for the parameter tuning.

The overall performance of each method was assessed through repeated applications of the methods with identical inputs. To become a method which can be confidently proposed as a means of predicting the muscle excitations occurring from a single frame of kinematic data they much show agreement with the known muscle excitations. The chosen hand shapes for the repeated applications are displayed in Figure 3.19. The performance measures selected, to be examined over the repeated applications, were: the muscle excitation and joint angle correlations and the time taken. The differences between the input and the resultant joint angles of the output inputted into the musculoskeletal model were considered - observing the difference in these sets of angles, correlation between them and time taken in each application. Through comparison of the muscle excitations, the end goal outputs from the muscle excitation prediction methods can be observed. The comparison of the joint angles

also provides the level of confidence to be had in the choice to assess each method with the joint angles; if the muscle excitation match and the joint angles agree with the outcome of this assessment then it holds that this is a valid means for performance assessment. Though the time taken is not of great concern for this application of the predictive model, it was considered potentially useful for future applications. The proposed solution was then concluded from the judged best performance across all of these categories. The results achieved form this evaluation method can be seen in Table 4.5.

To further validate the selected methods, experiment data of an equilibrium hand shape have been tested with each; these data included both the recorded joint angles and muscle excitations for the hand shape seen in Figure 3.20. This test allowed for the assessment of the methods with experimental data. Additionally, the tested equilibrium hand shape was not used during the tuning of the cost functions and, therefore, was an appropriate test of the predictive performance of each method with unseen data. The resultant muscle excitations found from the validation method employed can be seen in Table 4.6.

Reviewing the validation and evaluation tests highlighted the hybrid combination of a PSO technique followed by a GD method as the superior muscle excitation prediction method. This method offered a confident muscle excitation accuracy, with consistent repeatability. Furthermore, this method was one of two methods able to provide the desirable muscle excitations in a test with a recording of the equilibrium hand shape. This method has been used to determine the muscle excitations found in ADL from the single kinematic frames of averaged hand shapes found across ADL recordings, the results of which are presented within the next section.

6.4 Muscle Excitations of Common Hand Shapes

Following proposal of a means for predicting the muscle excitations from a single frame of kinematic data, the hand shapes of ADL were inputting. This was performed with the aim to determine the muscle excitations of ADL. Hand motion data seen in modern ADL has been collected with the portable motion capture system and a taxonomy common hand shapes has been created from these data. The model introduced in Section 3.1.2 has been implemented with the hand shapes presented in Section 5.2 to determine the muscle excitations from the collected data. The determination of the muscle excitations performed to achieve these common hand shapes would provide the knowledge required for EMG controlled upper-limb prostheses.

The taxonomy of hand shapes used as inputs into this method, presented by Figures 5.1 and 5.2 for the left and right hands respectively. These represent the

functional hand shapes found within ADL. To implement this model with the hand shapes of ADL the Cartesian co-ordinates of the cluster centroids were converted into the required joint angles, applying the vector dot product shown by (2.4). The PSO and GD hybrid optimisation method was then employed in order to converge on the closest muscle excitations which results in the desired joint angles, providing a prediction of the muscle excitations of the inputted hand shape. The mean of the absolute differences between the desired and outputted joint angles was calculated as a measure of evaluating of the results.

The GD hybrid method was selected to examine the data collected during ADL, due to the superior balance of accuracy, consistency and computational time which it demonstrated. To perform this process on the 40 and 24 common hand shapes found in ADL for the, respectively, left and right hands it took three hours 58 minutes and 12 seconds. This was performed on a computer with Windows 10, 32 GB random access memory (RAM) , Intel Core i7-7700 processor and MATLAB 2020b (9.9.0.1570001). The muscle excitations for all of the hand shapes recorded during ADL have been calculated and can be seen in Tables 6.2 and 6.3. Within these tables each row represents one of these common hand shapes, each column the extrinsic muscles of the hand and each element displays the found muscle excitation for the respective muscle as a fraction of maximum muscle excitation during the performance of each hand shape. The muscles observed are the: flexor digitorum superficialis (FDS), flexor digitorum profundus (FDP), extensor digitorum (ED), extensor indicis (EI), extensor pollicis longus (EPL), extensor pollicis brevis (EPB), flexor pollicis longus (FPL) and abductor pollicis longus (APL). The resultant actions performed by activations of each of these muscle groups can be seen in Table 2.1. Images of the hand taking on the outputted joint angles, for the left and right hands respectively, are shown in Figure 6.3 and 6.4. Comparing these hand shapes to those seen in Figure 5.1 and 5.2, receptively, visualises the error of the implemented technique. When implemented with all of the hand shapes found in ADL the outputs were found to differ from the desired joint angles by an average of 19.3 degrees. The full collection of hand shapes showed a correlation between the determined and desired hand shapes of 0.58. This was, respectively, composed of average joint angle differences of 19.6 degrees and 19.3 degrees and correlations of 0.55 and 0.61 for the left and right hands. Though this joint angle correlation was low, the strong performance that this method demonstrated when predicting the muscle excitation during validation, in spite of a comparatively lower joint angle correlation, provides confidence in the generated outputs.

Table 6.2: The predicted muscle excitations for the hand shapes, from the left hand, presented in the introduced taxonomy of hand shapes.

Hand Shape	Muscle																	
	FDSL	FDSR	FDSM	FDSI	FDPL	FDPR	FDPM	FDPI	EDCL	EDCR	EDCM	EDCI	EDM	EIP	EPL	EPB	FPL	APL
1	0.00	0.00	0.00	0.00	0.00	0.00	0.00	0.00	0.27	0.37	0.37	0.20	0.26	0.03	0.00	0.00	1.00	0.00
2	0.15	0.14	0.13	0.22	0.36	0.21	0.32	0.28	0.00	0.00	0.00	0.00	0.00	0.00	0.00	0.00	1.00	0.00
3	0.00	0.00	0.02	0.00	0.00	0.00	0.12	0.10	0.00	1.00	0.00	0.00	0.00	0.00	0.00	0.00	0.45	0.00
4	0.13	0.13	0.07	0.00	0.24	0.15	0.17	0.02	0.00	0.00	0.00	0.22	0.00	0.03	0.00	0.00	1.00	0.00
5	0.08	0.11	0.09	0.14	0.26	0.18	0.26	0.23	0.00	0.00	0.00	0.00	0.00	0.00	0.00	0.00	1.00	0.00
6	0.03	0.00	0.00	0.00	0.12	0.00	0.00	0.14	0.00	1.00	0.52	0.21	0.00	0.00	0.00	0.00	0.10	0.00
7	0.00	0.00	0.00	0.00	0.00	0.00	0.00	0.00	0.25	0.67	0.68	0.07	0.23	0.01	0.00	0.00	1.00	0.00
8	0.00	0.00	0.00	0.00	0.00	0.00	0.00	0.00	0.34	0.66	0.63	0.21	0.32	0.03	0.00	0.00	1.00	0.00
9	0.00	0.04	0.00	0.04	0.00	0.06	0.00	0.07	0.27	0.00	0.34	0.00	0.27	0.00	0.00	0.00	1.00	0.00
10	0.13	0.00	0.00	0.00	0.29	0.00	0.00	0.00	0.00	0.63	0.66	0.23	0.00	0.00	0.00	0.00	1.00	0.00
11	0.00	0.00	0.00	0.00	0.00	0.00	0.00	0.02	0.03	0.14	0.14	0.08	0.02	0.01	0.00	0.00	1.00	0.00
12	0.00	0.00	0.00	0.00	0.00	0.00	0.00	0.01	0.25	0.52	0.50	0.24	0.24	0.00	0.00	0.00	1.00	0.00
13	0.00	0.00	0.00	0.00	0.00	0.00	0.00	0.22	0.13	0.21	0.26	0.12	0.14	0.03	0.00	0.00	1.00	0.00
14	0.13	0.16	0.13	0.00	0.30	0.20	0.32	0.04	0.00	0.00	0.00	0.16	0.00	0.02	0.00	0.00	1.00	0.00
15	0.00	0.00	0.00	0.00	0.00	0.00	0.00	0.01	0.25	1.00	0.26	0.22	0.25	0.03	0.00	0.00	0.28	0.00
16	0.00	0.00	0.00	0.00	0.00	0.00	0.00	0.04	0.04	0.10	0.34	0.15	0.00	0.02	0.00	0.00	1.00	0.00
17	0.13	0.14	0.08	0.12	0.24	0.15	0.18	0.15	0.00	0.00	0.00	0.00	0.00	0.00	0.00	0.00	1.00	0.00
18	0.00	0.00	0.00	0.00	0.00	0.00	0.00	0.06	0.26	1.00	0.19	0.03	0.24	0.00	0.00	0.00	0.22	0.00
19	0.00	0.00	0.00	0.00	0.00	0.00	0.00	0.00	0.20	1.00	0.26	0.15	0.19	0.02	0.00	0.00	0.33	0.00
20	0.00	0.00	0.00	0.00	0.00	0.00	0.00	0.04	0.27	0.23	0.19	0.22	0.26	0.03	0.00	0.00	1.00	0.00

21	0.00	0.00	0.00	0.00	0.13	0.00	0.00	0.00	0.00	0.56	0.61	0.21	0.00	0.03	0.00	0.00	1.00	0.00
22	0.15	0.15	0.13	0.00	0.36	0.21	0.32	0.07	0.00	0.00	0.00	0.06	0.00	0.01	0.00	0.00	1.00	0.00
23	0.00	0.00	0.00	0.00	0.00	0.00	0.00	0.00	0.24	0.48	0.49	0.18	0.23	0.03	0.00	0.00	1.00	0.00
24	0.05	0.05	0.00	0.00	0.15	0.11	0.00	0.00	0.00	0.00	1.00	0.19	0.00	0.03	0.00	0.00	0.26	0.00
25	0.13	0.00	0.00	0.00	0.31	0.00	0.00	0.20	0.00	0.16	0.12	0.00	0.00	0.00	0.00	0.00	1.00	0.00
26	0.09	0.06	0.00	0.00	0.20	0.10	0.02	0.00	0.00	0.00	0.01	0.00	0.00	0.05	0.00	0.00	1.00	0.00
27	0.11	0.11	0.08	0.00	0.28	0.18	0.23	0.03	0.00	0.00	0.00	0.04	0.00	1.00	0.00	0.00	0.19	0.00
28	0.10	0.00	0.00	0.00	0.32	0.00	0.00	0.02	0.00	0.50	0.59	0.19	0.00	0.03	0.00	0.00	1.00	0.00
29	0.00	0.00	0.00	0.00	0.00	0.00	0.00	0.14	0.28	0.63	0.54	0.00	0.27	0.01	0.00	0.00	1.00	0.00
30	0.00	0.00	0.00	0.00	0.00	0.00	0.00	0.03	0.26	0.15	0.04	0.00	0.24	0.06	0.00	0.00	1.00	0.00
31	0.00	0.12	0.00	0.00	0.00	0.19	0.02	0.23	0.14	0.00	0.12	0.24	0.12	0.04	0.00	0.00	1.00	0.00
32	0.04	0.00	0.00	0.00	0.17	0.02	0.02	0.00	0.00	0.00	0.02	0.16	0.00	0.02	0.00	0.00	1.00	0.00
33	0.07	0.14	0.00	0.17	0.19	0.17	0.01	0.21	0.00	0.00	1.00	0.00	0.00	0.00	0.00	0.00	0.17	0.00
34	0.00	0.00	0.05	0.14	0.00	0.00	0.14	0.13	0.04	0.12	0.00	0.00	0.00	0.00	0.00	0.00	1.00	0.00
35	0.00	0.13	0.07	0.15	0.00	0.17	0.21	0.20	0.26	0.00	0.00	0.00	0.25	0.00	0.00	0.00	1.00	0.00
36	0.13	0.13	0.00	0.00	0.33	0.19	0.00	0.19	0.00	0.00	0.49	0.20	0.00	0.03	0.00	0.00	1.00	0.00
37	0.00	0.13	0.08	0.00	0.00	0.19	0.25	0.00	0.05	0.00	0.00	0.16	0.00	0.03	0.00	0.00	1.00	0.00
38	0.00	0.00	0.00	0.02	0.00	0.00	0.00	0.08	0.27	1.00	0.33	0.00	0.26	0.00	0.00	0.00	0.30	0.00
39	0.00	0.00	0.00	0.00	0.00	0.00	0.00	0.00	0.16	0.34	0.43	0.09	0.14	0.01	0.00	0.00	1.00	0.00
40	0.10	0.10	0.00	0.00	0.33	0.20	0.00	0.12	0.00	0.00	0.16	0.07	0.00	0.02	0.00	0.00	1.00	0.00

Table 6.3: The predicted muscle excitations for the hand shapes, from the right hand, presented in the introduced taxonomy of hand shapes.

Hand Shape	Muscle																	
	FDSL	FDSR	FDSM	FDSI	FDPL	FDPR	FDPM	FDPI	EDCL	EDCR	EDCM	EDCI	EDM	EIP	EPL	EPB	FPL	APL
1	0.00	0.00	0.00	0.00	0.00	0.00	0.00	0.02	0.08	0.16	0.15	0.07	0.08	0.01	0.00	0.00	1.00	0.00
2	0.09	0.08	0.06	0.11	0.23	0.14	0.21	0.19	0.00	0.00	0.00	0.00	0.00	0.00	0.00	0.00	1.00	0.00
3	0.00	0.00	0.00	0.00	0.00	0.00	0.00	0.10	0.30	0.48	0.41	0.00	0.29	0.00	0.00	0.00	1.00	0.00
4	0.00	0.00	0.00	0.00	0.00	0.00	0.00	0.02	0.23	0.36	0.35	0.15	0.21	0.02	0.00	0.00	1.00	0.00
5	0.00	0.00	0.00	0.00	0.00	0.00	0.00	0.03	0.28	0.67	0.64	0.10	0.26	0.02	0.00	0.00	1.00	0.00
6	0.00	0.00	0.04	0.14	0.00	0.00	0.14	0.13	0.06	0.11	0.00	0.00	0.03	0.00	0.00	0.00	1.00	0.00
7	0.09	0.10	0.00	0.00	0.30	0.19	0.00	0.12	0.00	0.00	0.20	0.04	0.00	0.01	0.00	0.00	1.00	0.00
8	0.10	0.08	0.00	0.00	0.21	0.12	0.02	0.00	0.00	0.00	0.01	0.03	0.00	0.00	0.00	0.00	1.00	0.00
9	0.11	0.11	0.10	0.00	0.33	0.20	0.28	0.02	0.00	0.00	0.00	0.14	0.00	0.02	0.00	0.00	1.00	0.00
10	0.00	0.00	0.00	0.00	0.00	0.00	0.00	0.00	0.30	0.61	0.59	0.21	0.29	0.03	0.00	0.00	1.00	0.00
11	0.00	0.14	0.10	0.17	0.00	0.18	0.26	0.26	0.12	0.00	0.00	0.00	0.12	0.00	0.00	0.00	1.00	0.00
12	0.15	0.15	0.12	0.19	0.33	0.19	0.30	0.25	0.00	0.00	0.00	0.00	0.00	0.00	0.00	0.00	1.00	0.00
13	0.00	0.00	0.00	0.06	0.00	0.00	0.03	0.17	0.00	0.50	0.02	0.00	0.00	0.00	0.00	0.00	1.00	0.00
14	0.11	0.15	0.11	0.00	0.27	0.19	0.27	0.04	0.00	0.00	0.00	0.16	0.00	0.02	0.00	0.00	1.00	0.00
15	0.00	0.00	0.00	0.00	0.00	0.00	0.00	0.07	0.02	0.16	0.35	0.12	0.00	0.02	0.00	0.00	1.00	0.00
16	0.00	0.00	0.00	0.00	0.00	0.02	0.00	0.00	0.00	1.00	0.19	0.15	0.00	0.00	0.00	0.00	0.27	0.00
17	0.00	0.00	0.00	0.00	0.00	0.09	0.00	0.15	0.17	1.00	0.21	0.07	0.16	0.00	0.00	0.00	0.16	0.00
18	0.09	0.10	0.00	0.00	0.27	0.18	0.00	0.15	0.00	0.00	0.55	0.21	0.00	0.00	0.00	0.00	1.00	0.00
19	0.00	0.00	0.00	0.00	0.00	0.00	0.00	0.01	0.14	0.18	0.10	0.04	0.13	0.01	0.00	0.00	1.00	0.00
20	0.01	0.00	0.00	0.00	0.20	0.00	0.00	0.07	0.00	0.62	0.77	0.21	0.00	0.03	0.00	0.00	1.00	0.00
21	0.00	0.00	0.00	0.00	0.00	0.00	0.00	0.00	0.25	0.40	0.36	0.20	0.25	0.03	0.00	0.00	1.00	0.00
22	0.00	0.04	0.00	0.04	0.00	0.06	0.00	0.07	0.27	0.00	0.34	0.00	0.27	0.00	0.00	0.00	1.00	0.00
23	0.15	0.15	0.10	0.15	0.29	0.17	0.24	0.19	0.00	0.00	0.00	0.00	0.00	0.00	0.00	0.00	1.00	0.00
24	0.00	0.00	0.00	0.00	0.31	0.00	0.00	0.02	0.00	0.62	1.00	0.24	0.00	0.04	0.00	0.00	0.56	0.00

Figure 6.3: The hand shapes, for the left hand, created from the predicted muscle excitations of hand shapes from the introduced taxonomy of hand shapes, using the proposed prediction technique.

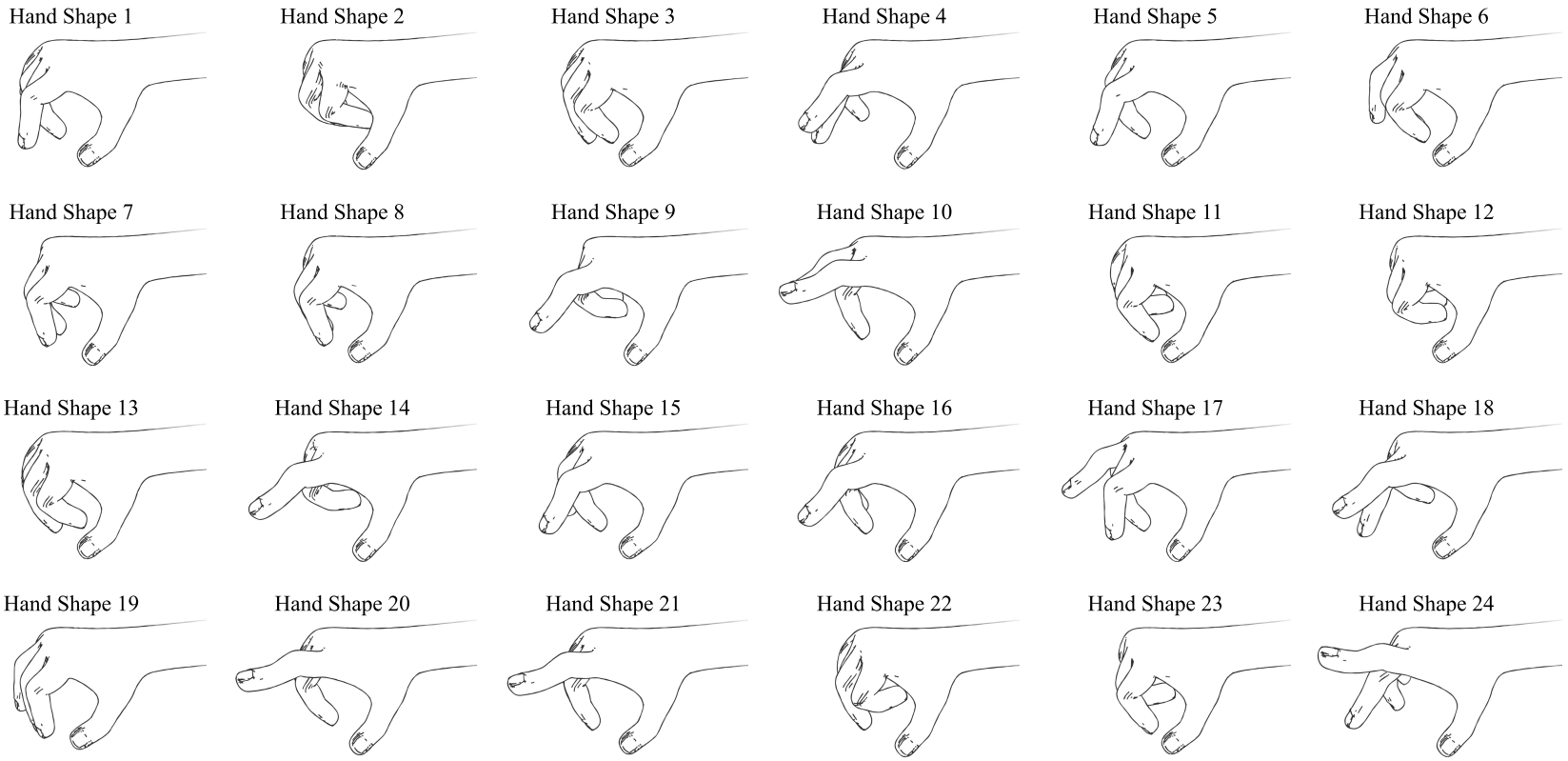

Figure 6.4: The hand shapes, for the right hand, created from the predicted muscle excitations of hand shapes from the introduced taxonomy of hand shapes, using the proposed prediction technique.

6.5 Discussion

The applications of different optimisation methods to predict muscle excitations from a single frame of kinematic data have been presented and each was tested on data collected during ADL. The accuracy and computational time of each has been examined. The hybrid method, an application of a PSO method followed by a GD technique, has been highlighted as the best and, in turn, claimed to be the proposed solution.

The cost functions for each of the selected optimisation methods were tuned with the hand shapes presented in Figure 3.19. When considered in repeated applications, inputting the validation hand shapes, all methods showed an average correlation to the inputted joint angles greater than 0.70. The brute-force search and GD method provided the lowest correlations between predicted and know muscle excitations during validation, respectively showing correlations of 0.46 and 0.22 - without these, all of the recorded muscle excitation correlations were above 0.60. This means of evaluation was able to identify key differences in the applications and results of the selected methods, providing options for the selection of a proposed solution. All of the methods were tested with an input of an equilibrium hand shape; in this test the PSO and PSO followed by GD methods were the only methods to present the correct solution - zero muscle excitations across all muscles.

The proposed solution to determining muscle excitations from kinematic data is a combination of a musculoskeletal model [9] and the PSO with GD hybrid optimisation method. This method was selected for the superior balance in performance, across all of the assessment categories observed, demonstrated. This method displayed superior muscle correlation performance when tested in ten repeated applications, showing a correlation of 0.74 between the known and predicted muscle excitations; this unsurpassed performance was key to the selection of this technique. Through these ten applications, this method displayed a very low variation across all of the measured fields. Across the ten applications the outputted joint angles showed a correlation to those desired of 0.74. A standalone implementation of PSO was able to provide a higher joint angle correlation but was hindered by the lower muscle excitation correlation it displayed. The average time taken by the PSO and GD hybrid optimisation method, to provide predictions of the muscle excitations, was 173 seconds. For this study computational time was not of high importance and, therefore, this slower performance did not provide any detriment the selection of this method. Further highlighting the performance capabilities of this method was that it was one of only two methods to produce the desired equilibrium validation results, the other method being a singular implementation of PSO.

When implemented with the hand shapes found in ADL, by the portable motion capture system, the proposed solution was able to provide muscle excitations creating hand shapes with an average difference of 19.3 degrees from those inputted, with a correlation to these of 0.58. In an application of the chosen musculoskeletal model [173], adequate control of a robotic hand was achieved with a correlation, to the performed hand motions, greater than 0.55; therefore, the correlation of 0.58 observed here provides promising results for this prediction technique. The EPL, EPB and APL all exhibited zero excitation; this raised concern that the implementation of muscle redundancies was providing inaccurate results. However, these results were also found when the chosen technique was applied without muscle redundancy considerations. It could be argued that consideration of external forces would influence these muscles and should be tested and, dependently, considered for future implementations. Hand motion data collected with a portable motion capture system have found the hand shapes occurring within ADL. The combination of an existing musculoskeletal model [9] and optimisation techniques has been implemented to determine the muscle excitations of these hand shapes found in ADL. The employed method has been validated and evaluated with hand shape data including muscle excitations; the proposed predictive method performed the best out of all of the examined techniques. Weighting the influence of the joint errors in the cost function, from the results of the Leap Motion controller (LMC) validation experiment, aided application with the collected ADL data. The determination of the muscle excitations performed in ADL would provide knowledge useful for the development of EMG controlled upper-limb prostheses.

The use of optimisation techniques with a musculoskeletal model has shown to be a plausible means of predicting hand muscle excitations. The proposed hybrid technique was able to determine muscle excitations replicating the desired hand shapes, observed during ADL, with an average error of 19.3 degrees and average correlation, to the desired hand shapes, of 0.58. The exclusion of external forces in the recorded data leads to potential inaccuracies in the predicted muscle excitations for the specific use cases recorded. The musculoskeletal model utilised during this application did not observe the intrinsic muscles of the hand - weighting a large focus of any results obtained towards application with prosthetic hand devices. Due to these omissions, an upper-limb device created from these results which desires a controllable gripping strength would require additional controllers to be used; several alternative methods of grasping control have been shown to be feasible, with some studies finding that visual feedback was sufficient [3, 59–62, 65, 68–70]. Furthermore, the exclusive consideration of extrinsic muscles of the hand from the model provides possible limitations to the accuracy of predictions made employing it. However, this work provides a framework to implement a musculoskeletal model with optimisation

techniques for the prediction of hand muscle excitation, enabling the ability to apply different or updated models. This work shows potential in aiding the design and development of EMG controlled upper-limb prostheses by determining the muscle excitations performed during ADL.

Chapter 7

AirGo

As shown in Chapter 2, the currently employed method for measuring hand angles is inaccurate and shows low repeatability. This highlights a need for a more accurate and reliable solution, with particular focus given to an increase of the inter-rater reliability. In this chapter, a novel means for the measurement of hand joint angle data within a clinical setting has been introduced. A description of the device, validation methods, steps taken during the clinical trial and analysis methods performed can be seen provided in Chapter 3. Previously favoured methods are reflected upon, with the limitations and possible solutions highlighted. The proposed solution to these exposed issues has been described within this chapter. The suitability of this proposed solution is discussed, with reference to the results from the validation of the portable motion capture system and the clinical study performed, presented in Chapter 4. A discussion around this work and the resultant data provides a conclusion to this chapter, with empathise on the improvements the introduced device provides to an occupational health therapy clinic.

7.1 Introduction

When evaluating the performance of the human hand an important measure is the active range of motion of the digits. This can be of aid when evaluating the rehabilitation progress of an injured hand, the capabilities of full and partial prosthetic hands and the adoption progress of upper-limb prostheses. Measuring the active range of motion of the digits during rehabilitation or adoption of upper-limb prostheses enables the assessment of the rehabilitation progress; through this, the rehabilitation routine can be altered to further gain greater progress or focus can be given to the weak performing digits in an upper-limb prosthesis. The currently employed measurement device is a goniometer; however, this device lacks the desirable speed, accuracy and consistency for such measurements. Therefore there is a need to improve the measurement devices used to enable improvements to hand rehabilitation and upper-limb prostheses evaluation and adoption. The improvement that would be gained from the employment of a new device, over a goniometer, has been assessed based on the speed, accuracy and consistency of the measurements obtained.

As highlighted in Section 2.10, there have been studies indicating the poor performance of goniometers for hand joint angle measurements [239, 240] and several showcasing new methods or technology aiming to provide an improvement to this [116, 241–248]. The time taken and reliability of the current state-of-the-art are highlighted as significant issues within the literature [116, 247]. Particularly, this showed low inter-rater reliability - indications suggesting that seeing a different clinical staff member on a different visit affects the results more than patient progress would [239, 244, 247]. Additionally, the manual goniometer, implemented commonly within clinics, requires contact with the patient, possibly leading to contamination of the collected measurements. The current state-of-the-art leaves much room for improvement on many fronts and attempts at creating alternative measuring devices have shown promise but lack clinical evaluation [116, 241–248].

The proposed clinical hand angle measuring device, the AirGo (abbreviated from Air Goniometer), has been validated against a state-of-the-art motion capture studio and tested within a hand clinic. Though the accuracy found in validation of the Leap Motion controller (LMC) has shown only marginal improvement over a goniometer, 18.4 degrees, it was still suggested for clinical measurements due to the support shown within the literature [111–116]. It should be highlighted that the validation was performed on a portable system and that the LMC is likely to provide superior accuracy if validated with a PC, as it is used in the AirGo system. The proposed solution offers an ease of use and high reliability of the results, as well as a far quicker time to gather all of the measurements for both hands. The LMC has been employed

along with JavaScript (JS) code to extract the Cartesian locations of the hand joints and, subsequently, calculate the joint angle to form AirGo. These resultant joint angles are displayed within a Hypertext Markup Language (HTML) body.

Here, the proposed solution is introduced, broken down into the physical build and the scripts used for front- and back-end development. The results of the clinical trial are discussed, in relation to the validation performed for the LMC and the demands of a clinical setting. Following these, a discussion compares the AirGo system with the current state-of-the-art and investigates the worth of employing AirGo within clinics.

7.2 Proposed Solution

The AirGo system uses an LMC to calculate the joint angles of a presented hand. This results in faster and more accurate collection of patient data, compared to the currently employed method, with no need for contact between clinical staff and the patients.

In Section 4.1 the a portable system employing the LMC was found to provide a set of choreographed hand shapes within 18.4 degrees, compared to a state-of-the-art motion capture system. As the AirGO system utilises the LMC, and calculates the angles in the same manner, these validation results are implicit of the accuracy of the AirGo system.

In a clinical trail performed with AirGo, the proposed device was seen to be able to record the joint angles within a matter of seconds. This provides a vast improvement to the goniometer, typically taking several minutes to perform the same measurements [116]. Additionally, employment of the AirGo system could alleviate the need of a clinical staff for hand joint angle measurements. Provided the front-end is modified to receive a unique identifier from the patient and direct them through the collection, the device could be set up in the clinic to measure patients prior to their appointments. Furthering this development, AirGo enables the possibility of patients recording from home if necessary. The ease of use of the device means that the patients would only need start the recording and present their hands. The time saved by clinic staff could be used for the treatment of more patients. If a clinical staff is present to oversee the recording, the method still remains contactless; the the clinical staff operates the computer the patient only needs to present their hands. This provides a consistency in measurement results, as the clinical staff member is not able to contaminate results through physical interaction with the patient.

7.2.1 Physical Build

A stand was built to support the LMC whilst the patients used AirGo. This was built for clinical application to aid in the collection of measurements. The vertical positioning of the LMC means that the user can place their elbow on the table and present their hand to the LMC with ease. A built-in height adjustment mechanism allows for the device to be compatible with different users, irregardless of their forearm length. This assists the LMC to find the hand accurately in the space. These adjustable settings were designed such that the centre of the LMC could exist in fine scale intervals between known extremes of forearm lengths. Removal of the physical build would result in a less comfortable user experiences but a reduced cost - of consideration if mass deployment was undertaken.

The initial build of the stand for this system can be seen in Figure 7.1. Each of the components were laser cut from a five millimetre thick acrylic sheet and permanent fixtures were attached with epoxy. Acrylic chosen as it was cheap and accessible and the ability to accurately provide the desired patterns highlighted the laser cut as the selected production method. The base of the system was bent into the desired shape using an acrylic bending machine. The base was bent to ensure that all of weight of the system sits through the centre of the base, creating a stable stand platform which supports the LMC confidently. Sections were cut out of the side to make it so that the stand could be easily picked up and transported. A pocket for the backboard was added to the top of the base, to hold it upright, and house the height adjusting mechanism. Adhesive rubber pads where attached underneath the base to keep the stand stable whilst in use. Though movement does not affect the angle readings, this provided an ease of use. The backboard sits in the pocket of the base and was used to hold the LMC in place during data collection. The adjustable height of the stand was achieved using a moving pin on the base which locks into teeth on back board. The locking pin is three millimetres heigh and the teeth were cut with two and a half millimetres between each one, allowing high level of accuracy during adjustments. At the centre top of the backboard a hole was cut to house the LMC; this was created one millimetres narrower than the LMC. The LMC was placed on the back of the top board, in a recessed hole with an identical width and height to the LMC and three millimetres deep. To support the LMC within the system a clip was fashioned; this lifts up to allow the LMC to be placed into the recess and then will naturally sit down and exert a pressure which holds the LMC within this recess.

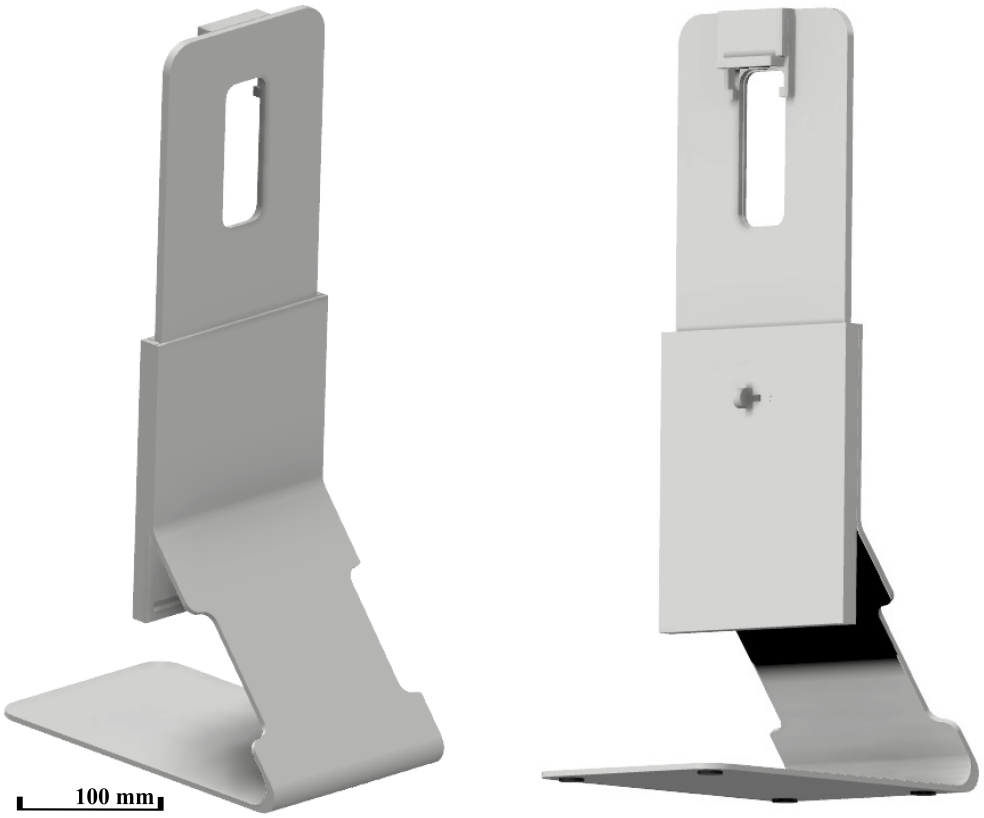

(a) The front view of the first iteration of the stand for AirGo.

(b) The rear view of the first iteration of the stand for AirGo.

Figure 7.1: The front and rear views of the first iteration of the stand for AirGo.

Preliminary experiments with the first iteration of AirGo identified that the LMC performed best when a hand was presented perpendicularly to the long side. Henceforth, the stand was modified to allow the LMC to sit at an angle more suited for data collection. The time frame of the clinical trial resulting in this being solved by the removal of the hole and attachment of the LMC with a suitable adhesive. Given more time, a new top part would be laser cut with the LMC hole rotated appropriately. The final form of the AirGo stand can be seen in Figure 3.5. After implementation it was found that, in this orientation, the LMC was able to pick up the hands more consistently - this setting was adopted for the duration of the clinical trial.

The stand was proven to provide useful functionality during the clinical trial. Though not necessary, this was seen to provide a more comfortable user experience than if the LMC was to be place on a horizontal surface and the hand outstretched. The physical body also helped indicate to the user where to place their hands; for many patients this is a new item and presenting the LMC only would be disorientating.

The height adjustment provided aid to the LMC when locating the presented hands. Following alteration to the orientation of the LMC, the device was able to work with no other issues. Future iterations of AirGo aim to reproduce the clasping mechanism for the LMC in this orientation.

7.2.2 Front-End Code

The screen displayed in an application of AirGo can be seen in Figure 3.6. In the current state, this would be presented to both the patient and clinical staff. The numerical values provide clinical staff with an indication of performance, displaying the best measurement taken so far for each joint and the resultant total active motion (TAM). The gauges display the live, smoothed and best performance for a selected digit, allowing the clinical staff to isolate a single digit and encourage the patient to flex further.

Figure 7.2 presents version 1.1 of AirGo, the main addition to version 1.2 was the addition of the patient identifier input box and save button. When pressed, the save button stores the displayed values in a text file named by the value given in the patient identifier box, current recording time and the number of recordings previously taken for the observed patient - aiding future reference of the measurements taken.

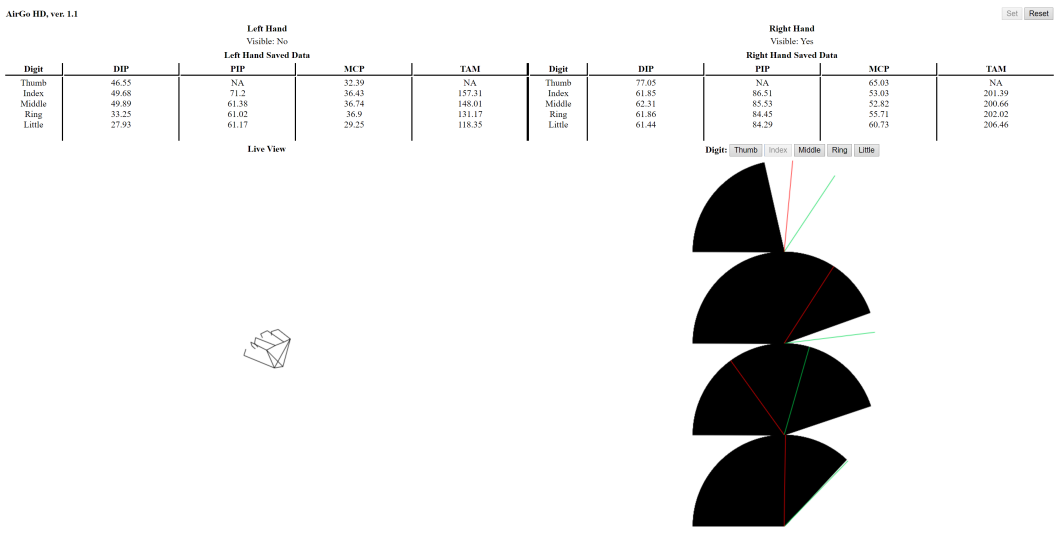

Figure 7.2: The first iteration of the display for the AirGo system.

The AirGo screen consists of: version number, an interactive text box and three buttons, indication of the hands seen, tables of the maximum joint angles reached, a live view of the hands presented and gauge style indications of the joint angles for a selected digit. In the top left of the screen the name AirGo, followed by the

version number, is displayed. The top right of the screen hosts interactive elements of the script, this includes: providing a unique patient ID (to enable patient progress tracking), a set button (to set a current best for the user), a save button (which saves the current observations under the unique patient identifier, the current time and visit number) and a reset button (refreshing the script for the next patient). The indication of the hands seen by the LMC is displayed as a simple "Yes" or "No" to assure the user that the correct hand is being recognised. The table shown updates with the smoothed joint angle for each joint of each digit and respective TAM; the TAM for a digit is calculated from the summation of the constituent joints.

The live view provides a three-dimensional (3D) wire frame image of the current LMC observations. This was used to ensure that the captured information was close to the real life scenario. The live view of the hand was achieved using a canvas drawn on the HTML page, updating the image based on the results gathered from the LMC by the JS script. Gauges of the current flexion degree, for each joint of a selected digit, were created to provide a relative indication of the flexion achieved. These gauges were also created through a canvas drawn on the HTML page, extracting the required data to display from the JS script. This display was also considered as a user motivator to flex a digit further, with future implementations hoping to also include a personal best from all measurements taken for the current patient.

The tables and canvas images displayed were coded to resize with the screen so that the monitor, browser or window position adopted in a use would not matter - the correct information would always display correctly. The set button sets the currently seen hand joint angles as the target flexion for the other hand. These target values were used, rather than absolute bests, as an aim for the patients as not everyone will exhibit the same natural flexion. The creation of a patient specific target severs to provide a more realist aim, intending to lead towards more motivated patients.

One future modification is to split the information displayed between the clinician staff and patient. For the current implementation within a clinical study the information has been reduced and amalgamated on a single screen. Further information, sought by the clinical staff would be saved following the measurements for later reference. For the patient, future implementations plan to display the virtual representation of the presented hand and achieved joint angles. This aims to focus motivation on the patient to further flex their joints, through a gamification of the task. Additional to this, the ability to reload past recordings and personal best would aid patient motivation.

7.2.3 Back-End Code

In order to extract the positional co-ordinates of he hand from the LMC and, in turn, calculate and present the required data, several JS scripts were executed within the HTML script. These produce a loop, updating with measurements from the LMC and performing any necessary calculations each iteration. Any interaction with the AirGo screen, such as the buttons in the top right, executes specified JS scripts written to execute the requested functions.

Upon start the Leap Service programme initiates a local websocket, this is accessed by the JS code to gather the data from the LMC. From the LMC the 3D Cartesian locations of each of the joints, for the presented hands, are found. Using the animation loop of the current browser, the values obtained from the LMC are continually updated. The obtained values are stored as JS variables for later access by the code.

The joint angles are calculated for each joint, in turn, using the vector dot product in 3D space, utilising (2.4). To achieve this the joints more proximal and more distal to a selected joint; when calculating the including the distal interphalangeal (DIP) angle the tip of a digit was considered as the joint more distal. These joint are transformed to make the currently considered joint the origin of the Cartesian space, from which the dot product rule was directly applied with inputs of the other joints locations to determine the angle between them - providing the joint angle of the currently considered joint. This was converted into degrees, from radians, and subtracted from 180 degrees to provide the flexion angle of the joint (the commonly considered clinical measure). The abduction and adduction of the digits is not considered and, therefore, been omitted during these calculations. Smoothing was applied to avoid the potential of any anomalous data contaminating the collected measurements. If data has been collected for a hand for 100, consecutive, frames the the mean and standard deviation of this 100 set of frames are calculated. Each of the recorded angles from each of these frames is compared to the two standard deviations away from the mean, a frame found outside of this is removed. The average of the remaining frames provides the smoothed angle, to be displayed on the AirGo screen.

The TAM value was calculated with the summation of the DIP, proximal interphalangeal (PIP) and metacarpophalangeal (MCP) joint angles. The TAM of the thumb was not calculated due to the lower number of joints, resulting in a measure it not comparable with the other digits. The joint angles of the carpometacarpal (CMC) joint (flexion and extension and abduction and abduction) are not considered in observations the hands joints and, due to this, have not been considered here.

Following the calculation of the joint angles, the `getElementById` function was

used to update the cells of the HTML table accordingly. Each cell in the HTML front-end script was labelled with an `id` property, this is then accessed by the `getElementById` function and the variable stored under that `id` updated by the JS script - updated each iteration of the embedded JS script. The `getElementById` function was also used to extract the x, y and z Cartesian co-ordinates of the joints, for display in the live view area. These values were drawn onto the created canvas using the `beginPath`, `moveTo` and `lineTo` functions. The `beginPath` starts a new drawing on the canvas, the `moveTo` function defines the start point of the line to be drawn and the `lineTo` draws a line between this start point and specified position. These functions are used to draw connecting lines between each of the joint locations, resulting in a wire frame representation of the hand. The gauges, displaying the requested joint angles, also use the `beginPath`, `moveTo` and `lineTo` functions to update the dedicated canvases. These function draw a line representative of the percentage of 180 degrees that the observed angle comes to. The space be between the current angle and a zero degree representation with line is then filled to display as arc from zero degrees to the observed angle. All of the aforementioned are updated with each cycle of the JS loop.

When a, unique, identifying value is typed into the patient identifier box this value is held by the HTML script and later extracted by the JS script using the `getElementById` function. Utilising this value with the name of the later saved file provides a unique identifier for the measurements taken for each patient. Upon pressing the set button a boolean variable, `set`, is switched from false to true; this variable is queried each loop and if found true then the currently seen hand is set as the ideal joint angles These joint angles are stored in separate variable, to later be refereed in order to drawn comparisons. When the "Save" button is pressed the smoothed joint angles at that moment in time are written into a string variable, tabulating these values, and saved as a text file. The JS save script then creates a route for the HTML to download the file from, clicks the link to begin the download and subsequently removes the link. This file is named by the patient identifier and the current date and time (obtained using the `Date` JS function), for later ease of reference. The reset button simply refreshes the browser page using the `location.reload()` function, this reloads the currently viewed webpage and, in turn, resets any stored data.

7.3 Clinical Trial

A clinical study implementing the AirGo system was performed during a hand clinic at University Hospitals Coventry & Warwickshire (UHCW). A total of 11 patients

were measured, voluntarily, following a visit to the clinic. Of these 11 patients, 16 trials were recorded; four of the patients were recorded in consecutive visits.

The results of this clinical trail are presented in Section 4.4, displayed within Table 4.9. Measurements of joint angles required took less than 30 seconds, for each patient, and required no expertise or prior knowledge to operate the device, only for the patient to present their hand to the LMC.

7.4 Discussion

The currently employed method for hand joint angle measurements, a goniometer, lacks the desired accuracy and reliability and requires prior knowledge and expertise to operate. The introduced AirGo system was able to measure the joint angles of the hands within a fraction of the time taken for measurements with a goniometer and showed a superior accuracy, with no need for prior knowledge of the system. Following a clinical study, the AirGo system has been shown to be applicable within a clinical environment. The ability to store the data with the AirGo system allows for an ease of measurement comparisons and the possibility to quickly review patient progress. Additionally, the use of measurements taken from each patient to provide a goal to aim for provides an achievable aim for each patient - the gamification of the system leads to a more motivated patient. Utilisation of data recorded from each patient as the respective target angles, compared to an absolute best, also means that any natural limitations of patient are be accounted for; this provides a patient specific clinical assessment.

Though designed for clinical application, there is not restriction to use in a clinical environment and there is no reason for the patient to not perform this measurement collection at home (given the LMC is provided for them and they have a PC meeting the requirements). The LMC is inexpensive and could be loaned to several patients and does not enforce heavy demands on a PC. With a limited number of LMCs, AirGo could still find use in application before or after clinical visits, with self measurement acquisition being possible.

In a study to validate a portable motion capture system the LMC was shown to provide adequate measurement accuracy; theory suggests the possibility of a higher accuracy with the AirGo system when implemented with a PC with higher specifications. The use of the LMC in a clinical environment is also supported by the literature, proving to provide an accuracy holding clinical relevance [111–116].

Application of the device within a clinical environment severed to prove the capability of the device to provide the desired properties of a measurement system

AirGo was quick to provide data with high consistency in measurements without requiring expertise or contact. The smoothing applied to the data provided a more reliable reading; however, this did result in an, approximately, two second delay to the data. The LMC would sometimes label the detected hand incorrectly, the live view of the virtual hand and seen hand indicators provide the necessary knowledge of an error occurrence - with removal and representing the desired hand commonly fixing this issue. The display is functional but offers little in terms of a user friendly experience, if deployed within clinics it would be preferred that this is redesigned to provide a cleaner and easier to understand interface. It was observed that, throughout the clinical trial, patient interest was peaked by the displayed hands; this digital visualisation of the hand serves to potential aid the adoption rate of the device and result in a greater willingness of patients to participate. AirGo was able to measure all of the joint angles for the presented hands in a matter of seconds; the currently employed goniometer has been shown to take several minutes to produce the same results [116].

Observations of the recorded data concluded that, comparing the MCP angle of the known injured digit on each hand gave the most confident results for predicting injury (eight out of 11 patients correctly predicted). Observing the MCP angle exclusively was also among the methods which presented the highest number of progressed patients. Though these results are not conclusive, as it is unknown whether the patients did progress, the ability to predict the correct injury with an accuracy greater than 70% highlights this analysis method as a possible means of quickly identifying patient progress. Knowledge of the precise validity and repeatability of this method is limited, suggested future work includes a comparison of this system with a state-of-the-art motion capture studio over several repeated recordings. In a study implementing the LMC for hand digit joint angle measurements [116], it was seen that the accuracy of the wrist rotation was lower when the elbow was not seen. During measurements, the AirGo does not view the elbow position; however, the wrist angles are not measure and, therefore, this was not seen as a problem. This knowledge, however, would influence future changes if wrist angle observations were added.

The proposed solution has demonstrated, within a clinical environment, several advantages over the currently employed joint angle measurement method. The required procurement of several LMCs may result in a limited adoption; however, The literature shows vast support for the creation a superior clinical measurement method [116, 239–248], with additional support seen for the use of the LMC [111–116].

Chapter 8

Conclusions and Future Work

This chapter highlights the conclusions drawn from the works of previous chapters. Included within this are discussions of the: created taxonomy of functional hand shapes, proposed technique to predict muscle excitations from kinematic data and suggested method to the measurement of joint angles within a clinical environment. The modern, updated, taxonomy of hand shapes, presented in Chapter 5, is reviewed. The resultant accuracy from the predictions of muscle excitations using kinematic data, seen in Chapter 6, is evaluated. The improvements offered, by AirGo, over the current clinically employed hand digit angle measurement device, highlighted in Chapter 7, are discussed. Additional to this, the recommendations for future work in all of these areas are presented.

8.1 Conclusions

This work has completed the set out objectives and provided knowledge of the hand shapes found in everyday modern life, with the importance and predictions of the muscle excitations for each also provided. A method for predicting the muscle excitations occurring within a single frame of kinetic data has been provided and an improved clinical method for measuring hand digit joint angles supplied.

The goal of creating a portable motion capture system has been met; the Leap Motion controller (LMC) and Next Unit of Computing (NUC) system has proven to be a viable means of collecting hand motion data during activities of daily living (ADL). It was found to collect natural, unencumbered, hand movements without problems. The system was validated against a state-of-the-art motion capture system and found to provide data within 14.2 mm, exhibiting a correlation between the two systems of 0.92. The clustering, with subsequent merger, of the collected data gave confident results, reducing all of collected data into 40 and 24 hand shapes, for the left and right hands respectively. These hand shapes were shown to represent all of the collected data within 12 mm for both hands. The found hand shapes formed the novel taxonomy introduced here, with information of each grouping readily available. The provided details of each group enabled manual intervention for a more concise and customised taxonomy of the hand shapes of ADL, to suit specific needs. The large focus that previous work has placed on grasps, tainted by the desire of a wider audience from industrial manufacturing robotics, limits the obtained results. This research aimed to capture all of the functional hand shapes present during ADL, with an unhindered focus on improving the quality of life for upper-limb prostheses users. The lack of video recordings of the collected data and the fact that no knowledge exists of the exact tasks being performed during the use of each hand shape leads to difficulties in designing task specific prostheses. This knowledge would enable task focused customisation during the development of the prosthetic devices, as the specific hand shape requirements during set tasks would be known. This could lead to the development of upper-limb prostheses with high usability whilst remaining at a low cost. Despite ample performance during validation, the data captured by the employed portable motion capture system still differed from those from the state-of-the-art. As post-processing of these data included reductions made with machine learning techniques, there is the potential that some information was lost in these choice. Any data loss could potentially mean that hand shapes occurring during ADL were missed. The data have been collected from a diverse range of participant ages, gender and activities, but there was a lack of left handed participants. This means that it is difficult to draw decisive conclusions relevant for all end users.

An existing musculoskeletal model has been implemented alongside optimisation techniques to provide predictions of hand muscle excitations from kinematic data. Following validation and evaluation of each of the selected methods, the use of a hybrid technique utilising a particle swarm optimisation (PSO) technique with gradient descent (GD) was concluded as the proposed solution. The deployment of this with the hand motion data collected during ADL was found to supply muscle excitations providing joint angles with an average pairwise difference to the inputted hand shape of 19.3 degrees and a correlation to this of 0.58. As the collected data did not include external forces, there were limited options to incorporate muscle redundancy into the predictive model. This limitation mean that, though the resultant muscle excitations will adequately perform the desired grasp, it is difficult to claim the results to be the optimal solutions. In order to enable the ability to vary the grasping pressure of a prostheses, the addition of a controller would be required; this limits the potential applications the of these results. Furthermore, the limited validation with experimental data means that certainty is not provided with this method. The lack of external forces and information of the exact task performed also means that there is no knowledge of wherever a grasp or gesture has been performed. Dependent on this, the gripping pressure and, in turn, muscle excitations may be different. This application has only considered the hand, with no concern of the position and rotation of the arm; alterations to muscle excitations may occur due to changes to hand location in space and the angle of the arm. Though the current implementation would work for hand prostheses, it would potentially not be applicable for more proximal amputations. The musculoskeletal model used works well when performing hand shape reproduction for prosthetic devices, but the fact that it does not consider the intrinsic muscles means that the results may not be the exact case for able bodied subjects. This has not been seen as detrimental to this project due to the focus on hand prostheses development, though would require consideration if further information was desired.

The LMC has been further utilised in a motion capture solution for the improvement of hand joint angle measurements in a hand therapy clinic; the resultant device has been named AirGo. The results of validation performed for the LMC support use of this device, shown to provide joint angles within 18.4 degrees when compared to a state-of-the-art motion capture system. A clinical trial performed has indicated the employability of this device within a clinical environment. Overall the AirGo offered a faster measurement time and greater reliability, without the need of contact between patient and clinical staff, when compared to the currently employed method. However, the accuracy showed no improvement over these methods during validation of the LMC. Additionally, the validation data were collected in a scenario different from that for which AirGo was designed and the clinical study performed

did not include results of an alternative method. This lack of end use validation data hinders the employability of AirGo at present. Furthering this, the cost of the devices required to use AirGo means that there is a commitment required for clinics to consider before the employment of this device.

The steps outlined by the objectives of this research have been successfully undertaken. Motion capture data of the hand during ADL has been collected and analysed. The common hand shapes performed during ADL have been observed and compared to the results of existing grasp taxonomies found within the literature. The muscle excitations of the functional hand shapes seen within ADL have been determined. Motion capture technology has been implemented to provide faster and more reliable measurements of the hand digit joint angles than the current clinical standard. The following list defines the original set of objectives, with sub-bullets outlining how each has been completed:

- Collect and analyse motion capture data of the hand to provide an understanding of the typical everyday hand motions.
  - A portable motion capture system has been created; utilising a LMC, NUC and external battery.
  - Hand motion data have been collected with 22 subjects during ADL, totalling 111 hours and 20 minutes.
- Determine the common hand shapes performed in everyday activities and compare these with previously developed taxonomies in the literature.
  - The common hand shapes seen during ADL have been found for the left and right hands, each collection respectively consisting of 40 and 24 hand shapes, following a k-means++ and merger of the recorded data.
  - These final results were compared to previous taxonomies, with the similarities and differences between the collections drawn.
- Develop and implement a musculoskeletal model based technique to determine muscle excitations from hand shapes observed in everyday life.
  - Optimisation methods have been performed alongside existing an musculoskeletal model to enable predictions of muscle excitations from a single frame of kinematic hand data.
  - The model has been validated using hand shapes with known muscle excitations, showing a 0.74 correlation between the predicted and know muscle excitations, and used to predict muscle excitations for the common hand shapes observed in ADL.
- Utilise motion capture technology to provide faster and more reliable measurements of the hand digit angle than the current clinical standard.

  - A clinic-ready device, AirGo, has been created utilising the LMC.
  - AirGo has been tested within a clinical environment, showing feasibility for the use of this device in practice.

This work has completed the aims set out, through utilisation of the devices and methods aforementioned. The aim to ascertain the most commonly used hand motions in modern ADL has been achieved through the implementation of the created portable motion capture system and subsequent machine learning approach based analysis. A means in which the quality of life of recipients of upper-limb prostheses can be increased and the cost of the devices reduced has been highlighted from this created taxonomy. An understanding of the muscle excitations performed during ADL has been provided through the application of an existing musculoskeletal model and optimisation techniques with the data collected during ADL. An improved method for clinical measurements of the hand joint angles has been supplied. The following list defines the original set of aims, with sub-bullets outlining how each has been achieved:

- Create a means by which the quality of life of recipients of upper-limb prostheses can be increased and the cost of the devices reduced.
  - A taxonomy of the functional hand shapes seen within ADL has been provided, with combined and individual results for both the left and right hands presented - providing an understanding of the demands from the hand during ADL.
  - The developed predictive model can suggest muscle excitations expected during the performance of these hand shapes, to aid the development of myoelectric prostheses.
  - AirGo has displayed faster and more consistent measurements for rehabilitation in clinics than the currently employed devices and offers a means of testing the performance of prosthetic hands.
- To ascertain the most commonly used hand motions in everyday tasks, including the use of modern day technology.
  - Data have been collected with the created portable motion capture system across a range of activities performed in regular ADL.
  - Machine learning was used to identify common hand shapes within the collected data.
- Provide a greater understanding of hand motion through mechanistic musculoskeletal modelling of the hand.
  - A predictive model has been created and employed to provide predictions of the muscle excitation which can cause the hand shapes seen during ADL.

  - The model has been shown to be able to predict muscle excitations from conventional motion capture Cartesian data formatted kinematic hand data.

- Improve the clinical methods employed to obtain angular displacement measurements for the hand digits.
  - AirGo has been shown to provide improved speed and consistency, in terms of data collection, over the currently employed clinical measurement methods.
  - The system was seen to be deployable within a clinical environment with the use of only an LMC and the JavaScript (JS) code.

8.2 Future Work

Future work is important to further the findings of this research and employment of the methods and results introduced. Increases to the collected data should continue to support the results and improvements to methods would hope to aid efficiency and accuracy of the introduced results, devices and prediction technique.

Regarding the data collected during ADL, an increase to the collected data would serve to cover a greater range of activities over a longer period of time - converging towards a full representation of hand shapes in, ever-changing, modern ADL. The majority of participants studied were right hand dominant, further data collection and analysis could be used to determine the differences seen between differing hand dominance. The analysis of this increased amount of data should consolidate the findings of this paper and require no further modifications to the analysis process. Additionally, if video recordings were captured alongside this collection, it would enable the determination of the exact application for each of the observed hand shapes. Though this could provide insightful information, and provide precise discrimination between gestures and grasps, it would likely result in less natural motions and tasks performed, as the participants would know their actions are begin recorded with less anonymity. A major limitation to this element of the study was the low accuracy observed, in comparison with state-of-the-art motion capture systems. Due to this, further work to this study would be to improve the devices used and continue data collection as developments are made in lightweight and low resource demanding motion capture devices.

Though including the summation of the muscle excitations within the cost function attempts to simulate the muscle redundancies, this does not provide an exact solution. Without knowledge of external forces imposed on the hand it is difficult to know how the internal muscle forces would distribute themselves, though weighting on muscle parameters such as moment arms and grouping flexors and extensors could aid in the

generation of more accurate muscle redundancies. However, there was no support found for this in the literature and this would need to be tested with experimental data. Aiding this, another future task would include collecting ADL data with knowledge of the external forces and electromyography (EMG) data, for use during further development of the predictive model and validation of the predictions. The limited validation data analysed with the introduced muscle excitation prediction technique highlights a need for the collection of data observing both the kinematics and kinetics of the hand. The current musculoskeletal model employed only considers the extrinsic muscles of the hand; as the technique discussed provides a framework in which the model could easily be updated, it is suggested that experiments with alternative models are undertaken. Use of a model with the hand and arm, including the extrinsic and intrinsic muscles of the hand, would help identify more accurate distribution of the excitations. As more optimisation techniques are developed and improvements are presented to existing techniques, the implementation of these within the framework presented is envisioned. Applications with alternative musculoskeletal models and optimisation algorithms would help to identify the most accurate possible predictions of the muscle excitations.

AirGo was solely used for measurements taken during a clinical application of the device, resulting in no comparable measure to evaluate the observed performance. A repeated clinical study with data simultaneously collected by the currently employed method would enable further evaluation of the device; allowing for comparisons of the time taken, accuracy and repeatability. The validation for the LMC was performed under conditions different to those seen during the employment of AirGo, suggesting a need to collect additional validation data for the use of the LMC with AirGo. Even so, this validation highlighted the imperfect accuracy of the LMC; as improvements are made to motion capture devices, future work would include replacing the currently used LMC. The current setup of the device allows for these changes, with a redesign of the head mount and alterations to application programming interface (API) being the only necessary changes to perform a replacement. As AirGo becomes closer to clinical application, improvements to the front-end code would provide a more comfortable user experience and promote the breadth of use for this device. The completion of these suggestions would bring AirGo closer to a recognised clinically viable device.

References

[1] B. Phillips, G. Zingalis, S. Ritter, and K. Mehta, "A review of current upper-limb prostheses for resource constrained settings," in *IEEE Global Humanitarian Technology Conference (GHTC)*. IEEE, Oct. 2015, pp. 52–58.

[2] L. Smail, C. Neal, C. Wilkins, and T. Packham, "Comfort and function remain key factors in upper limb prosthetic abandonment: Findings of a scoping review," *Disability and Rehabilitation: Assistive Technology*, pp. 1–10, Mar. 2020.

[3] J. W. Sensinger and S. Dosen, "A Review of Sensory Feedback in Upper-Limb Prostheses From the Perspective of Human Motor Control," *Frontiers in Neuroscience*, vol. 14, p. 345, Jun. 2020.

[4] N. Kerver, S. van Twillert, B. Maas, and C. K. van der Sluis, "User-relevant factors determining prosthesis choice in persons with major unilateral upper limb defects: A meta-synthesis of qualitative literature and focus group results," *PLoS ONE*, vol. 15, no. 6, Jun. 2020.

[5] G. Schlesinger, "Der mechanische Aufbau der künstlichen Glieder," in *Ersatzglieder und Arbeitshilfen*. Springer, Berlin, Heidelberg, 1919, pp. 321–661.

[6] J. R. Napier, "The Prehensile Movements of the Human Hand," *Bone & Joint Journal*, vol. 38-B, no. 4, pp. 902–913, Nov. 1956.

[7] M. R. Cutkosky, "On Grasp Choice, Grasp Models, and the Design of Hands for Manufacturing Tasks," *IEEE Transactions on Robotics and Automation*, vol. 5, no. 3, pp. 269–279, 1989.

[8] T. Feix, R. Pawlik, H.-B. Schmiedmayer, J. Romero, and D. Kragic, "A comprehensive grasp taxonomy," in *Robotics, Science and Systems: Workshop on Understanding the Human Hand for Advancing Robotic Manipulation*, Jun. 2009.

[9] D. Blana, E. K. Chadwick, A. J. van den Bogert, and W. M. Murray, "Real-time simulation of hand motion for prosthesis control," *Computer methods in biomechanics and biomedical engineering*, vol. 20, no. 5, pp. 540–549, Apr. 2017.

[10] J. L. Pons, R. Ceres, and F. Pfeiffer, "Multifingered dextrous robotics hand design and control: A review," *Robotica*, vol. 17, no. 6, pp. 661–674, Nov. 1999.

[11] F. Montagnani, M. Controzzi, and C. Cipriani, "Independent Long Fingers are not Essential for a Grasping Hand," *Scientific Reports*, vol. 6, p. 35545, Oct. 2016.

[12] T. Okada, "Object-Handling System for Manual Industry," *IEEE Transactions on Systems, Man, and Cybernetics*, vol. 9, no. 2, pp. 79–89, Feb. 1979.

[13] T. Okada, "Computer Control of Multijointed Finger System for Precise Object-Handling," *IEEE Transactions on Systems, Man, and Cybernetics*, vol. 12, no. 3, pp. 289–299, May 1982.

[14] M. Tavakoli, B. Enes, J. Santos, L. Marques, and A. T. de Almeida, "Underactuated anthropomorphic hands: Actuation strategies for a better functionality," *Robotics and Autonomous Systems*, vol. 74, pp. 267–282, Dec. 2015.

[15] V. Nanayakkara, G. Cotugno, N. Vitzilaios, D. Venetsanos, T. Nanayakkara, and M. Sahinkaya, "The Role of Morphology of the Thumb in Anthropomorphic Grasping: A Review," *Frontiers in Mechanical Engineering*, vol. 3, Jun. 2017.

[16] Pliny the Elder, *The Natural History of Pliny.* H. G. Bohn, 1857.

[17] G. von Berlichingen, *Lebens-Beschreibung des Herrn Gözens von Berlichingen.* Georg Olms Verlag, 1731.

[18] A. Paré, *Les Oeuvres d'Ambroise Paré.* A Paris: Chez Gabriel Buon, 1585.

[19] A. Magowska and M. Owecki, "Ireneusz Wierzejewski: Treatment of amputees of the upper limb in Poznan during the Great War," *International Orthopaedics*, vol. 46, no. 2, pp. 401–407, Feb. 2022.

[20] G. Vanghetti, *Vanghetti: Amputazioni, Disarticolozioni e Protesi - Google Scholar*, Florence, Italy, 1898.

[21] A. Ceci, "Dimostrazioni Pratiche: Archivio & Atti Società," *Pisa: Italiana di Chirurgia*, pp. 173–174, 1905.

[22] A. P. Ashhurst, "Cinematoplastic Amputations," *Annals of Surgery*, vol. 60, no. 6, pp. 750–755, Dec. 1914.

[23] F. Sauerbruch, "Chirurgische Vorarbeit für eine willkürlich bewegliche," *Hand Medizinische Klinik*, vol. 11, pp. 1125–1126, 1915.

[24] E. A. Brav, M. J. Fletcher, J. H. Kuitert, F. Leonard, H. B. Luscombe, W. F. Macdonald, A. W. Spittler, F. E. Vultee, and G. H. Woodard, "Cineplasty; an end-result study," *The Journal of Bone and Joint Surgery. American Volume*, vol. 39-A, no. 1, pp. 59–76, Jan. 1957.

[25] L. Brückner, "Die operation nach Sauerbruch-Lebsche-Vanghetti (Sauerbruch-Kineplastik)," *Operative Orthopädie und Traumatologie*, vol. 3, no. 3, pp. 186–195, Aug. 1991.

[26] W. G. Biedermann, "Neuer Sauerbrucharm mit neuer Technik und neuer Hand," *Orthopädie-Technik*, vol. 43, pp. 708–711, 1992.

[27] R. Reiter, "Eine Neue Eltronkunsthand," *Grenzgebiete Der Medizin*, vol. 1, no. 4, pp. 133–135, Sep. 1948.

[28] S. Bitzer and P. van der Smagt, "Learning EMG control of a robotic hand: Towards active prostheses," in *Proceedings 2006 IEEE International Conference on Robotics and Automation, 2006. ICRA 2006.* Orlando, FL, USA: IEEE, 2006, pp. 2819–2823.

[29] C. Castellini and P. van der Smagt, "Surface EMG in advanced hand prosthetics," *Biological Cybernetics*, vol. 100, no. 1, pp. 35–47, Jan. 2009.

[30] O. W. Samuel, M. G. Asogbon, Y. Geng, A. H. Al-Timemy, S. Pirbhulal, N. Ji, S. Chen, P. Fang, and G. Li, "Intelligent EMG Pattern Recognition Control Method for Upper-Limb Multifunctional Prostheses: Advances, Current Challenges, and Future Prospects," *IEEE Access*, vol. 7, pp. 10 150–10 165, 2019.

[31] O. S. Powar and K. Chemmangat, "Dynamic time warping for reducing the effect of force variation on myoelectric control of hand prostheses," *Journal of Electromyography and Kinesiology*, vol. 48, pp. 152–160, Oct. 2019.

[32] N. Parajuli, N. Sreenivasan, P. Bifulco, M. Cesarelli, S. Savino, V. Niola, D. Esposito, T. J. Hamilton, G. R. Naik, and U. Gunawardana, "Real-time EMG based pattern recognition control for hand prostheses: A review on existing methods, challenges and future implementation," *Sensors*, vol. 19, no. 20, p. 4596, 2019.

[33] A. Prakash, S. Sharma, and N. Sharma, "A compact-sized surface EMG sensor for myoelectric hand prosthesis," *Biomedical Engineering Letters*, vol. 9, no. 4, pp. 467–479, Nov. 2019.

[34] C. J. De Luca, "Control of upper-limb prostheses: A case for neuroelectric control," *Journal of medical engineering & technology*, vol. 2, no. 2, pp. 57–61, 1978.

[35] P. Zhou, M. Lowery, J. Dewald, and T. Kuiken, "Towards Improved Myoelectric Prosthesis Control: High Density Surface EMG Recording After Targeted Muscle Reinnervation," in *2005 IEEE Engineering in Medicine and Biology 27th Annual Conference.* Shanghai, China: IEEE, 2005, pp. 4064–4067.

[36] J. B. Hijjawi, T. A. Kuiken, R. D. Lipschutz, L. A. Miller, K. A. Stubblefield, and G. A. Dumanian, "Improved Myoelectric Prosthesis Control Accomplished Using Multiple Nerve Transfers," *Plastic and Reconstructive Surgery*, vol. 118, no. 7, pp. 1573–1578, Dec. 2006.

[37] L. A. Miller, K. A. Stubblefield, R. D. Lipschutz, B. A. Lock, and T. A. Kuiken, "Improved Myoelectric Prosthesis Control Using Targeted Reinnervation Surgery: A Case Series," *IEEE transactions on neural systems and rehabilitation engineering : a publication of the IEEE Engineering in Medicine and Biology Society*, vol. 16, no. 1, pp. 46–50, Feb. 2008.

[38] S. Salminger, A. Sturma, A. D. Roche, J. A. Mayer, C. Gstoettner, and O. C. Aszmann, "Outcomes, Challenges, and Pitfalls after Targeted Muscle Reinnervation in High-Level Amputees: Is It Worth the Effort?" *Plastic and Reconstructive Surgery*, vol. 144, no. 6, pp. 1037e–1043e, Dec. 2019.

[39] H. Myers, D. Lu, S. J. Gray, and F. Bruscino-Raiola, "Targeted muscle reinnervation to improve electromyography signals for advanced myoelectric prosthetic limbs: A series of seven patients," *ANZ Journal of Surgery*, vol. 90, no. 4, pp. 591–596, Apr. 2020.

[40] P. F. Pasquina, M. Evangelista, A. J. Carvalho, J. Lockhart, S. Griffin, G. Nanos, P. McKay, M. Hansen, D. Ipsen, J. Vandersea, J. Butkus, M. Miller, I. Murphy, and D. Hankin, "First-in-Man Demonstration of Fully Implanted Myoelectric Sensors for Control of an Advanced Electromechanical Arm by Transradial Amputees," *Journal of neuroscience methods*, vol. 244, pp. 85–93, Apr. 2015.

[41] M. Islam, S. Ahmad, F. Haque, M. B. I. Reaz, and M. A. S. Bhuiyan, "Force-Invariant Improved Feature Extraction Method for Upper-Limb Prostheses of Transradial Amputees," *Diagnostics*, vol. 11, no. 5, p. 843, 2021.

[42] C. Guger, W. Harkam, C. Hertnaes, and G. Pfurtscheller, "Prosthetic control by an EEG-based brain-computer interface (BCI)," in *Proc. Aaate 5th European Conference for the Advancement of Assistive Technology.* Citeseer, 1999, pp. 3–6.

[43] K. Ohnishi, R. F. Weir, and T. A. Kuiken, "Neural machine interfaces for controlling multifunctional powered upper-limb prostheses," *Expert Review of Medical Devices*, vol. 4, no. 1, pp. 43–53, Jan. 2007.

[44] J. V. V. Parr, S. J. Vine, M. R. Wilson, N. R. Harrison, and G. Wood, "Visual attention, EEG alpha power and T7-Fz connectivity are implicated in prosthetic hand control and can be optimized through gaze training," *Journal of NeuroEngineering and Rehabilitation*, vol. 16, no. 1, p. 52, Apr. 2019.

[45] I. Ruhunage, S. Mallikarachchi, D. Chinthaka, J. Sandaruwan, and T. D. Lalitharatne, "Hybrid EEG-EMG Signals Based Approach for Control of Hand Motions of a Transhumeral Prosthesis," in *2019 IEEE 1st Global Conference on Life Sciences and Technologies (LifeTech)*. Osaka, Japan: IEEE, Mar. 2019, pp. 50–53.

[46] B. Massa, S. Roccella, M. C. Carrozza, and P. Dario, "Design and development of an underactuated prosthetic hand," in *Proceedings 2002 IEEE International Conference on Robotics and Automation (Cat. No.02CH37292)*, vol. 4, May 2002, pp. 3374–3379 vol.4.

[47] I. M. Bullock and A. M. Dollar, "A two-fingered underactuated anthropomorphic manipulator based on human precision manipulation motions," in *2016 IEEE International Conference on Robotics and Automation (ICRA)*, May 2016, pp. 384–391.

[48] M. Tavakoli, B. Enes, L. Marques, and T. Feix, "Actuation Strategies of Bionic Hands for a Better Anthropomorphism," *Journal of Mechanisms and Robotics*, vol. 8, no. 4, Dec. 2015.

[49] S. Hirose and Y. Umetani, "The development of soft gripper for the versatile robot hand," *Mechanism and Machine Theory*, vol. 13, no. 3, pp. 351–359, Jan. 1978.

[50] G.-C. Jeong, Y. Kim, W. Choi, G. Gu, H.-J. Lee, M. B. Hong, and K. Kim, "On the Design of a Novel Underactuated Robotic Finger Prosthesis for Partial Hand Amputation," in *2019 IEEE 16th International Conference on Rehabilitation Robotics (ICORR)*, Jun. 2019, pp. 861–867.

[51] R. Abayasiri, R. S. T. Abayasiri, R. A. G. M. Gunawardhana, R. M. C. Premakumara, S. Mallikarachchi, R. Gopura, T. D. Lalitharatne, and D. G. K. Madusanka, "An Under-Actuated Hand Prosthesis with Finger Abduction and Adduction for Human Like Grasps," in *2020 6th International Conference on Control, Automation and Robotics (ICCAR)*, Apr. 2020, pp. 574–580.

[52] A. A. Adewuyi, L. J. Hargrove, and T. A. Kuiken, "Evaluating EMG feature and classifier selection for application to partial-hand prosthesis control," *Frontiers in neurorobotics*, vol. 10, p. 15, 2016.

[53] E. J. Earley, L. J. Hargrove, and T. A. Kuiken, "Dual window pattern recognition classifier for improved partial-hand prosthesis control," *Frontiers in neuroscience*, vol. 10, p. 58, 2016.

[54] R. G. Gaston, J. W. Bracey, M. A. Tait, and B. J. Loeffler, "A Novel Muscle Transfer for Independent Digital Control of a Myoelectric Prosthesis: The Starfish Procedure," *The Journal of Hand Surgery*, vol. 44, no. 2, pp. 163–168, Feb. 2019.

[55] B. Murali, S. Huddle, and R. F. ff Weir, "Design and evaluation of a distally actuated powered finger prosthesis with self-contained transmission for individuals with partial hand loss," *Advances in Mechanical Engineering*, vol. 11, no. 4, p. 1687814019834114, Apr. 2019.

[56] R. Alturkistani, K. A, S. Devasahayam, R. Thomas, E. L. Colombini, C. A. Cifuentes, S. Homer-Vanniasinkam, H. A. Wurdemann, and M. Moazen, "Affordable passive 3D-printed prosthesis for persons with partial hand amputation," *Prosthetics and Orthotics International*, vol. 44, no. 2, pp. 92–98, Apr. 2020.

[57] T. Feix, J. Romero, H. B. Schmiedmayer, A. M. Dollar, and D. Kragic, "The GRASP Taxonomy of Human Grasp Types," *IEEE Transactions on Human-Machine Systems*, vol. 46, no. 1, pp. 66–77, Feb. 2016.

[58] J. S. Cuellar, G. Smit, P. Breedveld, A. A. Zadpoor, and D. Plettenburg, "Functional evaluation of a non-assembly 3D-printed hand prosthesis," *Proceedings of the Institution of Mechanical Engineers, Part H: Journal of Engineering in Medicine*, vol. 233, no. 11, pp. 1122–1131, Nov. 2019.

[59] A. Tufa, C. Lamberti, A. Davalli, and R. Sacchetti, "Experimental development of a sensory control system for an upper limb myoelectric prosthesis with cosmetic covering," *Journal of rehabilitation research and development*, vol. 35, pp. 14–26, 1998.

[60] C. Pasluosta, H. Tims, and A. Chiu, "Slippage Sensory Feedback and Nonlinear Force Control System for a Low-Cost Prosthetic Hand," *American Journal of Biomedical Sciences*, pp. 295–302, Oct. 2009.

[61] E. D. Engeberg and S. Meek, "Enhanced visual feedback for slip prevention with a prosthetic hand," *Prosthetics and Orthotics International*, vol. 36, no. 4, pp. 423–429, Dec. 2012.

[62] C. Cipriani, F. Zaccone, S. Micera, and M. Carrozza, "On the Shared Control of an EMG-Controlled Prosthetic Hand: Analysis of User–Prosthesis Interaction," *IEEE Transactions on Robotics*, vol. 24, no. 1, pp. 170–184, Feb. 2008.

[63] K. Kim and J. E. Colgate, "Haptic Feedback Enhances Grip Force Control of sEMG-Controlled Prosthetic Hands in Targeted Reinnervation Amputees," *IEEE Transactions on Neural Systems and Rehabilitation Engineering*, vol. 20, no. 6, pp. 798–805, Nov. 2012.

[64] H. Liu, D. Yang, L. Jiang, and S. Fan, "Development of a multi-DOF prosthetic hand with intrinsic actuation, intuitive control and sensory feedback," *Industrial Robot: An International Journal*, vol. 41, no. 4, pp. 381–392, Jun. 2014.

[65] H. J. Witteveen, H. S. Rietman, and P. H. Veltink, "Vibrotactile grasping force and hand aperture feedback for myoelectric forearm prosthesis users," *Prosthetics and Orthotics International*, vol. 39, no. 3, pp. 204–212, Jun. 2015.

[66] E. Battaglia, J. P. Clark, M. Bianchi, M. G. Catalano, A. Bicchi, and M. K. O'Malley, "Skin Stretch Haptic Feedback to Convey Closure Information in Anthropomorphic, Under-Actuated Upper Limb Soft Prostheses," *IEEE Transactions on Haptics*, vol. 12, no. 4, pp. 508–520, Oct. 2019.

[67] A. Ninu, S. Dosen, S. Muceli, F. Rattay, H. Dietl, and D. Farina, "Closed-Loop Control of Grasping With a Myoelectric Hand Prosthesis: Which Are the Relevant Feedback Variables for Force Control?" *IEEE Transactions on Neural Systems and Rehabilitation Engineering*, vol. 22, no. 5, pp. 1041–1052, Sep. 2014.

[68] R. Christiansen, J. L. Contreras-Vidal, R. B. Gillespie, P. A. Shewokis, and M. K. O'Malley, "Vibrotactile feedback of pose error enhances myoelectric control of a prosthetic hand," in *2013 World Haptics Conference (WHC)*. IEEE, 2013, pp. 531–536.

[69] C. E. Stepp and Y. Matsuoka, "Relative to direct haptic feedback, remote vibrotactile feedback improves but slows object manipulation," in *2010 Annual International Conference of the IEEE Engineering in Medicine and Biology*. Buenos Aires: IEEE, Aug. 2010, pp. 2089–2092.

[70] E. Raveh, S. Portnoy, and J. Friedman, "Adding vibrotactile feedback to a myoelectric-controlled hand improves performance when online visual feedback is disturbed," *Human Movement Science*, vol. 58, pp. 32–40, Apr. 2018.

[71] J. Y. Zheng, C. Kalpakjian, M. Larrága-Martínez, C. A. Chestek, and D. H. Gates, "Priorities for the design and control of upper limb prostheses: A focus

group study," *Disability and Health Journal*, vol. 12, no. 4, pp. 706–711, Oct. 2019.

[72] I. M. Bullock, J. Z. Zheng, S. D. L. Rosa, C. Guertler, and A. M. Dollar, "Grasp Frequency and Usage in Daily Household and Machine Shop Tasks," *IEEE Transactions on Haptics*, vol. 6, no. 3, pp. 296–308, Jul. 2013.

[73] D. A. Huang, M. Ma, W. C. Ma, and K. M. Kitani, "How Do We Use Our Hands? Discovering a Diverse Set of Common Grasps," in *Proceedings of the IEEE Conference on Computer Vision and Pattern Recognition*, 2015, pp. 666–675.

[74] J. Liu, F. Feng, Y. C. Nakamura, and N. S. Pollard, "A taxonomy of everyday grasps in action," in *2014 IEEE-RAS International Conference on Humanoid Robots*, Nov. 2014, pp. 573–580.

[75] M. Vergara, J. L. Sancho-Bru, V. Gracia-Ibáñez, and A. Pérez-González, "An introductory study of common grasps used by adults during performance of activities of daily living," *Journal of Hand Therapy*, vol. 27, no. 3, pp. 225–234, Jul. 2014.

[76] T. Feix, I. M. Bullock, and A. M. Dollar, "Analysis of Human Grasping Behavior: Object Characteristics and Grasp Type," *IEEE Transactions on Haptics*, vol. 7, no. 3, pp. 311–323, Jul. 2014.

[77] A. M. Dollar, "Classifying human hand use and the activities of daily living," in *The Human Hand as an Inspiration for Robot Hand Development*. Springer, 2014, pp. 201–216.

[78] J. Z. Zheng, S. De La Rosa, and A. M. Dollar, "An investigation of grasp type and frequency in daily household and machine shop tasks," in *Robotics and Automation (ICRA), 2011 IEEE International Conference On*. IEEE, 2011, pp. 4169–4175.

[79] S. Edwards, D. Buckland, and J. McCoy-Powlen, "Developmental and Functional Hand Grasps," *All Books and Monographs by WMU Authors*, Nov. 2002.

[80] S. Kita, M. W. Alibali, and M. Chu, "How do gestures influence thinking and speaking? The gesture-for-conceptualization hypothesis," *Psychological Review*, vol. 124, pp. 245–266, 2017.

[81] K. H. Mumford, S. Aussems, and S. Kita, "Encouraging pointing with the right hand, but not the left hand, gives right-handed 3-year-olds a linguistic advantage," *Developmental Science*, 2022.

[82] S. Kita, "How representational gestures help speaking," in *Language and Gesture*, 1st ed., D. McNeill, Ed. Cambridge University Press, Aug. 2000, pp. 162–185.

[83] S. Kita, *Speech Accompanying-Gesture: A Special Issue of Language and Cognitive Processes*. Psychology Press, 2020.

[84] S. Kita, "Interplay of Gaze, Hand, Torso Orientation and Language in Pointing," in *Pointing: Where Language, Culture, and Cognition Meet*. Psychology Press, 2003.

[85] S. Kita and A. Özyürek, "What does cross-linguistic variation in semantic coordination of speech and gesture reveal?: Evidence for an interface representation of spatial thinking and speaking," *Journal of Memory and Language*, vol. 48, no. 1, pp. 16–32, Jan. 2003.

[86] A. Melinger and S. Kita, "Conceptualisation load triggers gesture production," *Language and Cognitive Processes*, vol. 22, no. 4, pp. 473–500, Jun. 2007.

[87] A. B. Hostetter, M. W. Alibali, and S. Kita, "I see it in my hands' eye: Representational gestures reflect conceptual demands," *Language and cognitive processes*, vol. 22, no. 3, pp. 313–336, 2007.

[88] M. W. Alibali, S. Kita, and A. J. Young, "Gesture and the process of speech production: We think, therefore we gesture," *Language and Cognitive Processes*, vol. 15, no. 6, pp. 593–613, Dec. 2000.

[89] P. Chawla and R. M. Krauss, "Gesture and Speech in Spontaneous and Rehearsed Narratives," *Journal of Experimental Social Psychology*, vol. 30, no. 6, pp. 580–601, Nov. 1994.

[90] F. H. Rauscher, R. M. Krauss, and Y. Chen, "Gesture, Speech, and Lexical Access: The Role of Lexical Movements in Speech Production," *Psychological Science*, vol. 7, no. 4, pp. 226–231, Jul. 1996.

[91] R. M. Krauss, Y. Chen, and R. F. Gottesman, "Lexical gestures and lexical access: A processing model In McNeill D,(Ed.), Language and gesture (261–283)," 2001.

[92] K. J. Pine, H. Bird, and E. Kirk, "The effects of prohibiting gestures on children's lexical retrieval ability," *Developmental Science*, vol. 10, no. 6, pp. 747–754, Nov. 2007.

[93] J. E. Pyers, R. Magid, T. H. Gollan, and K. Emmorey, "Gesture Helps, Only If You Need It: Inhibiting Gesture Reduces Tip-of-the-Tongue Resolution for

Those With Weak Short-Term Memory," *Cognitive Science*, vol. 45, no. 1, 2021.

[94] S. Aussems and S. Kita, "Seeing iconic gestures while encoding events facilitates children's memory of these events," *Child development*, vol. 90, no. 4, pp. 1123–1137, 2019.

[95] P. Ginns and V. King, "Pointing and tracing enhance computer-based learning," *Educational Technology Research and Development*, vol. 69, no. 3, pp. 1387–1403, Jun. 2021.

[96] N. Lacombe, T. Dias, and G. Petitpierre, "Can Gestures Give us Access to Thought? A Systematic Literature Review on the Role of Co-thought and Co-speech Gestures in Children with Intellectual Disabilities," *Journal of Nonverbal Behavior*, vol. 46, no. 2, pp. 119–136, Jun. 2022.

[97] A. Chiera, A. Ansani, I. Sessa, V. Cataldo, L. Schettino, and I. Poggi, "Gestures and pauses to help thought: Hands, voice, and silence in the tourist guide's speech," *Cognitive Processing*, Dec. 2022.

[98] H. Du and E. Charbon, "3D Hand Model Fitting for Virtual Keyboard System," in *IEEE Workshop on Applications of Computer Vision, 2007. WACV '07*, Feb. 2007, p. 31.

[99] J. Qi, G. Jiang, G. Li, Y. Sun, and B. Tao, "Surface EMG hand gesture recognition system based on PCA and GRNN," *Neural Computing and Applications*, Mar. 2019.

[100] Leap Motion, "Leap Motion Controller," Leap Motion, California, United States, 2016.

[101] D. Bachmann, F. Weichert, and G. Rinkenauer, "Evaluation of the Leap Motion Controller as a New Contact-Free Pointing Device," *Sensors*, vol. 15, no. 1, pp. 214–233, Dec. 2014.

[102] J. C. Coelho and F. J. Verbeek, "Pointing task evaluation of leap motion controller in 3D virtual environment," *Creating the Difference*, vol. 78, pp. 78–85, 2014.

[103] J. Guna, G. Jakus, M. Pogačnik, S. Tomažič, and J. Sodnik, "An Analysis of the Precision and Reliability of the Leap Motion Sensor and Its Suitability for Static and Dynamic Tracking," *Sensors*, vol. 14, no. 2, pp. 3702–3720, Feb. 2014.

[104] N. Bizzotto, A. Costanzo, L. Bizzotto, D. Regis, A. Sandri, and B. Magnan, "Leap Motion Gesture Control With OsiriX in the Operating Room to Control Imaging," *Surgical innovation*, vol. 21, Apr. 2014.

[105] L. E. Potter, J. Araullo, and L. Carter, "The Leap Motion Controller: A View on Sign Language," in *Proceedings of the 25th Australian Computer-Human Interaction Conference: Augmentation, Application, Innovation, Collaboration*, ser. OzCHI '13. New York, NY, USA: ACM, 2013, pp. 175–178.

[106] C. Guardino, C.-H. Chuan, and E. Regina, "American Sign Language Recognition Using Leap Motion Sensor," Dec. 2014.

[107] M. Mohandes, S. Oladimeji, and M. Deriche, "Arabic Sign Language Recognition using the Leap Motion Controller," in *IEEE International Symposium on Industrial Electronics*, Jun. 2014.

[108] J. Tumsri and W. Kimpan, "Thai Sign Language Translation Using Leap Motion Controller," *Proceedings of the International MultiConference of Engineers and Computer Scientists*, vol. 1, 2017.

[109] M. Funasaka, Y. Ishikawa, T. Masami, and K. Joe, "Sign Language Recognition using Leap Motion Controller," in *Proceedings of the International Conference on Parallel and Distributed Processing Techniques and Applications (PDPTA)*, 2015.

[110] G. Marin, F. Dominio, and P. Zanuttigh, "Hand gesture recognition with leap motion and kinect devices," in *Image Processing (ICIP), 2014 IEEE International Conference On*. IEEE, 2014, pp. 1565–1569.

[111] M. Khademi, H. Mousavi Hondori, A. McKenzie, L. Dodakian, C. V. Lopes, and S. C. Cramer, "Free-hand interaction with leap motion controller for stroke rehabilitation," in *CHI '14 Extended Abstracts on Human Factors in Computing Systems*, ser. CHI EA '14. New York, NY, USA: Association for Computing Machinery, Apr. 2014, pp. 1663–1668.

[112] M. Iosa, G. Morone, A. Fusco, M. Castagnoli, F. R. Fusco, L. Pratesi, and S. Paolucci, "Leap motion controlled videogame-based therapy for rehabilitation of elderly patients with subacute stroke: A feasibility pilot study," *Topics in Stroke Rehabilitation*, vol. 22, no. 4, pp. 306–316, Aug. 2015.

[113] D. E. Holmes, D. K. Charles, P. J. Morrow, S. McClean, and S. M. McDonough, "Using Fitt's Law to Model Arm Motion Tracked in 3D by a Leap Motion Controller for Virtual Reality Upper Arm Stroke Rehabilitation," in *2016*

IEEE 29th International Symposium on Computer-Based Medical Systems (CBMS), Jun. 2016, pp. 335–336.

[114] R. Fonk, S. Schneeweiss, U. Simon, and L. Engelhardt, "Hand Motion Capture from a 3D Leap Motion Controller for a Musculoskeletal Dynamic Simulation," *Sensors*, vol. 21, no. 4, p. 1199, Jan. 2021.

[115] A. H. Smeragliuolo, N. J. Hill, L. Disla, and D. Putrino, "Validation of the Leap Motion Controller using markered motion capture technology," *Journal of Biomechanics*, vol. 49, no. 9, pp. 1742–1750, Jun. 2016.

[116] K. Nizamis, N. H. M. Rijken, A. Mendes, M. M. H. P. Janssen, A. Bergsma, and B. F. J. M. Koopman, "A Novel Setup and Protocol to Measure the Range of Motion of the Wrist and the Hand," *Sensors*, vol. 18, no. 10, pp. 3230–3244, Oct. 2018.

[117] Vicon Motion Systems, "Vicon Nexus," Vicon Motion Systems, Oxford, England, Sep. 2020.

[118] K. Pearson, "LIII. On lines and planes of closest fit to systems of points in space," *The London, Edinburgh, and Dublin Philosophical Magazine and Journal of Science*, vol. 2, no. 11, pp. 559–572, Nov. 1901.

[119] E. Beltrami, "Sulle funzioni bilineari," *Giomale di Matematiche ad Uso degli Studenti Delle Universita*, vol. 11, pp. 98–106, 1873.

[120] C. Jordan, "Mémoire sur les formes bilinéaires." *Journal de Mathématiques Pures et Appliquées*, vol. 19, pp. 35–54, 1874.

[121] H. Lu, K. N. Plataniotis, and A. N. Venetsanopoulos, "Uncorrelated Multilinear Principal Component Analysis for Unsupervised Multilinear Subspace Learning," *IEEE Transactions on Neural Networks*, vol. 20, no. 11, pp. 1820–1836, Nov. 2009.

[122] L. van der Maaten and G. Hinton, "Visualizing data using t-SNE." *Journal of machine learning research*, vol. 9, no. 11, 2008.

[123] S. Kullback and R. A. Leibler, "On Information and Sufficiency," *The Annals of Mathematical Statistics*, vol. 22, no. 1, pp. 79–86, Mar. 1951.

[124] J. O. Ramsay and B. W. Silverman, *Functional Data Analysis*. Springer, 1997.

[125] K. Pearson, "VII. Note on regression and inheritance in the case of two parents," *proceedings of the royal society of London*, vol. 58, no. 347-352, pp. 240–242, 1895.

[126] W. S. McCulloch and W. Pitts, "A logical calculus of the ideas immanent in nervous activity," *The bulletin of mathematical biophysics*, vol. 5, no. 4, pp. 115–133, 1943.

[127] C. Szegedy, W. Liu, Y. Jia, P. Sermanet, S. Reed, D. Anguelov, D. Erhan, V. Vanhoucke, and A. Rabinovich, "Going deeper with convolutions," in *Proceedings of the IEEE Conference on Computer Vision and Pattern Recognition*, 2015, pp. 1–9.

[128] H. Friedrich, V. Grossmann, M. Ehrenmann, O. Rogalla, R. Zöllner, and R. Dillmann, "Towards cognitive elementary operators: Grasp classification using neural network classifiers," in *Proceedings of the IASTED International Conference on Intelligent Systems and Control (ISC)*, vol. 1, 1999, pp. 88–93.

[129] C. Stanton, A. Bogdanovych, and E. Ratanasena, "Teleoperation of a humanoid robot using full-body motion capture, example movements, and machine learning," *New Zealand.*, p. 10, 2012.

[130] A. Miller, "Gait event detection using a multilayer neural network," *Gait & Posture*, vol. 29, no. 4, pp. 542–545, Jun. 2009.

[131] E. Corona, A. Pumarola, G. Alenya, F. Moreno-Noguer, and G. Rogez, "GanHand: Predicting Human Grasp Affordances in Multi-Object Scenes," in *2020 IEEE/CVF Conference on Computer Vision and Pattern Recognition (CVPR)*. Seattle, WA, USA: IEEE, Jun. 2020, pp. 5030–5040.

[132] K. Pearson, "Mathematical contributions to the theory of evolution. XII.—On a generalised theory of alternative inheritance, with special reference to Mendel's laws," *Proceedings of the Royal Society of London*, vol. 72, no. 477-486, pp. 505–509, 1904.

[133] E. Fix and J. L. Hodges, "Discriminatory Analysis. Nonparametric Discrimination: Consistency Properties," *International Statistical Review / Revue Internationale de Statistique*, vol. 57, no. 3, pp. 238–247, 1989.

[134] J.-H. Chen and K.-T. Song, "Collision-Free Motion Planning for Human-Robot Collaborative Safety Under Cartesian Constraint," in *2018 IEEE International Conference on Robotics and Automation (ICRA)*. Brisbane, QLD: IEEE, May 2018, pp. 4348–4354.

[135] G. Heumer, H. B. Amor, and B. Jung, "Grasp Recognition for Uncalibrated Data Gloves: A Machine Learning Approach," *Presence: Teleoperators and Virtual Environments*, vol. 17, no. 2, pp. 121–142, Apr. 2008.

[136] P. M. Woodward, "Probability and information theory, with applications to radar. New York: McRaw-Hill Book Co. Inc," 1953.

[137] T. Simpson, *Mathematical Dissertations on a Variety of Physical and Analytical Subjects...* T. Woodward, 1743.

[138] W. A. Belson, "Matching and prediction on the principle of biological classification," *Journal of the Royal Statistical Society: Series C (Applied Statistics)*, vol. 8, no. 2, pp. 65–75, 1959.

[139] C. Gini, "Variabilità e mutabilità," *Cuppini, Bologna*, vol. 420, 1912.

[140] B. T. Jijo and A. M. Abdulazeez, "Classification based on decision tree algorithm for machine learning," *Journal of Applied Science and Technology Trends*, vol. 2, no. 01, pp. 20–28, 2021.

[141] X. Zhang, X. Chen, Y. Li, V. Lantz, K. Wang, and J. Yang, "A Framework for Hand Gesture Recognition Based on Accelerometer and EMG Sensors," *IEEE Transactions on Systems, Man, and Cybernetics - Part A: Systems and Humans*, vol. 41, no. 6, pp. 1064–1076, Nov. 2011.

[142] G. Pappalardo, S. Cafiso, A. Di Graziano, and A. Severino, "Decision tree method to analyze the performance of lane support systems," *Sustainability*, vol. 13, no. 2, p. 846, 2021.

[143] N. Yuvaraj, V. Chang, B. Gobinathan, A. Pinagapani, S. Kannan, G. Dhiman, and A. R. Rajan, "Automatic detection of cyberbullying using multi-feature based artificial intelligence with deep decision tree classification," *Computers & Electrical Engineering*, vol. 92, p. 107186, Jun. 2021.

[144] L. Fraiwan and O. Hassanin, "Computer-aided identification of degenerative neuromuscular diseases based on gait dynamics and ensemble decision tree classifiers," *PLoS ONE*, vol. 16, no. 6, Jun. 2021.

[145] J. MacQueen, "Some methods for classification and analysis of multivariate observations," in *Proceedings of the Fifth Berkeley Symposium on Mathematical Statistics and Probability*, vol. 1. Oakland, CA, USA, 1967, pp. 281–297.

[146] H. Steinhaus, "Sur la division des corps matériels en parties," *Bull. Acad. Polon. Sci*, vol. 1, no. 804, p. 801, 1956.

[147] S. Lloyd, "Least squares quantization in PCM," *IEEE transactions on information theory*, vol. 28, no. 2, pp. 129–137, 1982.

[148] A. P. Dempster, N. M. Laird, and D. B. Rubin, "Maximum likelihood from incomplete data via the EM algorithm," *Journal of the Royal Statistical Society: Series B (Methodological)*, vol. 39, no. 1, pp. 1–22, 1977.

[149] L. Tanco and A. Hilton, "Realistic synthesis of novel human movements from a database of motion capture examples," in *Proceedings Workshop on Human Motion*. Los Alamitos, CA, USA: IEEE Comput. Soc, 2000, pp. 137–142.

[150] I. Kapsouras and N. Nikolaidis, "Action recognition on motion capture data using a dynemes and forward differences representation," *Journal of Visual Communication and Image Representation*, vol. 25, no. 6, pp. 1432–1445, Aug. 2014.

[151] D. Leightley, B. Li, J. S. McPhee, M. H. Yap, and J. Darby, "Exemplar-Based Human Action Recognition with Template Matching from a Stream of Motion Capture," in *Lecture Notes in Computer Science*, A. Campilho and M. Kamel, Eds., vol. 8815. Cham: Springer, 2014, pp. 12–20.

[152] Q. Gu, J. Peng, and Z. Deng, "Compression of Human Motion Capture Data Using Motion Pattern Indexing," *Computer Graphics Forum*, vol. 28, no. 1, pp. 1–12, Mar. 2009.

[153] W. Thong, S. Parent, J. Wu, C.-E. Aubin, H. Labelle, and S. Kadoury, "Three-dimensional morphology study of surgical adolescent idiopathic scoliosis patient from encoded geometric models," *European Spine Journal*, vol. 25, no. 10, pp. 3104–3113, Oct. 2016.

[154] T. Caliński and J. Harabasz, "A dendrite method for cluster analysis," *Communications in Statistics-theory and Methods*, vol. 3, no. 1, pp. 1–27, 1974.

[155] D. L. Davies and D. W. Bouldin, "A cluster separation measure," *IEEE transactions on pattern analysis and machine intelligence*, no. 2, pp. 224–227, 1979.

[156] P. J. Rousseeuw, "Silhouettes: A graphical aid to the interpretation and validation of cluster analysis," *Journal of Computational and Applied Mathematics*, vol. 20, pp. 53–65, Nov. 1987.

[157] H. Rijpkema and M. Girard, "Computer Animation of Knowledge-based Human Grasping," in *Proceedings of the 18th Annual Conference on Computer Graphics and Interactive Techniques*, ser. SIGGRAPH '91. New York, NY, USA: ACM, 1991, pp. 339–348.

[158] J. Biggs and K. Horch, "A three-dimensional kinematic model of the human long finger and the muscles that actuate it," *Medical Engineering & Physics*, vol. 21, no. 9, pp. 625–639, Nov. 1999.

[159] M. M. Rahman, T. T. Choudhury, S. N. Sidek, and A. B. Awang, "Mathematical Modeling and Trajectory Planning of Hand Finger Movements," in *Proceedings of the 2014 First International Conference on Systems Informatics, Modelling and Simulation*, ser. SIMS '14. Washington, DC, USA: IEEE Computer Society, 2014, pp. 53–57.

[160] S. Cobos, M. Ferre, M. Angel Sánchez-Urán, and J. Ortego, "Constraints for Realistic Hand Manipulation," *The 10th Annual International Workshop on Presence, October 25-27 Barcelona, Spain*, Feb. 2007.

[161] S. Cobos, M. Ferre, M. A. S. Uran, J. Ortego, and C. Pena, "Efficient human hand kinematics for manipulation tasks," in *2008 IEEE/RSJ International Conference on Intelligent Robots and Systems*, Sep. 2008, pp. 2246–2251.

[162] F. Chen Chen, S. Appendino, A. Battezzato, A. Favetto, M. Mousavi, and F. Pescarmona, "Constraint Study for a Hand Exoskeleton: Human Hand Kinematics and Dynamics," *Journal of Robotics*, 2013.

[163] A. Murgia, P. J. Kyberd, P. H. Chappell, and C. M. Light, "Marker placement to describe the wrist movements during activities of daily living in cyclical tasks," *Clinical Biomechanics (Bristol, Avon)*, vol. 19, no. 3, pp. 248–254, Mar. 2004.

[164] N. Jiang, J. L. Vest-Nielsen, S. Muceli, and D. Farina, "EMG-based simultaneous and proportional estimation of wrist/hand kinematics in uni-lateral trans-radial amputees," *Journal of NeuroEngineering and Rehabilitation*, vol. 9, p. 42, Jun. 2012.

[165] M. A. Lemay and P. E. Crago, "A dynamic model for simulating movements of the elbow, forearm, and wrist," *Journal of Biomechanics*, vol. 29, no. 10, pp. 1319–1330, Oct. 1996.

[166] V. Caggiano, H. Wang, G. Durandau, M. Sartori, and V. Kumar, "MyoSuite - A contact-rich simulation suite for musculoskeletal motor control," May 2022.

[167] Aristotle and M. C. Nussbaum, *De Motu Animalium*, 1st ed. Princeton, N.J.: Princeton University Press, 1985.

[168] R. D. Crowninshield, R. C. Johnston, J. G. Andrews, and R. A. Brand, "A biomechanical investigation of the human hip," *Journal of Biomechanics*, vol. 11, no. 1, pp. 75–85, Jan. 1978.

[169] F. L. Buczek, E. W. Sinsel, D. S. Gloekler, B. M. Wimer, C. M. Warren, and J. Z. Wu, "Kinematic performance of a six degree-of-freedom hand model (6DHand) for use in occupational biomechanics," *Journal of Biomechanics*, vol. 44, no. 9, pp. 1805–1809, 2011.

[170] R. W. Bisseling and A. L. Hof, "Handling of impact forces in inverse dynamics," *Journal of Biomechanics*, vol. 39, no. 13, pp. 2438–44, 2006.

[171] J. A. Sterner, S. K. Reaves, A. L. Aguinaldo, S. J. Hazelwood, and S. M. Klisch, "Inverse dynamics analysis of youth pitching arm kinetics using body composition imaging," *Sports Biomechanics*, vol. 21, no. 9, pp. 993–1007, Oct. 2022.

[172] D. C. McFarland, B. I. Binder-Markey, J. A. Nichols, S. J. Wohlman, M. de Bruin, and W. M. Murray, "A Musculoskeletal Model of the Hand and Wrist Capable of Simulating Functional Tasks," *IEEE Transactions on Biomedical Engineering*, 2022.

[173] D. Blana, A. J. van Den Bogert, W. M. Murray, A. Ganguly, A. Krasoulis, K. Nazarpour, and E. K. Chadwick, "Model-based control of individual finger movements for prosthetic hand function," *IEEE Transactions on Neural Systems and Rehabilitation Engineering*, vol. 28, no. 3, pp. 612–620, 2020.

[174] M. B. Sabick, M. R. Torry, R. L. Lawton, and R. J. Hawkins, "Valgus torque in youth baseball pitchers: A biomechanical study," *Journal of Shoulder and Elbow Surgery*, vol. 13, no. 3, pp. 349–355, May 2004.

[175] J. C. Garner, C. MacDonald, C. Wade, A. Johnson, and M. A. Ford, "The Influence of Body Composition on Youth Throwing Kinetics," *Pediatric Exercise Science*, vol. 23, no. 3, pp. 379–387, Aug. 2011.

[176] J. D. Darke, E. M. Dandekar, A. L. Aguinaldo, S. J. Hazelwood, and S. M. Klisch, "Effects of Game Pitch Count and Body Mass Index on Pitching Biomechanics in 9- to 10-Year-Old Baseball Athletes," *Orthopaedic Journal of Sports Medicine*, vol. 6, no. 4, p. 2325967118765655, Apr. 2018.

[177] K. M. DeGoede and J. A. Ashton-Miller, "Biomechanical simulations of forward fall arrests: Effects of upper extremity arrest strategy, gender and aging-related declines in muscle strength," *Journal of Biomechanics*, vol. 36, no. 3, pp. 413–420, Mar. 2003.

[178] R. Happee and F. C. T. van der Helm, "The control of shoulder muscles during goal directed movements, an inverse dynamic analysis," *Journal of Biomechanics*, vol. 28, no. 10, pp. 1179–1191, Oct. 1995.

[179] J. Rasmussen, M. Damsgaard, E. Surma, S. Tørholm, M. de Zee, and V. Vondrak, "AnyBody - a software system for ergonomic optimization," Jan. 2003.

[180] L. Engelhardt, M. Melzner, L. Havelkova, P. Fiala, P. Christen, S. Dendorfer, and U. Simon, "A new musculoskeletal AnyBody™ detailed hand model," *Computer Methods in Biomechanics and Biomedical Engineering*, vol. 24, no. 7, pp. 777–787, May 2021.

[181] L. Engelhardt, F. Niemeyer, P. Christen, R. Müller, K. Stock, M. Blauth, K. Urban, A. Ignatius, and U. Simon, "Simulating Metaphyseal Fracture Healing in the Distal Radius," *Biomechanics*, vol. 1, no. 1, pp. 29–42, Jun. 2021.

[182] W. Tsang, K. Singh, and E. Fiume, "Helping hand: An anatomically accurate inverse dynamics solution for unconstrained hand motion," in *Proceedings of the 2005 ACM SIGGRAPH/Eurographics Symposium on Computer Animation*, 2005, pp. 319–328.

[183] M. Günther, V. A. Sholukha, D. Kessler, V. Wank, and R. Blickhan, "Dealing with Skin Motion and Wobbling Masses in Inverse Dynamics," *Journal of Mechanics in Medicine and Biology*, vol. 03, no. 03n04, pp. 309–335, Sep. 2003.

[184] S. J. Wohlman and W. M. Murray, "Bridging the gap between cadaveric and in vivo experiments: A biomechanical model evaluating thumb-tip endpoint forces," *Journal of biomechanics*, vol. 46, no. 5, pp. 1014–1020, Mar. 2013.

[185] D. C. McFarland, J. A. Nichols, M. S. Bednar, S. J. Wohlman, and W. M. Murray, "Corrigendum to "Connecting the wrist to the hand: A simulation study exploring changes in thumb-tip endpoint force following wrist surgery" [J. Biomech. 58 (2017) 97–104]," *Journal of biomechanics*, vol. 139, p. 110859, Jun. 2022.

[186] K. R. S. Holzbaur, W. M. Murray, and S. L. Delp, "A Model of the Upper Extremity for Simulating Musculoskeletal Surgery and Analyzing Neuromuscular Control," p. 12, 2005.

[187] A. Nasr, S. Bell, J. He, R. L. Whittaker, N. Jiang, C. R. Dickerson, and J. McPhee, "MuscleNET: Mapping electromyography to kinematic and dynamic biomechanical variables by machine learning," *Journal of Neural Engineering*, vol. 18, no. 4, p. 0460d3, 2021.

[188] K. A. Hao and J. A. Nichols, "Simulating finger-tip force using two common contact models: Hunt-Crossley and elastic foundation," *Journal of Biomechanics*, vol. 119, p. 110334, Apr. 2021.

[189] K. M. DeGoede, J. A. Ashton-Miller, A. B. Schultz, and N. B. Alexander, "Biomechanical Factors Affecting the Peak Hand Reaction Force During the Bimanual Arrest of a Moving Mass," *Journal of Biomechanical Engineering*, vol. 124, no. 1, pp. 107–112, Oct. 2001.

[190] L. J. Lattimer, J. L. Lanovaz, J. P. Farthing, S. Madill, S. Y. Kim, S. Robinovitch, and C. M. Arnold, "Biomechanical and physiological age differences in a simulated forward fall on outstretched hands in women," *Clinical Biomechanics*, vol. 52, pp. 102–108, Feb. 2018.

[191] H. S. Legg, C. M. Arnold, J. P. Farthing, and J. L. Lanovaz, "Age differences in upper extremity joint moments and strength during a laboratory-based tether-release forward fall arrest in older women," *Journal of Biomechanics*, vol. 138, p. 111107, Jun. 2022.

[192] J. Borrelli, R. Creath, K. Westlake, and M. W. Rogers, "Test-retest reliability of the FALL FIT system for assessing and training protective arm reactions in response to a forward fall," *MethodsX*, vol. 9, p. 101702, Jan. 2022.

[193] P. Hahn, H. Krimmer, A. Hradetzky, and U. Lanz, "Quantitative analysis of the linkage between the interphalangeal joints of the index finger: An in vivo study," *Journal of Hand Surgery*, vol. 20, no. 5, pp. 696–699, 1995.

[194] P. H. Holguín, Á. A. Rico, L. P. Gómez, and L. M. Munuera, "The coordinate movement of the interphalangeal joints: A cinematic study," *Clinical Orthopaedics and Related Research*, vol. 362, pp. 117–124, 1999.

[195] T. Abaci, M. Mortara, G. Patane, M. Spagnulo, F. Vexo, and D. Thalmann, "Bridging geometry and semantics for object manipulation and grasping," in *Proceedings of Workshop towards Semantic Virtual Environments'(SVE 2005) Workshop*, Villars, Switzerland, 2005, pp. 110–119.

[196] M. J. Rainbow, A. L. Wolff, J. J. Crisco, and S. W. Wolfe, "Functional kinematics of the wrist," *Journal of Hand Surgery (European Volume)*, vol. 41, no. 1, pp. 7–21, Jan. 2016.

[197] Y. Smirnov, D. Smirnov, A. Popov, and S. Yakovenko, "Solving musculoskeletal biomechanics with machine learning," *PeerJ Computer Science*, vol. 7, pp. 663–683, Aug. 2021.

[198] A. J. van den Bogert, D. Blana, and D. Heinrich, "Implicit methods for efficient musculoskeletal simulation and optimal control," *Procedia IUTAM*, vol. 2, pp. 297–316, 2011.

[199] H. H. Rosenbrock, "Some general implicit processes for the numerical solution of differential equations," *The Computer Journal*, vol. 5, no. 4, pp. 329–330, 1963.

[200] S. A. Khomami and S. Shamekhi, "Persian sign language recognition using IMU and surface EMG sensors," *Measurement*, vol. 168, p. 108471, Jan. 2021.

[201] B. Saeed, M. Zia-ur-Rehman, S. O. Gilani, F. Amin, A. Waris, M. Jamil, and M. Shafique, "Leveraging ANN and LDA Classifiers for Characterizing Different Hand Movements Using EMG Signals," *Arabian Journal for Science and Engineering*, vol. 46, no. 2, pp. 1761–1769, Feb. 2021.

[202] R. Zaman, Y. Xiang, R. Rakshit, and J. Yang, "Muscle Force Prediction in OpenSim Using Skeleton Motion Optimization Results As Input Data," in *Volume 1: 39th Computers and Information in Engineering Conference*. Anaheim, California, USA: American Society of Mechanical Engineers, Aug. 2019.

[203] M. Manzano and G. Serrancolí, "A factorization-based algorithm to predict EMG data using only kinematics information," *International Journal for Numerical Methods in Biomedical Engineering*, vol. 37, no. 7, 2021.

[204] C. J. De Luca, A. Adam, R. Wotiz, L. D. Gilmore, and S. H. Nawab, "Decomposition of Surface EMG Signals," *Journal of Neurophysiology*, vol. 96, no. 3, pp. 1646–1657, Sep. 2006.

[205] A. Holobar, M. A. Minetto, A. Botter, F. Negro, and D. Farina, "Experimental analysis of accuracy in the identification of motor unit spike trains from high-density surface EMG," *IEEE Transactions on Neural Systems and Rehabilitation Engineering*, vol. 18, no. 3, pp. 221–229, 2010.

[206] J. S. Uribe, F. L. Vale, and E. Dakwar, "Electromyographic monitoring and its anatomical implications in minimally invasive spine surgery," *Spine*, vol. 35, no. 26S, pp. S368–S374, 2010.

[207] T. Sugiarto, C.-L. Hsu, C.-T. Sun, W.-C. Hsu, S.-H. Ye, and K.-T. Lu, "Surface EMG vs. High-Density EMG: Tradeoff Between Performance and Usability for Head Orientation Prediction in VR Application," *IEEE Access*, vol. 9, pp. 45 418–45 427, 2021.

[208] S. Shin, Y. Baek, J. Lee, Y. Eun, and S. H. Son, "Korean sign language recognition using EMG and IMU sensors based on group-dependent NN models," in *2017 IEEE Symposium Series on Computational Intelligence (SSCI)*, Nov. 2017, pp. 1–7.

[209] J. Wu, L. Sun, and R. Jafari, "A Wearable System for Recognizing American Sign Language in Real-Time Using IMU and Surface EMG Sensors," *IEEE Journal of Biomedical and Health Informatics*, vol. 20, no. 5, pp. 1281–1290, Sep. 2016.

[210] A. L. C. Ruiz, C. Pontonnier, A. Sorel, and G. Dumont, "Identifying representative muscle synergies in overhead football throws," *Computer Methods in Biomechanics and Biomedical Engineering*, p. 2, 2015.

[211] M. M. Nazifi, H. U. Yoon, K. Beschorner, and P. Hur, "Shared and task-specific muscle synergies during normal walking and slipping," *Frontiers in human neuroscience*, vol. 11, p. 40, 2017.

[212] J. H. Holland, *Adaptation in Natural and Artificial Systems: An Introductory Analysis with Applications to Biology, Control, and Artificial Intelligence*. MIT Press, Apr. 1992.

[213] A. J. K. van Soest and L. J. R. R. Casius, "The merits of a parallel genetic algorithm in solving hard optimiszation problems," *Journal of Biomechanical Engineering*, pp. 125–141, 2003.

[214] A. U. Nair, D. G. Taggart, and F. J. Vetter, "Optimizing cardiac material parameters with a genetic algorithm," *Journal of Biomechanics*, vol. 40, no. 7, pp. 1646–50, 2007.

[215] N. Wang, Z. Li, Y. Zhong, and X. Zhang, "Assistive Torque of Ankle Exoskeleton Based on a Simple Biomechanical Model and a Genetic Algorithm," in *Intelligent Robotics and Applications*, ser. Lecture Notes in Computer Science, X.-J. Liu, Z. Nie, J. Yu, F. Xie, and R. Song, Eds. Cham: Springer International Publishing, 2021, pp. 780–790.

[216] W. S. You, J. Casebier, J. Mandich, and R. Balasubramanian, "Genetic Algorithm-Based Optimization for the Geometric Design of a Novel Orthopedic Implant," *IEEE Transactions on Biomedical Engineering*, vol. 68, no. 12, pp. 3620–3627, Dec. 2021.

[217] J. Jabari Lotf, M. Abdollahi Azgomi, and M. R. Ebrahimi Dishabi, "An improved influence maximization method for social networks based on genetic algorithm," *Physica A: Statistical Mechanics and its Applications*, vol. 586, p. 126480, Jan. 2022.

[218] M. Squires, X. Tao, S. Elangovan, R. Gururajan, X. Zhou, and U. R. Acharya, "A novel genetic algorithm based system for the scheduling of medical treatments," *Expert Systems with Applications*, vol. 195, p. 116464, Jun. 2022.

[219] J. Kennedy and R. Eberhart, "Particle swarm optimization," in *Proceedings of ICNN'95 - International Conference on Neural Networks*, vol. 4, Nov. 1995, pp. 1942–1948 vol.4.

[220] R. Poli, J. Kennedy, and T. Blackwell, "Particle swarm optimization: An overview," *Swarm Intelligence*, vol. 1, no. 1, pp. 33–57, Oct. 2007.

[221] Y. Shi and R. Eberhart, "A modified particle swarm optimizer," in *1998 IEEE International Conference on Evolutionary Computation Proceedings. IEEE World Congress on Computational Intelligence (Cat. No.98TH8360)*, May 1998, pp. 69–73.

[222] J. F. Schutte, B. Koh, J. A. Reinbolt, R. T. Haftka, A. D. George, and B. J. Fregly, "Evaluation of a Particle Swarm Algorithm For Biomechanical Optimization," *Journal of biomechanical engineering*, vol. 127, no. 3, pp. 465–474, Jun. 2005.

[223] S. Saini, D. R. Bt Awang Rambli, M. N. B. Zakaria, and S. Bt Sulaiman, "A Review on Particle Swarm Optimization Algorithm and Its Variants to Human Motion Tracking," *Mathematical Problems in Engineering*, vol. 2014, Nov. 2014.

[224] S. Saini, N. Zakaria, D. R. A. Rambli, and S. Sulaiman, "Markerless Human Motion Tracking Using Hierarchical Multi-Swarm Cooperative Particle Swarm Optimization," *PLoS ONE*, vol. 10, no. 5, May 2015.

[225] B. Kwolek, T. Krzeszowski, A. Gagalowicz, K. Wojciechowski, and H. Josinski, "Real-Time Multi-view Human Motion Tracking Using Particle Swarm Optimization with Resampling," in *Articulated Motion and Deformable Objects*, ser. Lecture Notes in Computer Science, F. J. Perales, R. B. Fisher, and T. B. Moeslund, Eds. Berlin, Heidelberg: Springer, 2012, pp. 92–101.

[226] X. Chang, P. Yi, and Q. Zhang, "Key Frames Extraction from Human Motion Capture Data Based on Hybrid Particle Swarm Optimization Algorithm," in *Recent Developments in Intelligent Information and Database Systems*, ser. Studies in Computational Intelligence, D. Król, L. Madeyski, and N. T. Nguyen, Eds. Cham: Springer International Publishing, 2016, pp. 335–342.

[227] N. Rokbani, E. Benbousaada, B. Ammar, and A. Alimi, "Biped robot control using particle swarm optimization," in *Conference Proceedings - IEEE International Conference on Systems, Man and Cybernetics*, Oct. 2010, pp. 506–512.

[228] A. Cauchy, "Méthode générale pour la résolution des systèmes d'équations simultanées," *C.R. Acad. Sci. Paris*, vol. 25, pp. 536–538, 1847.

[229] L. F. Richardson, "The approximate arithmetical solution by finite differences with an application to stresses in masonry dams," *Philosophical Transactions of the Royal Society of London*, vol. 210, pp. 307–357, 1911.

[230] R. V. Southwell, *Relaxation Methods In Engineering Science A Treatise On Approximate Computation.* Oxford, England: Oxford University Press, 1940.

[231] E. Todorov and W. Li, "Optimal control methods suitable for biomechanical systems," in *Proceedings of the 25th Annual International Conference of the IEEE Engineering in Medicine and Biology Society (IEEE Cat. No.03CH37439).* Cancun, Mexico: IEEE, 2003, pp. 1758–1761.

[232] V. De Sapio, O. Khatib, and S. Delp, "Least action principles and their application to constrained and task-level problems in robotics and biomechanics," *Multibody System Dynamics*, vol. 19, no. 3, pp. 303–322, Apr. 2008.

[233] W. Wu, K. R. Saul, and H. H. Huang, "Using Reinforcement Learning to Estimate Human Joint Moments From Electromyography or Joint Kinematics: An Alternative Solution to Musculoskeletal-Based Biomechanics," *Journal of Biomechanical Engineering*, vol. 143, no. 4, p. 044502, Apr. 2021.

[234] S. L. Smith, B. Dherin, D. G. T. Barrett, and S. De, "On the Origin of Implicit Regularization in Stochastic Gradient Descent," *arXiv:2101.12176 [cs, stat]*, Jan. 2021.

[235] S. H. Haji and A. M. Abdulazeez, "Comparison of optimization techniques based on gradient descent algorithm: A review," *PalArch's Journal of Archaeology of Egypt/Egyptology*, vol. 18, no. 4, pp. 2715–2743, 2021.

[236] B. B. Alagoz, "Fractional order linear time invariant system stabilization by brute-force search," *Transactions of the Institute of Measurement and Control*, vol. 40, no. 5, pp. 1447–1456, Mar. 2018.

[237] S. Suzuki, M. Fujiwara, Y. Makino, and H. Shinoda, "Radiation Pressure Field Reconstruction for Ultrasound Midair Haptics by Greedy Algorithm With Brute-Force Search," *IEEE Transactions on Haptics*, vol. 14, no. 4, pp. 914–921, Oct. 2021.

[238] A. Nadian-Ghomsheh, B. Farahani, and M. Kavian, "A hierarchical privacy-preserving IoT architecture for vision-based hand rehabilitation assessment," *Multimedia Tools and Applications*, vol. 80, no. 20, pp. 31 357–31 380, Aug. 2021.

[239] E. Lewis, L. Fors, and W. Tharion, "Interrater and Intrarater Reliability of Finger Goniometric Measurements," *The American journal of occupational therapy : official publication of the American Occupational Therapy Association*, vol. 64, pp. 555–561, Jul. 2010.

[240] K. H. McVeigh, P. M. Murray, M. G. Heckman, B. Rawal, and J. J. Peterson, "Accuracy and Validity of Goniometer and Visual Assessments of Angular Joint Positions of the Hand and Wrist," *The Journal of Hand Surgery*, vol. 41, no. 4, pp. 21–35, Apr. 2016.

[241] T. I. Carter, B. Pansy, A. L. Wolff, H. J. Hillstrom, S. I. Backus, M. Lenhoff, and S. W. Wolfe, "Accuracy and Reliability of Three Different Techniques for Manual Goniometry for Wrist Motion: A Cadaveric Study," *The Journal of Hand Surgery*, vol. 34, no. 8, pp. 1422–1428, 2009.

[242] D. Blonna, P. C. Zarkadas, J. S. Fitzsimmons, and S. W. O'Driscoll, "Accuracy and inter-observer reliability of visual estimation compared to clinical goniometry of the elbow," *Knee Surgery, Sports Traumatology, Arthroscopy*, vol. 20, no. 7, pp. 1378–1385, Jul. 2012.

[243] G. E. Hancock, T. Hepworth, and K. Wembridge, "Accuracy and reliability of knee goniometry methods," *Journal of Experimental Orthopaedics*, vol. 5, pp. 46–52, Oct. 2018.

[244] M. Shamsi, M. Mirzaei, and S. S. Khabiri, "Universal goniometer and electrogoniometer intra-examiner reliability in measuring the knee range of motion during active knee extension test in patients with chronic low back pain with short hamstring muscle," *BMC Sports Science, Medicine and Rehabilitation*, vol. 11, no. 1, pp. 4–9, Mar. 2019.

[245] D. A. Krause, M. S. Boyd, A. N. Hager, E. C. Smoyer, A. T. Thompson, and J. H. Hollman, "Reliability and Accuracy of a Goniometer Mobile Device Application for Video Measurement of the Functional Movement Screen Deep Squat Test," *International Journal of Sports Physical Therapy*, vol. 10, no. 1, pp. 37–44, Feb. 2015.

[246] N. W. Williams, J. M. T. Penrose, C. M. Caddy, E. Barnes, D. R. Hose, and P. Harley, "A Goniometric Glove for Clinical Hand Assessment: Construction, calibration and validation," *Journal of Hand Surgery*, Nov. 2016.

[247] L. Reissner, G. Fischer, R. List, W. R. Taylor, P. Giovanoli, and M. Calcagni, "Minimal detectable difference of the finger and wrist range of motion: Comparison of goniometry and 3D motion analysis," *Journal of Orthopaedic Surgery and Research*, vol. 14, no. 1, pp. 173–183, Jun. 2019.

[248] J. Z. Zhao, P. E. Blazar, A. N. Mora, and B. E. Earp, "Range of Motion Measurements of the Fingers Via Smartphone Photography," *Hand (New York, N.Y.)*, vol. 15, no. 5, pp. 679–685, Sep. 2020.

[249] Blender Online Community, "Blender - a 3D modelling and rendering package," Blender Foundation, Amsterdam, Netherlands, Jun. 2021.

Appendices

The following pages provide supporting material for the results and conclusions drawn from this research. Within the work, references have been made to the appropriate sections and items here when relevant.

Appendix A: Ethical Approval

The following section provides the documents acquired from the ethical approval granted for this study. The confirmation of Biomedical & Scientific Research Ethics Committee approval is shown in Figures A.1 and A.1; the supporting documents follow, including: the participant information leaflet, in Figures A.3, A.4, A.5, A.6 and A.7, the participant consent form, in Figure A.8, and the participant questionnaire, in Figure A.9. The confirmation of Research Ethics Committee approval is shown in Figures A.10, A.11, A.12, A.13, A.14, and A.15.

PRIVATE
Mr Callum Thornton
School of Engineering
University of Warwick
Coventry
CV4 7AL

4 October 2018

Dear Mr Thornton,

Study Title and BSREC Reference: *Modelling and Analysis of Hand Motion in Everyday Activities with Application to prosthetic Hand Technology* REGO-2018-2210

Thank you for submitting the revisions to the above-named study to the University of Warwick's Biomedical and Scientific Research Ethics Sub-Committee for approval.

I am pleased to confirm that approval is granted.

In undertaking your study, you are required to comply with the University of Warwick's *Research Data Management Policy*, details of which may be found on the Research and Impact Services' webpages, under "Codes of Practice & Policies" » "Research Code of Practice" » "Data & Records" » "Research Data Management Policy", at:
http://www2.warwick.ac.uk/services/ris/research_integrity/code_of_practice_and_policies/research_code_of_practice/datacollection_retention/research_data_mgt_policy

You are also required to comply with the University of Warwick's *Information Classification and Handling Procedure*, details of which may be found on the University's Governance webpages, under "Governance" » "Information Security" » "Information Classification and Handling Procedure", at:
http://www2.warwick.ac.uk/services/gov/informationsecurity/handling.
Investigators should familiarise themselves with the classifications of information defined therein, and the requirements for the storage and transportation of information within the different classifications:

Information Classifications:
http://www2.warwick.ac.uk/services/gov/informationsecurity/handling/classifications
Handling Electronic Information:
http://www2.warwick.ac.uk/services/gov/informationsecurity/handling/electronic/
Handling Paper or other media
http://www2.warwick.ac.uk/services/gov/informationsecurity/handling/paper/.

Please also be aware that BSREC grants **ethical approval** for studies. **The seeking and obtaining of *all* other necessary approvals is the responsibility of the investigator.**

These other approvals may include, but are not limited to:

Figure A.1: The Biomedical & Scientific Research Ethics Committee approval confirmation document for hand motion capture, page one.

1. Any necessary agreements, approvals, or permissions required in order to comply with the University of Warwick's Financial Regulations and Procedures.
2. Any necessary approval or permission required in order to comply with the University of Warwick's Quality Management System and Standard Operating Procedures for the governance, acquisition, storage, use, and disposal of human samples for research.
3. All relevant University, Faculty, and Divisional/Departmental approvals, if an employee or student of the University of Warwick.
4. Approval from the applicant's academic supervisor and course/module leader (as appropriate), if a student of the University of Warwick.
5. NHS Trust R&D Management Approval, for research studies undertaken in NHS Trusts.
6. NHS Trust Clinical Audit Approval, for clinical audit studies undertaken in NHS Trusts.
7. Approval from Departmental or Divisional Heads, as required under local procedures, within Health and Social Care organisations hosting the study.
8. Local ethical approval for studies undertaken overseas, or in other HE institutions in the UK.
9. Approval from Heads (or delegates thereof) of UK Medical Schools, for studies involving medical students as participants.
10. Permission from Warwick Medical School to access medical students or medical student data for research or evaluation purposes.
11. NHS Trust Caldicott Guardian Approval, for studies where identifiable data is being transferred outside of the direct clinical care team. Individual NHS Trust procedures vary in their implementation of Caldicott guidance, and local guidance must be sought.
12. Any other approval required by the institution hosting the study, or by the applicant's employer.

There is no requirement to supply documentary evidence of any of the above to BSREC, but applicants should hold such evidence in their Study Master File for University of Warwick auditing and monitoring purposes. You may be required to supply evidence of any necessary approvals to other University functions, e.g. The Finance Office, Research & Impact Services (RIS), or your Department/School.

May I take this opportunity to wish you success with your study, and to remind you that any Substantial Amendments to your study require approval from BSREC before they may be implemented.

Yours sincerely

pp. [redacted]

Dr David Ellard
Chair
Biomedical and Scientific
Research Ethics Sub-Committee

Biomedical and Scientific
Research Ethics Sub-Committee
Research & Impact Services
University of Warwick
Coventry, CV4 8UW.
E: BSREC@Warwick.ac.uk

http://www2.warwick.ac.uk/services/ris/research_integrity/researchethicscommittees/biomed

Figure A.2: The Biomedical & Scientific Research Ethics Committee approval confirmation document for hand motion capture, page two.

Participant Information Leaflet

Study Title: **Modelling and Analysis of Hand Motion in Everyday Activities with Application to Prosthetic Hand Technology**

Investigator: **Callum Thornton**

Introduction

You are invited to take part in a study. Before you decide, you need to understand why the study is being done and what it would involve for you. Please take the time to read the following information carefully. Talk to others about the study if you wish.

Part 1 tells you the purpose of the study and what will happen to you if you take part.
Part 2 gives you more detailed information about the conduct of the study.

Please ask if there is anything that is not clear or if you would like more information. Take time to decide whether or not you wish to take part.

PART 1

What is the study about?

My research aims to create a mechanistic mathematical model of the human hand in order to give a greater understanding of how the hand works and, through the application of this knowledge, reduce the cost of upper limb prostheses. This study is being used to evaluate current state-of-the-art in taxonomies of common hand grasps used in everyday activities and update these taxonomies to include modern day, finer scale, tasks (such as the use of keyboards and mobile phones).

Do I have to take part?

It is entirely up to you to decide. I will describe the study and go through this information sheet, which I will give to you to keep. If you choose to participate, you will be asked to sign a consent form to confirm that you have agreed to take part. You will be free to pause the experiment or withdraw at any time, without giving a reason and this will not affect you or your circumstances in any way.

Figure A.3: The Biomedical & Scientific Research Ethics Committee approved participant information leaflet for the conducted study, page one.

What will happen to me if I take part?

The Leap Motion experiment can be performed anywhere, this will most likely be in your regular working environment. You will be required to wear a headband (on which the Leap Motion controller will be attached) and have a pocket-sized computer (used to collect the data) in close proximity (this may be on your person or beside you on a desk). This experiment can be carried out wherever you would like for as long as you would like. You will then be asked to treat this time as you normally would, performing tasks as you normally would. Once the experiment has started the Leap Motion controller will look for hands in its field of vision, fit hand models to any hands it finds and send these models to the computer, which then only records the positional data from the models. If you are unable to wear a headband, for medical or religious reasons, you will not be able to take part in the study – please let us know immediately if you have any worries.

If the VICON experiment is being performed you will be in the VICON Gait Laboratory at the University. Your digit length, knuckle width, wrist width and hand length will need to be measured and then reflective markers attached to your hand, with medical grade double sided tape. You will then be asked to perform typical everyday tasks with a range of common household items within the laboratory. This will include: holding a mug, operating a smartphone, removing a screw cap from a jar, holding a blunt kitchen knife, squeezing a tube of toothpaste, holding a key, picking up coins and carrying a bag. The positions of the reflective markers are recorded by infrared cameras, located around the room, to collect the motion capture data. You may be asked to repeat some of these tasks with a non-invasive pressure, EEG and/or EMG sensing device to find the pressure applied by the hand, electrical activity of the brain and/or electrical activity of the muscles (respectively) when the tasks are performed.

What are the possible disadvantages, side effects, risks, and/or discomforts of taking part in this study?

All the equipment is non-invasive, therefore should not pose any risk or side effect. If, however, at any time during the study you feel irritation from the equipment used you are free to pause, or stop the experiment completely.

What are the possible benefits of taking part in this study?

There will be no direct, individual, benefits from taking part in this study; however, as this is a research project focused on health care the results will give wider, long term, benefits and impacts. The overall project aims to enhance the design and reduce the cost of upper limb prostheses, the data collected in this study will help towards this goal.

Expenses and payments

There are no expenses or payments involved with the participation of this study.

What will happen when the study ends?

Once the experiment has finished that is all that will be required from you. The data collected will be stored for up to 10 years, per University policy (or in line with the new University regulations, if changed). Further detail on how the data is stored is included in Part 2.

Will my taking part be kept confidential?

Yes. We will follow strict ethical and legal practice and all information about you will be handled in confidence. All data will be kept on an encrypted memory stick and it will be ensured that these are safely stored in a locked cupboard within one of the supervisor's

Figure A.4: The Biomedical & Scientific Research Ethics Committee approved participant information leaflet for the conducted study, page two.

office. Data will be stored for up to 10 years according to University policy (or in line with the new University regulations if changed). The data will only be accessible by the PhD student and the supervisors for this project. The signed consent form will be will be locked in a draw in the supervisor's office, away from the laboratory.

What if there is a problem?

Any complaint about the way you have been dealt with during the study or any possible harm that you might suffer will be addressed. Detailed information is given in Part 2.

This concludes Part 1.

If the information in Part 1 has interested you and you are considering participation, please read the additional information in Part 2 before making any decision.

Figure A.5: The Biomedical & Scientific Research Ethics Committee approved participant information leaflet for the conducted study, page three.

PART 2

Who is organising and funding the study?

This study is EPSRC (Engineering and Physical Sciences Research Council) and UHCW (University Hospitals Coventry and Warwickshire NHS Trust) funded.

What will happen if I don't want to carry on being part of the study?

Participation in this study is entirely voluntary. Refusal to participate will not affect you in any way. If you decide to take part in the study you will need to sign a consent form, which states that you have given your consent to participate.

If you agree to participate, you may nevertheless withdraw from the study at any time without affecting you in any way.

You have the right to withdraw from the study completely and decline any further contact by study staff after you withdraw. Withdrawal from the study will not affect your usual care or any care benefits you may be entitled to. If you do choose to withdraw from the study any data collected will be immediately deleted.

What if there is a problem?

This study is covered by the University of Warwick's insurance and indemnity cover. If you have an issue, please contact the Chief Investigator of the study:

Callum Thornton
Biomedical and Biological Laboratory
School of Engineering
University of Warwick
Coventry
CV4 7ES
Tel: 07477 631 867
Email: c.thornton@warwick.ac.uk

Who should I contact if I wish to make a complaint?

Any complaint about the way you have been dealt with during the study or any possible harm you might have suffered will be addressed. Please address your complaint to the person below, who is a senior University of Warwick official entirely independent of this study:

Head of Research Governance
Research & Impact Services
University House
University of Warwick
Coventry
CV4 8UW
Tel: 024 76 522746
Email: researchgovernance@warwick.ac.uk

Figure A.6: The Biomedical & Scientific Research Ethics Committee approved participant information leaflet for the conducted study, page four.

Will my taking part be kept confidential?

All participants will be assigned a study number which will be the number under which all their data will be recorded – this will ensure that their data is anonymised. All data will be saved to an encrypted USB stick for further analysis. Only myself, my supervisors in the School of Engineering and collaborators and co-supervisor at WMS and UHCW will have access to the data collected.

What will happen to the results of the study?

Results will be used, anonymised, in publications for journals, my thesis and posters and presentations at conferences, workshops and an annual internal symposium.

Who has reviewed the study?

This study has been reviewed and given favourable opinion by the University of Warwick's Biomedical and Scientific Research Ethics Committee (BSREC): REGO-2018-2210.

What if I want more information about the study?

If you have any questions about any aspect of the study, or your participation in it, not answered by this participant information leaflet, please contact:

Callum Thornton
Biomedical and Biological Laboratory
School of Engineering
University of Warwick
Coventry
CV4 7ES
Tel: 07477 631 867
Email: c.thornton@warwick.ac.uk

Thank you for taking the time to read this participant information leaflet.

Figure A.7: The Biomedical & Scientific Research Ethics Committee approved participant information leaflet for the conducted study, page five.

BIOMEDICAL AND SCIENTIFIC RESEARCH ETHICS COMMITTEE APPROVED CONSENT FORM

Study Number:

Patient Identification Number for this study:

Title of Project: Modelling and Analysis of Hand Motion in Everyday Activities with Application to Prosthetic Hand Technology

Name of Researcher(s): Mr. Callum Thornton, Prof. Michael Chappell, Dr. Neil Evans and Dr. Joseph Hardwicke

Please initial boxes

1. I confirm that I have read and understand the information sheet dated 3rd August 2018 for the above study. I have had the opportunity to consider the information, ask questions and have had these answered satisfactorily. ☐
2. I understand that my participation is voluntary and that I am free to withdraw at any time without giving any reason, without my medical, social care, education, or legal rights being affected. ☐
3. I understand that relevant sections of my medical notes and data collected during the study, may be looked at by individuals from The University of Warwick, from regulatory authorities (or from a relevant NHS Trust), where it is relevant to my taking part in this study. I give permission for these individuals to have access to my records. ☐
4. I agree to take part in the above study. ☐

Name of Participant	Date	Signature
Name of Person taking consent	Date	Signature

3rd August 2018, version 2

1

Figure A.8: The Biomedical & Scientific Research Ethics Committee approved participant consent form for the conducted study.

BIOMEDICAL AND SCIENTIFIC RESEARCH ETHICS COMMITTEE APPROVED QUESTIONNAIRE

Study Number:

Patient Identification Number for this study:

Title of Project: Modelling and Analysis of Hand Motion in Everyday Activities with Application to Prosthetic Hand Technology

Name of Researcher(s): Mr. Callum Thornton, Prof. Michael Chappell, Dr. Neil Evans and Dr. Joseph Hardwicke

1. Age: _____
2. Gender: _____
3. Dominate hand: _____
4. Do you have any hand impairments? (if yes please specify below) _____
5. Do you have any current medical conditions? (if yes please specify below) _____

If yes to question 4 please specify below,

If yes to question 5 please specify below,

3rd August 2018, version 2

1

Figure A.9: The Biomedical & Scientific Research Ethics Committee approved participant questionnaire for the conducted study.

NHS
Health Research Authority

North East - York Research Ethics Committee
NHSBT Newcastle Blood Donor Centre
Holland Drive
Newcastle upon Tyne
NE2 4NQ

Telephone: 0207 1048091

Please note: This is the favourable opinion of the REC only and does not allow you to start your study at NHS sites in England until you receive HRA Approval

11 May 2018

Dr Joseph Hardwicke
Consultant Plastic Surgeon/Honorary Associate Professor
University Hospitals of Coventry and Warwickshire NHS Trust
Clifford Bridge Road
Coventry
CV2 2DX

Dear Dr Hardwicke

Study title:	**A sensorimotor PROsthesis for the upper LIMB. The PROLIMB study.**
REC reference:	**18/NE/0174**
Protocol number:	**JH382118**
IRAS project ID:	**243525**

The Proportionate Review Sub-committee of the North East - York Research Ethics Committee reviewed the above application via correspondence.

We plan to publish your research summary wording for the above study on the HRA website, together with your contact details. Publication will be no earlier than three months from the date of this favourable opinion letter. The expectation is that this information will be published for all studies that receive an ethical opinion but should you wish to provide a substitute contact point, wish to make a request to defer, or require further information, please contact hra.studyregistration@nhs.net outlining the reasons for your request. Under very limited

A Research Ethics Committee established by the Health Research Authority

Figure A.10: The Research Ethics Committee approval confirmation document for the AirGo clinical trail, page one.

circumstances (e.g. for student research which has received an unfavourable opinion), it may be possible to grant an exemption to the publication of the study.

Ethical opinion

On behalf of the Committee, the sub-committee gave a **favourable ethical opinion** of the above research on the basis described in the application form, protocol and supporting documentation, subject to the conditions specified below.

Conditions of the favourable opinion

The REC favourable opinion is subject to the following conditions being met prior to the start of the study.

Management permission must be obtained from each host organisation prior to the start of the study at the site concerned.

Management permission should be sought from all NHS organisations involved in the study in accordance with NHS research governance arrangements. Each NHS organisation must confirm through the signing of agreements and/or other documents that it has given permission for the research to proceed (except where explicitly specified otherwise).

Guidance on applying for HRA and HCRW Approval (England and Wales)/ NHS permission for research is available in the Integrated Research Application System, www.hra.nhs.uk or at http://www.rdforum.nhs.uk.

Where a NHS organisation's role in the study is limited to identifying and referring potential participants to research sites ("participant identification centre"), guidance should be sought from the R&D office on the information it requires to give permission for this activity.

For non-NHS sites, site management permission should be obtained in accordance with the procedures of the relevant host organisation.

Sponsors are not required to notify the Committee of management permissions from host organisations.

Registration of Clinical Trials

All clinical trials (defined as the first four categories on the IRAS filter page) must be registered on a publically accessible database. This should be before the first participant is recruited but no later than 6 weeks after recruitment of the first participant.

There is no requirement to separately notify the REC but you should do so at the earliest opportunity e.g. when submitting an amendment. We will audit the registration details as part of the annual progress reporting process.

To ensure transparency in research, we strongly recommend that all research is registered but for non-clinical trials this is not currently mandatory.

If a sponsor wishes to request a deferral for study registration within the required timeframe, they should contact hra.studyregistration@nhs.net. The expectation is that all clinical trials will

Figure A.11: The Research Ethics Committee approval confirmation document for the AirGo clinical trail, page two.

be registered, however, in exceptional circumstances non registration may be permissible with prior agreement from the HRA. Guidance on where to register is provided on the HRA website.

It is the responsibility of the sponsor to ensure that all the conditions are complied with before the start of the study or its initiation at a particular site (as applicable).

Ethical review of research sites

The favourable opinion applies to all NHS sites taking part in the study, subject to management permission being obtained from the NHS/HSC R&D office prior to the start of the study (see "Conditions of the favourable opinion").

Summary of discussion at the meeting

Members stated that there needed to be more information in the Participant Information Sheet on the number of visits, the location of these visits and the time taken to collect data. The type of activities patients will be asked to perform also need to be included.

Members noted that on page 13 of the protocol, it stated that participants would have to wear the LMC (data capture device) for 6 hours in the home or familiar setting and queried whether this was a further additional visit. If so, there would need to be details included in the Participant Information Sheet.

Members noted that in the section "what is the purpose of the study" reference was made to patients who may choose to wear it (the old/new prosthesis) in the future. It seemed ambiguous and may be misinterpreted that patients would receive (if they choose) the body powered finger prosthesis after the study had finished. Members requested that this was made clearer in the Participant Information Sheet.

Members stated that the Participant Information Sheet, Page 2 "Why have I been invited to take part?", Line 4, "you" should read "your".

You confirmed that the above changes had been made.

Approved documents

The documents reviewed and approved were:

Document	*Version*	*Date*
Covering letter on headed paper		11 May 2018
IRAS Application Form [IRAS_Form_27042018]		27 April 2018
IRAS Checklist XML [Checklist_27042018]		27 April 2018
Letter from sponsor [243525_PROLIMB_Sponsor Letter]		17 April 2018
Participant consent form [243525_PROLIMB_Consent Form]	1.0	16 April 2018
Participant information sheet (PIS) [tracked and clean]	V1.1	09 May 2018
Research protocol or project proposal [243525_Protocol_PROLIMB]	1.0	16 April 2018
Summary CV for Chief Investigator (CI) [Summary CV for CI]	1.0	17 April 2018

Figure A.12: The Research Ethics Committee approval confirmation document for the AirGo clinical trail, page three.

Membership of the Proportionate Review Sub-Committee

The members of the Sub-Committee who took part in the review are listed on the attached sheet.

Statement of compliance

The Committee is constituted in accordance with the Governance Arrangements for Research Ethics Committees and complies fully with the Standard Operating Procedures for Research Ethics Committees in the UK.

After ethical review

Reporting requirements

The attached document "After ethical review – guidance for researchers" gives detailed guidance on reporting requirements for studies with a favourable opinion, including:

- Notifying substantial amendments
- Adding new sites and investigators
- Notification of serious breaches of the protocol
- Progress and safety reports
- Notifying the end of the study

The HRA website also provides guidance on these topics, which is updated in the light of changes in reporting requirements or procedures.

User Feedback

The Health Research Authority is continually striving to provide a high quality service to all applicants and sponsors. You are invited to give your view of the service you have received and the application procedure. If you wish to make your views known please use the feedback form available on the HRA website:
http://www.hra.nhs.uk/about-the-hra/governance/quality-assurance/

HRA Training

We are pleased to welcome researchers and R&D staff at our training days – see details at http://www.hra.nhs.uk/hra-training/

With the Committee's best wishes for the success of this project.

18/NE/0174	**Please quote this number on all correspondence**

A Research Ethics Committee established by the Health Research Authority

Figure A.13: The Research Ethics Committee approval confirmation document for the AirGo clinical trail, page four.

Yours sincerely

[redacted]

pp
Mr Steve Chandler
Chair

Email: nrescommittee.northeast-york@nhs.net

Enclosures: *List of names and professions of members who took part in the review*

"After ethical review – guidance for researchers"

Copy to: Ms Ceri Jones

Miss Sonia Kandola, University Hospitals of Coventry and Warwickshire NHS Trust

A Research Ethics Committee established by the Health Research Authority

Figure A.14: The Research Ethics Committee approval confirmation document for the AirGo clinical trail, page five.

North East - York Research Ethics Committee

Attendance at PRS Sub-Committee of the REC meeting via correspondence

Committee Members:

Name	*Profession*	*Present*	*Notes*
Mr Steve Chandler (Chair)	Retired Consultant Medical Physicist	Yes	
Dr Mary Connor	Coaching & Mentoring Consultant	Yes	
Dr James Hobkirk	Lecturer in Physiology & Scientific Director of Cardio-thoracic Surgery	Yes	

Also in attendance:

Name	*Position (or reason for attending)*
Mrs Helen Wilson	REC Manager

A Research Ethics Committee established by the Health Research Authority

Figure A.15: The Research Ethics Committee approval confirmation document for the AirGo clinical trail, page six.

Appendix B: Preliminary Findings

The following section provides the participant information and results form the preliminary data collection and analysis performed. This preliminary data collection includes 62 hours and ten minutes of hand motion data from 13 participants. The data collected during the preliminary data collection has also been used within the final taxonomy of hand shapes presented in this study. Included here are: the anonymised participant information, in Table B.1, the resultant hand shapes found within the data collected, in Figures B.1 and B.2, bar charts of the number of occurrences and frame count for these hand shapes, in Figures B.3, B.4, B.5 and B.6, and tabulated characteristics of the hand shapes, in Tables B.2 and B.3.

Table B.1: The anonymised participant information from the preliminary data collection.

Participant	Recorded Time	Age	Dominant Hand	Gender
01	8 hours 10 minutes	45	Right	Female
02	5 hours 20 minutes	72	Right	Male
03	2 hours 30 minutes	30	Right	Female
04	2 hours 50 minutes	24	Left	Male
05	4 hours 50 minutes	24	Right	Female
06	6 hours 20 minutes	54	Right	Female
07	2 hours 10 minutes	22	Right	Female
08	6 hours 0 minutes	53	Right	Female
09	5 hours 20 minutes	47	Right	Female
10	2 hours 10 minutes	46	Right	Female
11	3 hours 20 minutes	75	Right	Female
12	3 hours 20 minutes	28	Right	Female
13	9 hours 50 minutes	26	Right	Male

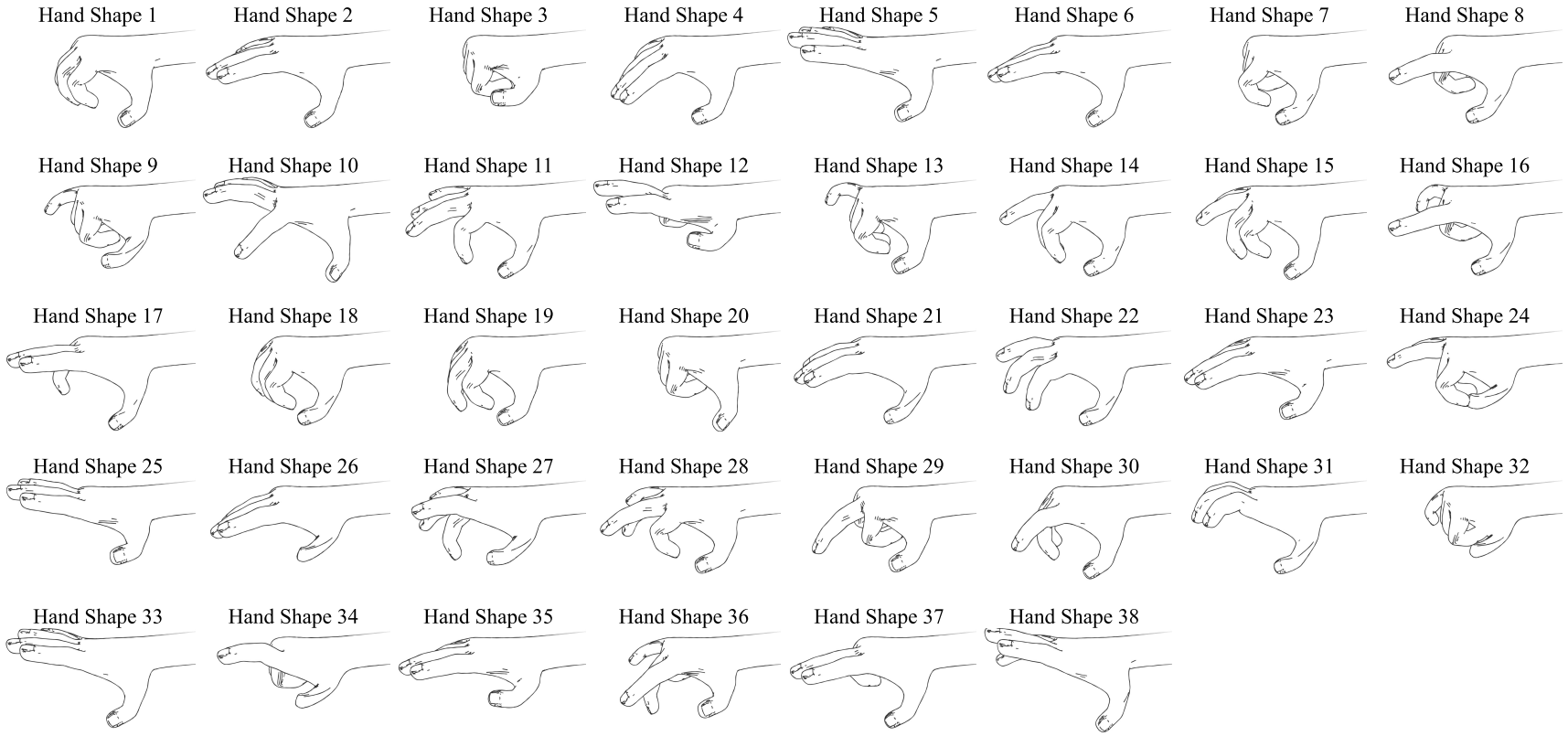

Figure B.1: The preliminary taxonomy of hand shapes for the left hand, provided by line art of the 38 cluster centroids.

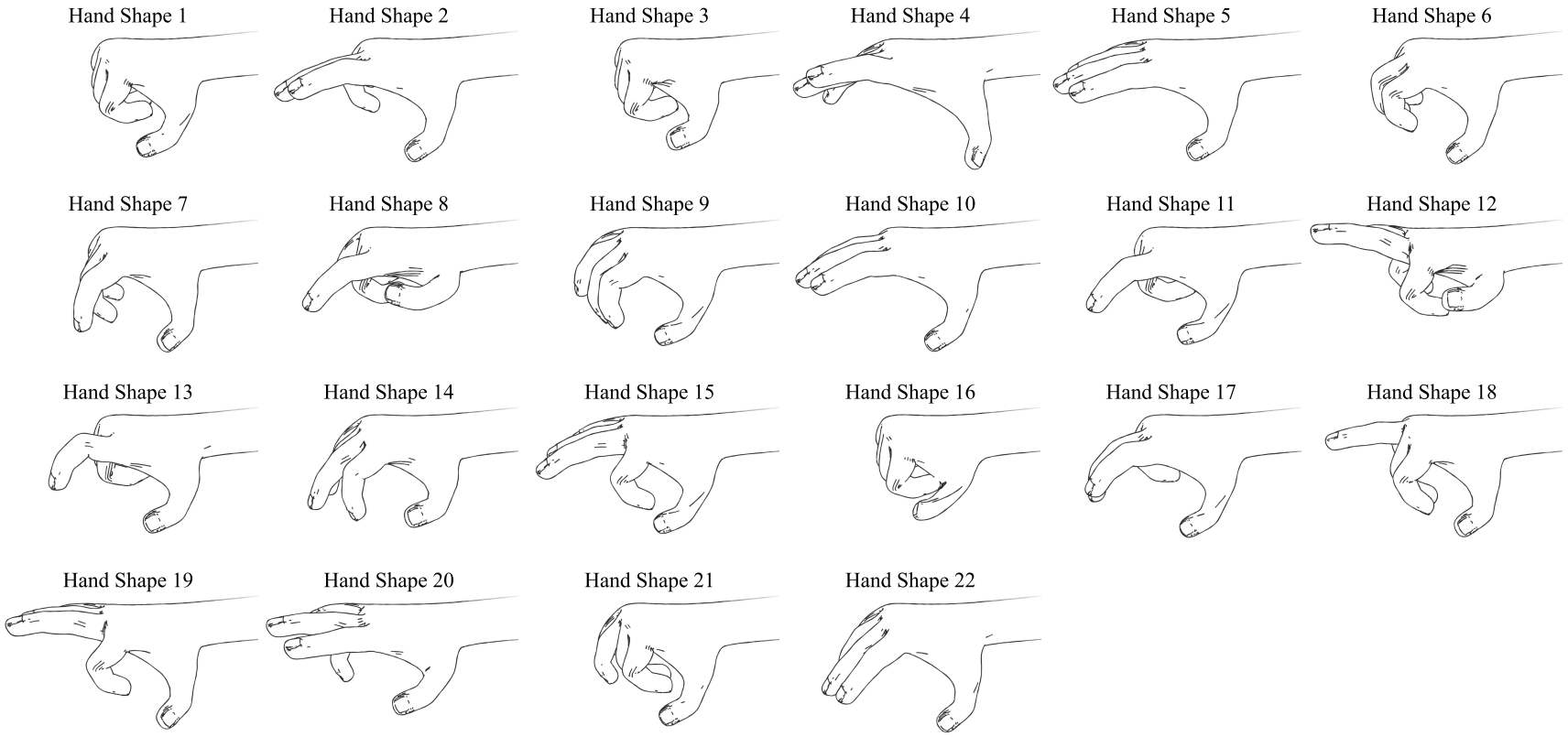

Figure B.2: The preliminary taxonomy of hand shapes for the right hand, provided by line art of the 22 cluster centroids.

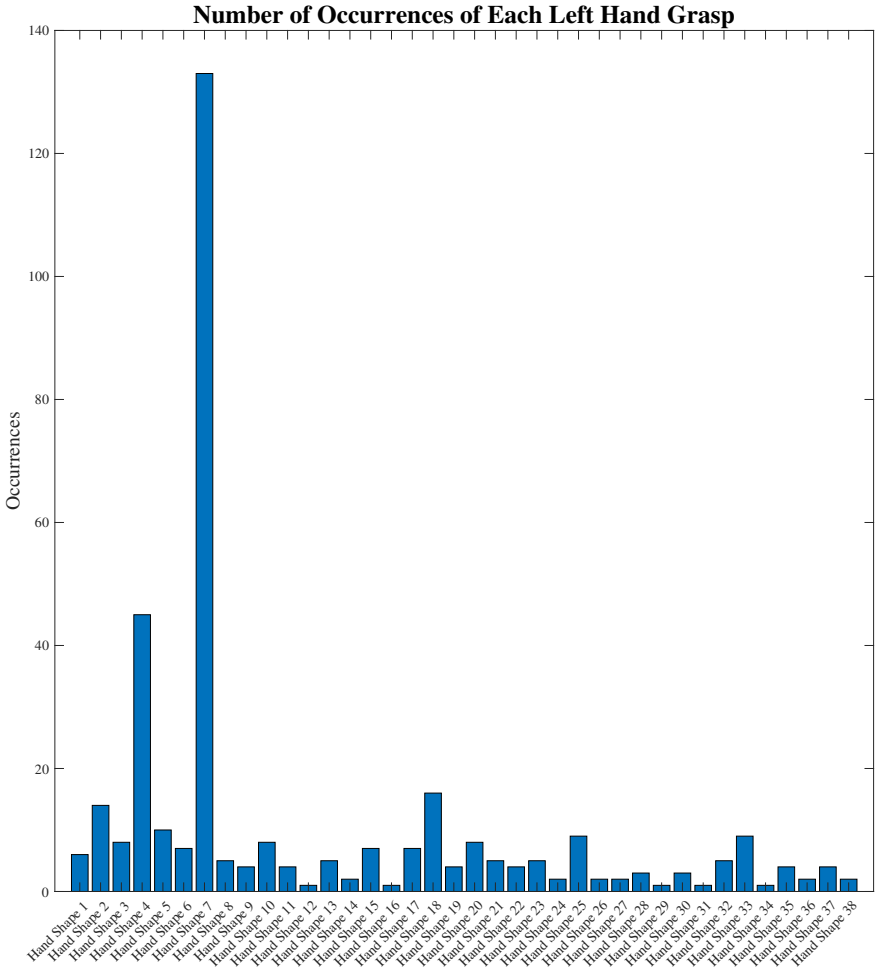

Figure B.3: A bar chart displaying the total number of occurrences of each hand shape for the left hand for the preliminary data analysis.

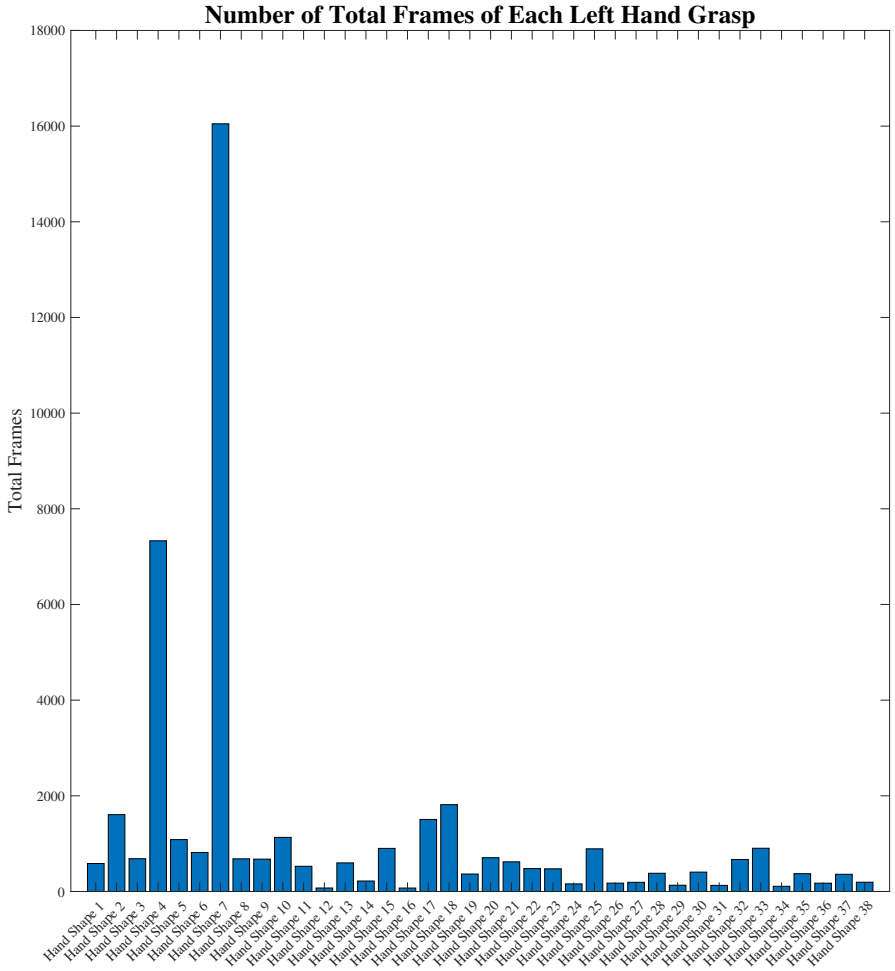

Figure B.4: A bar chart displaying the total number of frames each hand shape is seen within for the left hand for the preliminary data analysis.

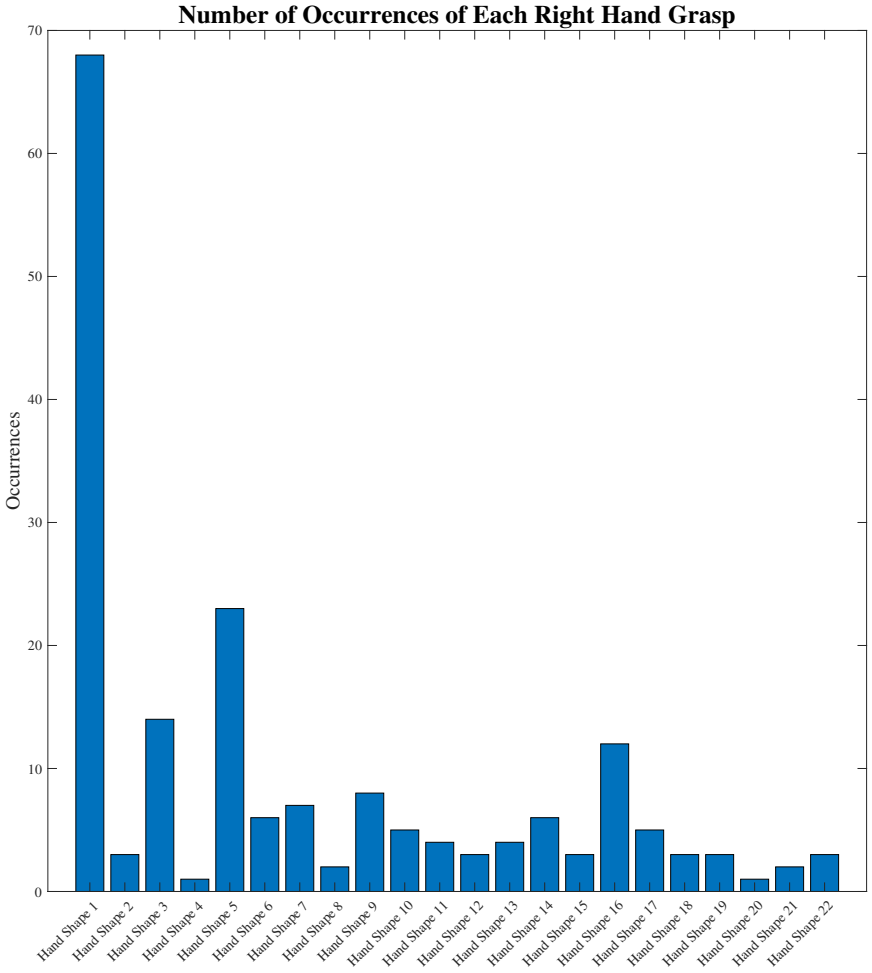

Figure B.5: A bar chart displaying the total number of occurrences of each hand shape for the right hand for the preliminary data analysis.

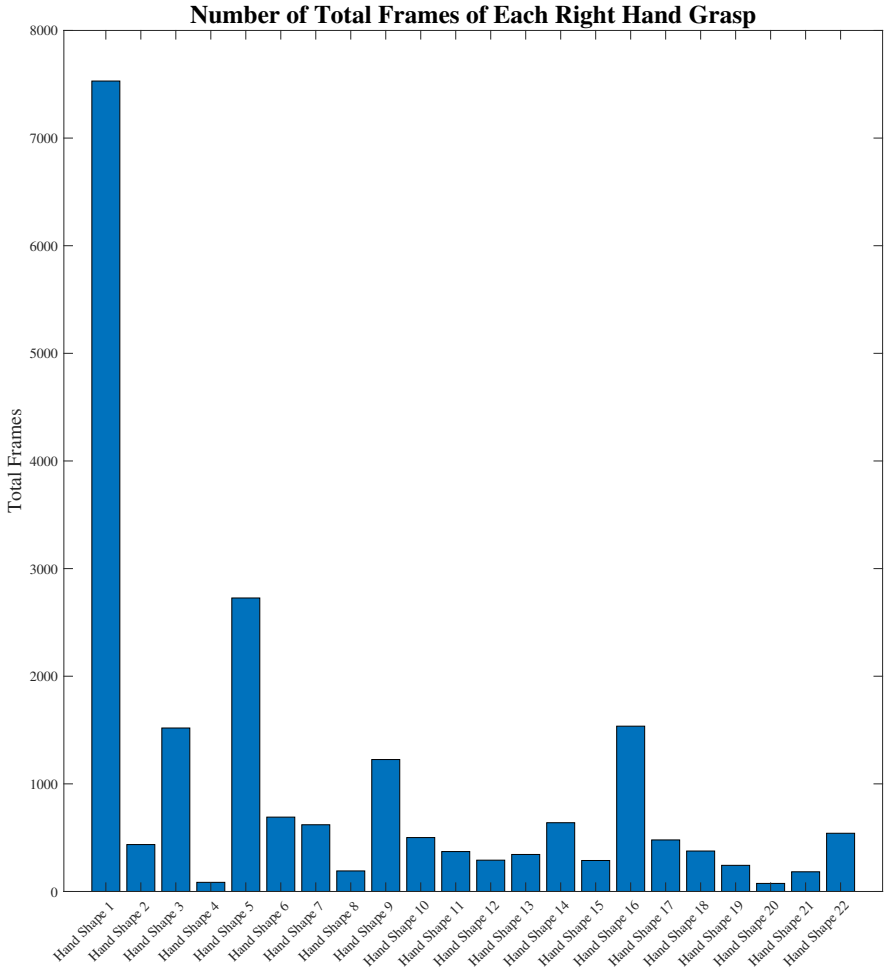

Figure B.6: A bar chart displaying the total number of frames each hand shape is seen within for the right hand for the preliminary data analysis.

Table B.2: The further hand shape cluster characteristics for the left hand for the preliminary data analysis.

Hand Shape	Percentage of Data / %	Total occurrences	Total Frames	Average Frames
1	0.07	6	585	98
2	0.19	14	1606	115
3	0.08	8	685	86
4	0.86	45	7331	163
5	0.13	10	1085	109
6	0.1	7	816	117
7	1.87	133	16048	121
8	0.08	5	683	137
9	0.08	4	677	169
10	0.13	8	1131	141
11	0.06	4	527	132
12	0.01	1	73	73
13	0.07	5	598	120
14	0.03	2	219	110
15	0.11	7	901	129
16	0.01	1	72	72
17	0.18	7	1506	215
18	0.21	16	1815	113
19	0.04	4	365	91
20	0.08	8	706	88
21	0.07	5	620	124
22	0.06	4	479	120
23	0.06	5	474	95
24	0.02	2	159	80
25	0.1	9	892	99
26	0.02	2	175	88
27	0.02	2	192	96
28	0.04	3	381	127
29	0.02	1	131	131
30	0.05	3	405	135
31	0.01	1	128	128
32	0.08	5	669	134
33	0.11	9	904	100
34	0.01	1	109	109
35	0.04	4	372	93
36	0.02	2	174	87
37	0.04	4	360	90
38	0.02	2	194	97

Table B.3: The further hand shape cluster characteristics for the right hand for the preliminary data analysis.

Hand Shape	Percentage of Data / %	Total occurrences	Total Frames	Average Frames
1	1.12	68	7530	111
2	0.06	3	436	145
3	0.23	14	1519	109
4	0.01	1	85	85
5	0.4	23	2727	119
6	0.1	6	691	115
7	0.09	7	620	89
8	0.03	2	191	96
9	0.18	8	1226	153
10	0.07	5	501	100
11	0.05	4	371	93
12	0.04	3	291	97
13	0.05	4	344	86
14	0.09	6	639	107
15	0.04	3	288	96
16	0.23	12	1536	128
17	0.07	5	479	96
18	0.06	3	376	125
19	0.04	3	243	81
20	0.01	1	75	75
21	0.03	2	183	92
22	0.08	3	541	180

Appendix C: Additional Analysis Findings

The following section provides additional results from the analysis performed. This includes: the scree plots from a principal component analysis (PCA) analysis of the collected hand motion data in Cartesian form, in Figures C.2 and C.1, the loading plots from a PCA analysis of the collected hand motion data in Cartesian form, in Figures C.3 and C.4, and the joint activity seen in the collected data with a threshold such that the thumb has been included, in Figures C.5 and C.6.

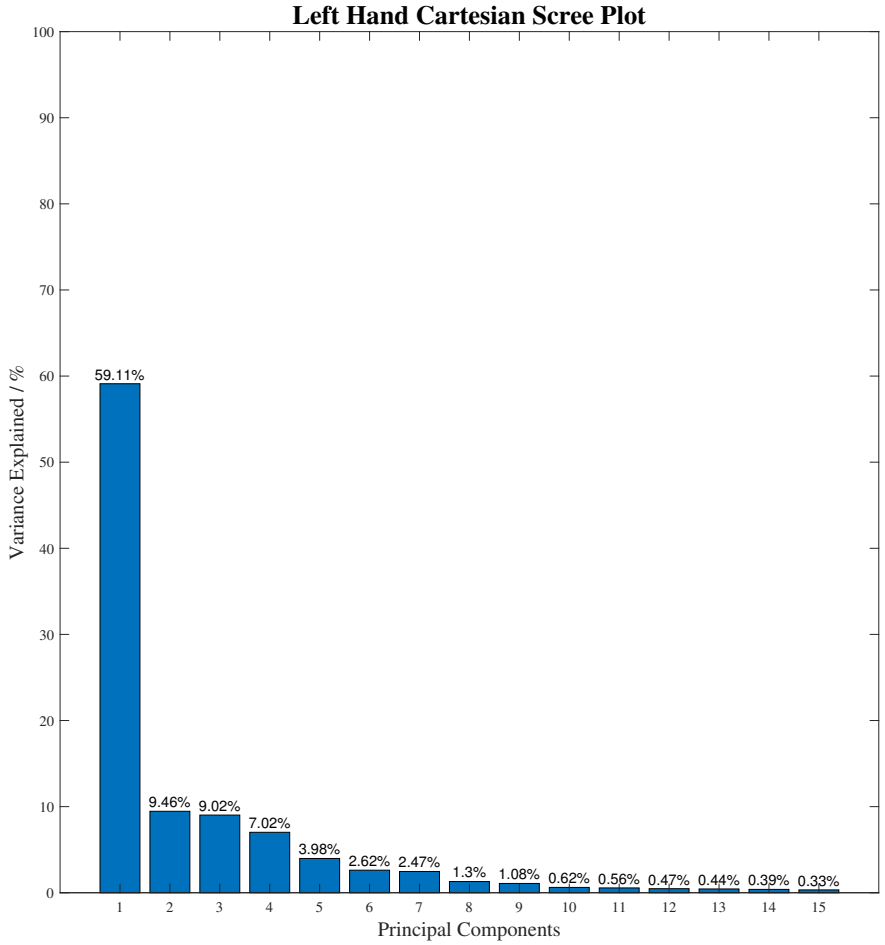

Figure C.1: A scree plot for the joint Cartesian co-ordinates of the left hand.

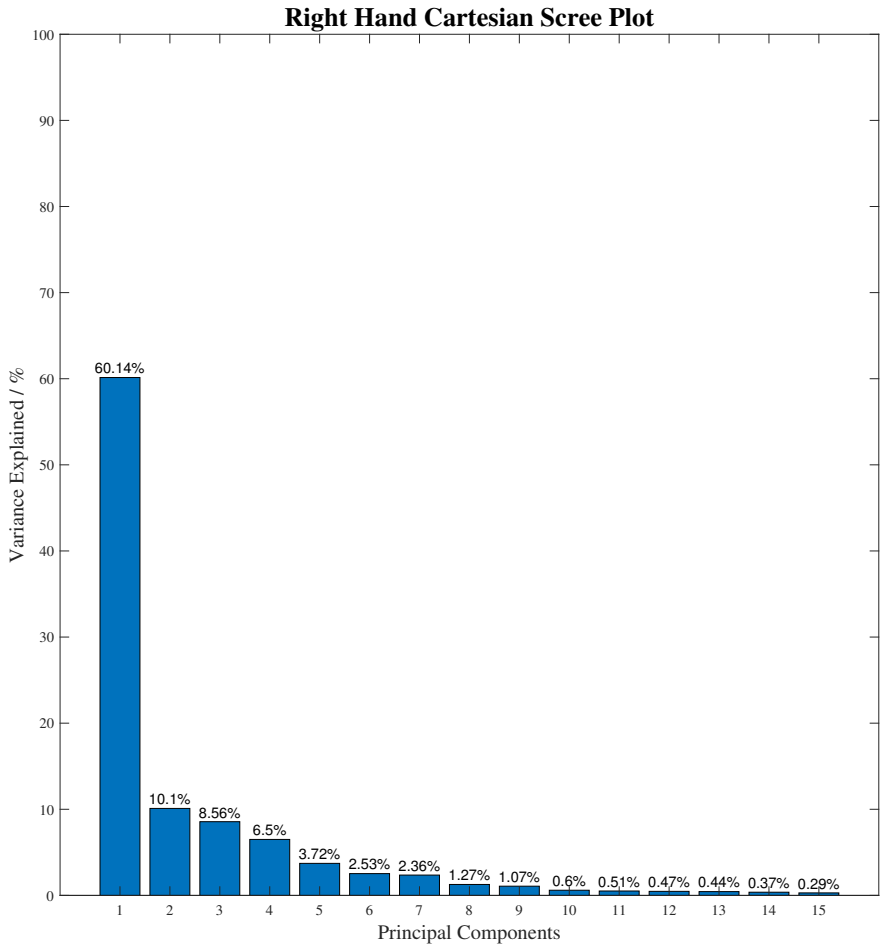

Figure C.2: A scree plot for the joint Cartesian co-ordinates of the right hand.

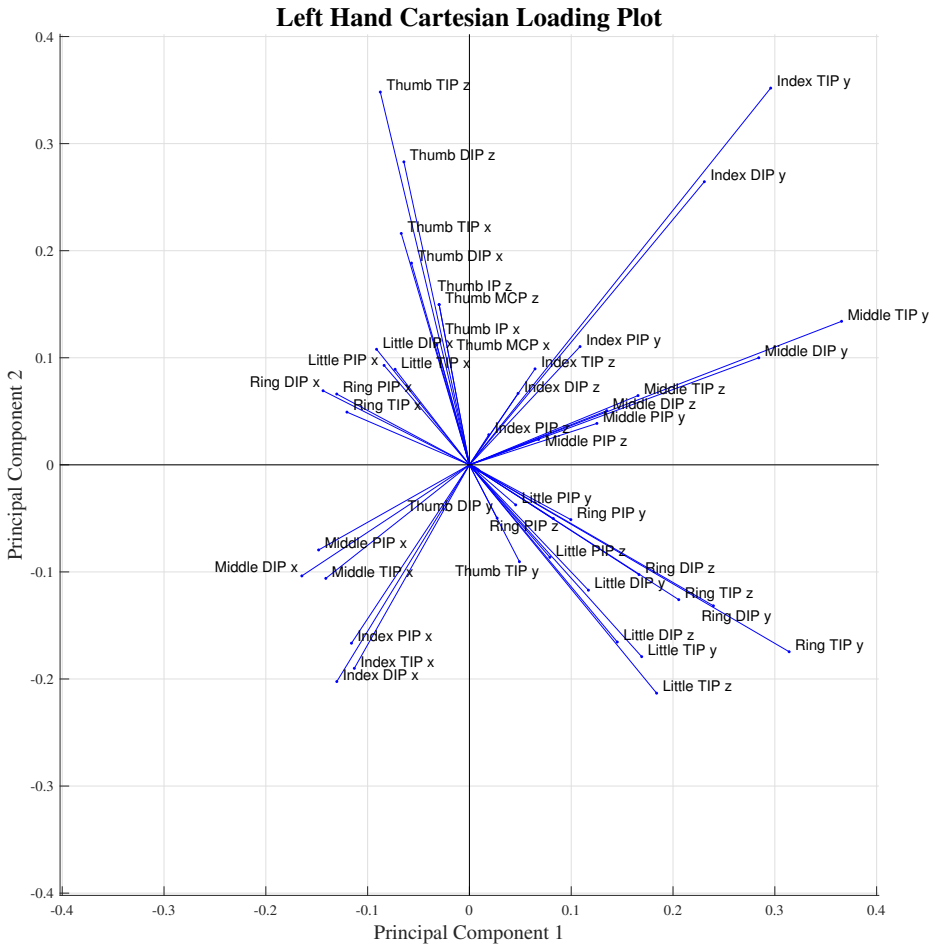

Figure C.3: A loading plot for the joint Cartesian co-ordinates of the left hand.

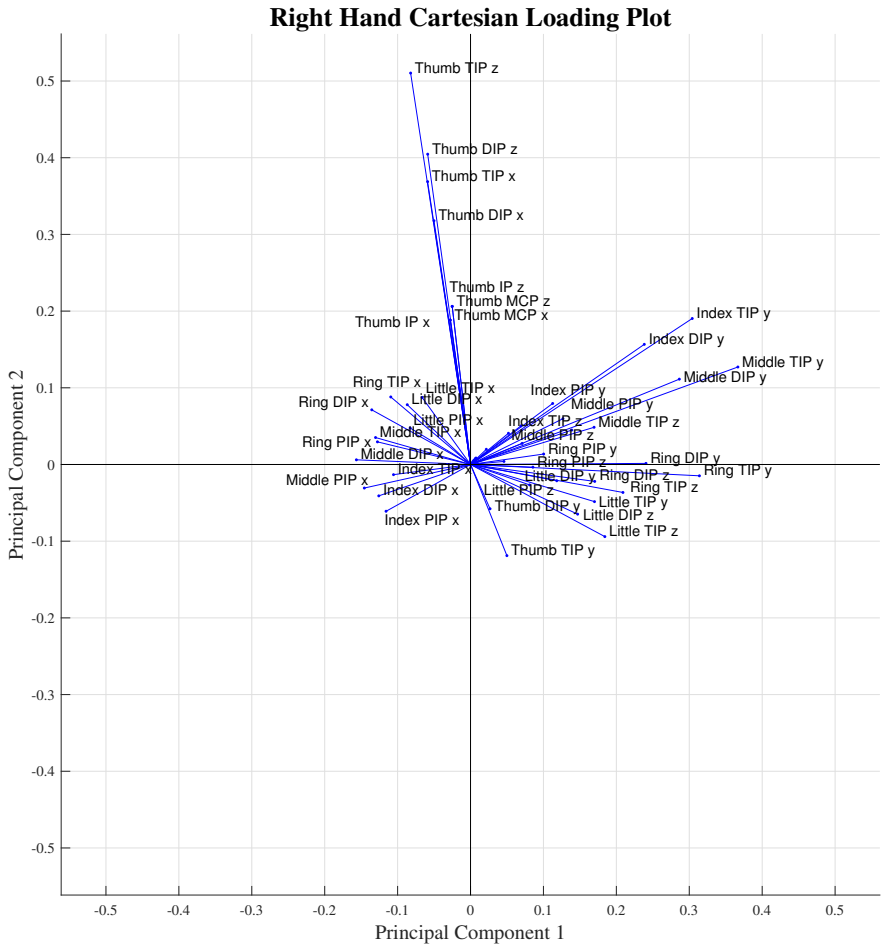

Figure C.4: A loading plot for the joint Cartesian co-ordinates of the right hand.

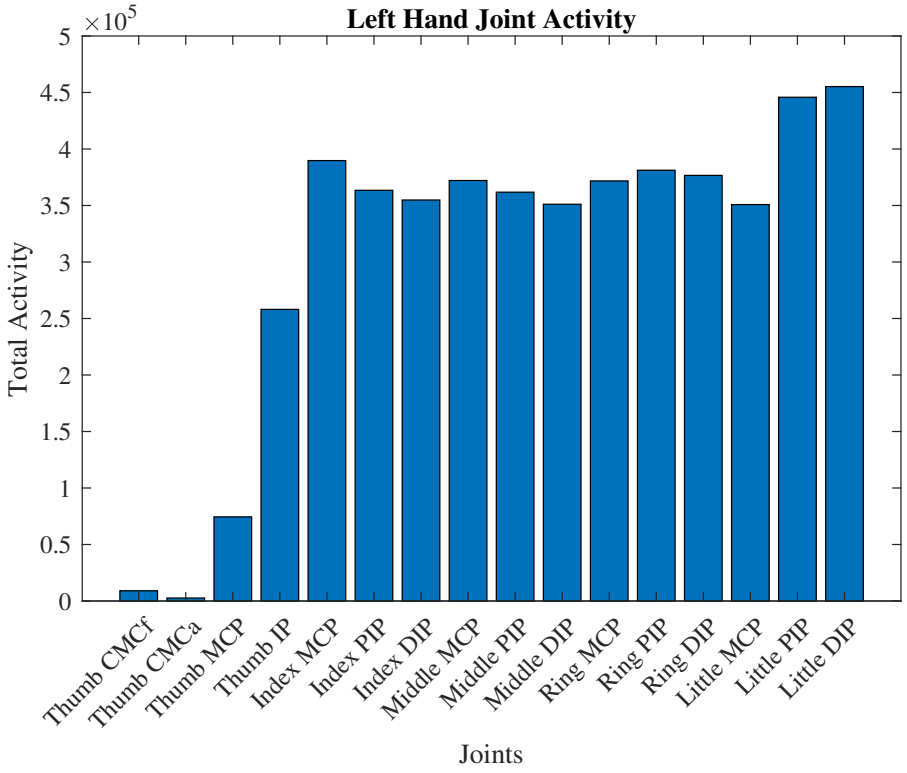

Figure C.5: The joint activity seen for each joint on the left during data collection, with a threshold altered to include all of the joints of the thumb.

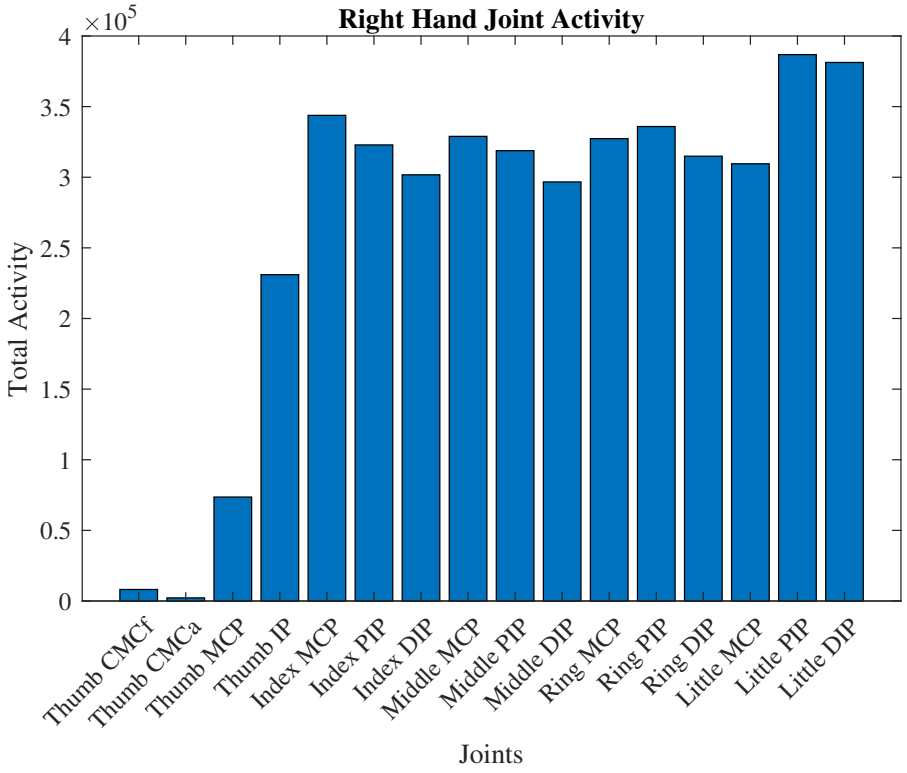

Figure C.6: The joint activity seen for each joint on the right during data collection, with a threshold altered to include all of the joints of the thumb.